# Design Aspects and Simulation of an Interconnected Hydragas (RTM) Roll Control Suspension

Rosam, Neil Daniel

*Award date:*
1995

*Awarding institution:*
University of Bath

# Design Aspects and Simulation of an Interconnected Hydragas® Roll Control Suspension

submitted by Neil Daniel Rosam
for the degree of PhD
of the University of Bath
1995





ProQuest LLC
789 East Eisenhower Parkway
P.O. Box 1346
Ann Arbor, MI 48106-1346

## SUMMARY

This thesis presents research work undertaken into the development of a novel, hydraulically operated roll control suspension based on established Hydragas® technology. A prototype system has been constructed and installed on a fluid interconnected Hydragas Austin Metro.

A computer simulation model of the vehicle with the active roll control system is presented. This model is implemented within a sophisticated dynamic fluid power simulation package and makes use of standard car and hydraulic models. Models of the passive and active Hydragas components are developed and validated against experimental test results.

Experimental testing has been carried out on the prototype vehicle in both passive and active modes. The results of this testing are compared with those obtained from the computer simulation model and there is found to be a good correlation between these results, providing confidence in the model. The active roll control system is shown to offer significant advantages over the passive vehicle in terms of roll attitude during both steady state and transient manoeuvres.

Suggestions are made for improvements to the roll control system from the perspectives of both performance and production. A thorough investigation is made into possible alternative control methods. Control system parameters and a number of controller command signals are investigated over a wide range of operating conditions. A limited study is carried out into the use of artificial neural networks to determine vehicle lateral acceleration from speed and steering wheel angle data. A number of advantages are highlighted but further work is required to improve the system performance.

The prototype roll control active suspension is shown to provide improved handling performance and body roll attitude. The limited bandwidth requirements of the actuation system together with the simplicity of the control hydraulics result in a low cost, low power device with considerable promise.

# ACKNOWLEDGEMENTS

There is not room here to thank everybody who helped me during the course of this work, but if there are any grievances I will add names for a small fee.

Firstly, my thanks go to my supervisor, Jos Darling, whose advice and guidance has been superb and to Alex Moulton who not only supported the project financially but also gave valuable technical support. The work was also funded by the S.E.R.C. under grant no. 91301940. Thanks must also go to those at the Rover car company, particularly Julian Buckingham, for the use of their test track and their interest in the project.

The work was made considerably easier by the virtually free consultancy offered by the dynamic(s) duo of Togs and Lionel and considerably less labourious by the skilled hands of Dave the Lathe. Unfortunately, the many and particularly varied denizens of 4E 3.33 have in no way helped me work towards this thesis but have made my three-and-a-bit years here very enjoyable. They are, in chronological order, Lee, Donkey, Volker, Jennie and Dave.

Finally, thanks to Jane for being kind and supportive when I needed it most and being generous when student poverty reared its ugly head.

## CONTENTS

# Nomenclature

Terminology adopted in this work relating to the vehicle follows the standards outlined in SAE J670e [ 1 ]. Nomenclature specified here covers only those equations used in the text of the thesis, including appendices. Appendix 3 gives a full listing of the parametric data used to define the computer vehicle model. The nomenclature is set out in logical sections.

## A) GENERAL

| | | |
|---|---|---|
| f | frequency | [Hz] |
| k | road roughness factor | |
| s | Laplace's operator | [rad/s] |
| t | time | [s] |
| K | control system gain | |
| S(f) | power spectral density | |
| $\omega$ | frequency | [rad/s] |

## B) THE VEHICLE

**1) subscripts**

| | |
|---|---|
| a,b | front and rear axle respectively |
| d | Hydragas suspension unit fluid displacer |
| eff | effective |
| gas | Hydragas suspension unit gas 'egg' |
| hp | hydraulic pump |
| s | sprung mass |
| sh | Hydragas active shuttle |

**2) vehicle dimensions and properties**

| | | |
|---|---|---|
| a | front axle to vehicle cg distance | [m] |
| b | vehicle cg to rear axle distance | [m] |
| h | roll centre height above ground | [m] |
| $m_s$ | sprung mass | [kg] |
| $z_{rc}$ | body cg to roll axis height | [m] |
| $I_w$ | vehicle yaw moment of inertia | [kgm$^2$] |
| PRMR | pitch rate moment ratio | |
| T | vehicle track | [m] |

**3) suspension characteristics**

| | | |
|---|---|---|
| B | fluid bulk modulus | |
| $p_d$ | suspension unit fluid displacer pressure | [bar] |
| $p_{gas}$ | suspension unit gas egg pressure | [bar] |
| $K_{da}$ | suspension drop angle rate | [N/m] |
| $K_h$ | suspension hydraulic rate | [N/m] |
| $K_p$ | suspension parasitic rate | [N/m] |
| $K_t$ | suspension taper rate | [N/m] |
| $Q_{Td}$ | total flow into fluid displacer | [m$^3$/s] |
| $Q_{gas}$ | flow into gas egg | [m$^3$/s] |

| | | |
|---|---|---|
| $V_d$ | suspension unit fluid displacer volume | [$m^3$] |
| $V_{gas}$ | gas volume in suspension unit gas egg | [$m^3$] |
| $\gamma$ | gas polytropic index | |

**4) dynamic quantities**

| | | |
|---|---|---|
| $a_1, a_2, a_3$ | measured accelerations at front, top and rear of car respectively | [$m/s^2$] |
| $a_y$ | body cg lateral acceleration | [$m/s^2$] |
| $a_\phi$ | body roll acceleration | [$rad/s^2$] |
| $a_\psi$ | body yaw acceleration | [$rad/s^2$] |
| x | body cg displacement parallel with vehicle longitudinal axis | [m] |
| y | body cg displacement parallel with vehicle lateral axis | [m] |
| z | body cg displacement parallel with vehicle vertical axis | [m] |
| $\phi$ | body roll angle | [rad] |
| $\phi_{susp}$ | suspension roll angle | [rad] |
| $\phi_{tyre}$ | tyre roll angle | [rad] |
| $\theta$ | body pitch angle | [rad] |
| $\psi$ | heading | [rad] |
| $\beta$ | vehicle slip angle | [rad] |
| $F_{Ly}$ | lateral linkage force | [N] |
| L | tyre lateral force | [N] |
| $L_T$ | lateral load transfer | [N] |
| $M_L$ | suspension linkage roll moment | [Nm] |
| $M_{La}$ | front suspension linkage roll moment | [Nm] |
| $M_{Lb}$ | rear suspension linkage roll moment | [Nm] |
| R | radius of turn in steerpad manoeuvre | [m] |
| U | vehicle forward speed | [m/s] |

**5) active roll control system**

| | | |
|---|---|---|
| $p_{max}$ | maximum system pressure | [bar] |
| $p_{hp}$ | hydraulic supply pressure | [bar] |
| $\Delta p_{sh}$ | shuttle differential pressure | [bar] |
| $x_{sh}$ | shuttle displacement | [m] |
| $v_{sh}$ | shuttle velocity | [m/s] |
| $A_{effsh}$ | shuttle displacer effective area | [$m^2$] |
| $D_{sh}$ | shuttle oil bore | [m] |
| $F_{max}$ | maximum net force on shuttle | [N] |
| $P_{max}$ | maximum hydraulic power output | [W] |
| $P_{mean}$ | mean hydraulic power output | [W] |
| $Q_{hp}$ | supply flow | [$m^3/s$] |
| $Q_{sh}$ | shuttle oil flow | [$m^3/s$] |
| $V_{sw}$ | oil swept volume in lane change | [$m^3$] |
| $\eta$ | actuation system overall efficiency | |

## C) NEURAL NETWORKS

| | |
|---|---|
| a | output from neuron |
| i | current neuron |
| j | next neuron |
| $\omega_{ij}$ | weighting of a neural network synapse |
| $\varphi$ | bias of a neuron |

## D) SHUTTLE END CAPS

| | | |
|---|---|---|
| $h$ | plate thickness | [m] |
| $q$ | load distribution (pressure) | [N/m$^2$] |
| $r$ | radius of plate | [m] |
| $w$ | plate deflection | [m] |
| $D$ | flexural rigidity | |
| $E$ | modulus of elasticity | |
| $M_r$ | radial bending moment | [Nm] |
| $M_t$ | tangential bending moment | [Nm] |
| $Q$ | shear load | [N] |
| $\nu$ | Poisson's ratio | |
| $\sigma_r$ | radial stress | [N/m$^2$] |
| $\sigma_{yield}$ | material yield stress | [N/m$^2$] |

## E) THEORETICAL MODEL OF HYDRAGAS UNIT

| | | |
|---|---|---|
| $A_{eff}$ | piston effective area | [m$^2$] |
| $L$ | length of radial section through displacer diaphragm | [m] |
| $r$ | radius of curved part of above section | [m] |
| $\Delta$ | included angle of curved part of above section | [ °] |
| $R_{eff}$ | piston effective radius | [m] |
| $R_0$ | minimum radius of piston | [m] |
| $U$ | maximum radius of unit (excluding turnover seals) | [m] |
| $X$ | displacement of piston | [m] |
| $\alpha$ | total taper angle of unit | [ °] |
| $\beta$ | piston taper angle | [ °] |
| $\kappa$ | skirt taper angle | [ °] |

# 1. Introduction

## 1.1 Introduction

Perhaps the greatest advance in vehicle suspension design since the introduction of the pneumatic tyre has come in recent years with the advent of controlled active suspensions. The design of such systems involves the combination of technologies from fields such as vehicle dynamics, control and fluid power engineering. The performance benefits of such systems must be weighed against the added complexity, weight and cost incurred if a practically realisable result is to be achieved.

This report outlines work carried out by the author at the University of Bath involving the design, development, testing and simulation of a novel low cost roll control system based on the established Hydragas® technology. A full 10 degree of freedom ( DOF ) non-linear simulation model is then used to investigate the performance of the roll control system and modifications to the prototype system are suggested.

## 1.2 The Suspension Compromise

### 1.2.1 Definition of Vehicle Suspension

A vehicle suspension is the arrangement supporting the body on its axles. This may be extended to include the tyres by defining a suspension as the means by which a vehicle's body motion is isolated from road surface excitation. Further, for passenger cars it should be characterised as keeping the vehicle tyres in contact with the road surface to enable the transmission of driving and cornering forces. This last point is important in emphasising the suspension's handling function.

### 1.2.2 A Background to Suspension Design

The design of vehicle suspension systems has traditionally been complicated by the need to compromise between a number of differing and often conflicting aspects of performance. These include :

- passenger perceived comfort
- tyre/ground contact force variations
- vehicle attitude control
- suspension working space

The importance of each of these factors will vary according to the requirement specification of the vehicle. In the majority of cases, a passively suspended vehicle with soft suspension elements will provide good sprung mass isolation from external (road ) disturbances whereas stiffer elements are used to maintain vehicle body attitude during manoeuvres. The purpose of a vehicle suspension is to provide the correct balance between these conflicting requirements.

### 1.2.3 A Brief History of Passenger Car Suspension Systems

Vehicle manufacturers have developed a number of solutions to partially overcome the suspension problem. Early cars extensively used solid axles mounted at each end on leaf springs. These were heavy and required a large amount of space. They are still used on heavy vehicles but are no longer considered appropriate for passenger cars.

The majority of small modern cars and a considerable number of larger cars make use of the transversely mounted engine incorporating front wheel drive, the main benefit being the significant saving in space. Disadvantages arise however due to high proportion of load taken on the front wheels and the dual role of the front wheels in steering and driving.

The high load on the front wheels and associated need for stiff suspension elements often results in a large lateral load transfer at the front axle during manoeuvres which in turn degrades the cornering

ability of the front tyres. This may cause an undesirable amount of understeer [ 2 ]. The combination of cornering and driving requirements of the tyre will decrease the efficiency of both resulting in loss of traction power and unstable steering torque during cornering [ 3 ]. These difficulties can be overcome to a certain extent by improving tyre performance, for example with low profile tyres, by the use of a limited slip differential and by adopting sophisticated independent suspension systems.

Due to lack of space caused by transverse-mounted engines, the majority of front wheel drive cars use suspensions of the Macpherson strut type. These are light, compact and low in price. However the small changes in camber and toe angles with vertical deflection give very little freedom in optimising these angles for given operating conditions. Ideally, tyre camber angles should be close to zero and the toe angles of each side the same (except in tight turns at very low speed ) for any body attitude.

The double wishbone arrangement is more costly and weighs more than a Macpherson strut but allows camber angle change with deflection to be optimised and reduces kingpin offset and hence the change of toe angle between the left and right wheels. The more complex multi-link suspension, available on many luxury modern cars [ 4 ] has the additional feature that the steering axis is not restricted by the position of the upper suspension link. It is also used to full effect on the MacLaren F1 road car [ 5 ].

The geometry of these systems can be altered to achieve specific goals but the overall performance is generally limited by the passive suspension elements used to transfer and dissipate force. For the majority of passenger vehicles, these elements consist of a helical spring and hydraulic damper or shock absorber. Excess suspension travel is generally prevented by stiff rubber bump and rebound stops.

Some vehicle manufacturers make use of the compressibility of gas to provide the spring element of the suspension. Air springs can be used in conjunction with conventional hydraulic dampers or in line with damper valves. These can offer an in-built rising rate, beneficial from the perspective of ride comfort and capable of maintaining near constant body resonant frequencies independent of load. (Since the rate rises similarly to the load, the body natural frequency, $\sqrt{K / M}$ , remains nearly constant). They also open up the possibility of fluid interconnection. Hydro-pneumatic suspension systems have been used most notably by Citroen and Rover ( formerly British Leyland ) with their Hydragas system.

### 1.2.4 Small Car Ride

In the 1950s, the small car concept was developed by Sir Alec Issigonis. The transverse-engined front wheel drive car offered maximum passenger space for a minimum volume of car. The wheels of most small cars are positioned at the four corners for optimum road holding and handling. This however leads to a high pitch stiffness due to the car's low pitch moment of inertia and relatively long wheelbase. It has long been recognised that this can lead to passenger discomfort. Mechanical or fluid interconnection can significantly reduce the pitch rate of a car and therefore make it more comfortable [ 6, 7 ].

## 1.3 Hydragas® Suspension

### 1.3.1 The Development of Hydragas®

The hydragas suspension system, designed by Moulton Developments Ltd, was a natural progression from the earlier Hydrolastic system used on many BMC cars such as the Mini. The Hydrolastic unit utilised conical rubber cone springs as the main spring elements. These were actuated by pistons attached to the upper suspension arms.

The Hydragas unit was developed due to the need to improve performance, cost, weight and uniformity. The rubber cone spring previously used on Hydrolastic units was replaced by a sealed chamber filled with nitrogen gas. A valve damper pack consisting of metal leaf springs and bleed holes was substituted for the earlier rubber damper valve.

### 1.3.2 Construction of the Hydragas Unit

The current Hydragas unit shown in figure 1.1, as used on the Rover Metro, is mounted above the upper suspension arm and is operated through a ball joint at a lever ratio of typically 4.5:1. The tapered piston supports the inner bead ring of the strengthened rubber diaphragm. The outer bead ring

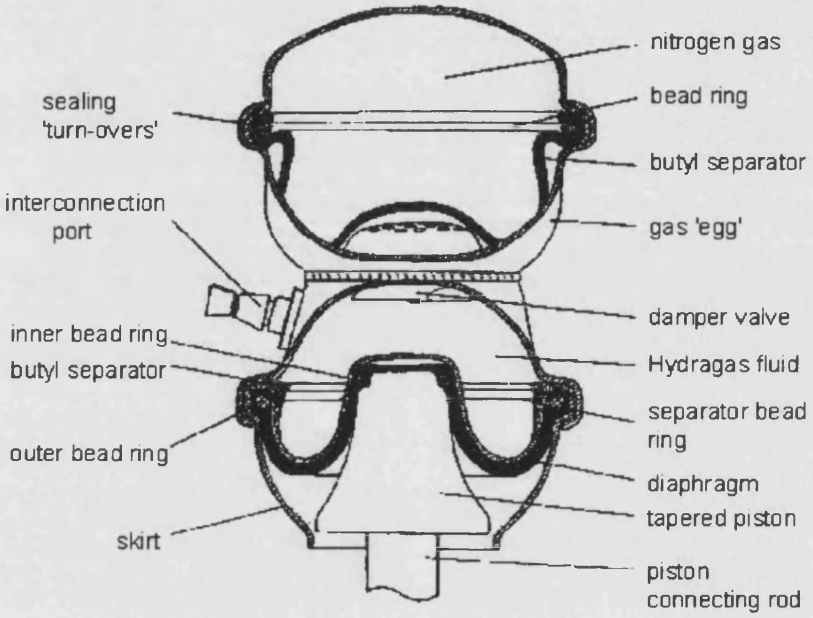


**Fig 1.1** *Construction of the Hydragas® Unit*

holds the diaphragm into the 'turn-over' of the pressed steel skirt. The diaphragm forms the fluid seal at the base of the unit. It is separated from the corrosive Hydragas fluid by a butyl liner held in place by a separate bead ring. Movement of the tapered piston and rolling diaphragm displaces fluid into and out of the lower chamber.

The body of the lower chamber comprises two pressed steel casings, the skirt and the upper section which houses the interconnection port. At the top of the displacer is the damper pack. The damper valve itself consists of a combination of bleed holes and metal leaf valves. This provides a different damper characteristic in the bump and rebound directions.

The upper chamber of the unit contains the gas 'egg'. A butyl separator contains the nitrogen gas, sealed to the casing by another bead ring. This flexes as fluid is forced into and out of the chamber, compressing and decompressing the gas.

The front and rear fluid displacers of the suspension units on each side are connected by an 11 mm bore synthetic fibre reinforced PA11 Polyamide pipe. These incorporate orifices which act as pitch dampers. The connections at each end are sealed with 'O' rings to prevent leakage of Hydragas fluid. Each pipe is approximately 3m long.

### 1.3.3 Operating Principles of the Interconnected Hydragas System

Operation of the interconnected Hydragas system is explained fully by Moulton and Best [ 8 ]. The system uses a water-based fluid as the working medium. The weight of the car is carried by the fluid at a pressure of about 29 bar. No pumps or glands are required as the entire system is hermetically sealed. The system is pressurised initially by means of Schraeder valves located near the front suspension units using a specially developed hand pump.

The system spring rate is obtained from a number of sources. In bounce, fluid is displaced to and from the lower chambers of the suspension units into the upper gas chambers. Compression of the encapsulated nitrogen gas causes the pressure in the unit to rise. The changing area of the rolling diaphragm as it is displaced also gives rise to a change in force. The system bounce rate is comprised of these two elements in conjunction with a drop angle rate due to the changing lever ratio of the suspension arm with displacement, and a parasitic rate due to the compliant bushes of the suspension system.

The fluid interconnection pipe which is located below and in parallel with the unit damper valves serves to reduce the system pitch rate as well as provide a means of balancing the load taken by the four wheels. In pitch, when the front wheels are moved upwards, fluid is displaced from the front to the rear at ( almost ) constant pressure. Little fluid is displaced into the upper chambers of the suspension units. The pitch rate is therefore comprised of the piston taper rate, the drop angle rate and the parasitic rate. There is no further compression of the nitrogen gas. Damping in the pitch mode is provided by the 3.3 mm diameter orifices located in the interconnection pipes. The Hydragas unit spring rate is the same in bounce and roll.

The bounce and pitch operating modes of the interconnected Hydragas suspension system are shown in figure 1.2.

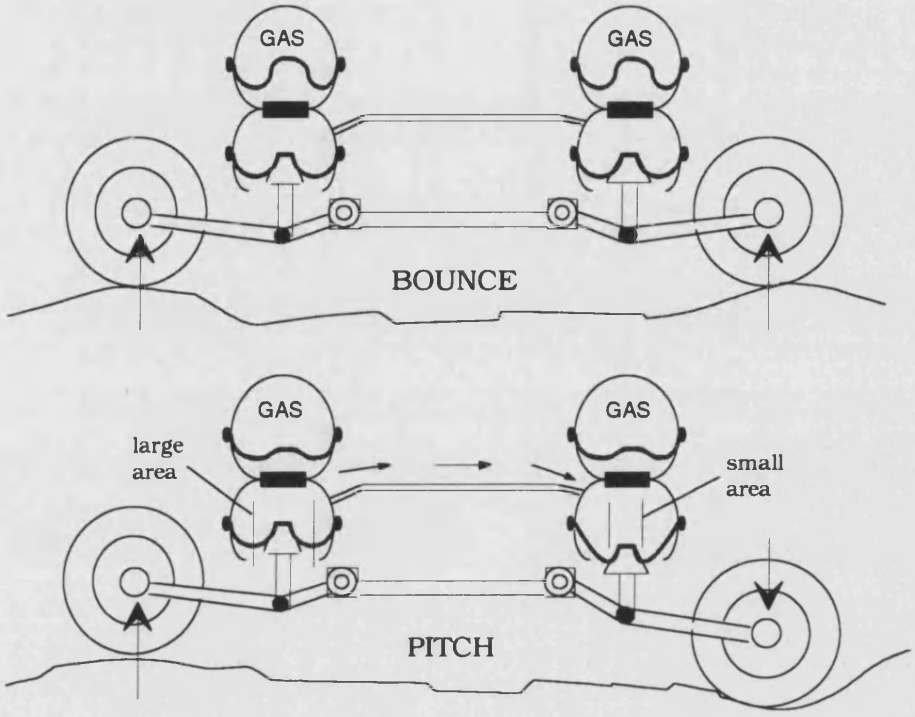


**Fig 1.2** *Operation of the Interconnected Hydragas System in Bounce and pitch*

### 1.3.4 Distribution of Wheel Rates

Numerical values for the Rover Metro lever ratios, bounce and pitch rates are quoted by Oldaker and Waide in [ 9 ]. The breakdown of these rates is shown in figure 1.3. The pitch rate is significantly lower than the identical bounce and roll rates. The pitch rate moment ratio (PRMR ) is 0.52 giving a reasonable pitch mode ride as explained in [ 9 ].

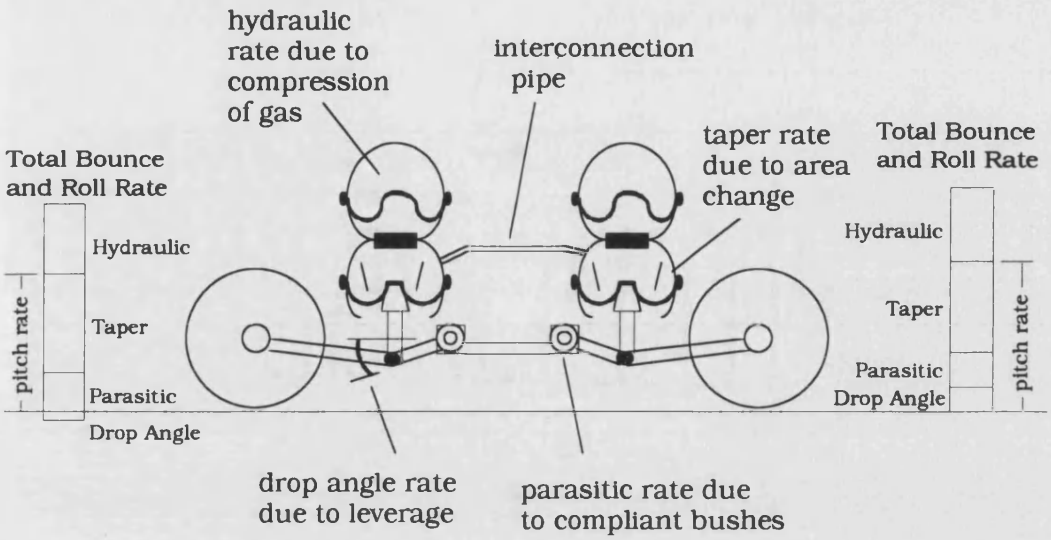


**Fig 1.3** *The Make-up of Rates in The Interconnected Hydragas Suspension System*

Roll stiffnesses are sufficient and the ratio between front and rear roll stiffness suitable for anti-roll bars not to be used. Due to the reduced pitch stiffness Anti-dive and anti-squat geometry of the suspension linkages is used to prevent excessive changes in vehicle pitch attitude during braking and acceleration. Pitch damping orifices are necessary in the interconnection lines of each side of the car to prevent undesirable oscillations following road disturbance inputs.

The ratios between the components making up the bounce rate of the car were chosen to give the correct amount of stiffening with load. Alone, the compression of gas provides too much increase of rate, whereas the drop angle and parasitic rates are almost independent of load or suspension deflection. The taper rate may be chosen to provide the correct amount of stiffening with load. Therefore, the hydraulic rate due to gas compression is balanced against the drop angle and parasitic rates.

The Hydragas® suspension has been used widely over a period of 21 years and has been fitted to over 10 million vehicles. Recognised as a good compromise solution to ride and handling requirements, the only major disadvantages are the limited unit displacement, which requires large lever ratios for acceptable wheel travel, large suspension unit forces and the sensitivity to temperature changes which may alter ride height.

## 1.4 Chassis Control

A number of methods can be used to improve the handling performance of a vehicle without significantly reducing the passenger ride quality. These include adaptations to the vehicle suspension, steering and braking systems and the drive train.

Perhaps the simplest method of increasing the vehicle roll rate of a car with a low bounce rate is the addition of torsional anti-roll bars. These act to reduce the car body roll angle during manoeuvres by resisting the motion of a wheel one side of the car relative to the wheel on the opposite side. Bounce motion is not effected. These tend to be used at the front of the car where the bounce stiffness is generally lower for reasons of ride in the pitch mode ( Olley, [ 10 ] ). In some cases, front and rear roll bars are used. The main disadvantage of anti-roll bars is the increased harshness of ride in the roll-rock mode.

Another method of improving chassis stability is four wheel steering ( 4WS ). At low forward speed, vehicle manoeuvring generally requires a high degree of yaw motion, for example in negotiating a roundabout. At higher forward speeds, however, lateral motion is of the greater significance, for example in lane changes on a motorway. The control law for a 4WS system turns the front and rear wheels in anti-phase at low speed, giving a tighter turning radius, but turns them in phase at higher speeds resulting in greater stability. The control law governing the phase difference between front and rear wheels is dependant on vehicle forward speed and steer angle.

Traction control and anti-lock braking systems ( ABS ) can be used to control the ground/tyre forces in acceleration and braking. They can also be used to control longitudinal tyre forces during lateral manoeuvres, thereby giving greater control over the tyre lateral forces and handling [ 11 ].

Passive suspension systems have been developed to a high level of sophistication. There is a limit to the compromise these systems can reach between the conflicting aspects of suspension performance mentioned previously. In recent years, a great deal of research has gone into the use of 'intelligent' active suspensions.

Many modern cars feature a number of these advanced systems. The action of these systems are to some extent coupled and the improvement of one system may well be to the detriment of another. Yokoya et al [ 12 ] cite the example of the close coupling between body roll and yaw response which

are key features of both active suspension and four wheel steering systems. Care should therefore be taken in the design of control systems where this coupling of functions is apparent. This has been evident in a number of prototype vehicles incorporating integral control of a number of advanced systems. Cars from Nissan [ 13 ] and Toyota [ 12 ] have integrated control systems in which the performance of the various 'intelligent' systems are optimised as a whole rather than individually.

## 1.5 Active Suspensions

### 1.5.1 What is an Active Suspension ?

An active suspension is capable not only of reacting to externally applied forces but of modulating these forces according to measured parameters. This implies that some external source must be used to provide the extra power requirements of the system. By modulating the suspension forces, the active suspension seeks to optimise the vehicle ride and handling functions for a given set of operating conditions. Ideally, the ride and handling functions of the suspension would be completely dissociated allowing body attitude to be controlled independently of sprung mass isolation.

The salient features to be considered in the design of an active suspension are discussed by Sharp and Crolla [ 14 ] and relate to ride and handling performance, safety particularly in failure modes, power consumption, capital cost, reliability, durability and ease of maintenance.

The performance of active suspensions has been investigated at great length and they have been shown to offer benefits of varying degree over conventional passive suspension systems. Sharp and Hassan [ 15 ] point to the ride advantages of active suspensions being apparent only where suspension working space is restricted. The major advantage of active systems is the ability to adapt to varying operating conditions.

Sharp and Crolla [ 14 ] emphasise the harshness of fully active systems at high frequency and the need to incorporate isolators in series, thus compromising the performance. They point out the economic advantages of slow active systems both in terms of capital cost and power consumption. Despite the good performance of semi-active and slow active systems, caution is recommended with

relation to extreme events such as potholes. They conclude that narrow bandwidth systems offer nearly all of the advantages of broad bandwidth systems and less disadvantages.

Sharp [ 16 ] states that significant improvements in performance are possible by the de-coupling of ride and handling functions. Slow active suspensions are highlighted as the most likely to provide a commercially available system. The performance of switchable damper systems is stated as not subjectively better than passive systems.

Disputing the above arguments, Wright and Williams [ 17 ] for Lotus point out that the above conclusions arise from an oversimplification of the suspension problem. The models used are of a single wheel station and therefore neglect many aspects of active suspension control. It is suggested that the control of vehicle attitude in a fully active system represents a saving in power ( as the actuators need not respond to inertial forces ). In contrast, in slow active systems attitude control represents a significant consumption of energy. Other advantages are cited, such as the safe failure modes ( which are due to the parallel passive springs rather than the hydraulic elements ) and the easy assimilation into integrated control systems.

A sober assessment of the current state of active suspension technology is given by Hillebrecht et. al. [ 18 ]. Comparisons between fully active, slow active and passive cars are given both objectively and subjectively. The slow active system was not rated highly by drivers although the results presented show a poor performance when compared with other, similar systems mentioned in this work. The benefits gained in ride and handling were small compared to the increased cost and power consumption incurred. The fully active system fared well both in objective tests and in the opinion of the test drivers but was discounted on the grounds of cost and complexity.

None of the above appraisals mention pure roll control systems, in which one of the most significant advantages of active systems is achieved at a substantially reduced cost using simple hardware and instrumentation together with low power consumption.

Research into active suspension design has progressed along different channels in academia and industry. Academics have largely involved themselves in the research of advanced control techniques using quarter car models to optimise the performance of a suspension at a single wheel station. In industry, however, more emphasis is naturally placed on finding practical systems which play off the ride or handling benefits of a suspension against additional cost.

Active suspension systems fall into a number of categories, each with different advantages and disadvantages based on performance, cost and complexity.

### 1.5.2 Categorisation of Active Suspension Systems

There are many approaches to active suspension design. Motor manufacturers tend to adopt either of two strategies. These are :

1. Full or limited state fully active suspensions offering the potential of high performance at a high cost, with considerable complexity and high power requirements

2. Semi-active or slow active suspensions offering some of the performance benefits of fully active systems at a lower cost and hardware intensity

A number of motor manufacturers have produced fully active suspension systems for prototype vehicles including Nissan [ 19 ], BMW [ 18 ] and Lotus [ 20 ], the former being technically a slow active system despite its name; however none have gone into production and such systems are generally limited to such fields as motor racing where cost is of less significance.

The main impetus of research is towards cheaper semi-active and slow active systems. Production cars are currently available with semi-active systems, which consume very little power, such as BMW and Lancia with a system from Boge, [ 21 ]; Ford, Renault and Jaguar using the Armstrong semi-active system [ 22 ] and Toyota with their own piezo TEMS [ 23 ]. Developments are continuously being made and recently the Citroen Xantia Activa has become the first production active roll controlled passenger car [ 24 ].

A brief outline of the main classifications of vehicle suspensions follows :

## PASSIVE

These systems comprise springs, dampers and in some instances, anti-roll bars. Control over sprung and unsprung mass dynamics is achieved by selection of suitable spring rates and damper characteristics. Neither spring nor damper rates can be changed by external signals, although the rates need not be linear. A rising spring rate is generally beneficial to the compromise between ride and attitude control of the vehicle and tends to keep body natural frequencies more nearly constant, independent of load. Dampers are normally asymmetric, offering greater resistance in rebound than in bump. The suspension stores and dissipates energy in response to road excitation, i.e. there is no net energy input to the system.

Passive systems can be modified and improved upon by the addition of compliant bushes which reduce ride harshness and allow for lateral compliance which can be used to improve handling. In addition, the careful choice of suspension geometry will control vehicle attitude and influence handling [ 25 ].

## SELF LEVELLING

Self levelling suspensions are essentially passive systems with some provision to maintain a steady ride height independent of static loading. Typically, a pump will be required for this operation but self energising systems have been produced [ 26 ] in which energy input from road undulations is used to displace the working fluid. Self levelling is seen most commonly on Citroen cars with oleo-pneumatic suspension, first seen on the 1955 DS model [ 6 ] and has been offered on a number of luxury and U.S. cars [ 26 ]. They allow the full suspension travel to be used under any loading conditions. The response time of such a system is typically a number of seconds. This avoids unnecessary operation over rough ground which would otherwise consume power.

Prototype dynamic self levelling systems are under development [ 27 ]. These continuously monitor the vehicle ride height and adjust it accordingly. Response time is necessarily faster than for steady state self levelling systems and so accordingly, power requirements are increased.

## SEMI-ACTIVE (DISSIPATIVE)

In these systems, the rate of energy dissipation in the dampers is varied according to some control law. This is based on the desired response to the road conditions and the vehicle speed. A common approach is to control the force applied by a variable damper in the same way as that produced by a fully active system, except that when the fully active system supplies energy, the equivalent semi-active system merely switches off, exerting no force.

Theoretically, the performance of semi-active suspensions is almost as good as that of fully active suspension systems [ 15 ]. The power requirement for a variable damper system is low and hence this type of system is currently popular. However a semi-active damper arrangement is still only capable of dissipating energy in response to road inputs and so can be considered an optimal passive suspension. A typical quarter car layout of a semi-active suspension is shown in figure 1.4.

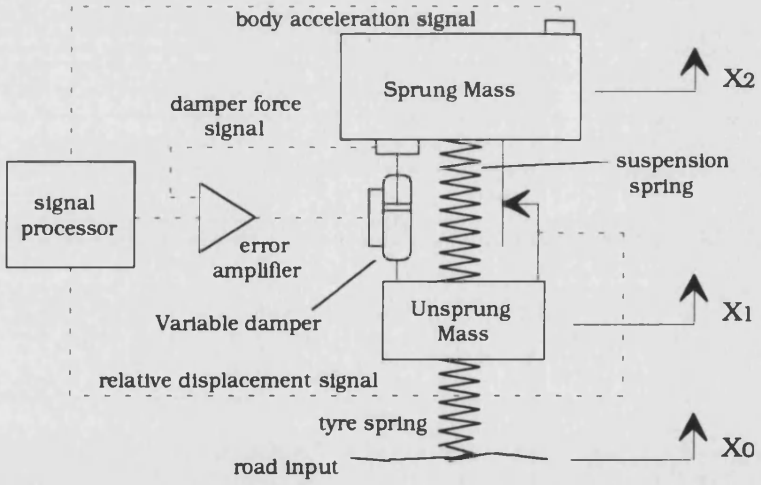


**Fig 1.4** *Typical Layout of a Semi-Active Suspension System*

A number of production cars are available [ 21, 22, 23 ] with switchable damper systems. These allow the car to exchange between two or more discrete damper settings, typically soft ( for reduction of harshness at high frequency ) and hard (for reduction of sprung mass oscillation at low frequency). Research is in progress into continuously variable dampers [ 28, 29 ] but such systems are not currently available on production cars.

Although ride may be improved with semi-active systems, only limited control of handling or roll during manoeuvres is possible.

## SLOW ACTIVE (REACTIVE)

These are low bandwidth active suspensions. The active element ( actuator ) has a limited bandwidth ( typically around 3 Hz ) beyond which it is effectively rigid. The slow active system will therefore have a lower performance but conversely a lower power requirement than a fully active system (q.v.). The actuator is mounted in series with a passive spring which provides sprung mass isolation above the bandwidth of the active element. A typical arrangement is shown for a quarter car in figure 1.5.

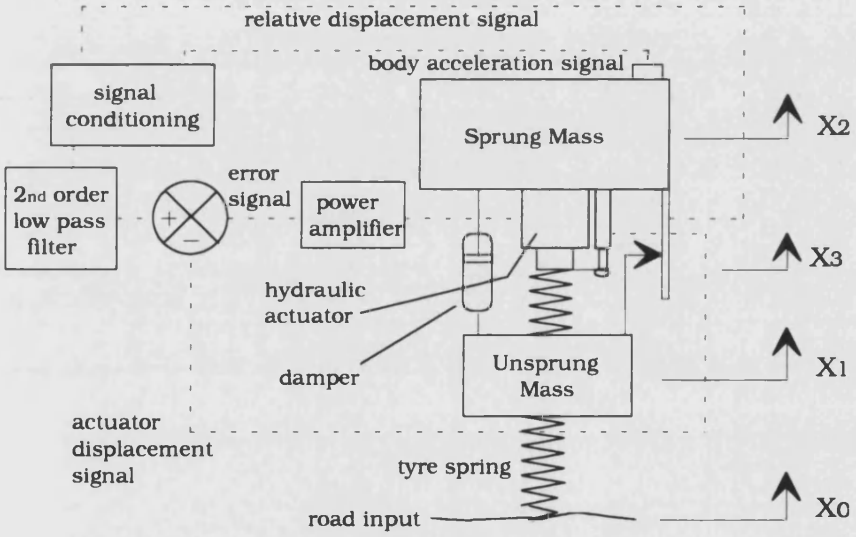


**Fig 1.5** *Quarter Car Representation of a Slow Active Suspension*

The control bandwidth is a compromise solution based on cost and ride improvement and is chosen to provide sufficient control over the sprung mass main ride frequencies and vehicle attitude during manoeuvres, with the possible benefit of improving handling. Wheel load fluctuations and road noise are controlled principally by the passive elements which do this to good effect in passive systems. It has been determined [ 15 ] that the benefits of fully active systems are only apparent below wheel hop frequency and that control of the unsprung mass resonant frequencies is not greatly

improved over passive systems. Unsprung mass natural frequencies will usually be above the slow active system bandwidth.

Since the active element is in series with the passive spring, it must also support the static weight of the vehicle body. The kerb steady state pressure and associated system power requirement will therefore be high. The problem can be largely alleviated by incorporating a further passive support spring in parallel with the actuator.

It has been shown that system performance can be further enhanced by employing a variable damper rate, as in the semi-active system [ 30 ]. This presents a problem with 'in-line' fluid dampers such as that used in the Hydragas system, where size, accessibility and integrity of sealing are major considerations.

There are a number of differing approaches to slow active suspension design. The majority of these have made use of fluid based suspension systems with gas spring elements. Systems developed by Pirelli [ 31 ] and Nissan [ 32 ] use an air pump to alter the volume of gas in each air spring, thereby controlling vehicle attitude or body acceleration. This allows a soft spring rate to be used enhancing passenger comfort. The Nissan system allows the spring rate to be varied between soft and hard settings and also includes a switchable damper. The merits of varying the suspension spring rate are discussed by Sharp [ 16 ]. No active control is exerted over body attitude in manoeuvres.

The performance capabilities of pneumatic active suspensions are discussed by Sharp and Hassan in [ 33 ]. Active control with a bandwidth of 3 Hz significantly improves tyre load fluctuations, suspension working space requirement and ride comfort. A possible disadvantage is the large amount of space taken up by the suspension units due to relatively low working pressures, as indicated by Sharp and Hassan. A typical system of this type is shown in figure 1.6.

Other systems, based on hydro-pneumatic suspensions, control chassis movement by varying the volume of hydraulic oil in the suspension units according to a control law, as in the 1989 Toyota Celica prototype [ 34 ]. Automotive Products developed a system in which the hydraulic valve is operated by a tuned mass, spring and damper pendulum [ 35 ] which prevents the system from being excited by road inputs. The dynamic behaviour of this system must be optimised for a specific load condition and becomes sub-optimal away from this condition.

Generally, conventional automotive hydraulics are used to control the suspension displacement. Again, the aim is to minimise dynamic tyre load and body vertical acceleration and to respond to pay

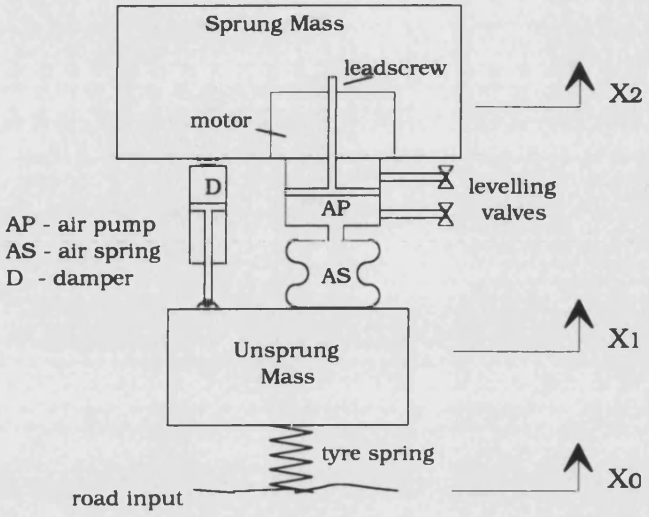


**Fig 1.6** *Example of a Pneumatic Slow Active Suspension*

load and handling induced changes in loading conditions. The size of the suspension units is generally smaller than for the pneumatic arrangements outlined above. The layout of a typical system is shown in figure 1.7.

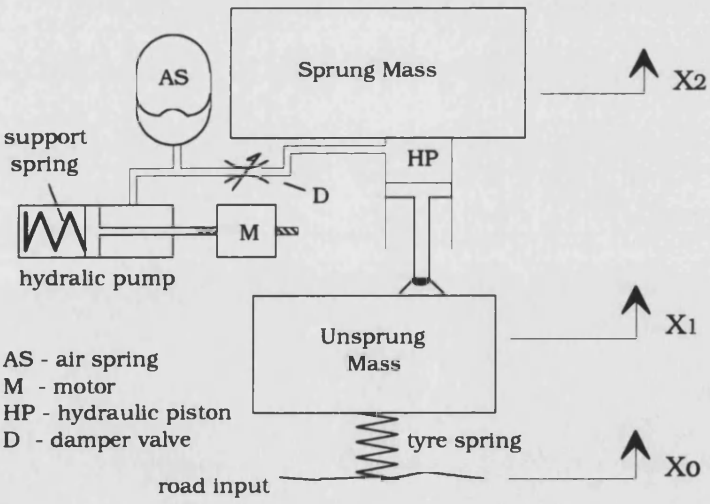


**Fig 1.7** *Example of a Hydro-Pneumatic Slow Active Suspension*

The power consumption of both the aforementioned systems is considerably less than that of a comparable fully active system.

## FULLY ACTIVE

In fully active suspension systems, the passive springs and dampers are replaced by hydraulic actuators at each wheel station. Control laws effectively substitute for spring rates and damper characteristics as system parameters. An active suspension will not react to an applied load or road disturbance unless it is specifically commanded to do so.

Active suspension was conceived in 1980 by Lotus [ 36, 37 ] as a solution to the problem of maintaining formula 1 racing cars' vehicle attitude during manoeuvres, while ensuring a reasonable level of comfort. At high speed, these cars develop large down forces, effectively increasing the vehicle static weight by up to 300%. Obviously, the optimisation of passive suspension parameters for such a wide range of vertical load was extremely difficult. The concept of active suspension was developed to satisfy the need for a suspension system which would perform well over a large range of operating conditions. The fully active concept has received much media attention [20, 38, 39 ] which has made the term 'active suspension' a familiar phrase.

Many prototype vehicles with fully active suspension have been produced. However despite reductions in the weight and cost of components no fully active system is commercially available on production vehicles. This is due to the large amount of hardware and measurement transducers necessary and the high power consumption associated with a broad bandwidth system. It should be noted however that for a fully active suspension to maintain body attitude during manoeuvres power is saved as the hydraulic actuators do not move. The reverse is true for a slow active suspension.

A possible arrangement for a fully active suspension system is shown in figure 1.8. Note that passive springs are used in parallel with the hydraulic actuators to support the vehicle static load and provide a fail-safe facility in the event of a malfunction in the active system. They do not otherwise effect system performance.

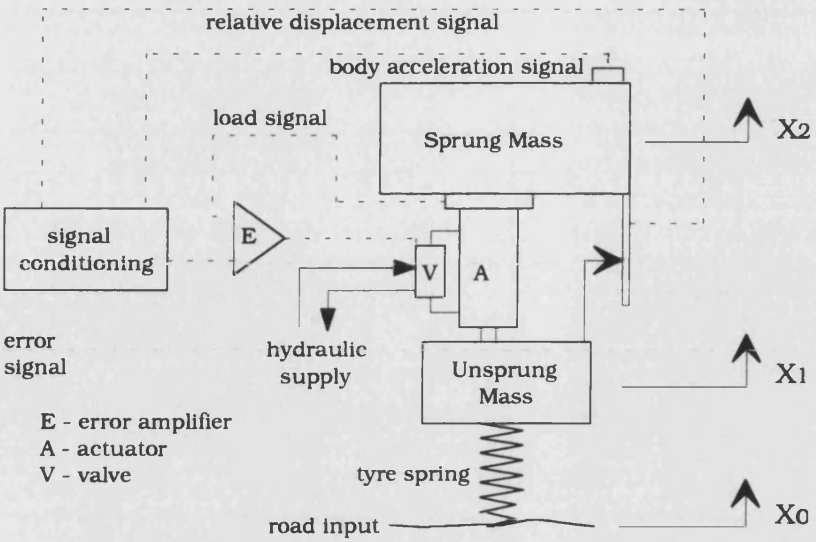


**Fig 1.8** *Quarter Car Representation of a Typical Fully Active Suspension*

All hydraulic control systems have a finite bandwidth, above which their response is sub-optimal. In fully active suspensions, the bandwidth of which are typically > 30 Hz, ride harshness due to high frequency road noise and vibration is a significant problem. At these high frequencies the hydraulic actuators are effectively rigid, transmitting vertical forces directly through to the vehicle body. The problem can, to some extent, be alleviated by mounting the actuators on flexible bushes. Unfortunately, this will inevitably compromise the system performance.

## ADAPTATION OF PARAMETERS

Suspension system parameters such as spring and damper rates and control circuit gains must usually be optimised for a particular set of operating conditions, for example road roughness, vehicle speed and static load. If conditions change ( which they inevitably will ) then those parameters are no longer optimal. A system in which the parameters can be dynamically changed to suit the operating conditions is known as adaptive [ 16 ].

Adaptation is possible with all the controlled suspension arrangements outlined above and a further example is the switching of a gas spring stiffness between hard and soft settings by opening up an extra volume of air at the same pressure [ 6, 31 ]. This does not remove the need to compromise

between ride and handling functions but implies optimisation of this compromise for any set of conditions.

### 1.5.3 Control of Active Suspensions

The previous section outlined the hardware configurations of a number of classes of suspension. Also important is the control methodology used to make these systems behave in the desired way. Once a strategy has been established, there are a number of ways to implement this in a control law. Some of the strategies used to control active suspensions are outlined below:

SELF-LEVELLING

These are the simplest form of active suspension and accordingly require the simplest control system. Wheel to body distance is measured using electronic or, more usually, mechanical means and compared with the desired position. The error is used to control the system and bring it to an acceptable position.

SEMI-ACTIVE

There are a number of possible approaches to designing a control strategy for a switchable damper system. Simple semi-active dampers rely on fast switching using continuously monitored states to provide the demand setting. A simple control scheme for a fast switchable damper is shown in figure 1.9. Fast switching can cause sharp changes in damper force and acoustic noise. A more sophisticated approach is to use an averaged level of the

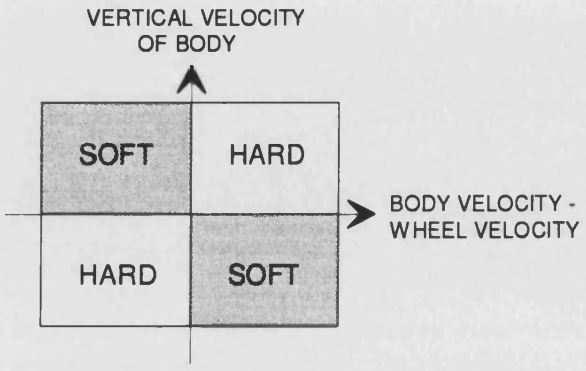


**Fig 1.9** *A Switchable Damper Control Scheme*

operating conditions, e.g. vehicle speed, road roughness and body motion states to determine a suitable level of damping [ 40 ].

One of the main factors in selecting a damper setting is the frequency of oscillation of the body. At low frequency, around the body main ride natural frequencies, a high level of damping is required to reduce sprung mass oscillation. At high frequency, however, a lower level of damping will decrease the transmission of road noise and high frequency vibration. Toyota [ 23 ] use a piezoelectric sensor measuring rate of change of damper force to determine the frequency of oscillation and hence select a damper setting.

Another factor is the manoeuvring condition of the vehicle. In straight line driving, damping can be soft to give the maximum comfort. During cornering, braking and accelerating however, a firmer setting should be chosen for safety and stability.

The amount of instrumentation used in the control of a semi-active suspension depends largely on the strategy employed and the method chosen to apply this strategy.

## SLOW ACTIVE

Again, there is a wide variety of systems available. Slow active systems often aim to control the body ride function within the system bandwidth, or the vehicle handling function by way of attitude control or both. Instrumentation requirements will vary depending on the goals of the system. Control will generally be exercised by the measurement of a number of states, usually including vehicle speed, various accelerations and displacements.

The use of road profile preview for slow active suspensions using both 'look ahead' and front to rear wheel delay has been investigated by Pilbeam and Sharp [ 41 ]. This study concluded that there were significant benefits to be gained in body isolation due to the rear suspension at the sprung mass resonant frequency using wheelbase preview which would be cheap to implement.

## FULLY ACTIVE

A full state feedback fully active suspension requires the extensive measurement of vehicle states, including a height above ground sensor and possibly a road profile preview sensor to predict suspension response. It has been argued [ 42 ] that preview of the road profile can significantly improve the ride performance of both full and limited state feedback fully active systems. Preview to the front wheels requires the use of an expensive proximity transducer whereas preview to the rear wheels is readily available from information gathered at the front wheels. However, Sharp [ 16 ] also points out that to achieve a preview time of 0.2 seconds, necessary to gain significant advantage, even at moderate speeds the sensor must read a profile a large distance ahead of the wheels.

The 'skyhook' damping phenomenon in which damping force is relative to the absolute vertical velocity of the vehicle body rather than the relative sprung to unsprung mass velocity is a common feature of many theoretical active suspension control systems. Difficulties lie in the actual measurement of this quantity and although integration of body vertical acceleration signals appears to be the most popular solution this may be subject to drift problems. Also, since the skyhook damping algorithm does not take into account wheel hop, for practical systems in which wheel motions will be transmitted to the vehicle body via the suspension linkages, additional wheel-to-body damping must be included to control wheel motion.

A further problem is encountered when driving up or down hills. The skyhook damper will generate a force proportional to the absolute vertical velocity of the body. It has been found that modest gradients can cause forces to be developed which would cause suspension deflections to exceed the travel of typical suspension spring elements [ 30 ].

Limited state feedback systems neglect the height above ground sensor to reduce instrumentation requirements and it has been shown that by the use of appropriate control laws they perform nearly as well as full state systems.

One of the main features of active suspensions is the de-coupling of the ride and handling functions, allowing each to be optimised in turn. This is made possible by sensing the motions of the sprung and unsprung masses separately. A computer determines the actuator motions necessary to satisfy both the body and wheels and distributes forces accordingly.

# 2. Active Roll Control

## 2.1 The Principles of Roll Control

### 2.1.1 Definition of Roll Control

It has been recognised that one of the most significant perceived benefits of an active suspension system is the reduction or elimination of body motions induced by manoeuvres [ 17 ].

Roll control involves the reduction or elimination of vehicle body roll during lateral manoeuvres. Body roll consists of three components: ground roll angle due to inclination of the road surface; suspension roll due to deflection of the suspension elements and tyre roll due to deformation of the tyres as shown in figure 2.1. Body roll relative to the ground therefore comprises suspension and tyre roll components.

$$\phi_{body} = \phi_{susp} + \phi_{tyre} \qquad (2.1)$$

Roll control suspension systems have a moderate bandwidth ( < 10 Hz ) and seek primarily to control body roll attitude. They are not intended to influence other vehicle modes such as bounce, pitch and wheel hop. These are controlled by the passive suspension elements such as springs and dampers, which also, naturally have an effect on the roll characteristics of the vehicle. Any further effects of the roll control system are secondary but may be significant as discussed later.

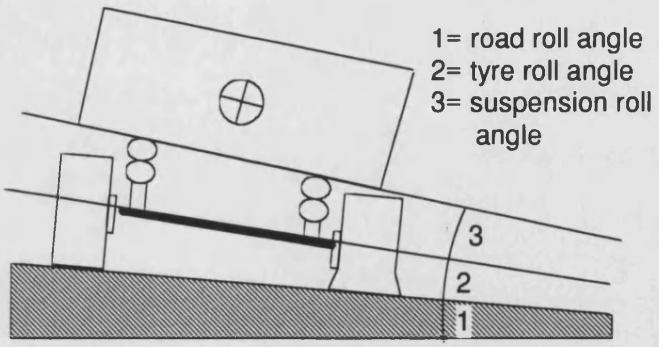


**Fig 2.1** *Components of Vehicle Total Body Roll Angle*

Passive vehicle roll attitude is strongly dependant on the magnitude of lateral acceleration. The roll angle of passenger vehicles is often compared on the basis of degrees per $5m/sec^2$ of lateral acceleration in a steady state or quasi-steady manoeuvre. Typical values for a passenger car can vary from 0.8 degrees for a high performance sports car ( Porsche 928 ) to 3.9 degrees for a softly sprung small car ( Ford Fiesta S ).

### 2.1.2 The Force Roll Centre and Body Roll

All forces between a car and the surface upon which it is travelling are transmitted through the tyres, or more specifically through a small area on the surface of the tyre called the contact patch. Lateral and longitudinal forces are developed by the tyres in these contact patches and are transmitted to the body primarily through the suspension linkages.

Due to suspension kinematics there is theoretically a single, imaginary point for the front and rear suspension on each side of the car through which these forces are said to act. Consequently there is no linkage force moment induced about this point. The force exerted on the wheel by the ground acts through the contact patch. The lateral component of the linkage force acting on each corner of the car is that lateral force generated by the tyre. This linkage force has a line of action between the tyre contact patch and the imaginary point (roll centre) found from the suspension geometry.

If the car suspension on either side is assumed to be symmetrical, there is a point on the body centre line which is the intersection of the lines of action of the suspension linkage forces. A lateral force applied to the body at this point will be reacted directly by the suspension links. As there is no unbalanced force in the springs, the vehicle body will not roll upon its suspension. This point is known as the force roll centre [ 43 ]. A typical construction used to find the instantaneous force roll centre for a double wishbone type suspension layout is shown in figure 2.2.

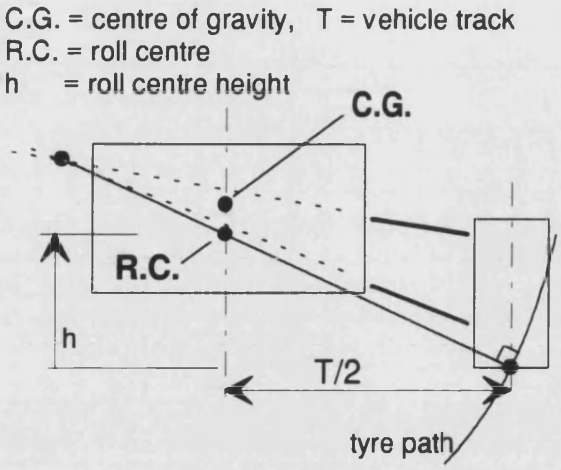


**Fig 2.2** *Construction for Roll Centre Location*

The analysis above is based on a number of assumptions but will be reasonably accurate for low lateral acceleration levels. At higher lateral accelerations, the location of the force roll centre is less simple. The most significant inaccuracies are caused by the assumption that the centre of the tyre contact patch lies at the intersection of the wheel centre plane and the ground and neglecting compliance in the suspension bushes. There will in practice be deformation of both the tyre carcass and the suspension bushes. However, a definition of the roll centre height which applies for all cases is:

$$h = \left(L_T / L\right) T \qquad (2.2)$$

where

| | |
|---|---|
| $h$ | is the roll centre height above ground |
| $L_T$ | is the lateral load transfer |
| $L$ | is the tyre lateral force |
| $T$ | is the vehicle track |

The above equation states simply that the moment on the vehicle body created by the c.g. being offset from the roll centre is reacted by a load transfer between the inside and outside wheels.

When a car manoeuvres, lateral forces act on the vehicle body through the suspension linkages. By the above approximation, the line of action of these forces passes through the roll axis. The roll axis will generally not be at the same height as the centre of gravity. Therefore a moment is developed

about the centre of gravity which results in a net linkage roll moment. This is opposed by a roll moment due to deflection of the primary and secondary suspension elements. Deflection of the suspension results in body roll during cornering manoeuvres. Body roll is defined as the rotation of the vehicle body relative to the ground plane. Suspension roll, conversely, is defined as the rotation of the body relative to a line joining the wheel centres of an axle and therefore does not include roll due to deflection of the tyres.

### 2.1.3 The Significance of Roll Stability

The phenomenon of body roll during lateral manoeuvres has a number of effects on the performance of a vehicle. The first and most obvious is the effect on driver comfort. The driver is very aware of body roll during cornering [ 17 ]. Severe roll angles result in changes in posture which can impair the driver's ability to maintain a steady course. The reaction between driver and the seat is reduced leading to a feeling of insecurity. In the extreme case, excessive body roll can increase the tendency to rollover.

Large roll angles can also have a significant effect on the vehicle's handling ability [ 44 ]. For most cars, large deflections of the suspension result in camber and toe changes of the wheels relative to the road. High camber angles reduce the cornering ability of the tyres while changes in wheel toe may reduce the front wheel steering angles and hence dynamic response to steering wheel inputs. Vehicle response during transient manoeuvres may be dulled as the different motions of the body are coupled. A secondary effect is the extra load transfer caused by lateral displacement of the body centre of gravity in roll.

Some of these effects can be deliberately used to influence the suspension geometry and associated handling characteristics but this may result in other penalties such as tyre scrub. It is clear that a system in which the vehicle roll angle during lateral manoeuvres is reduced would be beneficial from both a comfort and stability perspective, with the additional benefit that suspension geometry may be simplified.

### 2.1.4 Roll Control Methods

Vehicles employing soft suspension elements often suffer from excessive roll and pitch attitudes during manoeuvres such as cornering, accelerating and braking. Pitch attitude can, to some extent, be controlled by the adoption of anti-dive / anti-squat suspension linkage geometry. This leaves the problem of roll attitude control. A common solution is the use of anti-roll bars. These oppose the motion of the wheels of one side of the car relative to the opposite wheels reducing body roll but having a detrimental effect on ride quality in the roll-rock mode.

There is therefore a strong case for the use of active roll control systems which counteract body roll moments caused by lateral acceleration but do not effect ride quality. These are seen as a low cost and low power form of active suspension falling loosely into the slow active category mentioned previously. The main benefits of roll reduction are as follows:

- Improvement of driver and passenger comfort and perception of handling ability [ 17 ].
- Simplification of suspension geometry due to lack of camber and toe changes in manoeuvres [ 45 ].
- Improved tyre forces due to elimination of roll induced camber change [ 46 ].
- Reduction in tyre wear due to changes of track resulting from roll [ 46 ].
- Reduction in suspension working space [ 31 ].

There are a variety of approaches to the active reduction of body roll. A number of systems use rotary actuators mounted on anti-roll bars at the front and rear of the vehicle as shown in figure 2.3. These control the forces generated by the anti-roll bars and aim to cancel out the manoeuvre induced roll moment on the body. Systems have been developed by GKN and Sachs-Boge [ 47 ] and researched by many others [ 45, 48 ].

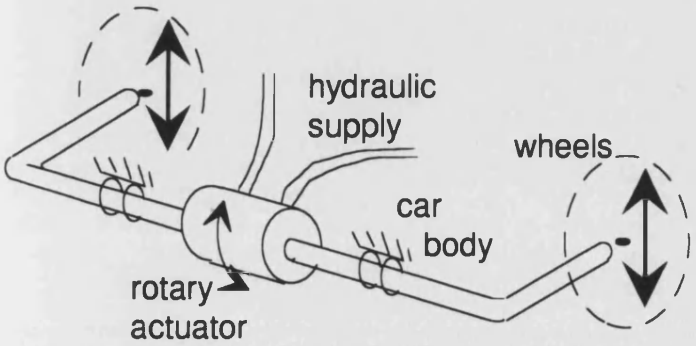


**Fig 2.3** *A Simple Rotary Actuator Active Anti-Roll Bar*

The GKN system utilises one valve to control both rotary actuators. The system, patented by Michael Mumford in 1987 is controlled by a lateral acceleration signal. Sharp and Pan [ 48 ] found that a valve bandwidth of 40 Hz was sufficient to control roll motion. They also investigated the influence on the response of the system of feeding forward a lateral acceleration derivative signal and feeding back an actuator velocity signal. The former was found to offer some benefits but was discarded on the grounds of practical realisation and high noise levels.

Darling, Dorey and Ross-Martin [ 45 ], investigating a similar system found the maximum power requirement to be 1.5 kW, though the average value would be considerably lower. They found through simulation that the dynamic lateral response of the active car was quicker than for a similar passive car.

The Sachs-Boge system differs from the GKN system in that is seeks to control the rotary actuators independently, with two valves. This allows the front-rear distribution of lateral load transfer to be controlled. The engine driven pump has been quoted as consuming 2 kW [ 47 ]. The system is controlled by steering wheel angle and speed signals which are in turn mapped to lateral acceleration. The use of lateral acceleration derivative in the forward path has also been considered. Both GKN and Sachs-Boge systems substantially reduce body roll but do not eliminate it entirely.

A potential problem with the use of rotary actuators in roll control systems is the cost of angular position measurement. An approach which avoids this problem is to mount a linear actuator at one end of each anti-roll bar. Such a system was fitted to the Citroen Activa [ 24 ]. Body roll attitude is controlled in a similar manner to using rotary actuators but using more conventional lower cost technology. During straight ahead driving, the actuators are connected to an additional gas spring which reduces the stiffness of the anti-roll bars, minimising their effect on ride quality.

A similar system has been investigated at the University of Bath [49 ] in which the two ports of the actuators are connected together during straight ahead driving. This research, again using one valve to control the front and rear actuators, examined the possibility of controlling the transient lateral load transfer distribution by introducing orifice dampers into the hydraulic lines to front or rear actuators.

Pirelli have developed a pneumatic system based on lateral acceleration measurement [ 31 ] with roll angle feedback closing the loop. The accelerometer is of low bandwidth (~ 7Hz) which seems low compared with those used in other systems. The steady state results showed show a significant

improvement in roll attitude however no transient results are presented. A response time of 0.6 seconds suggests that these may be poor. An improvement of this response time was said by the authors only to increase the system power consumption.

Nissan have introduced a slow active hydropneumatic suspension system on the Infiniti Q45 [ 19 ]. The system again uses lateral acceleration as the demand signal for roll control but controls four independent actuators. The results presented show the body roll angle to be reduced by only 50% in a steady state test. The authors point out that the tuning of vehicle attitude control must be based on a subjective judgement of comfort and vehicle performance limits.

A similar system was developed by Toyota for the Celica [ 34 ]. The lateral acceleration demand signal is complimented by a steering wheel velocity and forward speed signal with the intention of providing a degree of preview. The authors claim that a reduction in body roll angle reduces the mental stress and anxiety of the driver.

A further solution developed at Delft University of Technology [ 50 ] utilises electric motors to change the lever arm ratios of the suspension elements to reduce roll and pitch. This approach uses little power but is rather bulky.

The fluid nature of the Hydragas suspension lends itself to modification with respect to active suspension. One such system is under development by Anthony Best Dynamics [ 51, 52 ]. This is similar in function to the hydropneumatic systems developed by Nissan and Toyota. The vertical position of each corner of the vehicle is controlled independently by a valve regulating Hydragas fluid flow into and out of the suspension units in response to control signals. The hardware and control requirements for this system are relatively high and therefore would restrict the use of the system to luxury motor vehicles.

This thesis introduces a novel roll control suspension which makes full use of the benefits of existing Hydragas technology.

## 2.2 Hydragas® Roll Control System

### 2.2.1 Outline of the Hydragas Roll Control Method

The Hydragas roll control system utilises the fluid based nature of the suspension to achieve a reduction in body roll during cornering manoeuvres. The working fluid used in the Hydragas system is a water / glycol mix which is used for reasons of cost, low viscosity, good temperature stability and materials compatibility. However, this mixture is not suitable for conventional high pressure hydraulics which require lubrication, high viscosity and low corrosion. This creates potential problems with introducing hydraulic elements into the Hydragas system. Therefore any oil hydraulics used in the system must be completely sealed from the Hydragas fluid.

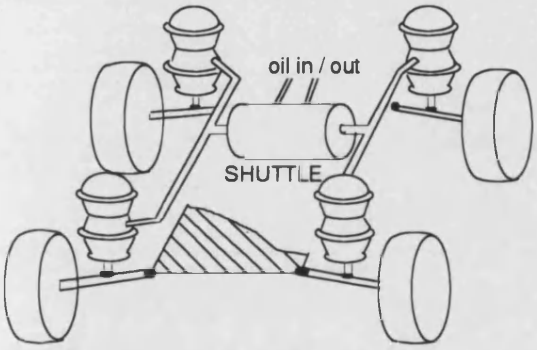


**Fig 2.4** *General Layout of the Hydragas Roll Control System*

The roll control system , shown diagrammatically in figure 2.4, uses a specially designed 'shuttle' device, similar in operation to a double ended equal area actuator to displace Hydragas fluid from the suspension units on the inside of a turn and into the units on the outside. This is achieved via the front to rear interconnection pipes and only one shuttle is necessary to control roll at the front and rear. The resulting imbalance in Hydragas unit pressures produces a roll moment opposing that due to the lateral acceleration. Therefore, an additional secondary suspension deflection is not required to balance the forces and the car remains level.

A schematic diagram of the shuttle is shown in figure 2.5. The oil pistons actuate tapered water

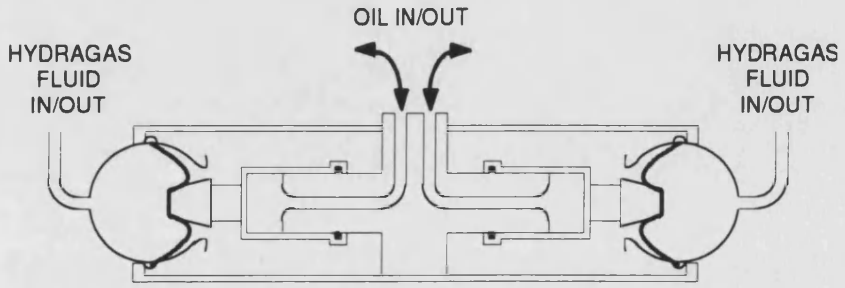


**Fig 2.5** *Schematic Representation of the Hydragas Roll Control Shuttle*

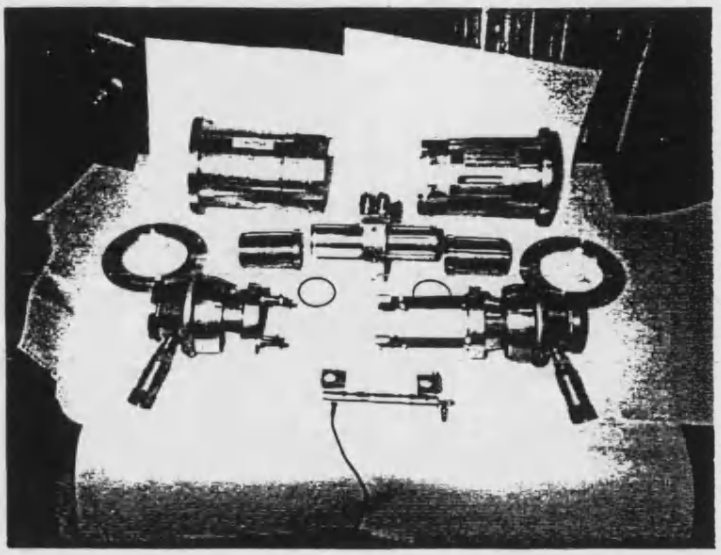

**Fig 2.6** *Disassembled Active Hydragas Shuttle*

pistons which in turn displace the diaphragms of the end effectors ( which are essentially the lower parts of Hydragas suspension units ) causing Hydragas fluid to be displaced. The tapered water pistons are connected together by restraining bolts so that the displacement of fluid out of one side of the shuttle will be matched by displacement of fluid into the other. Integrity of sealing of the Hydragas fluid is maintained by the hermetically sealed diaphragms. Figure 2.6 shows the disassembled shuttle including hydraulic fittings for attachment to the actuation circuit and the Hydragas fluid lines. Also shown is the linear displacement feedback transducer.

The shuttle was designed with low cost in mind but initial problems were encountered with failure of the oil piston. The brazed end cap deformed to a concave shape until failure of the cap occurred in a shear mode level with the inside wall of the cylinder. This necessitated a re-design of the oil piston which was subsequently machined as one piece. Proving calculations for the end section are presented in appendix 1.

The profile of the tapered water pistons is such that the body roll angle produced by the shuttle alone ( i.e. with the vehicle at kerb ) is approximately linear and proportional to the displacement of the shuttle, as shown in figure 2.7. The amount of roll which can be compensated for is limited by the volume of fluid displaced from the end effectors. The volume of fluid displaced is plotted against shuttle stroke in figure 2.8. The unequal volumes displaced from each side of the car combined with

the rolling diaphragm changing effective area led to a small increase in vehicle centre of gravity height as the shuttle was moved.

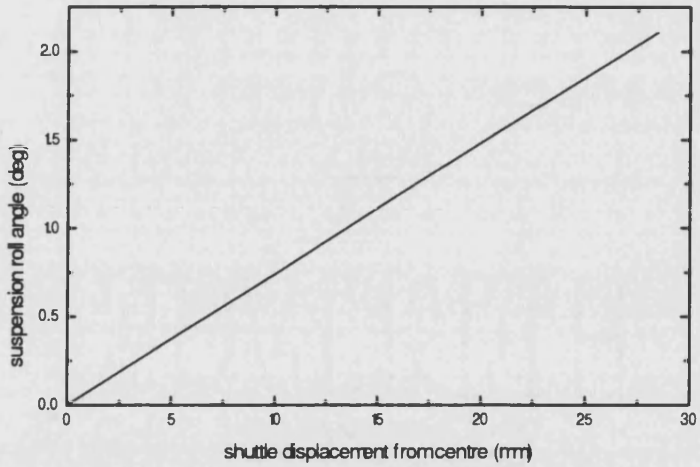


**Fig 2.7** *Predicted Body Suspension Roll Due to Displacement of the Shuttle*

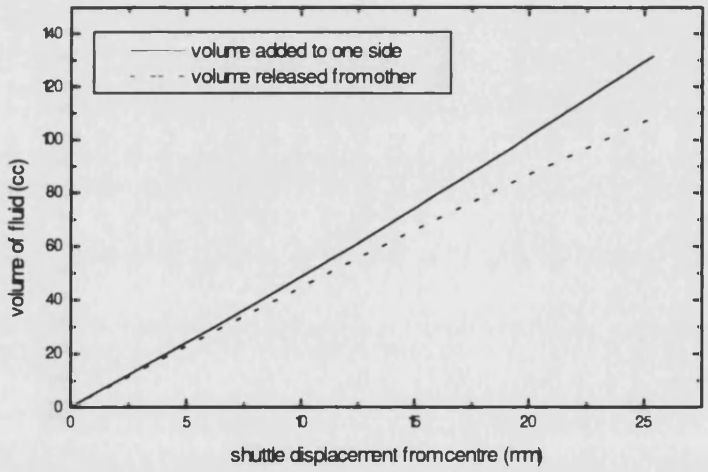


**Fig 2.8** *Volume of Fluid Added to and Removed From the Suspension Units*

### 2.2.2 Principles of Operation

The shuttle is not required to support the weight of the sprung mass as it is mounted across the two sides of the car. The pressures on each side of the car at kerb are equal, as are the effective areas of the end effector diaphragms. Therefore there is no net force on the shuttle at kerb. The shuttle only has to

react dynamic differential pressure fluctuations across the car caused by relative movement of the suspension elements. This reduces the power requirements of the system significantly. A block diagram representing the roll controlled vehicle system is shown in figure 2.9.

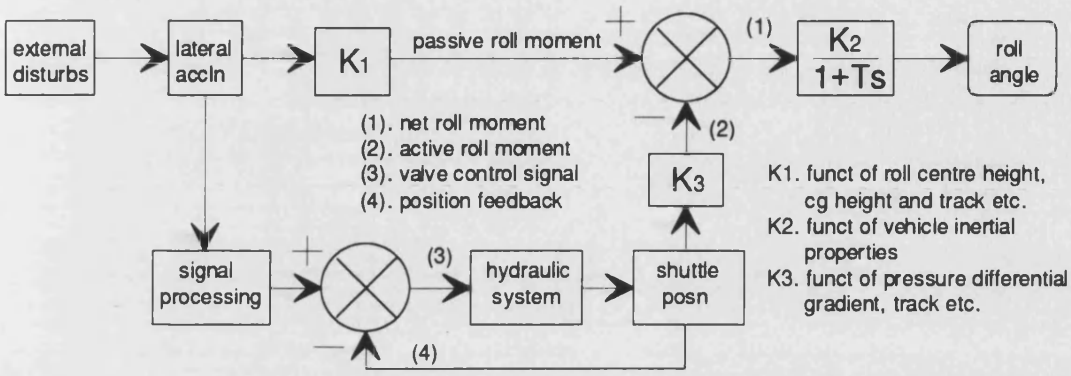


**Fig 2.9** *Block Diagram Representing the Simplified Active Vehicle System*

The negotiation of a severe lane change manoeuvre requires the shuttle to move to one end stop, back and to the other end stop, then finally to return to the centre stroke. The shuttle bore was 55 mm, its stroke 57 mm. The swept oil volume in an extreme lane change manoeuvre is therefore:

$$\begin{aligned} 2 \times 57 \times 2375 &= 2.71 \times 10^5 \, mm^3 \\ V_{sw} &= 0.27l \end{aligned} \tag{2.3}$$

The hydraulic system accumulator was sized on the assumption that it would provide sufficient fluid for a lane change manoeuvre without becoming discharged. The hydraulic pump was required to fill the accumulator in 5 seconds. The necessary flow was therefore approximately :

$$\begin{aligned} 0.27 \div 5 &= 0.054 L/s \\ Q_{hp} &= 3.24 L/\min \end{aligned} \tag{2.4}$$

In a severe lateral manoeuvre, the maximum pressure in the outside suspension units will rise to 40 bar. Pressure in the inside suspension units falls to a minimum of 25 bar. At this condition the shuttle piston outside effective area, $A_{effsh}$, is a maximum, 5900 mm$^2$. The shuttle effective inside area is a minimum, 3000 mm$^2$. The maximum net force acting on the shuttle is therefore:

$$\begin{aligned} F_{max} &= 5.9 \times 10^{-3} \times 40 \times 10^5 - 3.0 \times 10^{-3} \times 25 \times 10^5 \\ &= 16.1 kN \end{aligned} \tag{2.5}$$

This corresponds to a maximum pressure drop across the shuttle, $\Delta P_{sh}$ of 67.8 bar. Allowing for pressure drop through the hydraulic valves, a supply pressure, $P_{hp}$, of 85 bar was maintained.

A 1L accumulator was selected as a compromise between oil storage capacity and space requirements. Assuming adiabatic compression and expansion of the nitrogen gas with a polytropic index of 1.4 and taking the values calculated above for lower working pressure and stored fluid volume, the maximum pressure in the accumulator is:

$$\begin{aligned} P_{max} &= 85 \times (0.98 \div 0.71)^{1.4} \\ &= 133 bar \end{aligned} \qquad \textbf{(2.6)}$$

### 2.2.3 Prototype Hydraulic System

The hydraulic system used to power the roll control shuttle is shown in figure 2.10. Displacement of the shuttle was controlled by a Vickers closed centre valve KDG4V-3-2C28S-H-M-U-H7-20 capable of delivering 28 L/min and with a bandwidth of approximately 30 Hz. The prototype vehicle was fitted with a 24V Fenner electric power pack M09SA0,7 C07 R03 H 150 with integral motor,

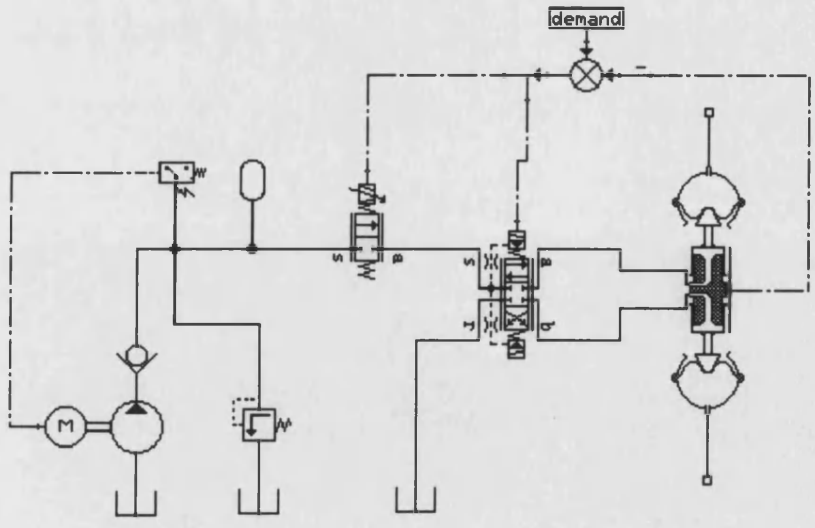


**Fig 2.10** *Hydraulic Circuit for Actuation of Prototype Roll Control Shuttle*

pump and tank. This supplied 4 L/min at 140 bar. A 1L accumulator was added to provide extra flow during demanding manoeuvres.

The cracking pressure of the relief valve was set at 140 bar. To prevent the power pack from working against this pressure continuously while the system was idle, a pressure switch ( Suco 0171 460 03 1 003 ) was included to turn the motor off at 140 bar. A dead band within the pressure switch meant that the motor was switched on again when system pressure fell below 125 bar. A check valve, a filter and a solenoid valve, to prevent oil leakage, were also included.

Electrical supply was from two 12V car batteries carried in the boot of the car.

### 2.2.4 Control Scheme

Analogue control was chosen for reasons of simplicity and cost. Figure 2.11 shows a block

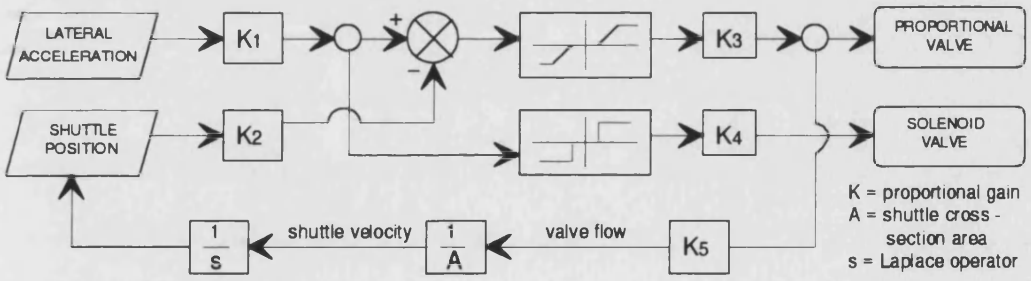


**Fig 2.11** *Basic Control Scheme for Hydragas Active Roll Control System*

diagram of the closed loop control system used to govern the shuttle position. In the development stages, the position demand signal came from a hand held joystick. This enabled the hydraulic system to be tested statically and to ensure its safety before testing on the road. A master switch was also available to shut the system down in the event of emergency. The joystick was later replaced by a J.P.B. accelerometer J.505-10 mounted laterally on the car body below the front bumper. This had a range of ± 10g with sensitivity 5.9 mV/g and natural frequency 378 Hz.

It was found that a linear relationship between lateral acceleration and shuttle position gave adequate roll control performance. Position feedback was supplied by an LVDT position transducer (

Penny & Giles HLP 190 BC1/75/3K ) mounted on the outer case of the shuttle. This monitored the movement of the tapered water pistons.

The demand voltage supplied to the proportional valve was the error between demand and actual shuttle positions, multiplied by a suitable gain. This demand was low-pass filtered ( bandwidth 20 Hz) to reduce the shuttle sensitivity to high frequency road disturbances. A deadband was used on the valve so that there was no response to very small lateral accelerations ( with the aim of reducing power consumption ).

The poppet solenoid valve, used to prevent oil leakage, was powered from the demand signal alone. Again a deadband was used to prevent it from constantly opening. However, when the system was tested statically it was found that the shuttle did not return to its centre position when the joystick was centred. This was because the demand had returned to zero, closing the solenoid valve. The problem was alleviated by introducing a time delay of approximately 1 second on the closing of the valve to allow the shuttle to centre. This had no effect on the dynamics of the hydraulic system.

The electrical circuit was protected from fluctuations in supply current by the use of a DC / DC converter ( Amplicon 92902150 ). This kept the electrical supply current within safe limits. A circuit breaker switch was included for safety purposes.

The system gain was chosen to give reasonable response times without causing instability. A suitable relationship between lateral acceleration and shuttle position was found so that suspension roll in manoeuvres was constant and approximately zero until the end stops of the shuttle were reached at around 4 $m/s^2$. Due to the integrating nature of the roll control system (an accelerometer being used to provide a position control signal), and the coupling between roll, pitch yaw and bounce, high gains may cause roll instability. Indeed, it was found that setting the loop gain too high resulted in unstable roll motion following any external disturbance of the car body. The gain was therefore lowered to an acceptable value. It was possible to use a higher loop gain when using the hand held joystick to provide a demand signal.

The hand held baton used to control the active system in static tests was carried in the front of the car for the dynamic tests. The active roll control system could then be turned on and off by means of a switch located at the base of the joystick. The hydraulic actuation system, as installed in the prototype vehicle, is shown in figures 2.12, 2.13. The majority of the electronics are housed within the case to

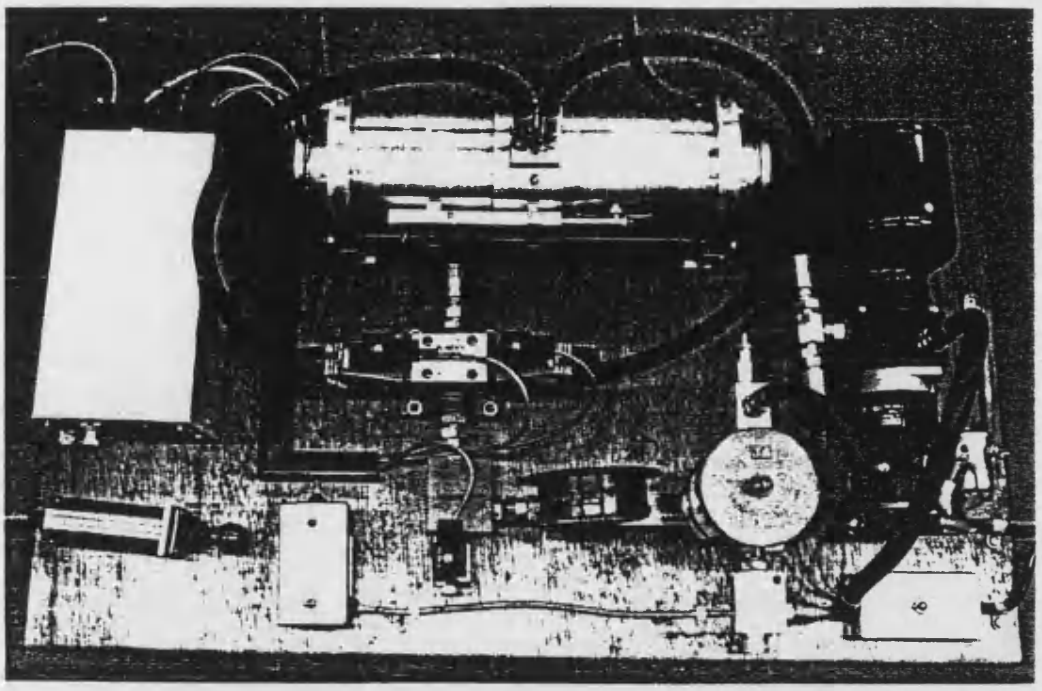

**Fig 2.12** *Hydragas Active Roll Control Actuation Circuit As Installed on Prototype Vehicle*

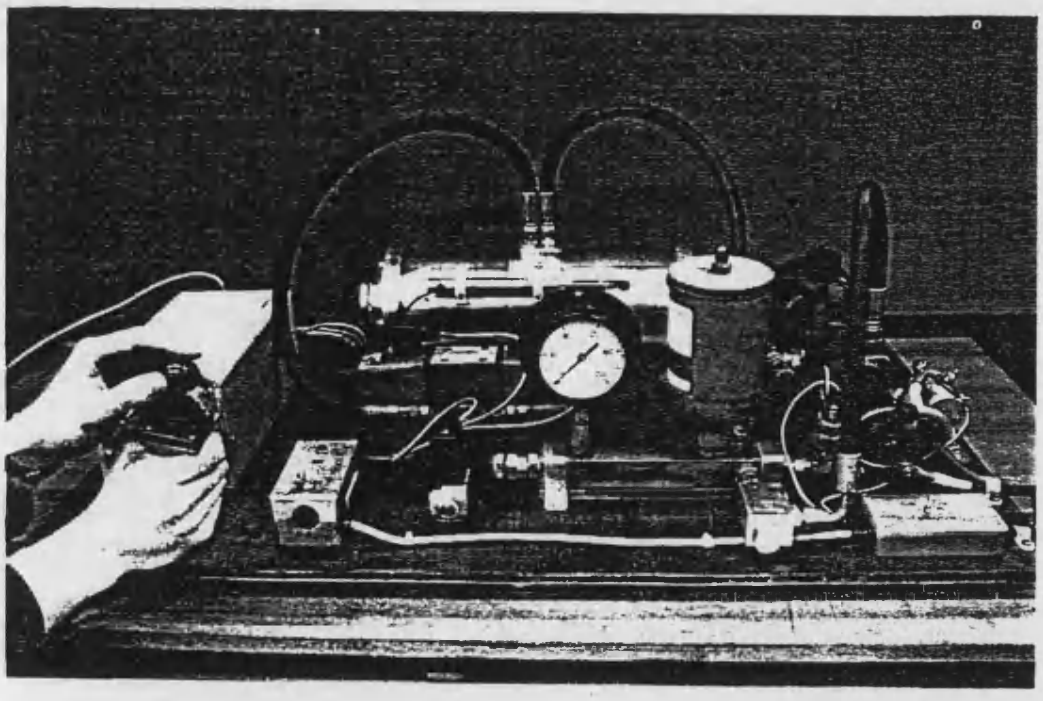

**Fig 2.13** *Prototype Hydraulic Actuation System Showing Operation of Joy-Stick*

the left of the board, including the control valve driver card. Isolating switches for the motor and the electronics are clearly visible.

# 3. Computer Simulation of Vehicle Systems

## 3.1 Review of Vehicle Modelling techniques

### 3.1.1 Introduction

Modelling of vehicle dynamic systems has come about as a result of the great expense and time required to produce prototype vehicles. It is evident that such mathematical models can provide valuable design information in significantly less time and for significantly less cost than a full prototype. The need for prototype vehicles is not completely annulled as they are still required for validation purposes and for subjective testing. However, the trial and error approach required for sensitivity studies can be markedly reduced.

In circumstances where complexity and non-linearity of a suspension system preclude a simplified linearised solution, there is a strong case for more sophisticated computer models. Computer simulation of vehicle dynamic systems can be carried out using specifically written code or general purpose vehicle dynamics packages. The main advantage of computer simulation is the reduction of calculation times. This allows complex non-linear systems to be analysed in a fraction of the time it would take for hand calculations.

The removal of repetitive and time consuming hand calculations allows the engineer to apply their knowledge of vehicle dynamics in a more constructive way. Adjustments can be made to vehicle parameters at little or no cost which renders the computer model a valuable design tool. The advent of general purpose vehicle dynamics software means that vehicle models and subsequent adjustments to these models can be achieved with little knowledge of computer programming.

### 3.1.2 The Quarter Car Model

There are several possible approaches to the modelling of vehicle suspension systems with varying applicability depending on the particular problem. The simplest and most commonly used representations are linearised models such as the quarter car shown in figure 3.1. Here, a single wheel station is modelled with an appropriate portion of the body mass. This has been used in many theoretical studies [ 53, 54, 55 ] to derive linear control laws for active suspensions in the ride function.

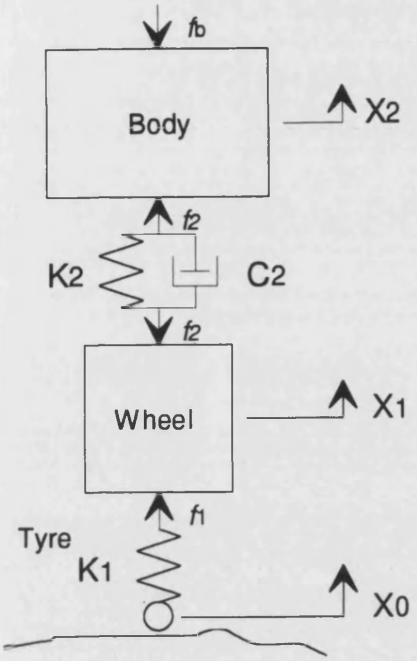


**Fig 3.1** *Quarter Car Model*

The quarter car representation assumes that the vertical response of the body at one corner is influenced predominantly by the suspension at that corner. The body pitch, roll, yaw, lateral and longitudinal degrees of freedom are neglected in this model together with engine and subframe motion.

Road inputs to the model are in the form of a power spectral density. A typical road is represented by the function :

$$S(f) = k \times U^{1.5} \times f^{-2.5} \qquad \textbf{(3.1)}$$

where :

| | | |
|---|---|---|
| $S(f)$ | is the power spectral density |
| $k$ | is the road roughness factor |
| U | is the vehicle forward speed |
| $f$ | is the relevant frequency |

The function is evaluated over a range of frequencies ( typically 0.25 - 20 Hz ) and body acceleration is weighted according to I.S.O. 2631 [ 56 ].

Although the above method is widely used and provides valuable design information, it does not take into account the highly non-linear nature of the majority of vehicle suspensions. Neither can it be used to predict vehicle geometric effects on ride such as the wheelbase filter effect [ 57 ]. Improvements can be made by adopting a half car model representing one side of the car. However no information can be gained on the behaviour of the vehicle in roll and the consequent effects on handling performance during manoeuvres. To address these issues, a more sophisticated approach must be adopted.

### 3.1.3 Multi-Body Kinematics and Dynamics Packages

Great accuracy and flexibility has been brought about by the use of general purpose multi-body kinematics and dynamics packages [ 58, 59 ]. These make use of the ever-increasing computing power available to examine the vehicle model in great detail. Suspension systems, for example are constructed from individual components and the kinematic interactions between these components are analysed. It is clear that such a system is capable of modelling vehicle dynamics to a high degree of accuracy.

However, this in itself can be a problem. To create a full vehicle model within these multi-body packages, a great amount of parametric data must already be known or estimated. This takes away the value of the model as a design tool. Simulation run times are likely to be long as a high computational effort is required. Furthermore, there is no provision within the majority of vehicle dynamics software packages for the addition of hydraulic components or controlled elements which are intrinsic in active suspension design.

For these reasons, there is case for a simpler three-dimensional vehicle model which can provide valuable design information without the large simulation effort and data requirements of the multi-body kinematics packages.

## 3.2 The BATH*fp* Vehicle Simulation Model

For the reasons outlined above, a full vehicle ride and handling model was developed at Bath University using the fluid power simulation package BATH*fp* [ 60 ].

### 3.2.1 BATH*fp* Simulation Environment

Research into the dynamic behaviour of hydraulic systems undertaken at the University of Bath prompted interest in the computer simulation of such systems. The result was a highly interactive state-of-the-art software package, BATH*fp*.

BATH*fp* is a mouse operated, menu driven dynamic package working on X-Windows/UNIX based Sun 4 / SPARC or SLC workstations. It was originally intended for the simulation of electro-hydraulic systems, containing an extensive library of standard hydraulic and control models. These libraries have been extended to cover a variety of different fields of engineering including the human respiratory system and vehicle transmission systems as well as the vehicle dynamics models used in this study.

BATH*fp* runs in the time domain using an enhanced version of the LSODA integrator. The integrator selects the most appropriate integration algorithm and automatically determines the optimum time step. The integrator also incorporates a handling mechanism for discontinuities. This method is ideal for 'stiff ' hydraulic systems which also contain many discontinuities such as actuator end stops.

Individual components are represented by icons which can be built up into a full system simulation model in the Circuit Drawing mode. A typical BATH*fp* screen is shown in figure 3.2. Components are connected by ports, visible on the model icons, which must be compatible to prevent non-rational attachments being made. In the Model Selection mode, a suitable model from the standard or user custom library is associated with each icon. This selection is made on the basis of compatibility with other models and appropriate complexity. Once each component has been allocated a model, the user enters the Parameter Definition mode.

At this stage, the circuit source code is generated. Component parameters, such as dimensions, are now set. Default settings are available to guide the inexperienced user to reasonable values. Once all parameters have been set, the simulation can be run. In the run mode, the duration and data output set are chosen; then the simulation is started.

Output data can be plotted as a time history, or results can be plotted against each other. The

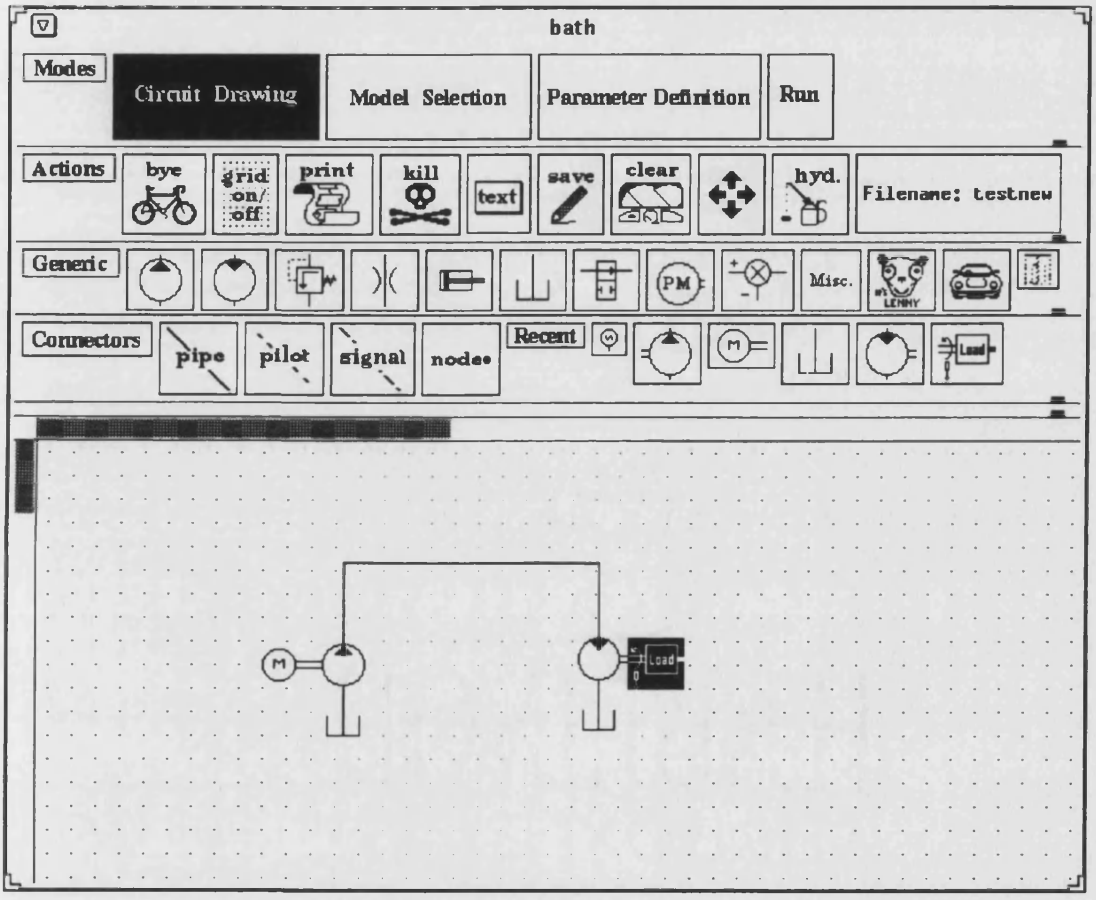


**Fig 3.2** *A Sample* BATH*fp Screen Showing a Simple Hydraulic Circuit*

graph window may then be manipulated for examination of particular areas of interest. Data may be exported for use in other packages, for example Matlab and data from previous runs may be imported for comparison with current results in, say, sensitivity analysis.

New models may be added by the operator using the BATH*mat* model adding tool and BATH*me* model editor. Code for these models may be written in FORTRAN 77 or C. Components may be

modelled using either instantaneous functions or dynamically by simultaneous differential equations. It was this feature which led to the development of the vehicle model set.

### 3.3.2 Causality Constraints on the Vehicle Model

The solubility of any system represented by two or more interacting, individually soluble models is governed by causality. The implication of this on time domain simulation, such as that used in BATH*fp*, is that if two models in a system are directly dependent on each other for information, then neither can be solved first and hence the overall system becomes insoluble. The condition is known as an algebraic loop.

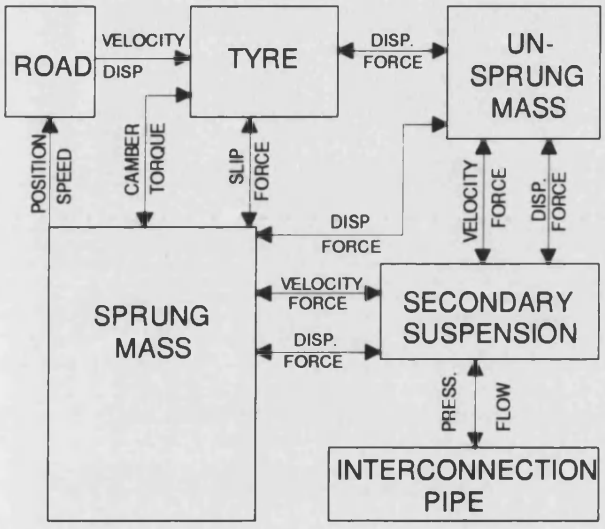


**Fig 3.3** *Block Diagram Showing the Transfer of Data Between Sub-Models of One Quarter of the Full Car Simulation Model*

Causality constraints are met in the BATH*fp* vehicle model by careful choice of the interactions between individual components. State variables are used where necessary which can be assigned initial values, therefore allowing the initial solution of one model and hence the solution of the models directly dependent on it. The current values of states are maintained throughout the integration procedure. External inputs to the vehicle model are defined at all times and therefore remove causality restrictions from the other models dependent on them. The transfer of information between the individual component models of a complete vehicle simulation with standard Interconnected Hydragas suspension is shown in figure 3.3.

### 3.2.3 The BATH*fp* Vehicle Simulation Suite of Models

The general philosophy of BATH*fp* leads to a separation of complex dynamic systems into far simpler component models. This philosophy led to the development of the vehicle model in its current form.

The BATH*fp* suite of vehicle models has been developed over a number of years [ 61, 62 ]. The full vehicle model is described by Ross-Martin and Darling in [ 63 ]. This model has been extensively validated by comparison with the multi-body package, ADAMS and experimental results. It was primarily developed as a tool for the development and analysis of active suspension systems.

The construction of the full vehicle model emulates that of a hydraulic circuit in its modular nature. The full vehicle is composed of a number of standard components. These include:

- Sprung mass ( body )
- Unsprung masses ( wheels )
- Tyres
- Driver
- Suspension components

Although the display is only of a half car ( figure 3.4 ), the models in fact represents both sides of the car. Two dimensional vectors are used to distinguish between the left and right hand sides. Further models representing external disturbances, i.e. road input and aerodynamic forces are also available.

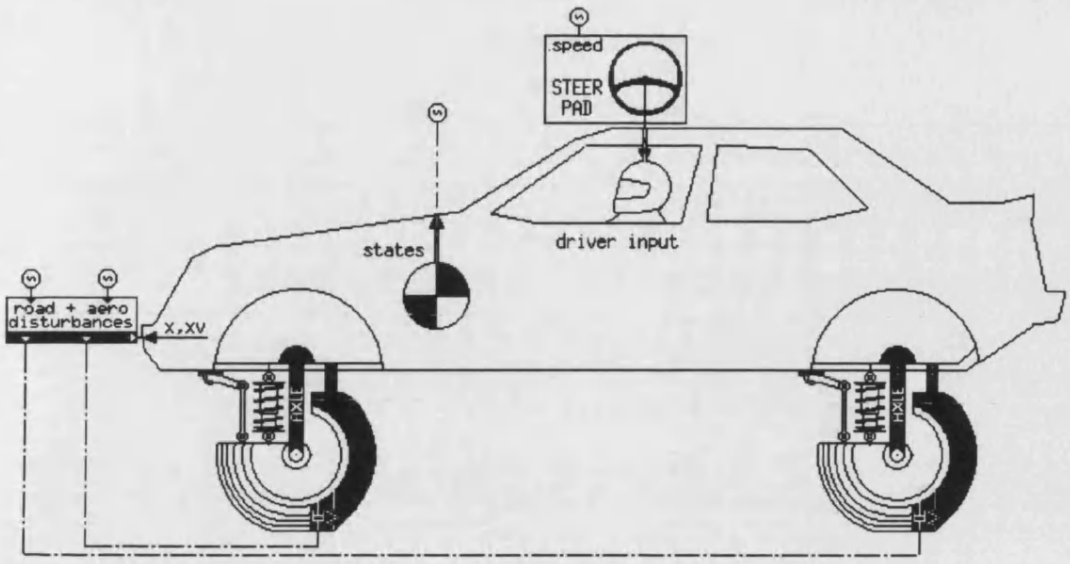


**Fig 3.4** *The* BATH*fp Vehicle Simulation Model*

Calculation of load transfer during manoeuvres is performed within the car body model using the force roll centre method [ 43 ] This constrains lateral forces to act on the body at the front and rear roll centres but does not restrict the body to roll about these points. The front and rear roll centres are found from the intersection of instantaneous perpendiculars to the tyre contact patch path at the contact patch. The contact patch path is defined by a polynomial function relating lateral displacement of the contact patch to relative displacement of the wheel to the body.

There are inherent errors in the use of the force roll centre method as outlined here due to lateral compliance of the tyres and to some degree the suspension linkages. This gives rise to changes in the contact path. The justification for this approach was the large saving in computational effort and the acceptable agreement between simulated and experimental results.

Wheel camber and toe values are calculated in submodels within the main sprung mass model. These are functions of suspension geometry and compliance characteristics. The car body is assumed rigid which is a reasonable assumption for low frequency testing, such as handling analysis. Suspension body roll and pitch angles are assumed to be small so that changes in pitch and roll inertia are negligible. The global and vehicle co-ordinate systems are shown in figure 3.5.

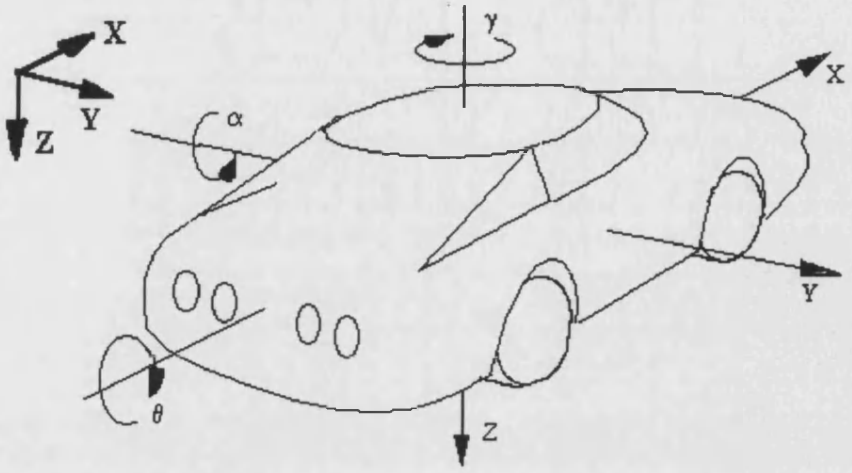


**Fig 3.5** *The Co-ordinate System Used for Modelling*

Tyre behaviour is predicted using one of a suite of models, ranging from a simple interpolation model to a full model based on the work of Pacejka [ 64 ]. The tyre is assumed to have a point contact with the road, thus neglecting any enveloping due to tyre deformation. This is a good approximation for road profiles comprising wavelengths greater than the tyre radius. Vertical stiffness and damping of the tyre are modelled linearly, providing sufficient accuracy over the normal load range of the tyre.

In the simple tyre model, tyre side forces and aligning torques are calculated by interpolating within data sets containing slip angle, camber angle and vertical load information. Longitudinal forces are based on relative vehicle body and tyre velocities and linear longitudinal slip stiffness. Dynamically, these are dependant on the distance travelled by the tyre in a function defined by the tyre relaxation length. The relationship between longitudinal and lateral tyre forces is based on the established frictional ellipse method.

Ride and handling studies are carried out independently using different model combinations. For handling studies, the road profile is assumed perfectly flat. This reduces simulation run times and prevents confusion in the results due to road noise. For ride studies, the calculation of longitudinal forces may be switched off, again to reduce run times. In any case, the movement of the wheels is restricted to the vertical direction on the assumption that only vertical displacement of the wheels is of interest in ride studies.

The driver model provides steering and braking or accelerating inputs to the car model. Open loop and closed loop speed and steer models are available. The former is used to evaluate vehicle transient

response, for example in step steer or lane change manoeuvres as defined in ISO 7401 [ 65 ]. Step, ramp and sinusoidal inputs are provided by a separate standard signal model. The latter model incorporates a closed loop P.I.D. steering controller to sustain the vehicle on a constant radius circular path for steerpad testing ( I.S.O. 4138 [ 66 ]). Speed is controlled using a P.I. controller.

Conventional suspension springs and dampers are represented by empirical models defining their characteristics in polynomial form. They provide output forces as functions of input displacements and velocities respectively. This was not considered sufficient for the modelling of the Hydragas suspension units as, for instance damper valve force is dependent not only on piston velocity but also on piston displacement due to the taper of the pistons. Therefore a more accurate model of the Hydragas units was required.

## 3.3 Modelling of the Interconnected Hydragas System

### 3.3.1 The Basic Hydragas Elements

New models were developed to represent the individual components of the Hydragas suspension units. The BATH*fp* iconic representation of a single Hydragas unit is shown in figure 3.6. The unit was split into the following discrete elements which can be seen clearly in the figure. These are:

1. Tapered piston and rolling diaphragm displacer
2. Fluid damper pack
3. Gas 'egg'

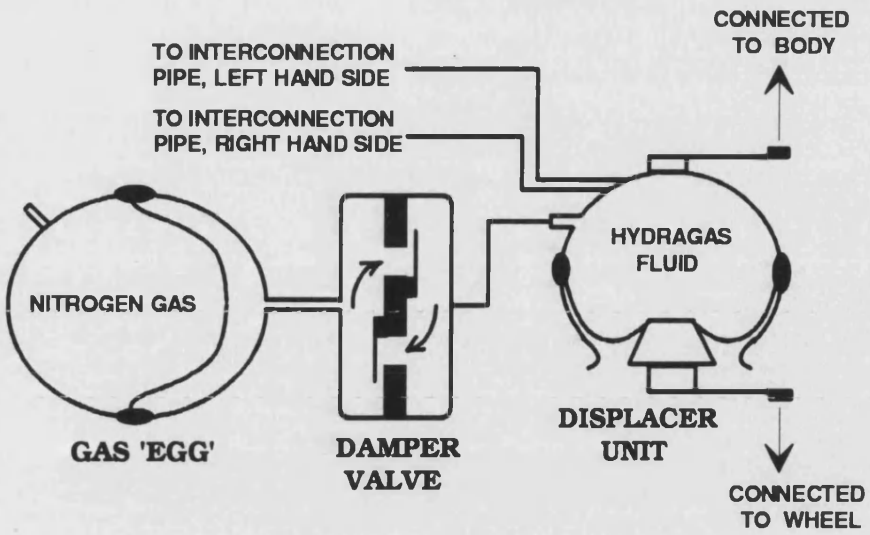


**Fig 3.6** *BATHfp Iconic Representation of a Single Hydragas Suspension Unit*

Causality restraints on the Hydragas models were met by using state variables in both the displacer and gas spring models. The exchange of data between hydragas unit models and with the car body and unsprung mass models is outlined in the sections below.

### 3.3.2 Front and Rear Fluid displacer models ( FDF0, FDR0 )

These models describe the lower chambers of the front and rear Hydragas suspension units, including the tapered piston and rolling diaphragm displacer. The model is defined by user supplied parameters describing fluid bulk modulus, nominal wheel centre to body eyebrow height, suspension arm lever ratio, drop angle and parasitic suspension rates and polynomial constants describing the relationship between piston displacement and diaphragm effective area.

Inputs received from other models are :

- unsprung mass vertical displacements and velocities ( from unsprung mass models )
- body eyebrow point vertical displacements and velocities ( from car body model )
- flow from left and right interconnection pipe models
- flow from gas springs through damper valve models

Outputs to other models are :

- vertical suspension forces ( to sprung and unsprung mass models )
- state pressures at left and right interconnection pipe and damper valve models

Also supplied by the model are internal variables measuring hydragas fluid volume, effective piston area and relative wheel to body displacement.

The front and rear fluid displacer elements were modelled using the fluid compressibility equation to predict pressure variations. The bulk modulus, B was modelled as a constant. This assumed a low range of pressures and absence of gas within the working fluid.

$$\frac{dp_d}{dt} = BQ_{Td}/V_d \qquad \textbf{(3.2)}$$

where: $B$ is the fluid bulk modulus

$Q_{Td}$ is the total flow into the model

$V_d$ is the displacer volume

Flow into the lower chamber from the damper valve and the interconnection port was summed with an equivalent flow due to the velocity of the piston. The total flow into the unit, along with a calculated fluid volume was used to find the derivative of pressure in the displacer. The rolling diaphragm was modelled using a $4^{th}$ order polynomial function to relate piston displacement to an effective diaphragm area. This function was determined from experimental data.

The experimental rig, used to provide steady state empirical data of diaphragm areas is shown in

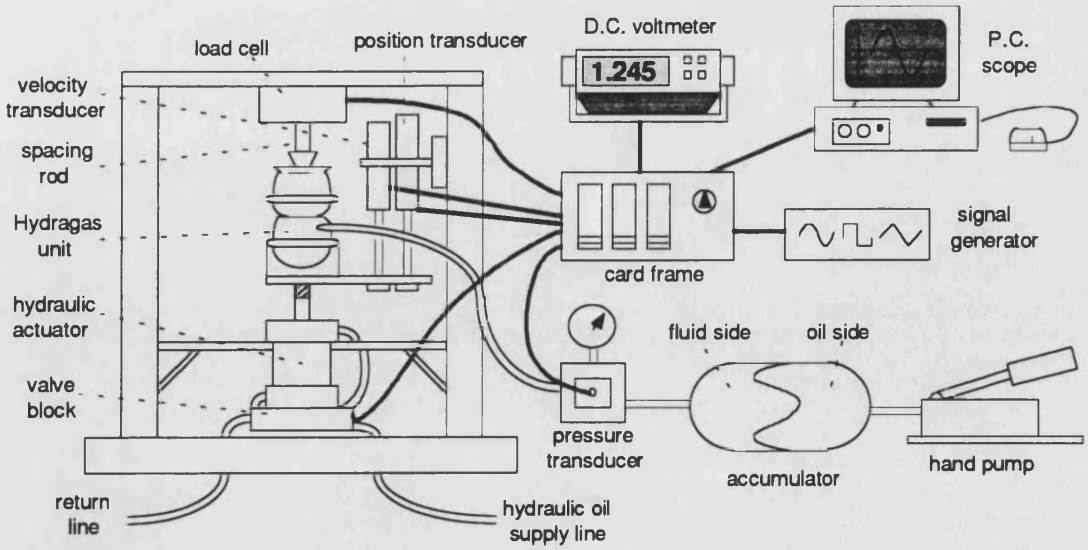


**Fig 3.6** *Experimental Rig Used to Find Hydragas Taper Rates and Validate Computer Model*

figure 3.6. The main body of the unit was displaced by a closed loop, position controlled hydraulic valve and actuator system fed by a high pressure supply. The unit piston was held stationary, giving a relative movement of the piston to the body.

A hand pump was used to pressurise hydraulic oil in one side of an accumulator. The other side contained Hydragas fluid and was connected to the interconnection port in the lower chamber of the unit. This arrangement was used to pressurise the Hydragas fluid in the unit to kerb pressure of 29 bar. The Hydragas unit was isolated from the charging accumulator during testing.

A pressure transducer was mounted at the interconnection port of the suspension unit to measure steady state or dynamic pressure. Applied load was measured using a load cell mounted at the end of the piston rod. Relative displacement and velocity were also measured. An arbitrary datum of piston displacement was chosen at the point where the skirt of the piston was level with the skirt of the body. This datum does not necessarily correspond to the datum used in previous testing of Hydragas units by Dunlop (q.v.).

Steady state readings of pressure and load were taken at various displacements and load was divided by pressure to give an effective diaphragm area. Characteristic curves of area versus

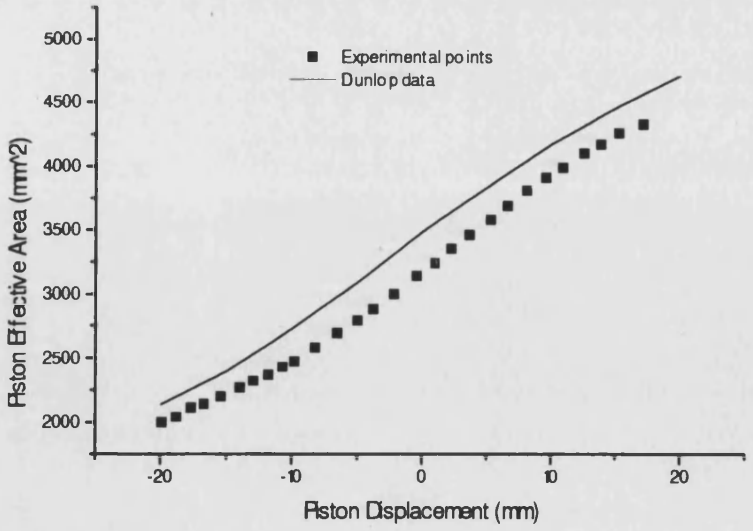


**Fig 3.7** *Variation of Front Hydragas Unit Piston Effective Area with Displacement*

displacement for front and rear suspension units are shown in figures 3.7, 3.8. These are compared with figures quoted by Dunlop. There is some quantitative discrepancy between these traces due to the arbitrary choice of datum position.

An analytical model was developed to describe the variation of piston effective area with displacement, based on the angles of piston and skirt taper. This is presented in appendix 2. It was not used in the BATH*fp* simulation as the approximation to profiled pistons and skirts was not as accurate as using empirical data.

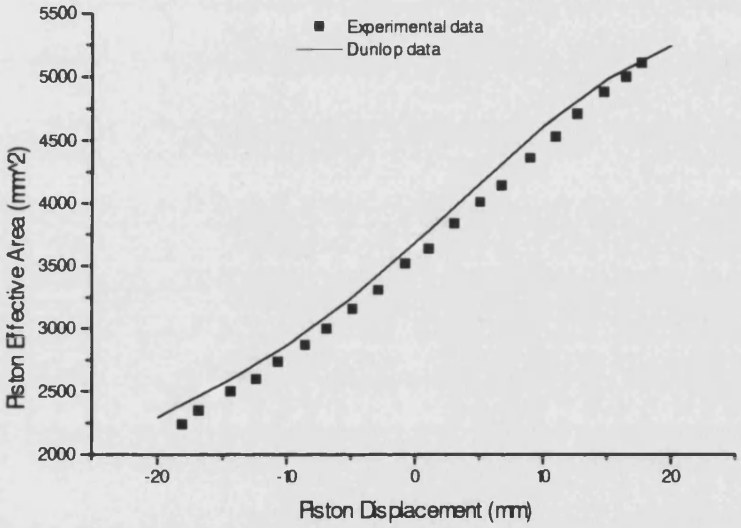


**Fig 3.8** *Variation of Rear Hydragas Unit Piston Effective Area with Displacement*

Suspension parasitic and drop angle rates were included in the displacer model as additional variations of force with suspension displacement. The suspension arm lever ratio was also included.

The pertinent equations used in the computer model are listed below following a glossary of terms used:

| | |
|---|---|
| X | relative displacement of the piston |
| AEFF | piston effective area |
| VREL | relative velocity of the piston |
| LEVER | mounted lever ratio of Hydragas unit |

| | |
|---|---|
| VF | volume of fluid in the displacer |
| VFDOT | derivative of above |
| FDROP | unit force due to drop angle rate |
| DROP | drop angle rate |
| FPARA | unit force due to parasitic rate |
| PARA | parasitic rate |
| QPIS | effective flow into unit due to movement of piston |
| QCON | flow into unit from interconnection lines |
| QSPR | flow into unit from gas spring |
| QTOT | total fluid flow into unit |
| P | Hydragas fluid pressure |
| PDOT | derivative of above |
| BULK | fluid bulk modulus |
| FHYD | force due to fluid pressure and piston effective area |
| FBOD | force on body from Hydragas unit |
| FWL | force on wheel from Hydragas unit |

$$X = (XWL - XBOD) / LEVER \tag{3.3}$$

AEFF = polynomial function of X

$$VREL = (VWL - VBOD) / LEVER \tag{3.4}$$

$$VFDOT = VREL \times AEFF \times 1000 \tag{3.5}$$

$$FDROP = X \times DROP \times LEVER \tag{3.6}$$

$$FPARA = X \times PARA \times LEVER \tag{3.7}$$

$$QPIS = -1 \times (VREL \times AEFF \times 60{,}000) \tag{3.8}$$

$$QTOT = QPIS + QCON + QSPR \tag{3.9}$$

$$PDOT = (BULK \times QTOT)/(VF \times 6{,}000{,}000) \tag{3.10}$$

$$FHYD = P \times AEFF \times 100{,}000 / LEVER \tag{3.11}$$

$$FWL = FHYD + FDROP + FPARA \tag{3.12}$$

$$FBOD = -1 \times FWL \tag{3.13}$$

### 3.3.3 Front and rear damper valve models ( DVF0, DVR0 )

These models describe the internal fluid damper packs between upper and lower chambers of the hydragas units. User supplied parameters give the polynomial constants describing the relationship between flow through and pressure drop across the valve in both bump and rebound directions.

Inputs received from other models are :

- pressure in the fluid displacer and gas spring models

Outputs to other models are :

- flow into fluid displacer and gas spring models

The model also supplies one internal variable measuring pressure drop across the valve.

The damper valve was modelled by interpolating between experimentally measured points relating flow to pressure drop across the valve. This method was used in preference to a theoretical orifice equation to achieve greater accuracy, particularly at low flows. Due to the non-linear rolling diaphragm displacer, a force / velocity characteristic was not used as the pressure and associated force are functions of both piston position and velocity. The empirical data was collected using a rig shown diagrammatically in figure 3.9. The working fluid was a 95/5 water to oil emulsion and was supplied under pressure by a combination of pumps. This fluid was selected as its properties were more similar

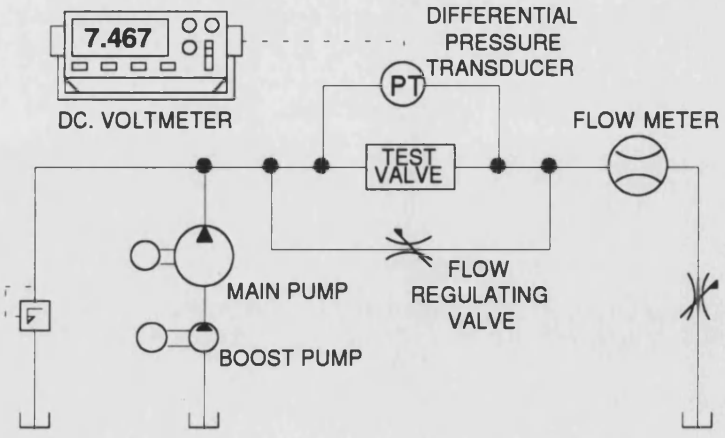


**Fig 3.9** *Test Rig Used to Determine Damper Valve Characteristics*

to Hydragas fluid than standard hydraulic oil.

Instrumentation consisted of a flow meter and a differential pressure transducer measuring pressure drop across the valve. Flow through the valve was modulated by a variable orifice in parallel with the test block. Both front and rear damper valves were tested in both directions to obtain a pressure / flow characteristic in bump and rebound. These characteristic curves are presented in figures 3.10, 3.11.

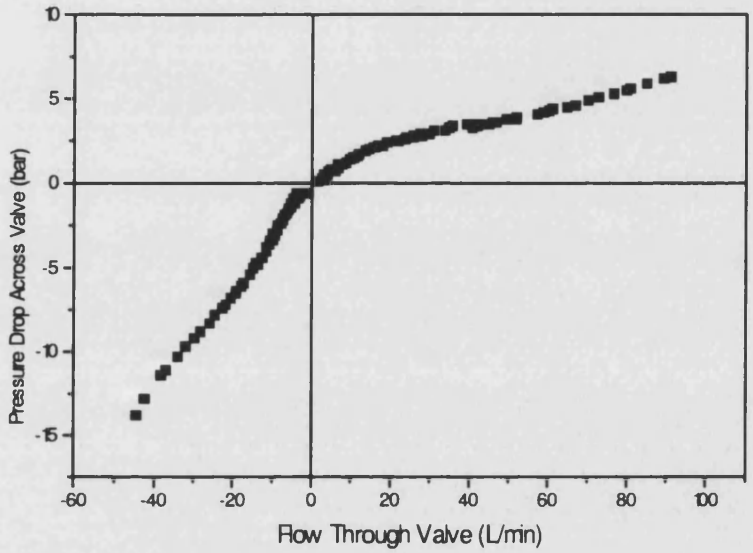


**Fig 3.10** *Pressure / Flow Characteristic for the Front Suspension Damper Valve*

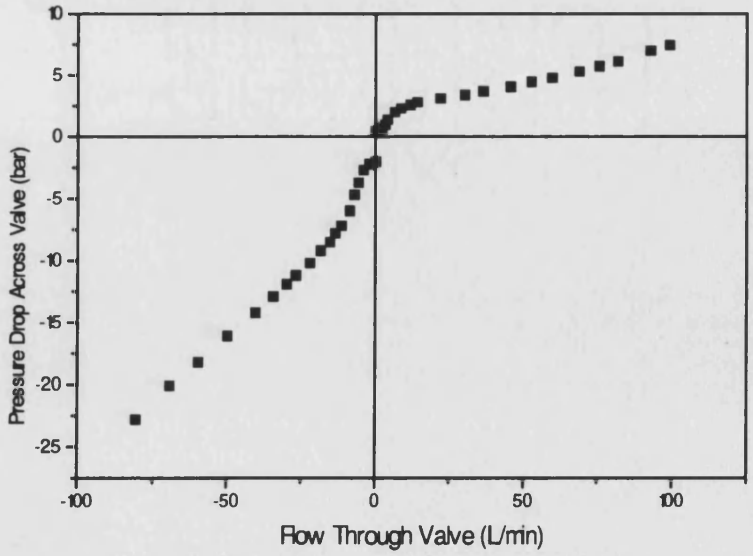


**Fig 3.11** *Pressure / Flow Characteristic for the Rear Suspension Damper Valve*

### 3.3.4 Gas spring model ( GS00 )

This model describes the nitrogen gas spring comprising the upper chamber of the Hydragas suspension unit. User supplied parameters define the gas spring volume, charge pressure and polytropic index.

The single input received is :

- flow from the fluid displacer through the damper valve model

the single output variable is :

- fluid pressure (to the damper valve model )

The model also supplies an internal variable measuring stored Hydragas fluid volume.

The gas 'egg' was modelled as a standard hydraulic accumulator with no restriction at its port. Initial gas volume at kerb is derived from pre-charge conditions using the ideal gas law

$$pV^{\gamma} = const \tag{3.14}$$

The variation of pressure is controlled by an adiabatic relationship with a user defined polytropic index for the expansion and compression of nitrogen gas.

$$\frac{dp_{gas}}{dt} = p_{gas}\gamma Q_{gas}/V_{gas} \tag{3.15}$$

where: $p_{gas}$ = gas pressure

$\gamma$ = polytropic index

$Q_{gas}$ = flow into chamber

$V_{gas}$ = volume of nitrogen gas

It was found that a polytropic index of 1.45 gave the best fit between experimental and simulated results. This value is high because of the long operating times and harsh operating cycles of the suspension units. Errors may arise due to the assumption of a constant polytropic index [ 67 ],

however these are likely to be insignificant when compared with other inaccuracies associated with tyre modelling.

The pertinent equations used in the computer model are listed below following a glossary of terms used:

| | |
|---|---|
| VINIT | initial volume of gas at kerb condition |
| VGAS | volume of nitrogen gas in gas egg |
| PINIT | initial pressure in gas egg at kerb condition |
| PATM | atmospheric pressure |
| P | pressure in gas egg |
| PDOT | derivative of above |
| BULK | Hydragas fluid bulk modulus |
| VF | volume of Hydragas fluid in gas egg |
| VFMIN | volume of fluid in gas egg at which it is considered discharged |
| VMAX | volume of gas egg |
| GAMMA | gas polytropic index |
| QIN | fluid flow into gas spring |

$$VGAS = VINIT \times \left( \frac{PINIT + PATM}{P + PATM} \right)^{\frac{1}{GAMMA}} \tag{3.16}$$

if fully discharged

$$VF = VMIN \tag{3.17}$$

$$PDOT = BULK \times QIN / VF \tag{3.18}$$

normal operating conditions

$$VF = VMAX - VGAS \tag{3.19}$$

$$PDOT = GAMMA \times (P + PATM) \times QIN / (VGAS \times 60) \tag{3.20}$$

### 3.3.5 The Interconnection Pipe

The interconnection pipes were modelled using standard hydraulic pipe model HP01. This dynamic, constant volume model included the effects of friction but not those of fluid inertia (because of the excessively long run times associated with the use of the fluid inertia models). Compressibility and cavitation are taken into account within the model.

The previous models simulate both sides of the vehicle using a two dimensional vector to distinguish between left and right. However the standard pipe models available are only capable of using scalar quantities. Therefore the interconnection pipes on each side were modelled using separate compressible volume pipe models. Standard non-linear orifices act as pitch dampers. It is possible to include the effects of fluid inertia within these pipe models for high frequency ride studies.

### 3.3.6 Full Vehicle Model

The BATH*fp* iconic representation of the full vehicle model incorporating Hydragas suspension units is shown in figure 3.12.

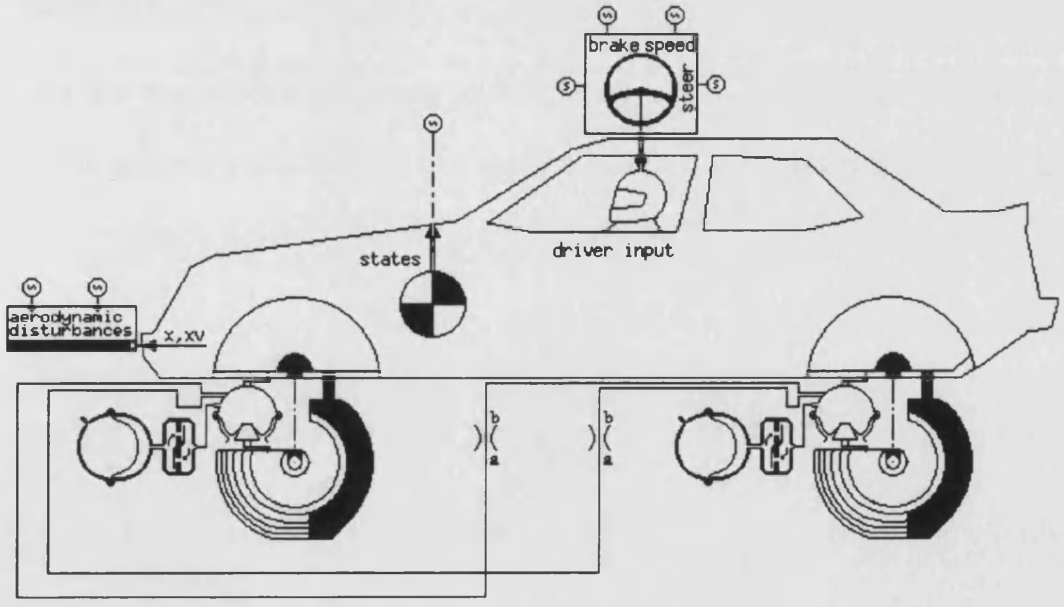


**Fig 3.12** *The* BATH*fp Vehicle Simulation Model Incorporating Hydragas Suspension*

## 3.4 Modelling of the Active Roll Control System

### 3.4.1 Hydragas® Specific Models

The BATH*fp* representation of the Hydragas active roll control vehicle is shown in figure 3.13.

The extensive library of hydraulic and control components within BATH*fp* made the description of active suspension systems relatively simple. Provided the porting arrangements between the hydraulic and mechanical systems are compatible the introduction of active elements into conventional suspension systems can be achieved by the addition of hydraulic and / or control components in the

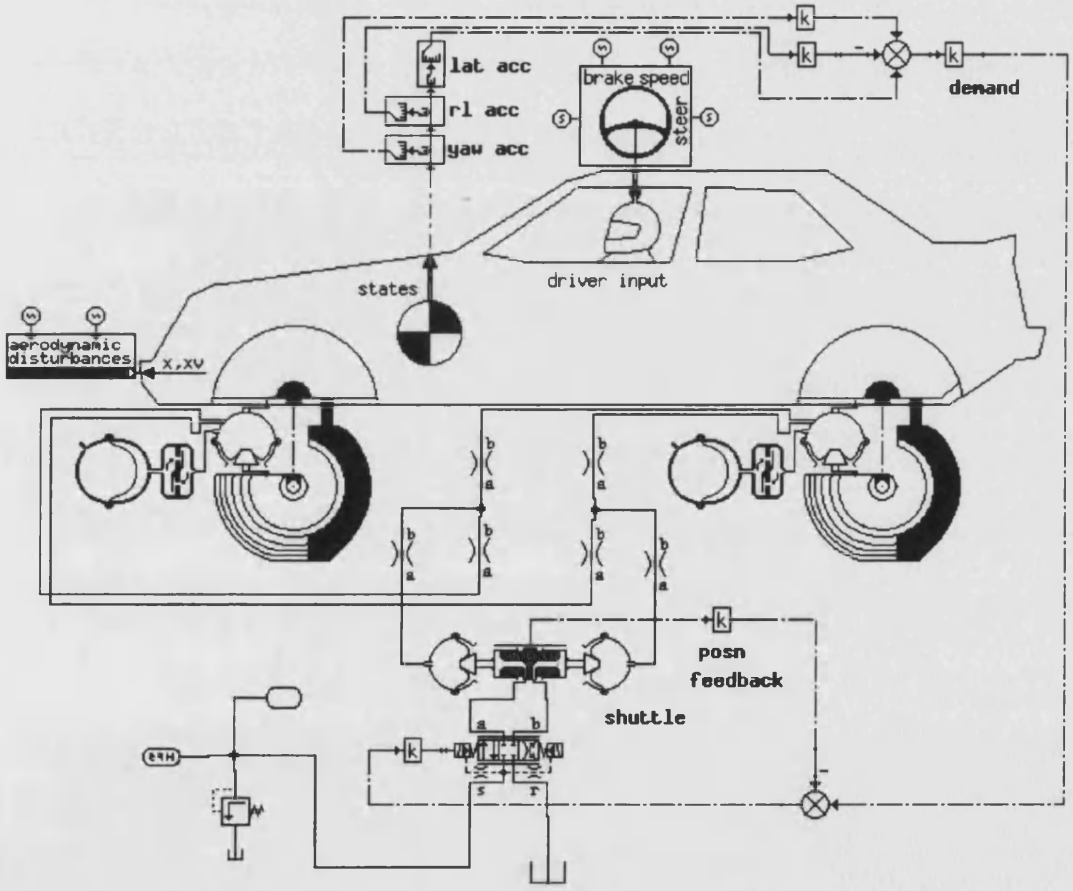


**Fig 3.13** BATH*fp Representation of the Hydragas Active Roll Control Vehicle*

circuit drawing mode.

Several component models were not available, however and were therefore developed specifically for the modelling of the Hydragas roll control circuit.

Models of specific proportional directional valves were available including the Vickers KDG3 valves. A 28 L/min valve was not included in the model library but the synthesis of this model from catalogue data was a simple matter of constructing an appropriate data file. It was found however that the basic valve model provided a performance equal to that of the specific model with less computational effort.

This basic proportional valve model included valve dynamics, the spool position responding as a critically damped second order system, and took into account the overlap of the Vickers valve. Leakage was assumed to vary linearly with pressure differential. The valve characteristics were defined using both steady state and frequency response performance data available from the manufacturers literature. Losses due to fluid compressibility, temperature changes and stiction forces were not included.

The Hydragas shuttle was modelled as three separate components, namely the hydraulic piston arrangement and two fluid filled end effectors. The hydraulic piston model was adapted from the standard double ended actuator model from the BATH*fp* library. The modifications allowed forces to be applied at both ends of the shuttle. The parameter defining the standard actuator rod diameter was removed as it was unnecessary. The end effectors were modified suspension fluid displacer models with piston area profiles taken from experimental data gathered by Moulton Developments Ltd at Bradford on Avon.

The standard BATH*fp* library of components did not include a pressure switch model. Therefore a model was written including the desired hysteretic effect.

### 3.4.2 Standard Hydraulic Models

Early simulation work included accurate modelling of the hydraulic components within the roll control system. The hydraulic power pack was modelled by combining motor, pump and tank models. The pump model used was an instantaneous model including loss terms due to slip, pressure dependant friction and speed dependant friction. These terms were derived from the manufacturers data. Although the model was intended for uni-directional rotation, it allowed the pump to act as a motor if prevailing conditions dictated that it should.

The dynamic motor model determined speed during transient and steady state operation by considering the shaft load torque, motor characteristics and the effective inertia of the pump and motor combination. These terms were again derived from the manufacturers data. A single overall efficiency term was included.

The pressure relief valve was modelled as a simple instantaneous device. Flow through the valve was assumed to be linear with respect to pressure drop once the cracking pressure was exceeded. The model did not account for valve dynamics. The check valve was also an instantaneous model having a linear relationship between pressure and flow. The model did not allow for valve saturation or spool dynamics.

In later simulations, where the performance of the system under continuous demand was not of relevance, the detailed model of the fluid power pack was replaced by a simple hydraulic flow source model, the maximum system pressure being dictated by the pressure relief valve.

The control system was also modelled using standard library components. The accelerometer lateral acceleration signal was generated by combining elements of body lateral, roll and yaw acceleration dependant on the accelerometer position. This was achieved by means of three models available as part of the vehicle dynamics model library. The models each selected the appropriate vehicle state from the body model and supplied this as a control output to be combined with the other such outputs in the correct proportions.

The shuttle position feedback was output directly by the shuttle model. The control system output was fed to the proportional valve model.

## 3.5 Validation of Hydragas Models

In order to ensure accurate modelling of the vehicle as a whole, the new suspension unit models were validated against experimental data. Testing was performed in a number of stages. Firstly, the kerb suspension rates were compared with those quoted by Oldaker in [ 9 ]. The results of this comparison are presented in table 3.1. It should be noted that the overall simulated rates and the

individual components making up these rates are consistent with the measured values. It can be seen that the hydraulic suspension rate does not have a significant influence on body pitch motion.

| | | SUSPENSION RATES (N/mm) | | | |
|---|---|---|---|---|---|
| | | FRONT | | REAR | |
| | | PITCH | BOUNCE | PITCH | BOUNCE |
| SIMULATED | HYDRAULIC | --- | 6.5 | --- | 6.8 |
| | DROP ANGLE | -1.0 | -1.0 | 2.0 | 2.0 |
| | PARASITIC | 2.8 | 2.8 | 3.0 | 3.0 |
| | TAPER | 12.1 | 12.1 | 12.4 | 12.4 |
| | **TOTAL** | **13.9** | **20.4** | **17.4** | **24.2** |
| MEASURED **TOTAL** | | **13.6** | **20.0** | **17.3** | **24.0** |

**Table 3.1** *Comparison of Simulated and Measured Hydragas Unit Rates*

In addition, simulated dynamic loads and pressures were compared with data measured on an experimental rig. This rig, also used for determination of effective diaphragm area as outlined earlier, is shown in figure 3.6. The hydragas unit piston was actuated sinusoidally at a number of frequencies, the demand actuator position being supplied by a signal generator. Readings were taken of piston load, hydragas fluid pressure measured outside the interconnection port, piston displacement and velocity. These are compared with the simulated results in figures 3.14 - 3.19.

It can be seen that the experimental input piston displacement was not perfectly sinusoidal which may account for some differences between simulated and experimental results. This was particularly noticeable at higher frequencies and the sharp peaks in actuator velocity account for the greater variation in experimental load and pressure compared to the simulated results at 5 Hz.

Also, the position of the pressure transducer outside the body of the unit may be the cause of discrepancies in the transient pressure readings. This had the effect of 'smoothing' transients for the experimental results. Nevertheless, correlation between the computer model and the measured dynamic behaviour is good.

For a complete validation of the interconnected Hydragas computer model, it was necessary to compare the results of the whole vehicle simulation with experimentally measured data. For this reason an interconnected Hydragas Metro was fitted with the active roll control system and tested.

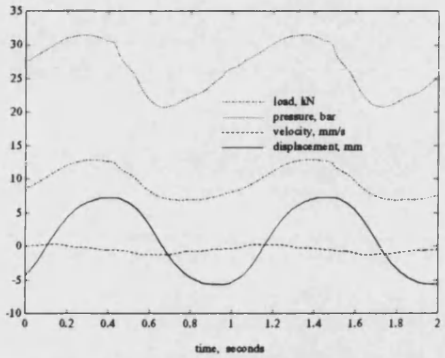


**Fig 3.14** *Results of Experimental Testing on Rear Hydragas Unit at 1Hz*

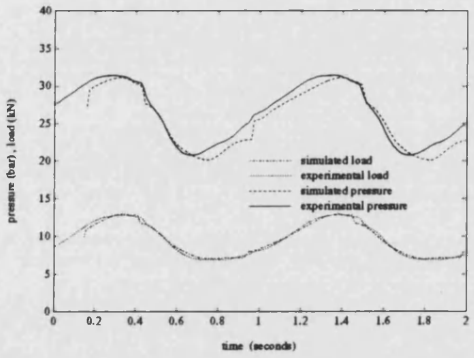


**Fig 3.15** *Comparison Between Experimental and Simulated Results at 1 Hz*

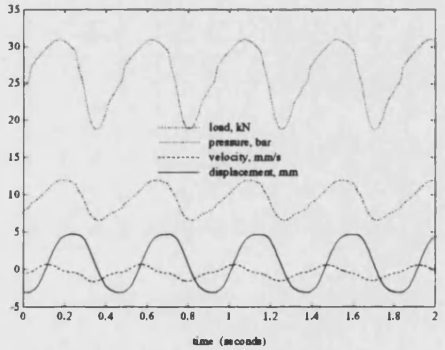


**Fig 3.16** *Results of Experimental Testing on Rear Hydragas Unit at 2 Hz*

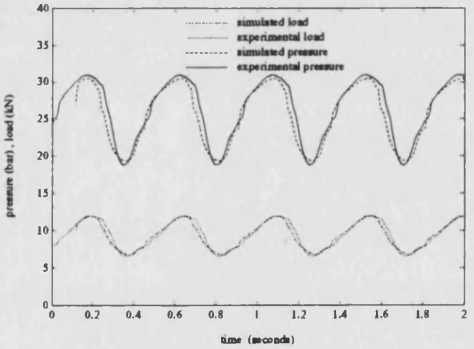


**Fig 3.17** *Comparison Between Experimental and Simulated Results at 2 Hz*

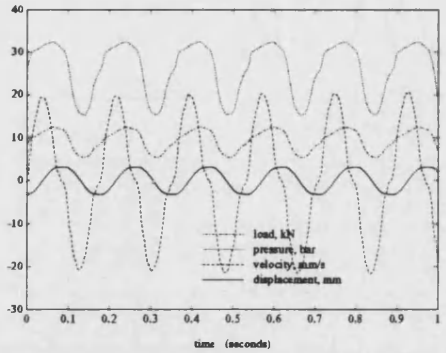


**Fig 3.18** *Results of Experimental Testing on Rear Hydragas Unit at 5 Hz*

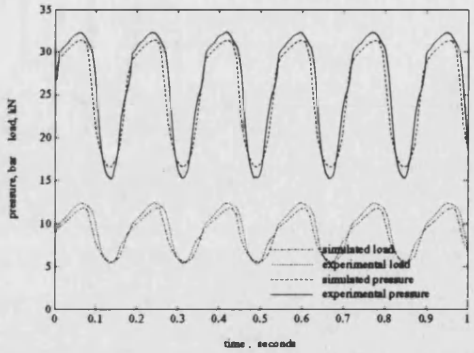


**Fig 3.19** *Comparison Between Experimental and Simulated Results at 5 Hz*

# 4. Experimental Vehicle Ride and Handling Tests

The vehicle tested was an Austin Metro 1.3 S , registration HHR 499 W. Initially employing independent Hydragas suspension units, the car was adapted for longitudinal interconnection by Moulton Developments Ltd. This vehicle was the original prototype developed to prove the benefits of interconnection on the Austin Metro.

The layout of the active roll control system on the boot of the metro is shown in figure 4.1. The batteries used to power both the motor and the electronics were housed in the box behind the shuttle, on top of which was an isolating switch which could be easily reached by the driver or passenger. The lengths of hydraulic pipework were kept to a minimum and pipes of equal length were used to connect the shuttle to the car interconnection lines on each side.

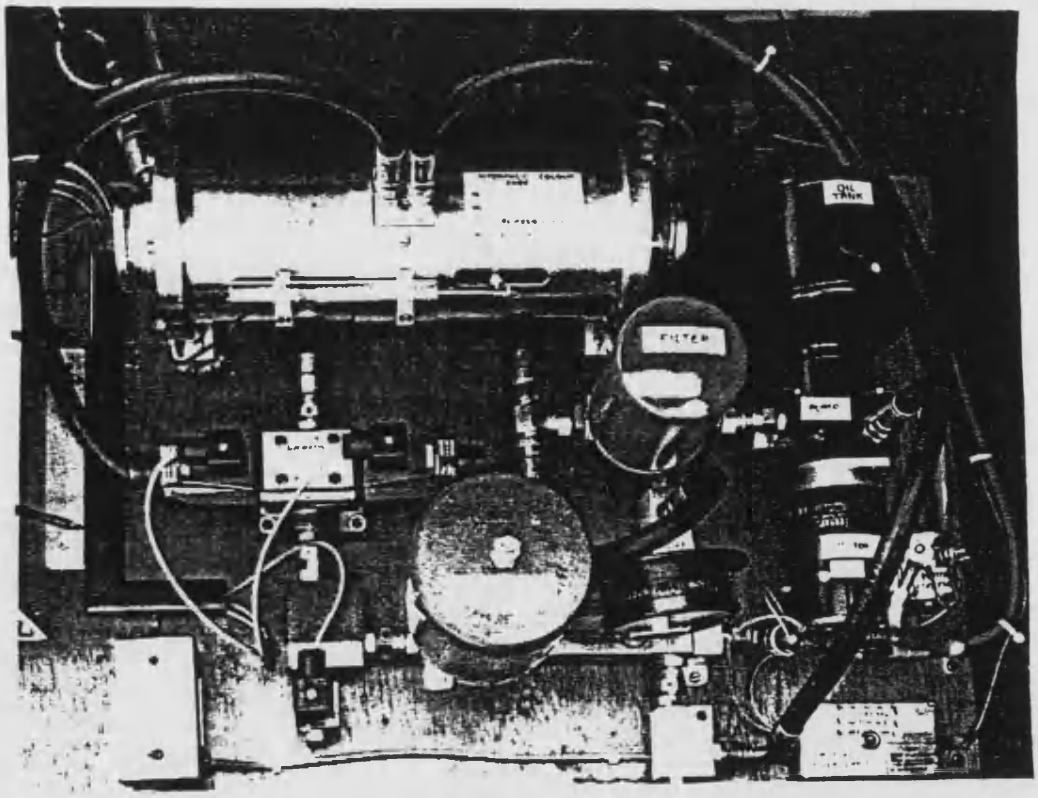

**Fig 4.1** *Hydragas Active Roll Control System Mounted on the Interconnected Metro*

## 4.1 Ride Testing

### 4.1.1 Test Set-up

Experimental vehicle ride testing was carried on the University four poster rig. A simple representation of this rig is shown in figure 4.2. The four wheels are supported by high pressure hydraulic cylinders which are controlled by two stage Vickers proportional valves. These valves receive, independently, signals from a control unit in conjunction with a P.C. and a tape player. The actuators may be controlled to move periodically in bounce, pitch, roll or warp motions or a sampled

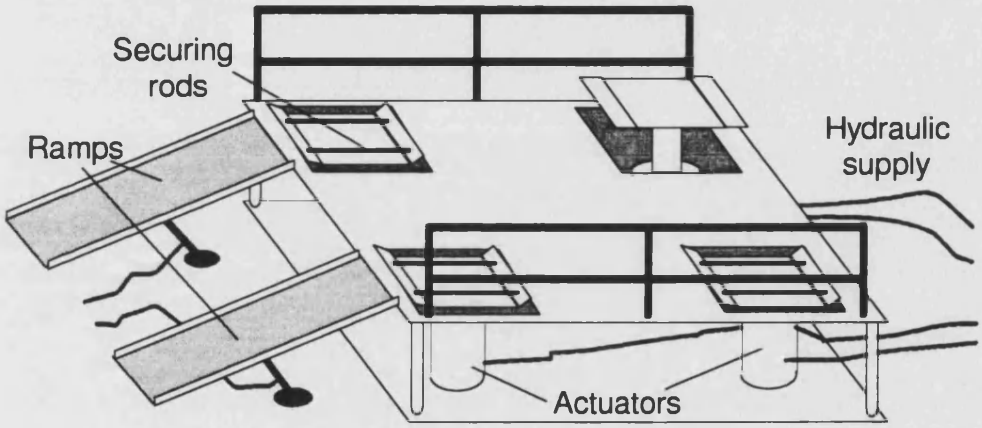


**Fig 4.2** *University of Bath Road Simulator 4-Poster Rig*

road profile may be followed.

The car was instrumented with three piezo-electric accelerometers mounted as shown in figure 4.3, as well as pull type position transducers measuring wheel to body displacement. The signals were fed to a separate P.C. with a data acquisition package ( Computerscope ). Furthermore, a Schlumberger Solartron 1250 frequency response analyser was used to control the frequency of motion and to analyse the frequency response of the vehicle.

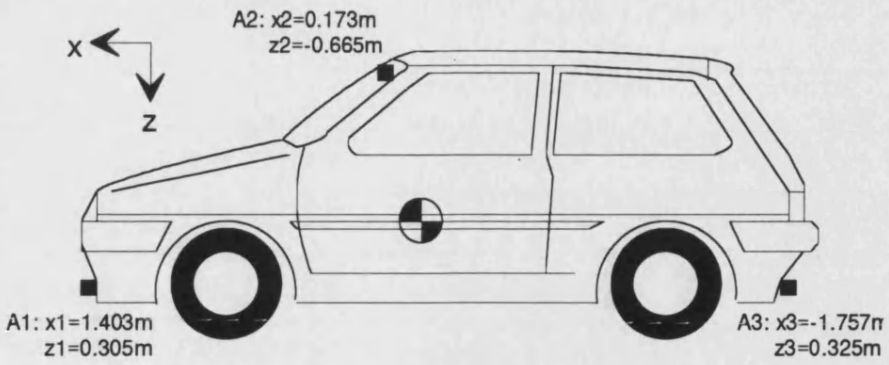


**Fig 4.3** *Positions of the Three Measurement Accelerometers*

### 4.1.2 Frequency Response Testing of the Vehicle

Frequency testing of the interconnected vehicle was carried out on the four poster rig in pitch, bounce and roll modes. Testing was performed with the aim of validating the frequency response of the computer model. For pitch and bounce excitation the accelerometers were mounted vertically, thus measuring vertical acceleration. For roll excitation, the accelerometers were mounted laterally. Vehicle accelerations were compared with input displacements in the frequency analysis and a transformation was used to find the displacement amplitude ratios as below.

$$20\log\left(\frac{y}{x}\right) = 20\log\left(\frac{\ddot{y}}{x}\right) - 40\log(\omega) \qquad \textbf{(4.1)}$$

where: y is the body displacement

x is the input displacement

ω is the excitation frequency

It should be noted that the only excess weight carried by the car was that of the data acquisition equipment and so the various modal frequencies may vary slightly from the 2 up condition used for simulation purposes. The frequency response of the car is shown in figures 4.4 - 4.6 for bounce, pitch and roll excitation. It was noted that the lateral movement of the vehicle due to compliance of the tyres was significant at some frequencies, particularly during roll excitation.

The main body pitch and bounce natural frequencies occur at around 2 Hz, the bounce natural frequency being slightly higher than for pitch. It is clear from the bounce plots that there is a strong influence on body motion at the front of the vehicle at around 16 Hz. This peak is less distinct at the rear of the vehicle, indicating that it may be caused by the oscillation of the engine on its mounts.

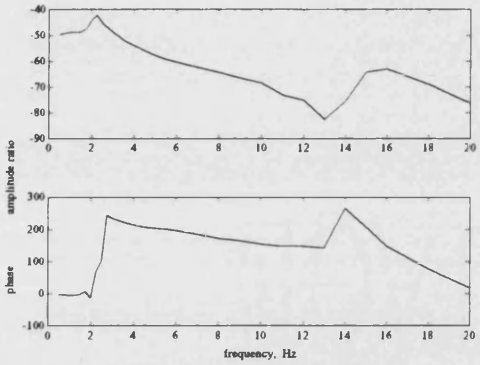


**Fig 4.4a** *Frequency Response of Metro at Front Accelerometer in Bounce*

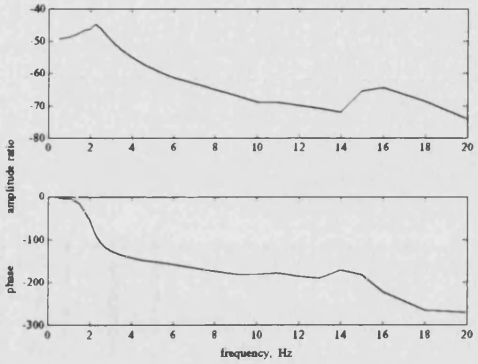


**Fig 4.4b** *Frequency Response of Metro at Rear Accelerometer in Bounce*

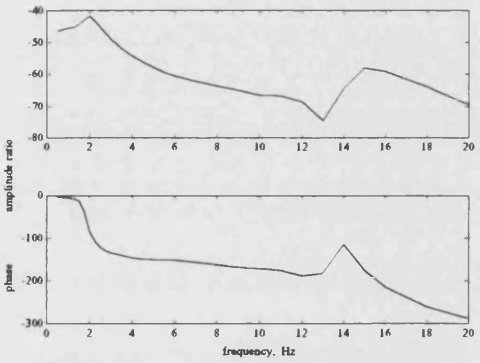


**Fig 4.5a** *Frequency Response of Metro at Front Accelerometer in Pitch*

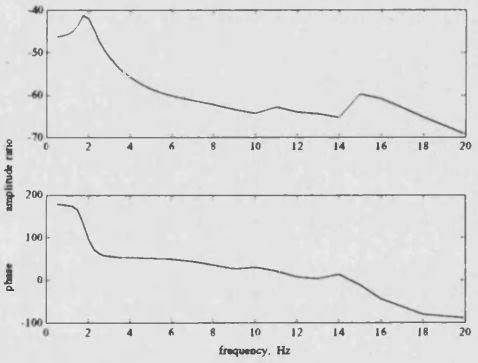


**Fig 4.5b** *Frequency Response of Metro at Rear Accelerometer in Pitch*

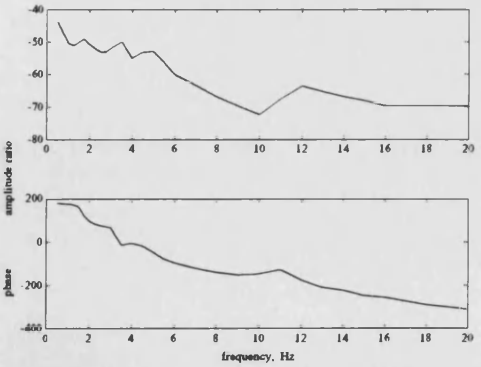


**Fig 4.6a** *Frequency Response of Metro at Front Accelerometer in Roll*

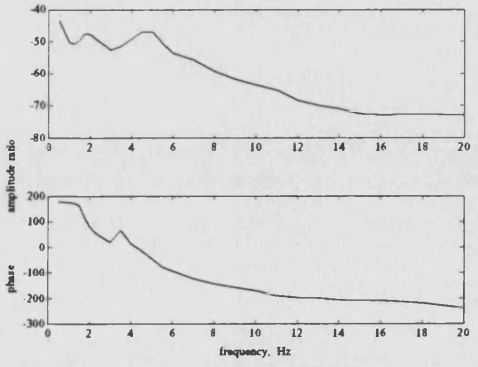


**Fig 4.6b** *Frequency Response of Metro at Rear Accelerometer in Roll*

The roll plots show rather indistinct peaks at around 2-4 Hz. It is likely that they represent the roll natural frequency of the body and also the lateral motion of the body on the tyres.

The signals from the three accelerometers recorded during a 2 Hz roll input are shown in figure 4.7. At this frequency the measured acceleration was greatest at the top of the car. When these signals are separated into lateral, roll and yaw components as shown in figure 4.8, it is clear that higher frequency components are present. This points to non-linear behaviour. It is also clear that for this type of disturbance there is a high degree of coupling between roll and lateral motions but little influence on yaw motion.

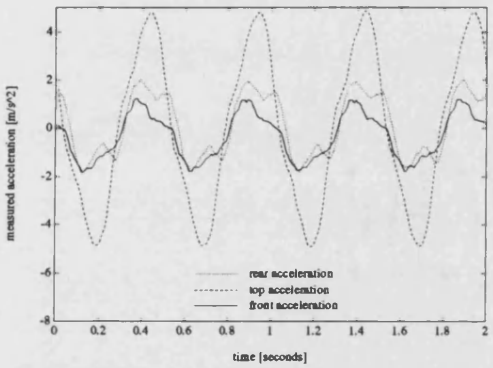


**Fig 4.7** *Measured Accelerations in 2 Hz Roll Excitation.*

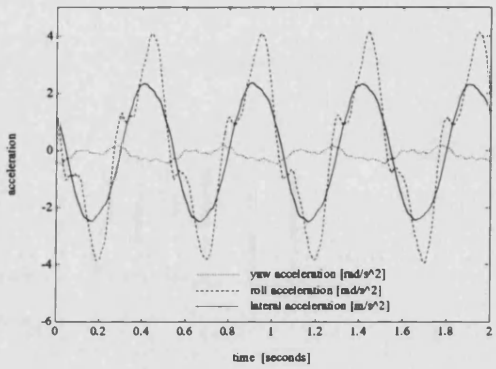


**Fig 4.8** *Components of Lateral, Yaw and Roll Accelerations in 2 Hz Roll Test*

### 4.1.3 Location of the Dynamic Roll Axis

The Kinematic roll centre is a well established concept [ 43 ] and provides a simple quantity to relate the lateral and roll motions of a car body. For ride purposes, it is also useful to determine the dynamic roll centre, defined here for free vibration as a nodal point about which the body rolls. The dynamic roll axis is therefore a longitudinal line joining these points. In free vibration at the modal frequency, lateral vibration on this axis will have zero amplitude. For more general forced vibration, the definition of the dynamic roll axis can be extended to mean the line which joins points of minimum lateral vibration amplitude. This concept is useful when considering the measurement of lateral acceleration on the vehicle body due to forcing inputs.

For this test, the three measurement accelerometers were mounted laterally as detailed previously and the car was excited in roll over a range of frequencies. The variation of acceleration amplitudes was recorded over a period covering a number of oscillations. This data was then processed to find the position of the dynamic roll centres above the front and rear axles. Note that the dynamic roll axis about which the body rolls does not necessarily coincide with the force roll centres used in lateral load transfer calculations. It is nevertheless useful to determine its location as it provides a quantity which can be used to analyse the roll and lateral motion characteristics of the vehicle.

The dynamic roll centres were found by calculating the heights above each axle at which average sideways acceleration is a minimum. The raw acceleration data was processed in Matlab using a series of functions to detrend the traces, find the components of lateral and roll accelerations and minimise functions of sideways acceleration with respect to vertical displacement from the body cg.

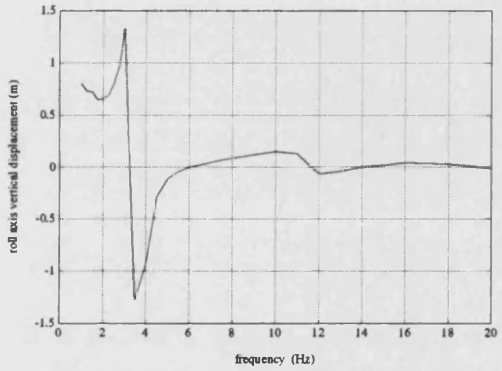


**Fig 4.9** *Variation in Dynamic Roll Axis Height with Frequency at Front Axle Position*

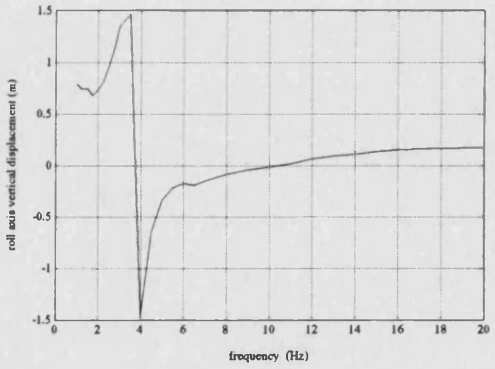


**Fig 4.10** *Variation in Dynamic Roll Axis Height with Frequency at Rear Axle Position*

The variation of roll centre heights versus frequency is shown in figures 4.9, 4.10. It can be seen that at a frequency of around 3 Hz at the front axle and 3.5 Hz at the rear axle, the roll centres moved sharply from below the centre of gravity to above it (note that SAE convention denotes displacement vertically downwards as positive). Below these frequencies the body lateral and roll motions were in phase. Above 3.5 Hz and 4 Hz respectively, the body lateral and roll motions were out of phase. There was a further discontinuity in roll centre height at the front axle at 12 Hz which was likely to be

caused by oscillation of the engine on its mounts. At high frequency (above 12 Hz), the dynamic roll centres were close to the c.g. position.

## 4.2 Static Testing of the Vehicle with Active Roll Control

### 4.2.1 Background to Testing

The prototype hydraulic active roll control system described previously was fitted to the test car for analysis. The hydraulic components were mounted on a board positioned in the boot of the car, along with batteries and the control system. The hydragas fluid outlets from the active shuttle were plumbed into the interconnection pipes of the car using ¼" B.S.P. flexible hosing. Sterling quick release couplings were incorporated into these lines so that the active system could be detached and reattached with a minimum of effort. A cut-off switch isolating the active system from its power supply was within easy reach of passenger and driver.

The system was initially controlled using a hand held electronic 'joy-stick' so that the shuttle could be actuated without a lateral acceleration demand. This allowed some of the basic performance properties of the system to be analysed independently of vehicle handling dynamics. Power supply to the control system was protected from fluctuations in supply current by the use of an Amplicon DC/DC converter.

Instrumentation included wheel-to-body height sensors in the form of pull-type position transducers, mounted on either side of the car at the front only, a differential pressure transducer measuring Hydragas fluid pressure difference across the car at the outlets of the shuttle, demand and feedback signals from the joystick and a position signal from an LVDT mounted on the shuttle. Finally a Hall effect ammeter measured the electric supply current into the power pack. Data were recorded using a P.C. based data acquisition package.

Power for the P.C. came from two 35 Ah 12V batteries via a Victron Atlas 750W inverter.

### 4.2.2 Performance Testing

The results presented are for a particular set of control system gains found experimentally to give system stability and reasonable response times suitable for roll control during manoeuvres. The response of the shuttle to a fast ramp input demand is shown in figures 4.11, 4.12. A time of 0.4 seconds to reach full stroke was found to be adequate to control vehicle attitude during manoeuvres. By calculating the maximum shuttle velocity it can be seen that the oil flow is considerably lower than that available from the proportional valve:

$$\begin{aligned} Q_{sh} &= 28 \times 10^{-3} \times 2206 \times 10^{-6} \times 60 \times 1000 \div 0.34 \\ &= 10.9L / \min \end{aligned} \tag{4.2}$$

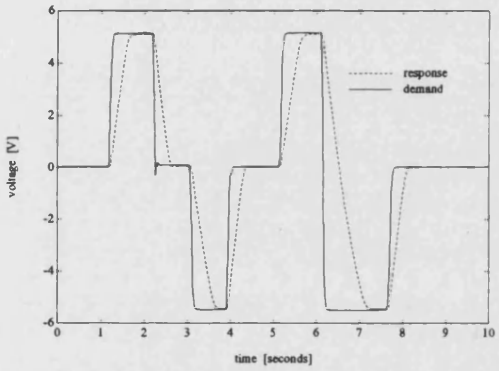


**Fig 4.11** *Response of Active Shuttle to a Fast Ramp Input From the Joy-stick*

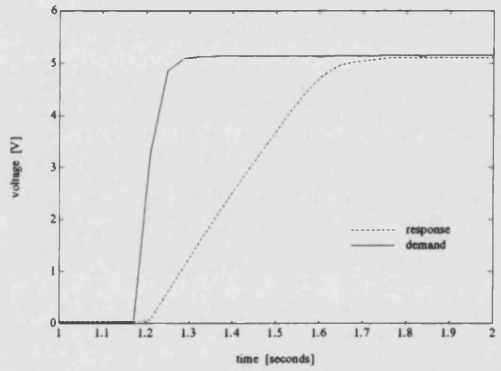


**Fig 4.12** *Detail of Active Shuttle Response to a Fast Ramp Input*

The body suspension roll due to this displacement of the shuttle is shown in figure 4.13. It can be seen that there is an overshoot of around 0.7° in one direction and a lesser overshoot in the other, probably due to friction in the suspension elements. The steady state roll angle achieved is around 3° in both directions.

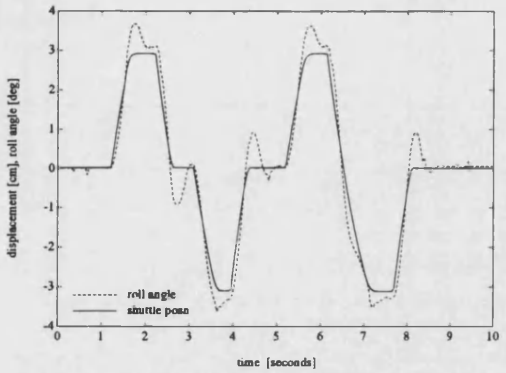


**Fig 4.13** *Roll Response to Displacement of the Shuttle for a Stationary Vehicle*

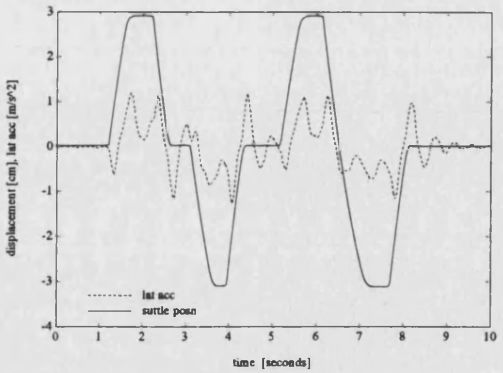


**Fig 4.14** *Lateral Acceleration Response Due to Roll Moment Input Generated by the Shuttle*

Figure 4.14 shows the consequence of the active roll control system on lateral acceleration. The applied roll moment causes a significant lateral acceleration to be recorded. This was a result of the coupling between the vehicle's lateral, roll and yaw motions. As lateral acceleration was to be the measured variable for non-stationary roll control, the effect is of importance. The control law used to govern suspension roll angle cannot be regarded as truly open loop as the output of the system has an effect on the input, i.e. a feedback path is present. The stability of the active roll control system is discussed further in chapters 6 and 7.

The influence of accumulator discharge is shown in figure 4.15. The accumulator supplies extra flow when the shuttle demand flow exceeds that available from the hydraulic pump. The accumulator is refilled during straight ahead driving when there is little or no demand from the actuator. Naturally, this additional supply of oil is not limitless and under extreme operating conditions, for instance in a slalom manoeuvre, the accumulator will become completely discharged. The system then relies on the pump alone to drive the actuator. It can be seen from the figure that the pump in isolation does not provide sufficient flow for good actuator response and this condition should be avoided if possible.

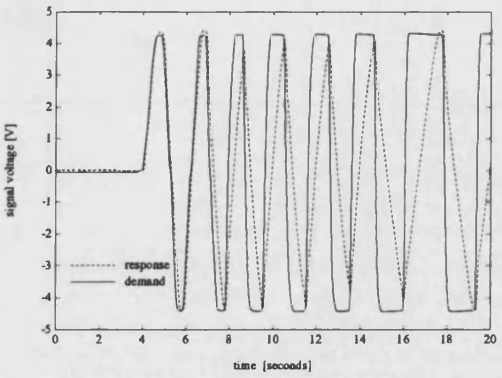


**Fig 4.15** *Effect of Accumulator Discharge on the Response of the Active Shuttle*

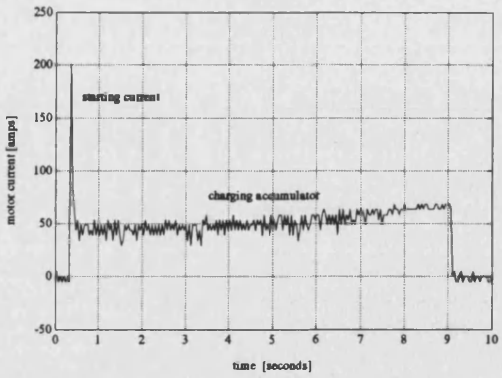


**Fig 4.16** *Current Delivered to Motor During Charge of the Accumulator (at 24V)*

The hydraulic power output of the pump was calculated from the time taken to fill the accumulator and the working pressures. The volume of oil stored by the accumulator at the maximum working pressure was 0.48 L, calculated using an isothermal relationship. The time taken by the pump to fill the accumulator was 9.0 seconds, giving a mean flow of 0.053 L/s ( 3.2 L/min ).

The mean pressure of the system was (140+60)/2 = 100 bar. Multiplying mean pressure difference across the shuttle by the mean flow into the shuttle gives a mean hydraulic power output, $P_{mean}$ of the system of 530 watts. Using the same flow rate and multiplying by the maximum system pressure (140 bar), the maximum power output, $P_{max}$, was 740 watts.

The electrical input current to the motor as the accumulator was charged is shown in figure 4.16. It is clear that a large current (200 amps) was required to start the motor. The frequent stopping and starting of the motor is therefore an undesirable feature. Following this the motor current dropped to a mean level of 40 amps, gradually building up to 70 amps as the pressure in the accumulator increased. The mean electrical power at a supply voltage of 24 V was 1.2 kW. The overall efficiency of the hydraulic power pack is :

$$\eta = \frac{530}{1200} = 44\% \qquad \textbf{(4.3)}$$

In normal driving conditions, the pump would operate only occasionally and so the mean power requirement would be considerably lower than the figures presented above.

## 4.3 Handling Tests

### 4.3.1 Instrumentation and Data Acquisition

Vehicle handling tests were carried out at the Rover test track at Gayden and at the University of Bath. In addition to the control transducers, from which measurement signals were available, the car was fitted with the following transducers:

- 3 piezo-electric accelerometers ( Access AMD CK/0 A10 +/- 10 g )
- 2 pull type displacement transducers ( Houston Scientific HSI 1850 - 0010 )
- 1 differential pressure transducer ( Sensotec model Z AD122 )
- 1 LVDT displacement transducer measuring steering rack position ( Penny and Giles HLP1905A1.200.8K/S )

The three accelerometers were mounted laterally under the front bumper, above the rear view mirror and below the rear bumper as shown in figure 4.3. Three accelerometers were required to resolve the components of lateral, roll and yaw acceleration from the measured signals.

The two pull type position transducers were mounted on the car body inside the engine compartment and attached to the top ball joints of the front suspension. These measured the suspension deflection on each side, from which the body suspension roll angle was calculated. Rear suspension deflections were not measured due to shortage of equipment and therefore the measured suspension roll angle assumed a rigid body.

The differential pressure transducer was mounted across the car as mentioned previously. This was sufficient to calculate the net forces imposed on the shuttle during manoeuvres and the overall active roll moment applied to the vehicle body. Steering angle was measured by a linear position transducer mounted on the steering rack. The relationship between steady state steering wheel angle and rack displacement was found to be linear. This transducer was useful in determining the car's handling behaviour and providing empirical steering inputs for simulation runs.

Information from the transducers was monitored using a P.C. based data acquisition package, Computerscope. A buffer of 20 seconds was used throughout testing with a sample rate of 25 Hz, sufficient to monitor the main handling modes. Data could be manipulated within the package so that quantities could be compared easily and exported as text files for processing in other packages. DC. values of measured parameters could be viewed using the monitor feature.

The P.C., card frame and computerscope hardware were secured in the passenger seat and footwell, with the keyboard positioned above the glove compartment on the dashboard so that the driver could control data acquisition 'in flight'. Results were saved onto the hard disk drive and onto floppy disks for analysis at a later stage.

### 4.3.2 Experimental Procedure

Three forms of handling test were performed: the slalom, step steer and steerpad manoeuvres. Slalom tests, as shown in figure 4.17, were performed with the intention of monitoring the dynamic behaviour of the vehicle and the active roll control system, in particular the degradation in roll control during repeated manoeuvres. As far as possible, the vehicle speed was maintained at a constant level as the car was manoeuvred through a number of equally spaced cones.

The step steer test gave an indication of the transient behaviour of the vehicle and the response of the active system. The car was driven in a straight line at constant speed and a step input was applied at the steering wheel. In reality the steering input resembled a rapid haversine. The car was then returned to straight ahead travel in a controlled manoeuvre.

**Fig 4.17** *The Slalom Manoeuvre*

The steerpad manoeuvre, shown in figure 4.18, gave an indication of the steady-state performance of the passive and active roll controlled vehicles. The car was driven in a constant radius while the speed was gradually increased, approximating steady-state behaviour. This

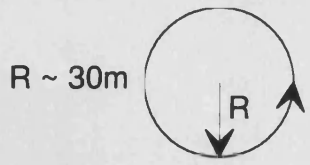


**Fig 4.18** *The Steerpad Manoeuvre*

test replaced earlier constant speed steerpad tests which proved lengthy to process and less indicative of the performance of the vehicle over a range of lateral accelerations.

Tests were carried out for both the passive ( active system disabled ) and active roll control vehicles in both directions ( clockwise and anti-clockwise ). Conditions for each were nearly identical. For all the active system tests, the demand control signal came from a separate accelerometer mounted laterally on the vehicle centre line. In the majority of tests, this was placed forward of and below the vehicle cg near the front bumper. The significance of this is discussed in the results section.

### 4.3.3 Data Processing

The experimental results were processed using Matlab [ 68 ]. Firstly, gains were applied to give parameter values in SI units. A simple transform was applied to the three sets of measured acceleration data to determine the separate components of lateral, roll and yaw acceleration relative to the vehicle cg. This transform related the components of lateral, roll and yaw acceleration to the positions of the three measurement accelerometers in the vehicle x and z directions with the cg as the origin. The measured accelerations comprised the following components:

$$\begin{aligned} A_1 &= A_{lat} + x_1 A_{yaw} - z_1 A_{roll} \\ A_2 &= A_{lat} + x_2 A_{yaw} - z_2 A_{roll} \\ A_3 &= A_{lat} + x_3 A_{yaw} - z_3 A_{roll} \end{aligned} \qquad \textbf{(4.4)}$$

$A_1$, $A_2$ and $A_3$ are the three measured accelerations at the front bumper, rear view mirror and rear bumper respectively. The x and z values are the longitudinal and vertical co-ordinates relative to the vehicle cg of the three accelerometers. The three equations may be rearranged to give expressions for lateral, roll and yaw accelerations. In this particular case, the equations are as follows:

$$\begin{aligned} A_{lat} &= 0.36A_1 + 0.321A_2 + 0.319A_3 \\ A_{yaw} &= 0.32A_1 - 6.47\times10^{-3}A_2 - 0.314A_3 \\ A_{roll} &= -0.625A_1 + 1.02A_2 - 0.398A_3 \end{aligned} \qquad \textbf{(4.5)}$$

Suspension roll angle was calculated by dividing the difference in suspension deflections by the distance between the position transducer mountings to give the inverse tangent of the roll angle.

### 4.3.4 Experimental Results

Comparisons of passive and active roll control vehicles during the three types of manoeuvre are presented. Sample traces are shown which were representative of the vehicle behaviour. These tests gave a good degree of repeatability.

STEERPAD MANOEUVRE

The main aim of the active Hydragas system was to reduce body roll angle during manoeuvres. The performance of the roll control system in realising this goal is shown visually in figures 4.19, 4.20 and graphically in figure 4.21. The figure shows steerpad manoeuvres in both clockwise and anti-clockwise directions. It can be seen that the active system was capable of cancelling out approximately 2.5 degrees of body suspension roll. The car body roll attitude was maintained at around zero degrees up to a lateral acceleration of around 0.4g. Beyond this point, the shuttle reached its end stops and was unable to displace any further fluid. As a result, the suspension roll angle increased at a rate similar to the passive system, therefore maintaining the reduction in roll attitude.

Statistical evidence has shown [ 69 ] that a cornering manoeuvre of above 0.4g is uncommon in everyday driving and can be regarded as severe. It is arguable therefore that a certain amount of body roll at lateral accelerations above this level is desirable from a safety perspective. It also gives the driver a 'feel' for the more extreme cornering manoeuvres.


**Fig 4.19** *Passive Car in 25 mph Steerpad Manoeuvre*


**Fig 4.20** *Active Car in 25 mph Steerpad Manoeuvre*

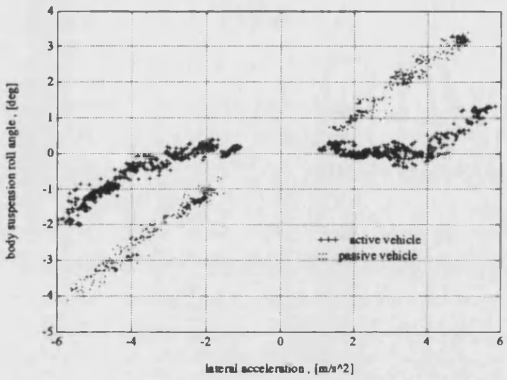


**Fig 4.21** *Body Suspension Roll Angle in Quasi-Steady State Steerpad Test*

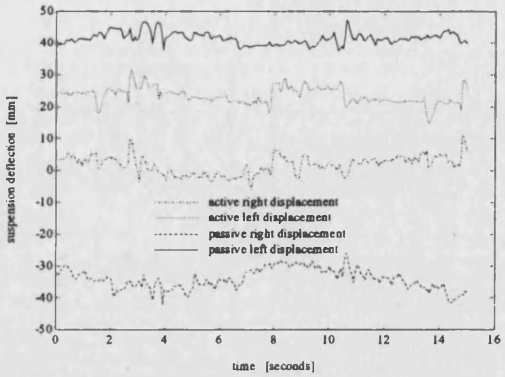


**Fig 4.22** *Suspension Deflections in 20m/s Steerpad Test*

Figure 4.22 shows how the body suspension roll angle was developed in a constant speed steerpad test. The suspension on the outside of the corner deflected in the bump direction while the suspension on the inside deflected in the rebound direction. However, for the active vehicle, the deflections were not equal in magnitude. It can be seen that the front suspension on the outside of the corner deflected little. However, the deflection of the front suspension on the inside of the corner was only partially prevented. Therefore, roll was reduced but there was a net lifting of the car body ('jacking'), i.e. the mean front suspension deflection was above zero.

The change of centre of gravity height with increasing lateral acceleration for the active vehicle is shown in figure 4.23. The cause of this was the changing diaphragm area of the active Hydragas shuttle. A deflection of the shuttle away from centre displaced more Hydragas fluid from one side than was drawn in by the other. There was therefore a net total displacement of fluid from the shuttle to the suspension during manoeuvres. Clearly there is considerable scatter on the experimental results but the trends are evident.

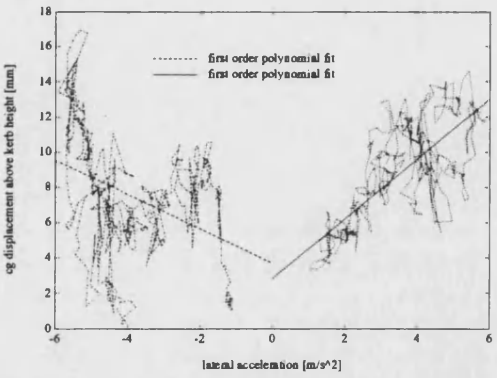


**Fig 4.23** *Change in Centre of Gravity Height with Lateral Acceleration for Active Vehicle*

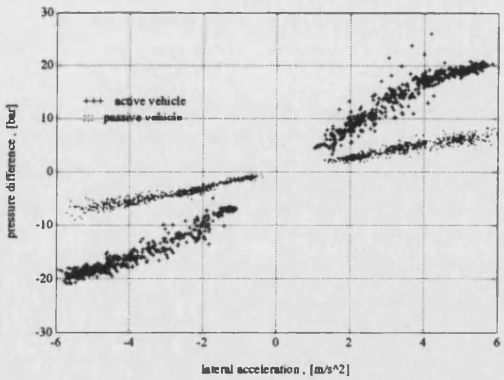


**Fig 4.24** *Pressure Difference Across the Car in Quasi- Steady State Steerpad Test*

The steady state Hydragas fluid pressure difference across the car is plotted against lateral acceleration in figure 4.24. This pressure difference , together with the other suspension forces mentioned previously, is a reaction to the roll moment acting on the vehicle during manoeuvres. The roll moment and associated pressure difference increases with lateral acceleration. This is apparent from the figure.

Since the suspension roll angle was reduced or eliminated by the active system, the passive secondary suspension effects (taper, parasitic and drop angle rates) were less important. Therefore, the active roll cancellation moment was generated by increasing the unit differential pressure to a greater extent than the passive vehicle by means of the active roll control shuttle. It is clear from the figure that beyond 0.4g, where the shuttle reached its end stop and the body started to roll, the change of pressure difference with lateral acceleration decreased to a level similar to that of the passive car.

The relationship between steering wheel angle and lateral acceleration is shown in figure 4.25. There was a tendency for both the passive and active vehicles to slightly understeer, with understeer increasing at high lateral accelerations. The active roll control system appeared to have only a small effect on the steady state steering characteristics of the car. However, the steering wheel angle for the active car was consistently smaller than for the passive car. The principal reason for this is the roll steer effect built in to the suspension geometry as a safety feature of the passive vehicle. With increasing roll, the steer angle of the wheels decreases. Without body roll, this effect is not apparent so the steering wheel angle required is less for a turn of similar radius.

In addition to the roll steer effect, there will be a change in handling characteristics caused by the elimination of taper, parasitic and drop angle rate effects and the associated front to rear load transfer distribution. This is explained more fully in due course. It is interesting to note that when the shuttle saturates at high lateral accelerations, the active vehicle steer characteristic changes.

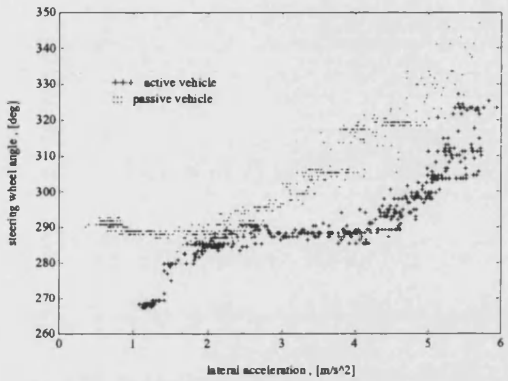


**Fig 4.25** *Steering Wheel Angle Change With Lateral Acceleration in Quasi-Steady State Steerpad Manoeuvre*

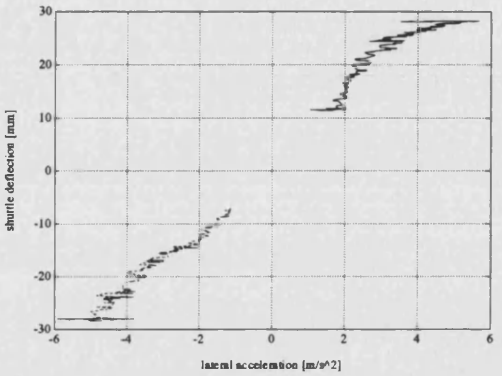


**Fig 4.26** *Displacement of Active Roll Control Shuttle in Response to Lateral Acceleration*

The movement of the roll control shuttle in response to the accelerometer demand signal is shown in figure 4.26. It is possibly not linear because the control system demand signal consisted in fact of lateral, yaw and roll components rather than pure lateral acceleration.

## SLALOM MANOEUVRE

The three measured acceleration signals for the passive vehicle are shown in figure 4.27. The sideways acceleration at the front of the car led that measured at the middle of the car which in turn led that measured at the rear. This was to be expected as the cornering forces used to steer the car are developed initially at the front wheels ( i.e. the steered wheels ). The magnitudes of the three accelerations were similar. When resolved into separate components of lateral, yaw and roll acceleration, as in figure 4.28, it can be seen that the lateral and yaw accelerations are of a greater magnitude than roll acceleration, with yaw leading lateral acceleration.

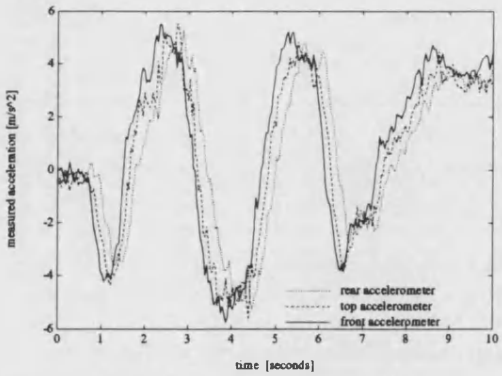


**Fig 4.27** *Measured Accelerations in Slalom Manoeuvre*

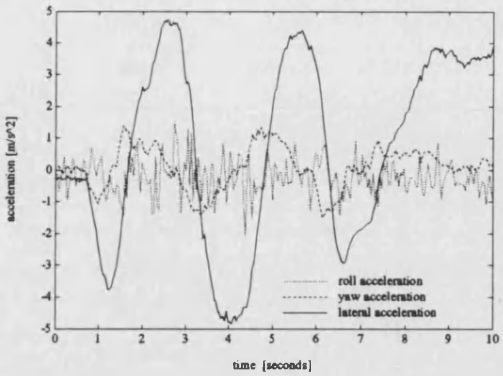


**Fig 4.28** *Components of Lateral, Yaw and Roll Acceleration in Slalom Manoeuvre*

The passive suspension roll angle variation is shown in figure 4.29. The roll angle slightly lagged the lateral acceleration which brought it about. The values of roll angle were quite high and subjectively felt considerable.

The effect of the active roll control system is demonstrated in figure 4.30. It can be seen that the suspension roll angle was considerably reduced when compared with the passive car. It is thought that the high frequency roll oscillation present was caused by road excitation and was not a function of the active vehicle handling dynamics. It was concluded that the response of the active system was sufficient to control the dynamic behaviour of the car. As the accumulator discharged, the performance of the system degraded, although the suspension roll angle was still lower than that of the passive car.

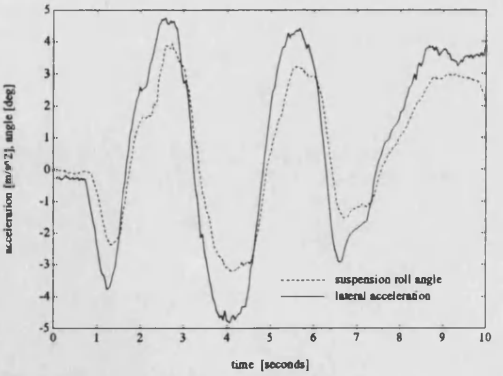


**Fig 4.29** *Suspension Roll Angle of the Passive Vehicle in a Slalom Manoeuvre*

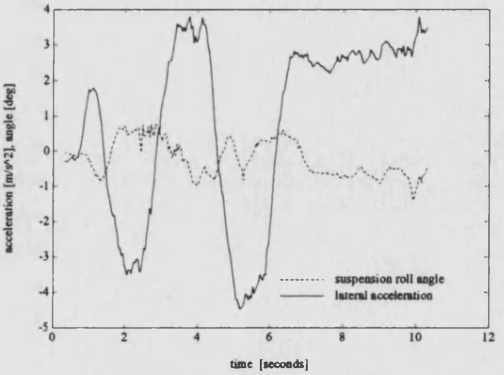


**Fig 4.30** *Suspension Roll Angle of the Active Vehicle in a Slalom Manoeuvre*

The degradation of system performance with time can be seen more clearly by plotting the suspension roll angle against lateral acceleration , figure 4.31. As the later cones were rounded, the roll angle became greater. Methods of preventing this reduction of performance are discussed in a latter section.

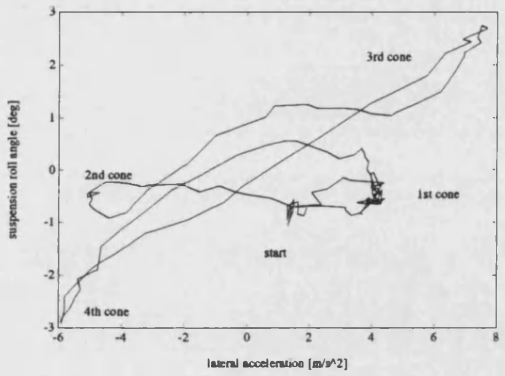


**Fig 4.31** *Suspension Roll Angle in Slalom Manoeuvre Plotted Against Lateral Acceleration*

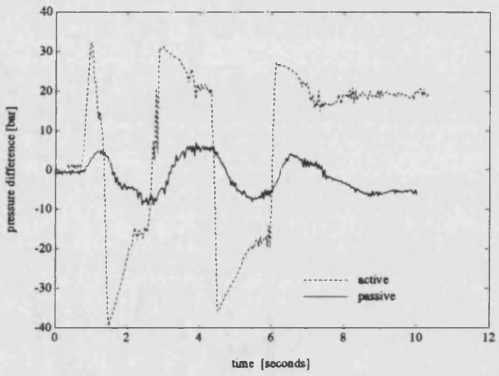


**Fig 4.32** *Pressure Difference Across the Car in a Slalom Manoeuvre*

The side to side pressure difference developed during the slalom manoeuvre is shown in figure 4.32. There was a substantial amount of noise in the pressure signal due to undulations in the road surface, however the overall trend for the passive car is clear. For the active vehicle, the results were more complicated. There were large transient peaks in pressure difference across the car when the lateral acceleration passed through zero ( i.e. the car changed direction ). This was found to be due to flow restrictions between the active hydragas shuttle and the suspension interconnection pipes into which the flow was passing. The magnitude of these transient peaks corresponds to an effective damper orifice of 2.5 mm bore. Unfortunately it was not possible to modify the prototype vehicle in order to remove this restriction and improve the active system performance.

Evidence that the transient pressure peaks were caused by a velocity effect is given in figure 4.33. The pressure difference is plotted along with shuttle position and velocity for the slalom manoeuvre. It is clear that the steady state pressure difference is dependant on the shuttle position whereas the transient peaks depend on the shuttle velocity.

The Hydragas fluid differential pressure was measured at the outlets of the active roll control shuttle where transients were particularly noticeable. Had it been measured in the suspension units themselves, the transient effects would have not have been as apparent. Therefore the sharp transient peaks were not transmitted through the suspension units to the car body and ride harshness was not a problem.

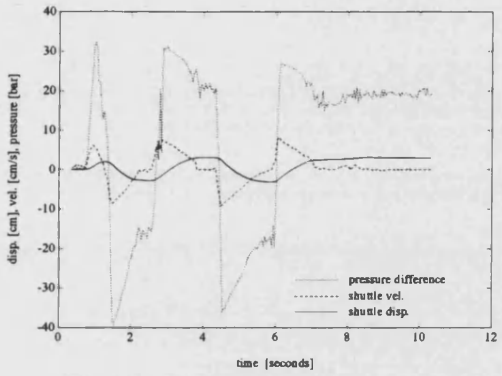


**Fig 4.33** *Side-to-side Pressure Difference in Slalom Manoeuvre with Shuttle Displacement and Velocity*

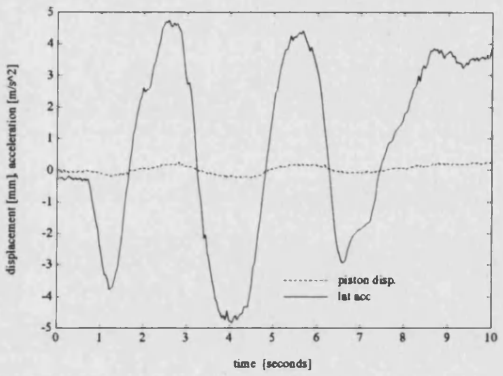


**Fig 4.34** *Shuttle Displacement due to External Disturbances in Passive Mode for Slalom Manoeuvre*

Figure 4.34 shows the movement of the roll control shuttle caused by external forces, i.e. road and inertial inputs, for the car in passive mode. It is clear from the figure that the shuttle displacement is minimal. It is important that the active shuttle is not excited by road disturbances as the feedback signal thus measured would result in additional valve flow and associated power consumption. Ride control was not the intention of the roll control system and would simply result in an increase in power consumption.

## STEP STEER MANOEUVRE

The lateral acceleration and resultant suspension roll angle for the passive car in response to a step input in steering wheel angle are presented in figure 4.35. It is evident that the roll angle lagged the lateral acceleration as the vehicle roll dynamics were slower than the generation of tyre side forces. The roll angle for the active system was considerably reduced as shown in figure 4.36. The active

system dynamics were fast enough to respond to the rapid lateral manoeuvre ( figure 4.37 ). This is due in part to the positioning of the demand accelerometer which provided a component of yaw acceleration as well as lateral acceleration.

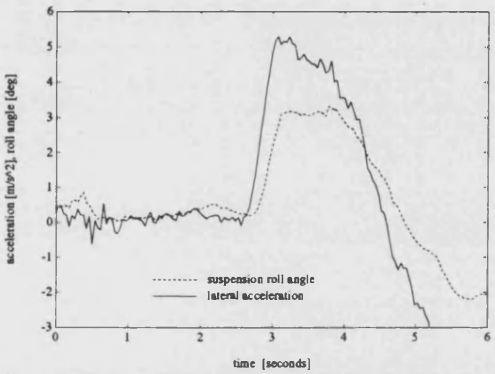


**Fig 4.35** *Suspension Roll Angle of Passive Vehicle in Step Steer Manoeuvre*

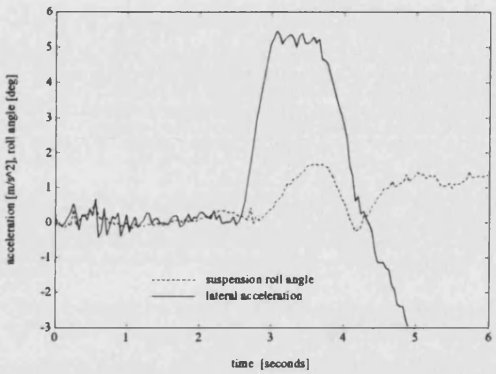


**Fig 4.36** *Suspension Roll Angle of Active Vehicle in Step Steer Manoeuvre*

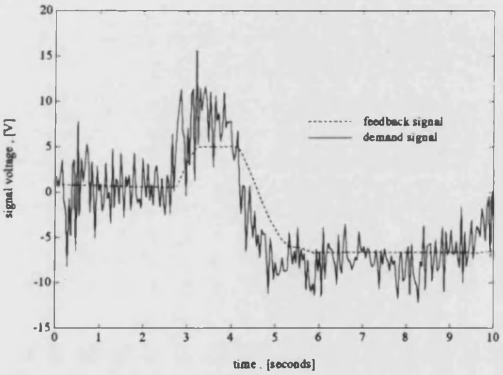


**Fig 4.37** *Demand and Feedback Signals in Active Vehicle Step Steer Manoeuvre*

The accelerometer was mounted initially on a bracket attached below the front bumper of the car. This was some 1.1m ahead of the vehicle cg. The vertical position was adjustable but was kept below the cg. height for reasons of stability. The measured acceleration therefore contained components of lateral, yaw and, to a lesser extent roll acceleration. In a cornering manoeuvre, yaw motion is developed before lateral motion ( see figure 4.28 ) as slip angles and tyre forces are generated at the front wheels before the rear wheels.

Because the system demand signal contained a component of yaw acceleration, it had a certain degree of preview of the lateral acceleration which followed. There was subsequently more time for

the active shuttle to react to the roll moment developed as a result of the lateral acceleration. Several accelerometer positions were investigated in this work.

In figure 4.38, a comparison is made between the active system with the accelerometer mounted at the front of the car and at the cg. longitudinal position. Direct comparison is difficult since it was not possible to achieve identical repeatable manoeuvres, however it was felt that the system using the accelerometer mounted at the cg. did not respond as quickly as that with the accelerometer mounted further forward. From a response viewpoint, the yaw acceleration 'preview' achieved by mounting the accelerometer forward of the cg. appears to be advantageous. The implications of this mounting position in extreme circumstances such as skidding, in which the magnitude of yaw acceleration is greater than would be the case in normal manoeuvring, are likely to be less desirable and therefore a compromise position slightly ahead of the cg. is recommended.

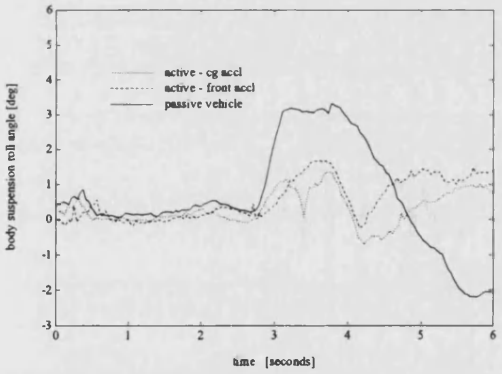


**Fig 4.38** *Suspension Roll Angle in Step Steer Manoeuvre for Passive and Active Car with Two Accelerometer Mounting Positions*

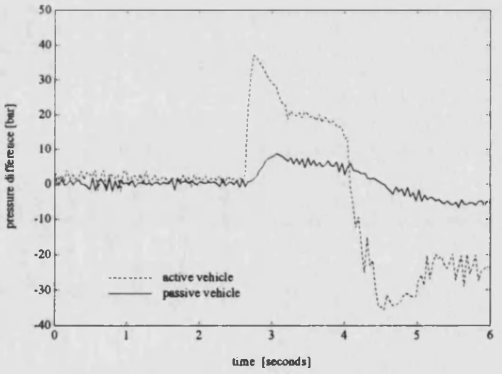


**Fig 4.39** *Side-to-side Pressure Difference for Passive and Active Cars in Step Steer Manoeuvre*

The side-to-side pressure difference for both passive and active vehicles is shown in figure 4.39. Again the transient peak is evident for the active system. Assuming no suspension roll and hence no roll cancellation moment due to suspension unit taper, parasitic and drop angle rates, the peak steady

state pressure difference of 8 bar corresponds to a suspension unit lateral load transfer of approximately 3 kN at a lateral acceleration of 0.5g.

The front to rear distribution of wheel load transfer is dependant on the suspension unit diaphragm areas and lever ratios. Since both of these parameters vary with suspension deflection it was inevitable that the passive and active vehicles would have different front to rear lateral load transfers during manoeuvres. This explains the difference in handling characteristics of the passive and active vehicles.

## EXTREME MANOEUVRES

Although it was not possible to take experimental measurements during extreme manoeuvres when the vehicle lost traction there were a number of effects worthy of note. The respective roll attitudes of the passive and active cars are shown for a lane change manoeuvre at 60 m.p.h. in figures 4.40, 4.41.

In the passive vehicle, excessive body roll during high lateral acceleration manoeuvres caused the suspension to run out of travel and reach its 'bump stops'. The major change in suspension rate caused by the bump stops led to a sudden variation in front to rear lateral load transfer distribution and a highly unpredictable handling characteristic.

In the active vehicle, the roll control elements prevented excessive suspension travel during violent manoeuvres. As a result, the suspension bump stops were not met, the suspension rates remained nearly linear and the front to rear lateral load transfer distribution was controlled. This meant that the limit lateral acceleration capability of the active vehicle was greater than that of the passive vehicle and it could be argued that the active vehicle was safer during violent manoeuvres.


**Fig 4.40** *Passive Car in Extreme Lane Change Manoeuvre at 60 mph.*


**Fig 4.41** *Active Car in Extreme Lane Change Manoeuvre at 60 mph.*

# 5. Vehicle Simulation Model Validation

## 5.1 Parametric Data for Vehicle model

Model parameters were derived by direct measurement and from data supplied by Rover Cars and Moulton Developments.

Mass and inertia properties of the sprung and unsprung masses were supplied by Rover and modified to include the effects of the driver, active roll control system and data acquisition equipment in the case of the sprung mass. The geometry of the vehicle was also supplied including c.g. positions of the car body and wheels and body eyebrow heights at kerb.

Tyre data was supplied in graphical form, giving cornering and longitudinal behaviour. Values were given for tyre vertical stiffness and rolling radius. Front and rear track, steering ratio and braking distribution were also supplied.

Vehicle suspension characteristics were derived from different sources. Data concerning the variation of wheel camber and toe with vertical deflection were supplied in graphical form. Polynomial curves were fitted to these graphs for incorporation into the BATH*fp* model. The tyre contact paths with vertical deflection were measured from drawings of the front and rear suspensions and curves were then fitted to these measured values. Suspension compliance characteristics were supplied by Rover.

## 5.2 Passive Vehicle Ride Simulation

### 5.2.1 Single Frequency Testing in Bounce, Pitch and Roll

The frequency response of the car body to single frequency road inputs was tested using the simulation model. The road input signal was provided by a single sinusoidal signal model. This was passed to the tyres via models which converted the demand signal to road displacement and velocity at

each wheel. Gains were applied so that the vehicle could be excited in bounce, pitch, roll and warp modes. Only the first three of these were considered. The variables examined were body accelerations at the cg. and the input displacement. These data were then processed in a similar manner to those measured experimentally using the four poster road simulation rig.

The body ride amplitude plots shown in figures 5.1 - 5.3 show that the computer simulation accurately predicted the body main ride frequencies in bounce, pitch and roll. The pitch natural frequency is slightly lower than that in bounce. The roll natural frequency is significantly higher. The prediction of wheel hop frequencies is not shown as they were above the frequency range of the simulation. Ride effects due to other component masses such as the engine are not apparent as the vehicle model did not include terms for these components.

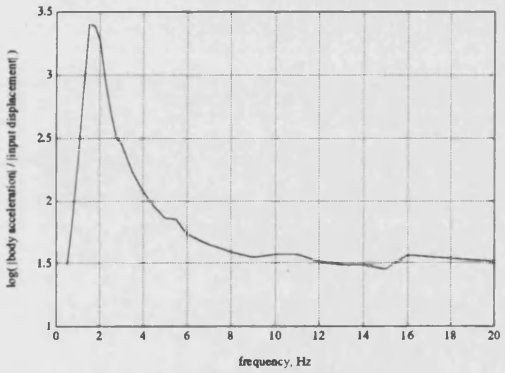


**Fig 5.1** *Simulated Frequency Response of Metro in Bounce Excitation*

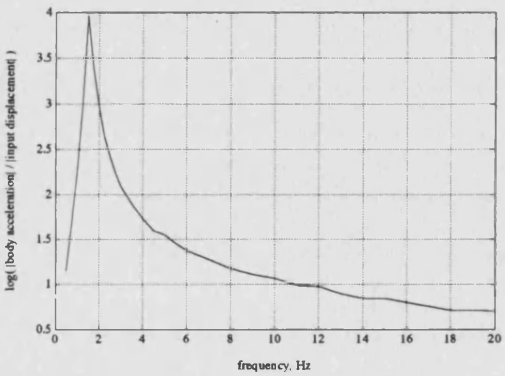


**Fig 5.2** *Simulated Frequency Response of Metro in Pitch Excitation*

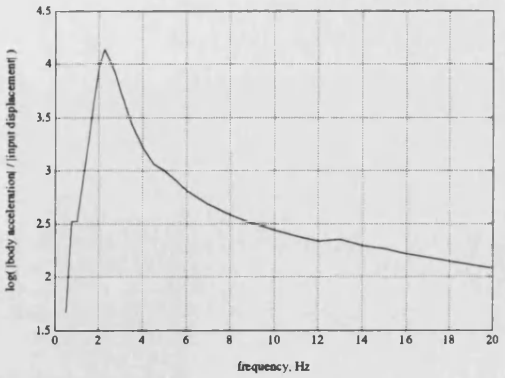


**Fig 5.3** *Simulated Frequency Response of Metro in Roll Excitation*

It would appear that the accuracy of the computer simulation is greatest at low frequency, and does not accurately predict wheel hop motions. For handling work this is sufficient as handling dynamics will be at low frequency ( < 10 Hz ).

### 5.2.2 Response of the Vehicle Model to a Sampled Test Track

In addition to the single frequency testing, the vehicle model was also subjected to a sampled real road input. The road used was the Moulenweg cobbled test track [ 70 ]. Sampled data was available for both tracks and a time delay was introduced between the front and rear wheels depending on the vehicle forward speed.

The simulation was then run with the vehicle travelling at different speeds. Body acceleration data were recorded and analysed using the Matlab suite of mathematical functions. Text files containing acceleration data in the time domain were manipulated such that power spectral densities of the various body accelerations were found. These are presented along with the power spectral density of the road itself at each speed.

**5 m/s :**

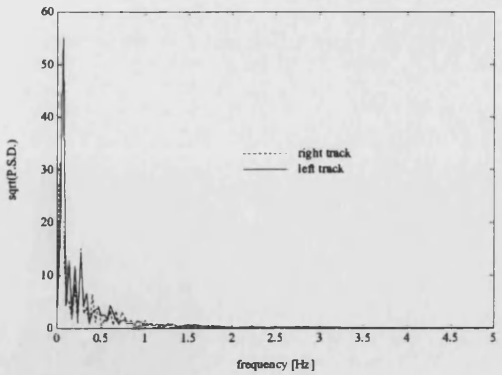


**Fig 5.4** *Power Spectrum of Road Displacement at 5 m/s*

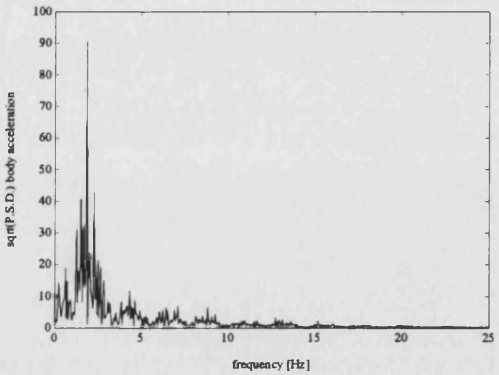


**Fig 5.5** *Power Spectrum of Body Vertical Acceleration at 5 m/s*

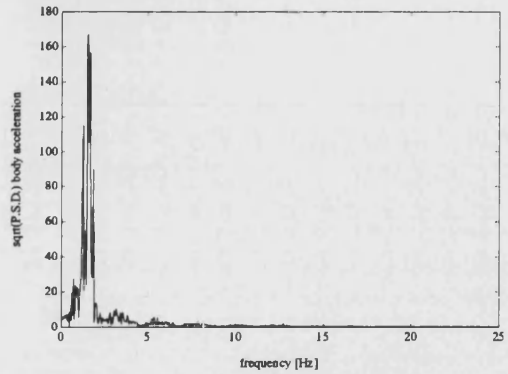


**Fig 5.6** *Power Spectrum of Body Pitch Acceleration at 5 m/s*

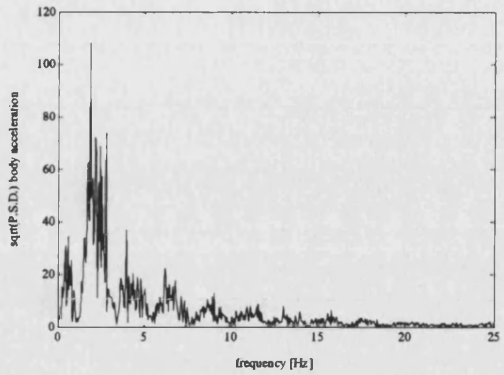


**Fig 5.7** *Power Spectrum of Body Roll Acceleration at 5 m/s*

**10 m/s :**

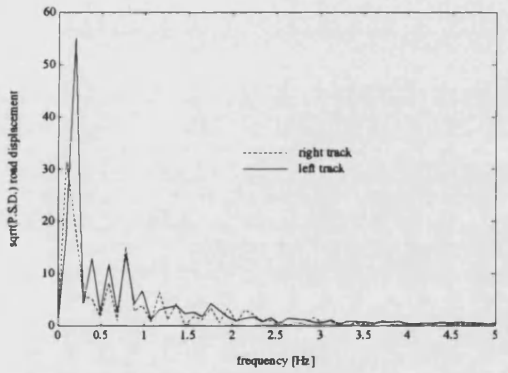


**Fig 5.8** *Power Spectrum of Road Displacement at 10 m/s*

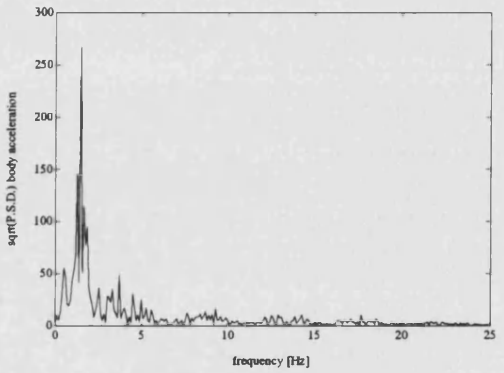


**Fig 5.9** *Power Spectrum of Body Vertical Acceleration at 10 m/s*

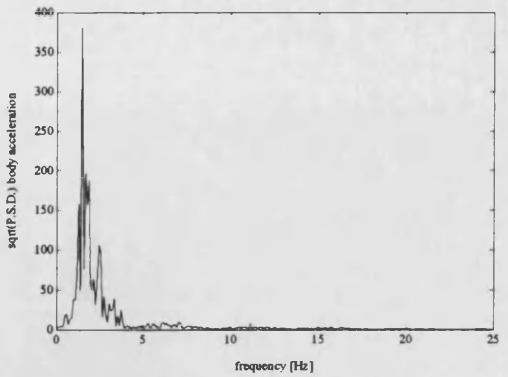


**Fig 5.10** *Power Spectrum of Body Pitch Acceleration at 10 m/s*

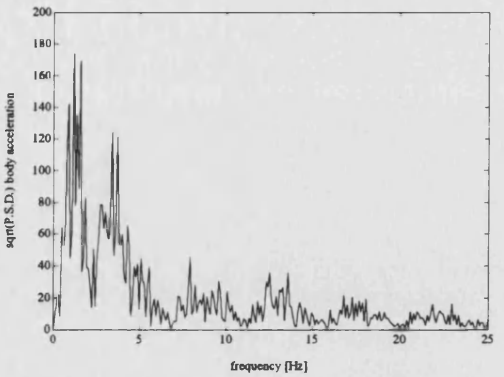


**Fig 5.11** *Power Spectrum of Body Roll Acceleration at 10 m/s*

**20 m/s :**

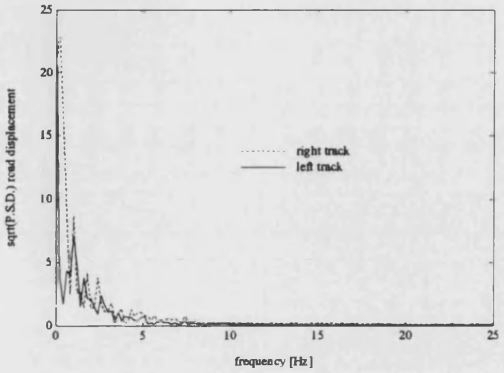


**Fig 5.12** *Power Spectrum of Road Vertical Displacement at 20 m/s*

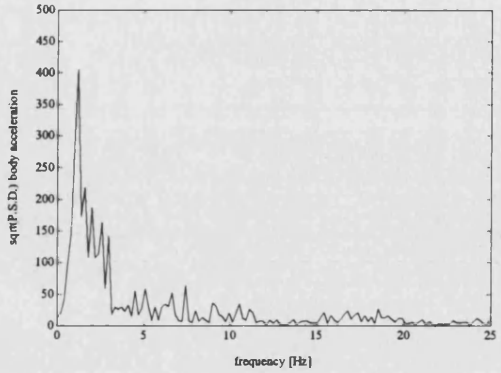


**Fig 5.13** *Power Spectrum of Body Vertical Acceleration at 20 m/s*

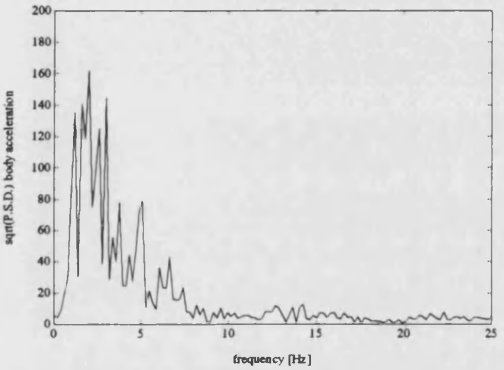


**Fig 5.14** *Power Spectrum of Body Pitch Acceleration at 20 m/s*

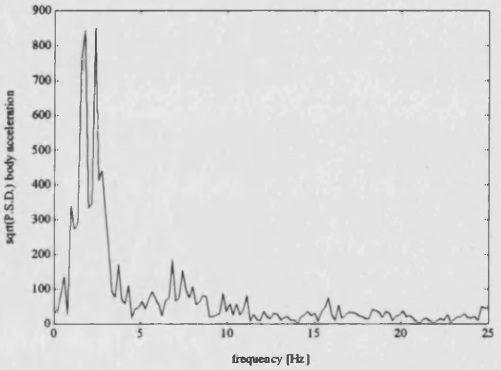


**Fig 5.15** *Power Spectrum of Body Roll Acceleration at 20 m/s*

The sampled right and left tracks of the road profile are shown in figure 5.16.

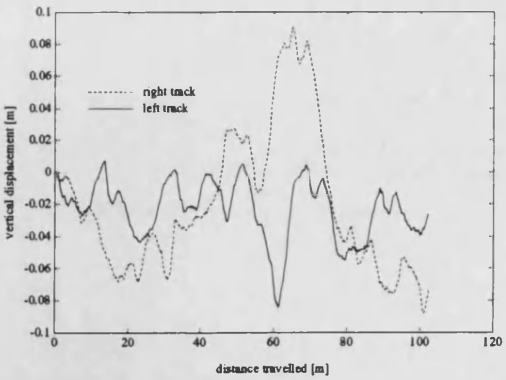


**Fig 5.16** *Left and Right Tracks of Sampled Road Profile*

Since the road displacement power spectral density at each of the three forward speeds has a rich frequency content in the range 0-5 Hz, the body response is dependant primarily on the secondary suspension and body inertial properties. The peak acceleration frequencies are the same as those identified in the single frequency excitation tests.

The magnitude of the peak value of vertical acceleration appears to increase with forward speed, while the frequency at which this peak occurs remains constant. The increase in magnitude may therefore be attributed to the increased road input power at that frequency at higher speeds. Roll acceleration magnitude also appears to increase with forward speed. The pitch results show a somewhat different trend. At 5 and 10 m/s, the power content of pitch oscillation appears to be largely concentrated at the pitch natural frequency. The magnitude of the peak value is greater for the higher speed. At 20 m/s however, pitch acceleration appears to be greatly reduced, particularly at the pitch natural frequency. The fluid interconnection seems to have a greater effect on pitch motion at high speed.

It is interesting to note that the body vertical acceleration response is influenced by the well known wheelbase filter effect [ 57 ]. Figure 5.9 shows distinct troughs in body acceleration P.S.D. at regular, approximately 4.5 Hz intervals. This, in combination with a forward speed of 10 m/s suggests a wavelength of approximately 2.2m, compared with a vehicle wheelbase of 2.269m.

### 5.2.3 Step Pitch Input Applied at the Wheels

This test aimed to compare the performance of both the interconnected and non interconnected Hydragas suspensions upon meeting an obstacle such as a kerb. The influence of the fluid interconnection inherent in the current Metro suspension system is shown in figures 5.17, 5.18. It can be seen that the reduced individual wheel rate arising from interconnection reduced the peak pitch acceleration felt by the passengers by over 0.1 $m/s^2$. However, the reduced pitch damping of the interconnected system was less able to control the pitch oscillation following the initial excitation. It can be concluded that the interconnection reduces ride harshness and improves comfort

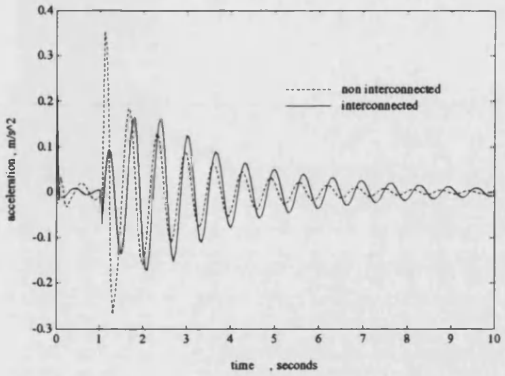


**Fig 5.17** *Bounce Acceleration Response to Step Pitch Input at the Wheels*

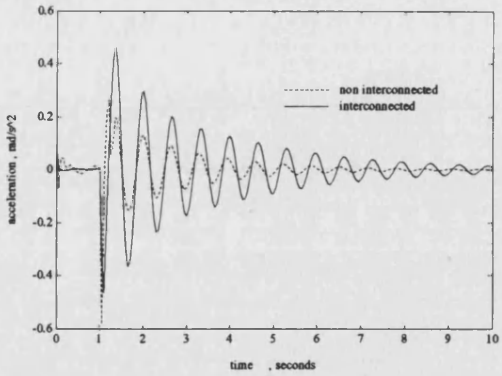


**Fig 5.18** *Pitch Acceleration Response to Step Pitch Input at the Wheels*

The comparison presented here is not truly representative of the difference between interconnected and non-interconnected vehicles since in practice they would employ different Hydragas unit spring and damping characteristics. However it is clear that the improvement in pitch rate gained by the adoption of longitudinal fluid interconnection must be offset against the resultant reduction in pitch damping. In any practical vehicle system, additional pitch dampers must be incorporated to prevent excessive body attitude, and indeed this is the case in the Interconnected Hydragas Rover Metro.

## 5.3 Passive Vehicle Handling Simulation

### 5.3.1 Steerpad Simulation

The simulated steerpad gives a measure of the quasi-steady state behaviour of the modelled vehicle. A closed loop driving force and steering controller was used to maintain a circular path over a range of fixed radii. The rate of speed change was low, so that the behaviour approximated that achieved under true steady state conditions. Tests were only carried out for left hand ( anti-clockwise ) turning, the model being perfectly symmetrical. Results are presented here as plots of calculated variables against lateral acceleration.

The simulated prediction of steady state suspension roll angle is shown in figure 5.19. Agreement between measurement and prediction was good both qualitatively and quantitatively. The relationship between roll angle and lateral acceleration is slightly non-linear, which is to be expected with

changing geometries. The computer prediction slightly over-predicts the experimental roll angle since the variable plotted for the simulation is total body roll rather than suspension roll. The prediction becomes less accurate at high lateral acceleration, above 5 $m/s^2$, although the maximum error does not exceed 0.5°.

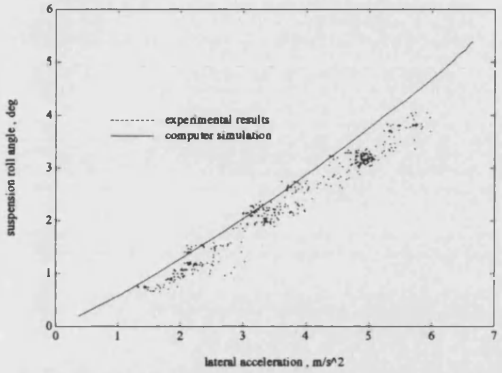


**Fig 5.19** *Experimental and Simulated Body Suspension Roll in Steerpad Test*

The suspension roll angle arose as a result of the suspension deflections shown in figure 5.20. The computer simulation is accurate up to a lateral acceleration of $3m/s^2$, at which point a highly non-linear effect is present in the experimental results. It was thought that a certain degree of 'suspension jacking' was present at high lateral acceleration. This is a function of the suspension geometry.

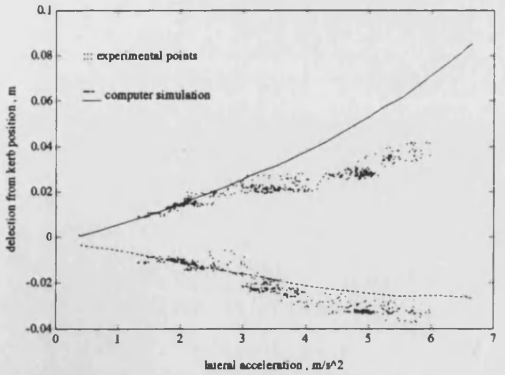


**Fig 5.20** *Experimental and Simulated Suspension Deflections in Steerpad Manoeuvre*

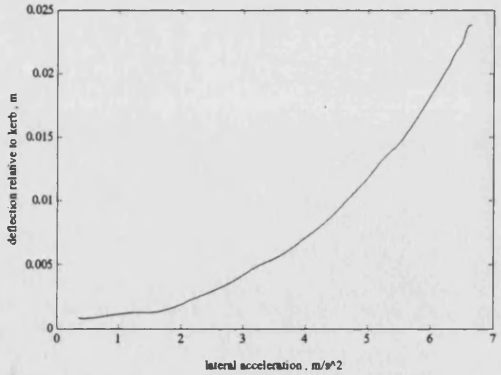


**Fig 5.21** *Change in Body Centre of Gravity Vertical Position in Steerpad Manoeuvre*

The jacking effect is not very clear in the experimental results due to the small magnitude of deflection and large amount of road noise present. However, it was clear from the computer simulation that there was a small increase in body height with lateral acceleration ( figure 5.21).

The simulated prediction of side-to-side pressure difference across the car is presented in figure 5.22. Agreement is good. This pressure difference cannot be directly related to a body roll moment because of the changing suspension unit piston effective areas. The simulated suspension linkage roll moment is shown in figure 5.23. It is clear that the relationship between this roll moment and lateral acceleration is almost linear for this manoeuvre. If the simulation results are to be believed, it would appear that lateral acceleration is a good measurement of suspension linkage roll moment in steady state manoeuvres.

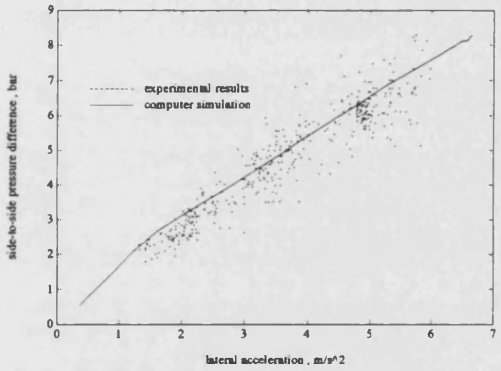


**Fig 5.22** *Pressure Difference Across the Car in Quasi-Steady State Steerpad Manoeuvre*

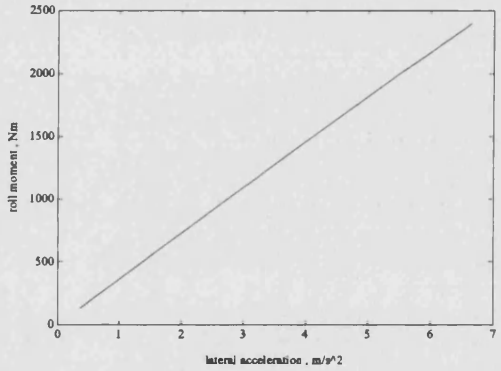


**Fig 5.23** *Simulated Suspension Linkage Roll Moment in Steerpad Manoeuvre*

The vehicle's steering characteristic is shown in figure 5.24. Like the experimental results, the simulation shows a small understeer gradient at low values of lateral acceleration. However at high lateral acceleration, above 5 m/ $s^2$, the simulation shows a marked increase in understeer gradient which was not apparent in the experimental tests, which were limited to an upper lateral acceleration of 6 $m/s^2$. This is explained in part by examining the front and rear axle slip angles ( figure 5.25 ). The high slip angle gradient at high lateral acceleration is indicative of low limit cornering stiffness at the front axle and non-linear tyre effects.

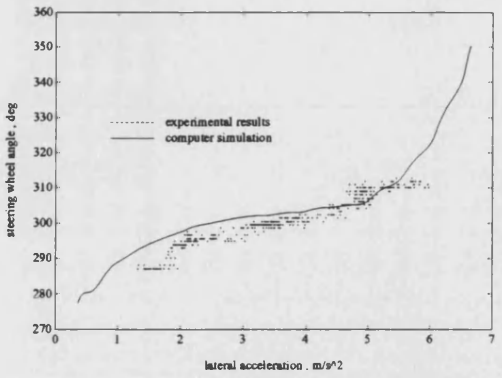


**Fig 5.24** *Experimental and Simulated Steering Wheel Angle in Steerpad Manoeuvre*

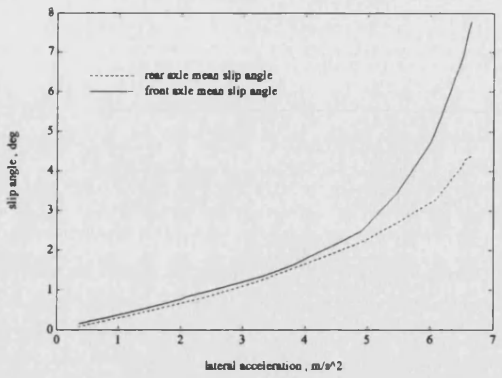


**Fig 5.25** *Simulated Mean Tyre Slip Angles at Front and Rear Axles in Steerpad Manoeuvre*

### 5.3.2 Step Steer Simulation

The step steer test was used to predict the transient dynamic behaviour of the vehicle. For comparison with experimental data, the same steering input was used. For later design and parameter studies a more theoretical fast ramp input was used. The manoeuvre was controlled using an open loop controller model. The simulation assumed a constant ( and zero ) driving torque throughout the manoeuvre and vehicle forward speed was lost due to 'scrub' between the road surface and the tyre. However this approximated the experimental conditions in which a constant throttle position was maintained during the manoeuvre.

A period of 2 seconds was allowed before the step steer was applied, allowing model transients to settle. All tests were right hand turns as the model behaviour in either direction was identical.

A comparison between the predicted and experimental vehicle lateral acceleration and suspension roll angle is shown in figure 5.26. The predicted lateral acceleration matches that recorded to a good degree of accuracy. The prediction of roll angle is reasonable, the maximum error being less than 0.2°.

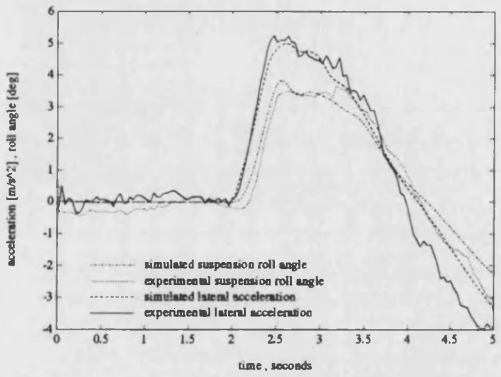


**Fig 5.26** *Lateral Acceleration and Suspension Roll Angle in Step Steer Manoeuvre*

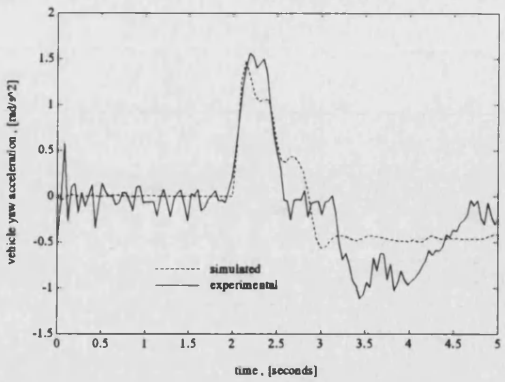


**Fig 5.27** *Experimental and Simulated Yaw Acceleration in Step Steer*

Figure 5.27 shows the yaw acceleration response to the step steer input. Agreement between experiment and prediction is good. Yaw acceleration led lateral acceleration in manoeuvres, a phenomenon put to use in the control of the active system. This is because cornering forces were developed at the front wheels first, then the rear wheels, as demonstrated in figure 5.28 showing the mean front and rear axle slip angles.

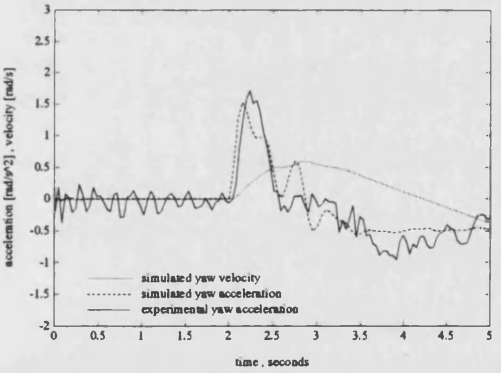


**Fig 5.27** *Yaw Acceleration and Velocity in Step Steer Manoeuvre*

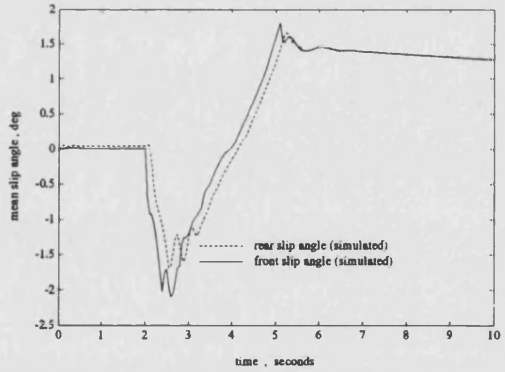


**Fig 5.28** *Front and Rear Axle Mean Slip Angles in Step Steer Manoeuvre*

The pressure difference between the two sides of the car during the step steer manoeuvre is shown in figure 5.29. The initial transient peak was a result of the damper restrictions between the upper and lower chambers of the Hydragas units. Once again, agreement is good. The predicted or experimental secondary suspension linkage roll moment in reaction to externally applied forces is a function of the suspension unit pressures and diaphragm effective areas in the no-roll case and also the drop angle

and parasitic suspension rates where body roll is non-zero. It is plotted together with a factored sum of the lateral and yaw body accelerations in figure 5.30. The relationship between these quantities is discussed further in chapter 7.

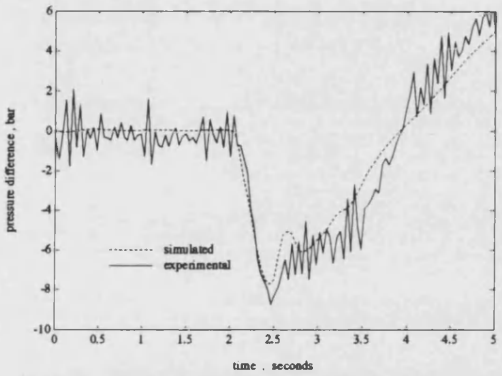


**Fig 5.29** *Side-to-Side Pressure Difference in Passive Step Steer Manoeuvre*

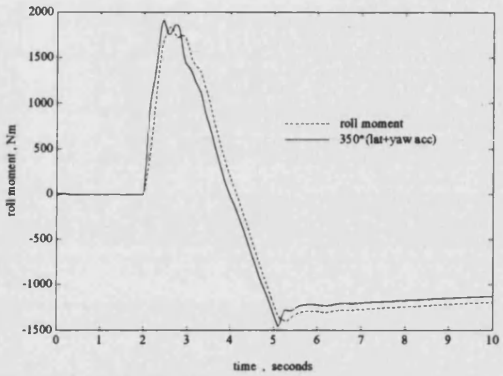


**Fig 5.30** *Total Suspension Linkage Roll Moment and Sum of Lateral and Yaw Accelerations in Step Steer*

### 5.3.3 Slalom Manoeuvre

The simulated slalom manoeuvre was again controlled using the open loop vehicle steer controller with a sinusoidal signal providing the demand steering wheel angle.

Figure 5.31 shows the three main body accelerations in the slalom manoeuvre. Yaw acceleration leads lateral acceleration by a margin of approximately $\pi/2$ rad. Roll acceleration is low in comparison with the two other modes and seems to be contain higher frequency effects. The roll angle response to this manoeuvre is shown in figure 5.32. The computer simulation appears to match the experimental results to a good degree of accuracy. The decrease in experimental lateral acceleration with time is due to the constant throttle position used for the test which results in speed being 'scrubbed off' in the cornering manoeuvre.

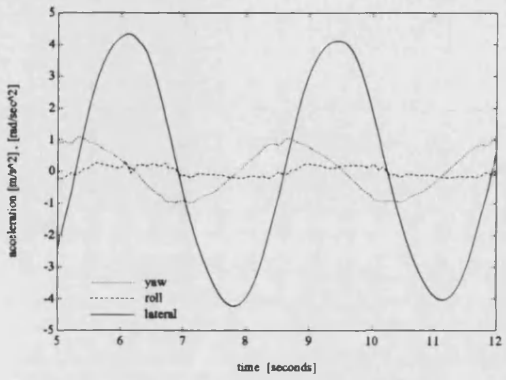


**Fig 5.31** *Simulated Body Accelerations in Passive Slalom Manoeuvre*

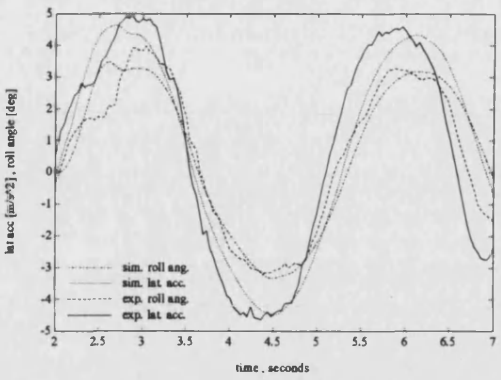


**Fig 5.32** *Experimental and Simulated Body Suspension Roll in Passive Slalom Manoeuvre*

Figure 5.33 shows the side-to-side pressure difference developed in the test. The dynamic pressure difference amounts to around 27% of the kerb steady state pressure in the suspension units (theoretically the kerb pressure difference is zero).

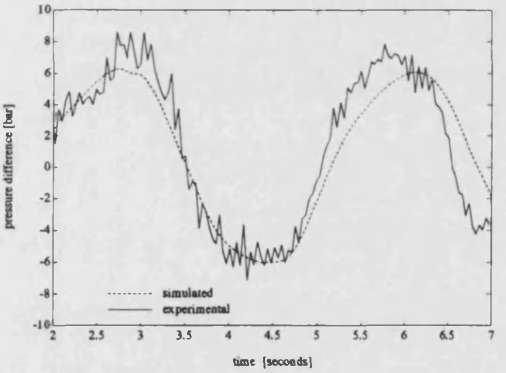


**Fig 5.33** *Side-to-Side Pressure Difference in Passive Slalom Manoeuvre*

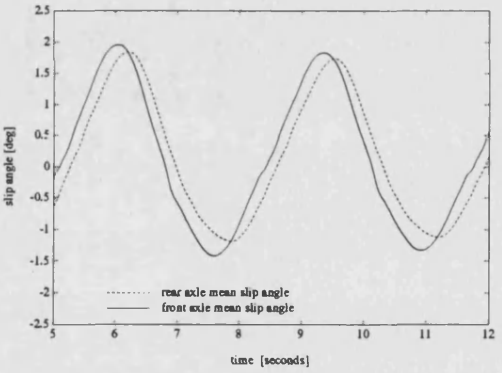


**Fig 5.34** *Simulated Slip Angles at Front and Rear Axles in Slalom Manoeuvre*

Figure 5.34 shows how slip angles developed at the front wheels lead those developed at the rear wheels. The amplitude of the mean front wheel slip angles is slightly higher than that of the rear wheels.

## 5.4 Active Vehicle Handling Simulation

While the passive computer vehicle model has been validated, it is important to ensure that the behaviour of the vehicle with active roll control is modelled accurately. Both the modelling of the hydraulic system dynamics and the interaction between the hydraulic and vehicle systems must be validated. For this purpose, further comparisons are made here with experimental results for the active vehicle ( i.e. with the active roll control system switched on ). Ride comparisons are not made as the active roll control shuttle was not intended to respond to road excitation.

## 5.5 Simulation of the Complete Active Roll Control Vehicle

The hydraulic and vehicle systems were combined by means of hydraulic hoses connecting the hydragas end effectors of the active shuttle to the front-to-rear vehicle interconnection pipes. Control system gains were selected to match the performance of the experimental vehicle. The active system demand signal came from a port on the vehicle body icon, supplying state variables for control purposes. In order to model the experimental driving accelerometer position under the front bumper of the car, components of yaw and roll accelerations were included in the control signal. The values of these components could be modified as system parameters.

The handling tests carried out were the same as for the passive vehicle.

### 5.5.1 Steerpad Test

The simulated reduction in quasi-steady state suspension roll angle compared to the passive vehicle is shown in figure 5.35. It can be seen that the simulation matched experimental results to a high degree of accuracy. There was a considerable amount of high frequency road noise in the experimental data.

Suspension roll angle was eliminated up to a lateral acceleration of 0.35g, after which roll increased gradually at the same rate as the passive vehicle. The simulation results show that the relationship between demand and feedback gains was not optimal; this was not immediately apparent from the experimental data due to the high amount of noise present. At low lateral acceleration levels, suspension roll angle has a negative value, i.e. the body leans into a gentle corner. By adjusting the feedback gain the suspension roll angle may be maintained at zero degrees up to the performance limit level of lateral acceleration ( figure 5.36).

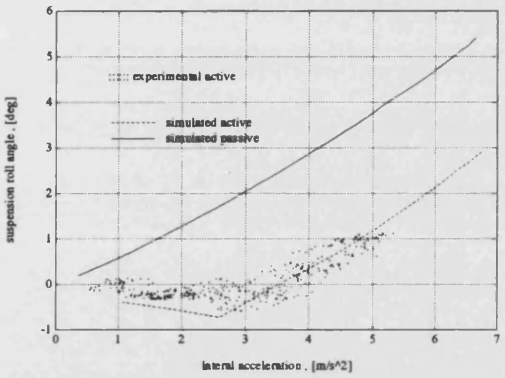


**Fig 5.35** *Reduction of Steady State Suspension Roll Angle by Active Hydragas Roll Control System*

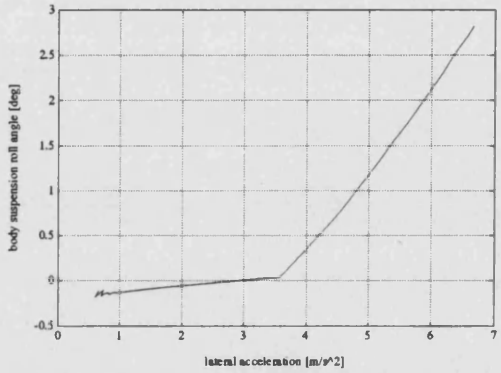


**Fig 5.36** *Improved Reduction of Steady State Roll Angle by Adjustment of Feedback Gain*

The non-linear roll characteristic of the active vehicle is reduced by the tapered pistons of the active fluid displacers which displace low volumes of fluid at small strokes ( i.e. at low lateral acceleration ), the displaced volume increasing with stroke. This is demonstrated in figure 5.37 in which the prototype system is compared with a system employing fluid displacers with a fixed effective area.

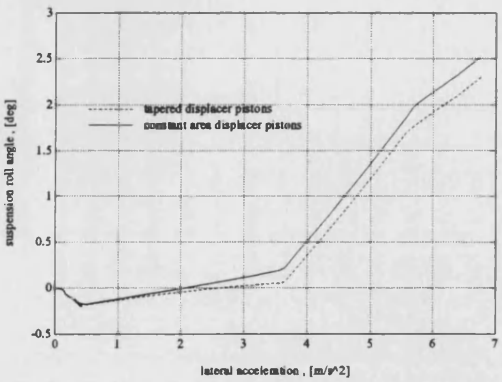


**Fig 5.37** *Comparison of Steady State Performance of Active Roll Control Systems Using Constant Area and Tapered Displacer Pistons*

The simulated side-to-side pressure difference is shown in figure 5.38. The simulation matches experimental results well for lateral accelerations below 0.3 g. Above this value, it slightly under-predicts the pressure difference. The most obvious feature of the graph is the change in slope above a lateral acceleration of 0.3 g. In this region, the shuttle was at the end of its stroke and no further increase in 'active' pressure difference was possible. The gradual increase in differential pressure beyond 0.3g was due to suspension deflection. Therefore the suspension roll moment opposing that due to lateral acceleration ( figure 5.39 ), was a combination of increased suspension unit pressure difference, piston taper rate and suspension parasitic and drop angle rate. In the region below 0.3 g lateral acceleration there was negligible body roll and hence the increasing suspension roll moment was due only to increasing pressure difference, hence the steeper slope.

The predicted suspension linkage roll moments for both passive and active vehicles are almost identical (figure 5.39). The slight difference at high lateral acceleration was thought to be due to the roll centre of the passive vehicle moving as a result of body roll.

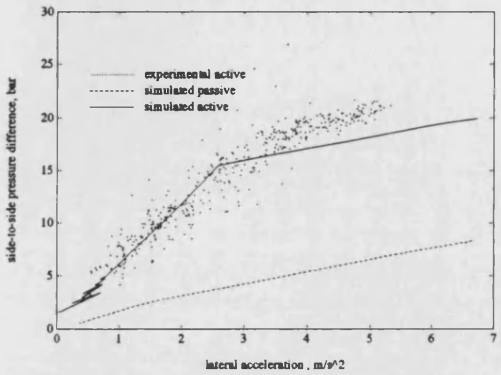


**Fig 5.38** *Side-to-side Pressure Difference Across the Vehicle in Steerpad Test*

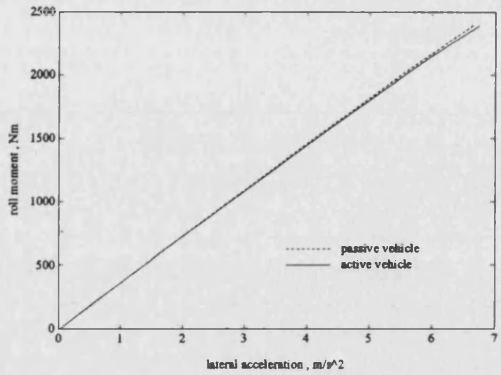


**Fig 5.39** *Suspension Linkage Roll Moment for Active and Passive Vehicles in Steerpad Manoeuvre*

The steering wheel angle required to maintain a circular path is shown in figure 5.40. The computer model appears to predict the steering wheel angle for the active vehicle less well at low lateral accelerations. It is likely that the experimental results were subject to error as maintaining a perfectly circular path was extremely difficult. The trends apparent for both experimental and simulated results are nonetheless similar. The effect of the active system is to reduce the required steering wheel angle to maintain a circular path. This is due to the lack of roll steer present in the passive vehicle tests.

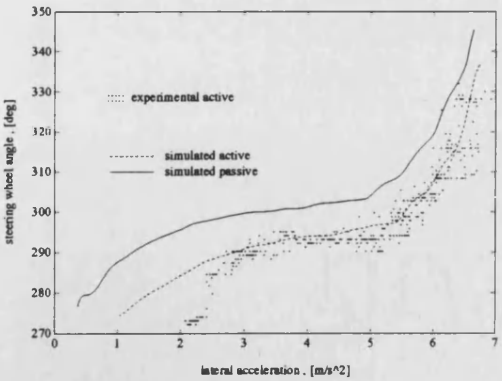


**Fig 5.40** *Steering Wheel Angle in Quasi-Steady State Steerpad Manoeuvre*

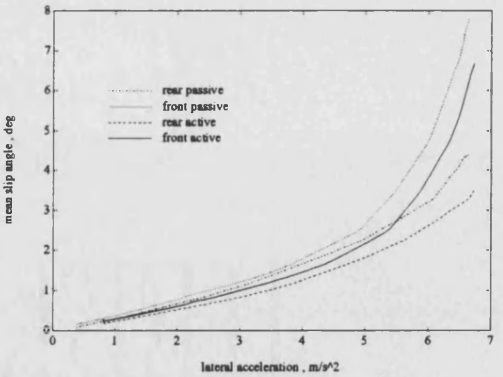


**Fig 5.41** *Front and Rear Axle Mean Slip Angles in Steerpad Manoeuvre*

The mean tyre slip angles at the front and rear wheels are shown in figure 5.41. The slip angles of both front and rear axles are lower for the active car, corresponding with the lower steering wheel angle.

The front left and right suspension deflections are shown in figure 5.42. The accuracy of the computer simulation decreases at high lateral acceleration but is reasonably good at low lateral acceleration. The jacking effect of the active roll control system due to the unequal areas of the fluid displacers is demonstrated in figure 5.43. The displacement of the body c.g. is consistently greater than for the passive vehicle

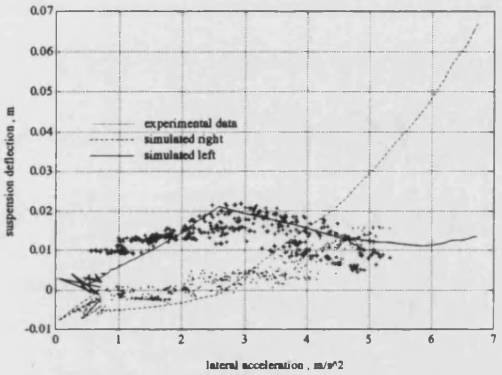


**Fig 5.42** *Front Suspension Deflections in Steerpad Manoeuvre*

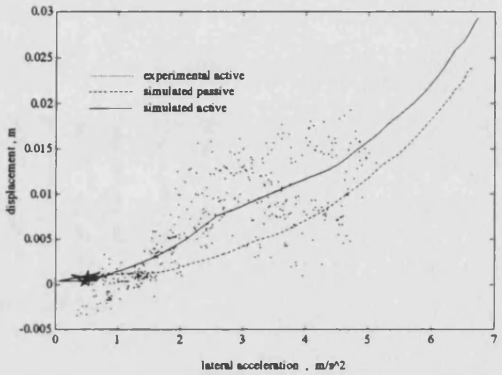


**Fig 5.43** *Change in Centre of Gravity Height in Steerpad Manoeuvre*

### 5.5.2 Step Steer Manoeuvre

The simulated lateral acceleration and suspension roll angle responses to the step steering wheel input are shown in figure 5.44. The simulation appears to model the behaviour of the active vehicle well. Roll attitude was reduced significantly by the active system as shown in figure 5.45, giving a comparison of passive and active angles.

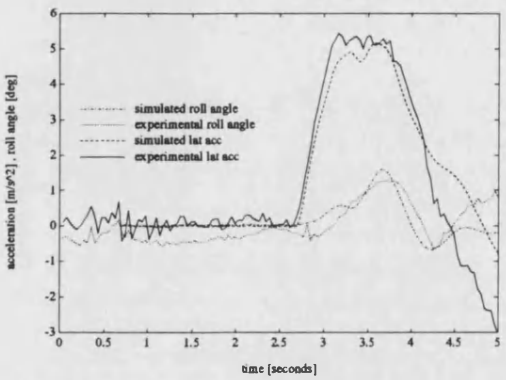


**Fig 5.44** *Lateral Acceleration and Suspension Roll Angle in Active Step Steer*

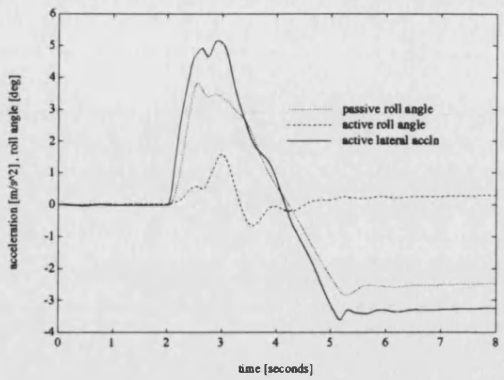


**Fig 5.45** *Simulated Active and Passive Roll Angle in Step Steer Manoeuvre*

The demand and response curves for the active shuttle are presented in figure 5.46. At peak demand, the lateral acceleration signal was saturated. It is likely that the transient peak in vehicle suspension roll angle above was due to limitations in the anti-roll capacity of the active system rather than lack of response. This is demonstrated by a less severe step steer manoeuvre in which the vehicle lateral acceleration was at all times within the anti-roll capabilities of the active system ( figure 5.47 ). The transient roll angle peak is considerably smaller ( less than ½° )

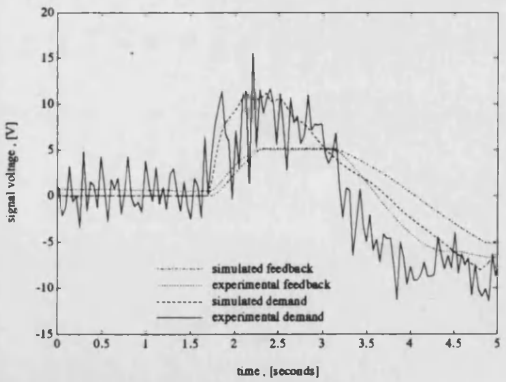


**Fig 5.46** *Experimental and Simulated Demand and Response of Shuttle in Active Step Steer Manoeuvre*

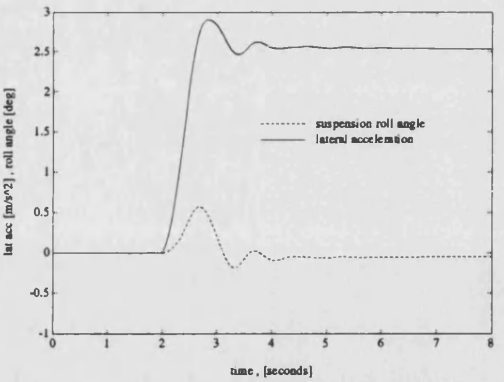


**Fig 5.47** *Simulated Lateral Acceleration and Roll Angle in Moderate Step Steer Test*

Figure 5.48 shows the yaw acceleration response to the step steer manoeuvre, comparing experimental with simulated results. Figure 5.49 shows the simulated yaw response of both passive and active vehicles.

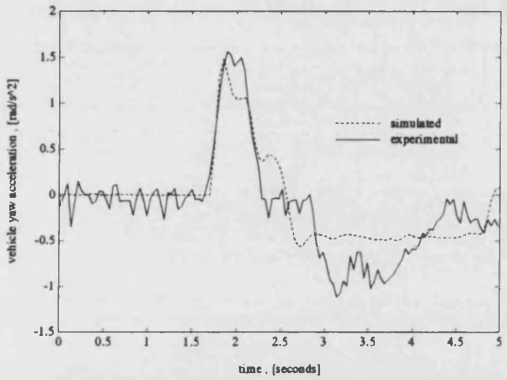


**Fig 5.48** *Yaw Acceleration Response to Step Steer Input*

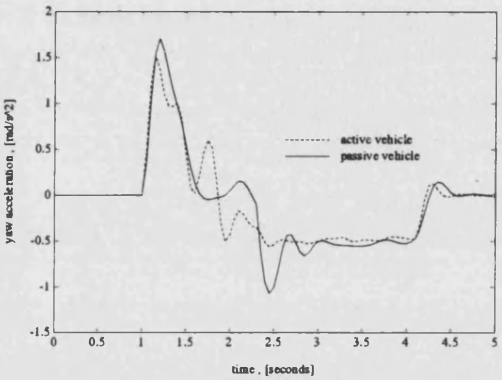


**Fig 5.49** *Yaw Acceleration for Passive and Active Vehicles in Step Steer*

The variation in side-to-side Hydragas fluid pressure for the step steer manoeuvre is shown in figure 5.50. Agreement is good between the simulated and experimental results. The large transient peak following the initial disturbance, far greater than that for the passive car, was not evident in early simulation work. It was found to be due in part to restrictions in the fluid flow path between the active hydragas displacers and the interconnection lines into which they fed. This was modelled by placing a single 3 mm bore orifice into each of the hydraulic connection lines between the shuttle and the car.

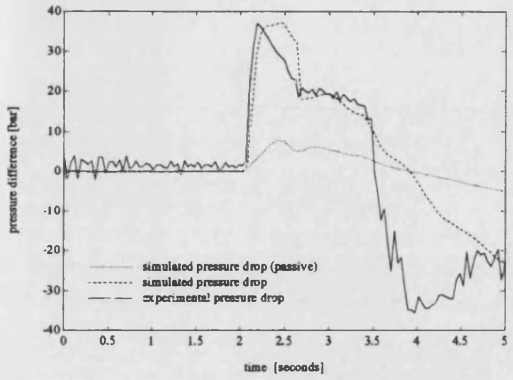


**Fig 5.50** *Experimental And Simulated Pressure Difference Across the Car in Step Steer Manoeuvre*

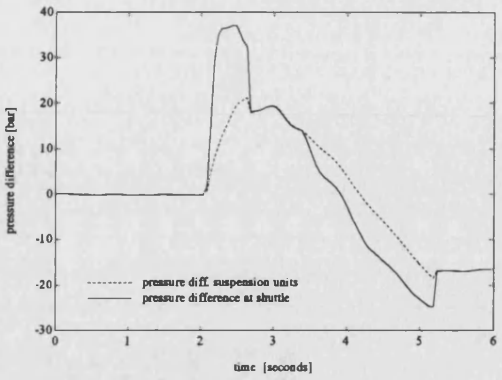


**Fig 5.51** *Pressure Difference Across Car Measured at the Active Shuttle Ports and at the Front Suspension Units*

As the side-to-side pressure difference was measured experimentally at the outlets of the shuttle, the transient peaks were particularly noticeable. Figure 5.51 shows the simulated pressure difference measured at the front and rear suspension units. Here the large transient peak was significantly reduced, explaining the fact that there was no apparent harshness felt by the passengers during the manoeuvre.

The relationship between secondary suspension pressure generated roll moment and the net force acting on the shuttle is shown in figure 5.52. The relationship is not linear and depends on whether a steady state or dynamic manoeuvre is being performed due to line pressure losses associated with fluid flow.

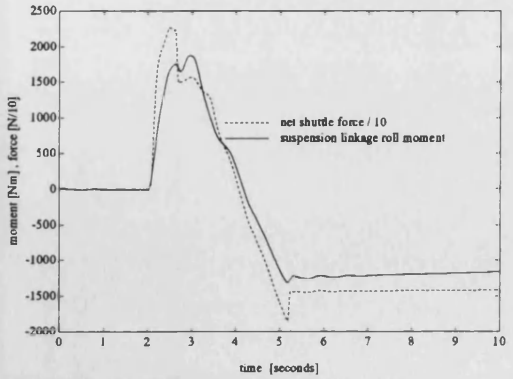


**Fig 5.53** *Simulated Suspension Linkage Roll Moment and Net Shuttle Force in Step Steer Manoeuvre*

### 5.5.3 Slalom Manoeuvre

The vehicle suspension roll attitude results for the active car in a slalom manoeuvre are presented in figure 5.54. It can be seen that the simulation does not predict the vehicle behaviour as accurately as for the previous tests. This is largely due to the assumption of a sinusoidal steering wheel input which was used for computer simulation purposes. This was necessary as the steering angle transducer failed during these tests. Body roll was not completely eliminated by the active system as the lateral acceleration levels involved were reasonably high.

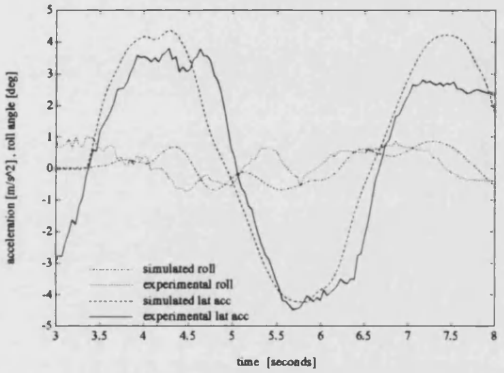


**Fig 5.54** *Experimental and Simulated Lateral Acceleration and Suspension Roll Angle in Slalom Manoeuvre*

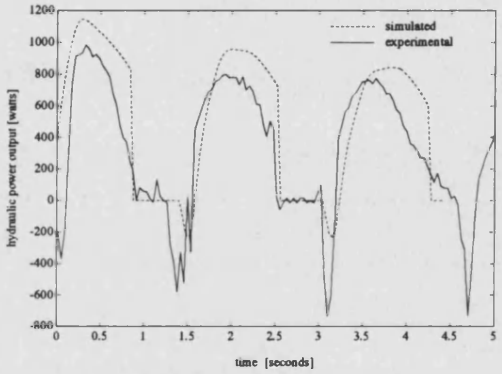


**Fig 5.55** *Experimental and Simulated Hydraulic Power Output of Active Hydragas Shuttle in Slalom Manoeuvre*

The hydraulic power output of the shuttle used in continuous running is shown in figure 5.55. The peak measured power output was 1 kW, successive peaks reducing in power as the accumulator became discharged. The simulated value was some 15% greater than this. The overestimation of the vehicle model is to be expected as pressure losses due to friction were neglected in the simulation model. The mean power output was 230 W for the experimental vehicle and 340 W for the computer simulation. These values would be considerably lower for normal driving in which the shuttle is not constantly operating.

The brief negative power peaks were a result of the self-centring nature of the roll control shuttle. The pressure differential and the difference in the effective piston areas across the shuttle served to return the shuttle to its central position. As well as reducing the hydraulic power requirement of the active system, this feature also serves as a fail safe function should hydraulic pressure be lost.

The flows and pressures used to calculate the hydraulic power are shown in figures 5.56, 5.57. The simulated oil flow through the shuttle rises less sharply than that measured experimentally ( by differentiating the shuttle position feedback signal and multiplying by the oil bore ). The sharp peaks apparent in the experimental trace may be due to the proportional valve deadband. A deadband was beneficial in that it prevented the shuttle from responding to small lateral disturbances such as road noise, but it also caused the shuttle to jump to a non-centre position when demand exceeded the deadband value.

The oil pressure difference across the shuttle shows a marked difference between experimental and simulated results. This is because the experimental values were calculated from the water pressure results and the effective diaphragm areas of the two sides of the shuttle. Therefore they take no account of the fact that while the shuttle was at it's end stops the oil side pressure difference rose to the relief valve cracking pressure.

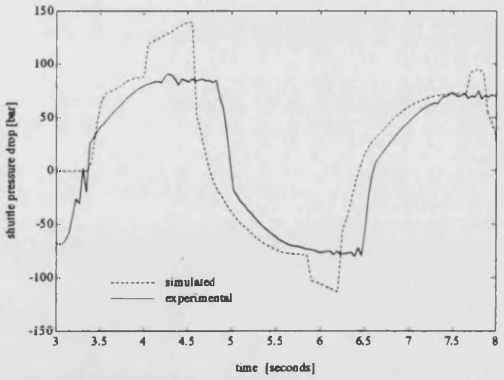


**Fig 5.56** *Experimental and Simulated Oil Pressure Difference Across the Shuttle in Slalom Manoeuvre*

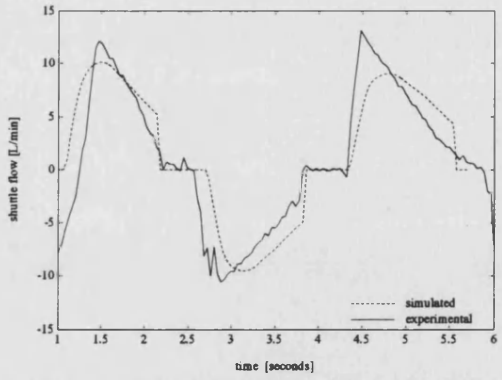


**Fig 5.57** *Experimental and Simulated Oil Flow Through the Valve in Slalom Test*

The Hydragas fluid pressure differential (figure 5.58) again shows good agreement between simulated and experimental results. The transient peaks are again slightly sharper for the

experimental trace. The simulated pressure difference is slightly higher than that measured experimentally.

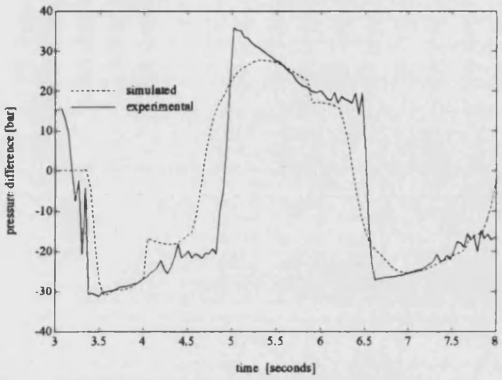


**Fig 5.58** *Experimental and Simulated Hydragas Fluid Pressure Difference Across the Vehicle in Slalom Manoeuvre*

# 6 Improvements to the Active Roll Control System Using BATH*fp* as a Design Tool

## 6.1 Introduction

As discussed in the previous two chapters, the performance of the prototype active roll control system installed on the interconnected Hydragas Metro was adequate but not ideal. The prototype system was originally designed on the basis of correct function and was optimised neither for cost nor performance. Once a validated computer model of the roll controlled vehicle had been developed, BATH*fp* could be used for its intended purpose, as a design tool to determine the sensitivity of system performance to a number of system parameters. The optimisation of the hydraulic system is presented in this chapter.

## 6.2 Determination of Dynamic Requirements

The dynamic requirements of roll control systems depend largely on the disturbance inputs and roll outputs specified. In the case of handling inputs, such as tyre lateral forces and aerodynamic forces, the requirement is to minimise roll. For ride purposes however, the requirements may differ. Roll control systems are not expected to respond to very high frequency road disturbances since this would represent a large, unnecessary power consumption. Neither are they expected to respond to low frequency road undulations. Although such systems can be designed to respond to high frequency road disturbances the work presented here will only consider handling requirements.

### 6.2.1 Disturbance Input Types

Handling disturbance inputs can be divided into four main categories:

1. Driver steering inputs.
2. Unintentional driver disturbances such as braking, accelerating and changing gear. The effect of these is primarily to influence forces developed at the tyres.
3. Tyre force disturbances due to changes in the road surface, such as road friction changes.
4. Aerodynamic disturbances, particularly side winds.

Methods are available to predict the bandwidths of types 2-4, however of primary importance in this study is the vehicle response to driver controlled steering inputs.

### 6.2.2 Driver Steering Inputs

The response of human operators in control tasks has been studied at length [ 71 ]. A bandwidth of 10 rad/s ( 1.6 Hz ) is considered appropriate for controlled driver inputs. This may be regarded as an upper limit of human response and hence an appropriate control system bandwidth. Under normal conditions, the bandwidth of steering inputs may be expected to be considerably lower than this value.

## 6.3 Reduction of Hydraulic Shuttle Bore

One of the major problems of the existing prototype roll control system was it's inability to sustain adequate roll attitude control under continuous and repetitive manoeuvring. The reason for this shortcoming was the hydraulic accumulator, which provided additional fluid flow to cover heavy demand. Under continuous demand, the accumulator did not have sufficient time to recharge and eventually became completely discharged, at which point the system became reliant on the pump alone for fluid supply.

The removal of the accumulator from the active system oil hydraulic circuit necessitated a reduction in the shuttle oil piston bore. This was done with the intention of reducing the mean flow requirements and hence reducing the size of the hydraulic pump required. Conversely, the mean pressure drop across the shuttle rose and a maximum system pressure of 140 bar was set for the modified system.

The minimum shuttle bore is dictated by the supply pressure, in this case a maximum of 140 bar. Allowing for 20 bar pipe and valve losses, the maximum pressure drop across the shuttle must not exceed 120 bar. From 2.2.2, we have the maximum force exerted on the shuttle during a lateral manoeuvre:

$$F_{max} = 16.1kN \tag{6.1}$$

therefore the minimum shuttle area:

$$\begin{aligned} A_{sh\,min} &= 16.1 \times 10^3 / 140 \times 10^5 \\ &= 1.15 \times 10^{-3} m^2 \end{aligned} \tag{6.2}$$

giving a minimum bore:

$$D_{sh\,min} = 38.3mm \tag{6.3}$$

The maximum experimental driver steering input frequency which caused the shuttle to just reach it's end stops was 0.3 Hz. For this analysis, a maximum frequency of 0.5 Hz is assumed, allowing for extreme manoeuvres. We can now calculate the maximum flow required by the system. The shuttle position is given by:

$$x_{sh} = \frac{0.057}{2} \times \sin(2 \times \pi \times 0.5 \times t) \tag{6.4}$$

and its velocity by:

$$v_{sh} = \frac{0.057 \times 2 \times \pi \times 0.5}{2} \times \cos(2 \times \pi \times 0.5 \times t) \tag{6.5}$$

Therefore the maximum shuttle velocity in a lateral manoeuvre is 0.090m/s. Multiplying by the oil piston cross sectional area gives a maximum flow of:

$$\begin{aligned} Q_{sh\,max} &= 1.03 \times 10^{-4} m^3 / s \\ &= 6.2 L / \min \end{aligned} \tag{6.6}$$

The main effect of this modification was to place all demand for oil flow on the pump. Despite the reduction in shuttle bore, a larger capacity pump was still required to provide sufficient flow for fast transient manoeuvres. A 7 L/min pump was found to be necessary to replace the 5 L/min unit used in the prototype vehicle.

An electric pump was not deemed to be suitable for the production vehicle. Hence it was replaced by an engine driven power steering pump drawing from a separate tank. Power requirements for the pump were reduced by piloting the pressure relief valve remotely from downstream of the non return-valve. Therefore, when not in use, the pump would discharge to tank at nominally zero pressure.

## 6.4 Optimisation of the Proportional Valve

### 6.4.1 Simple Directional valve

The valve used for the prototype vehicle was a large and expensive industrial valve, unsuitable for use in the automotive industry. BATH*fp* was used to investigate the possibility of using a smaller, lower bandwidth valve. Initially, investigations were made into using a simpler 4-port, 3 way directional valve with 'dead band' closed loop control. This was found to give a shuttle response capable of reducing body roll but required high frequency oscillations of the valve spool which would significantly reduce the life of the valve.

Figures 6.1 - 6.4 show the performance of the system with simple directional valves of two natural frequencies. It is clear that the operation of the valve has an adverse effect on the handling characteristics of the vehicle and it is likely that problems would arise with ride harshness and

excessive noise. The roll control capability of the system seems to improve only slightly as the frequency of the valve is increased.

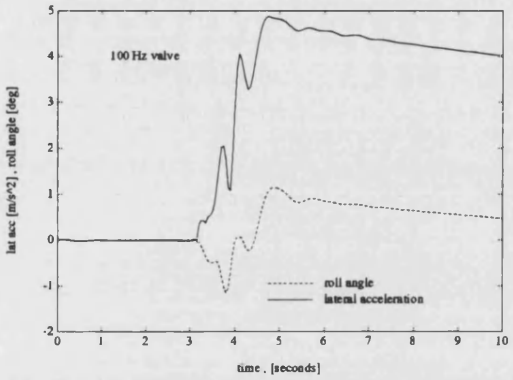


**Fig 6.1** *Roll Response in a Step Steer Test for Active Roll Controlled Vehicle Using 25 Hz Simple Directional Valve*

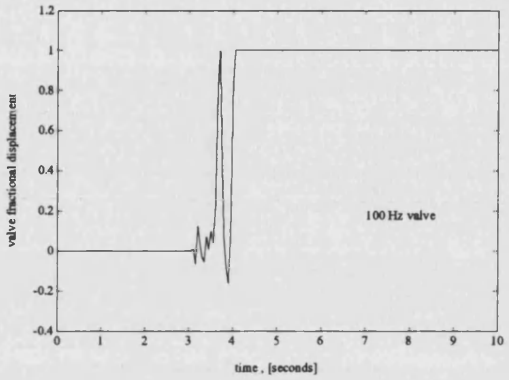


**Fig 6.2** *Valve Spool Fractional Displacement During Step Steer for 25 Hz Simple Directional Valve*

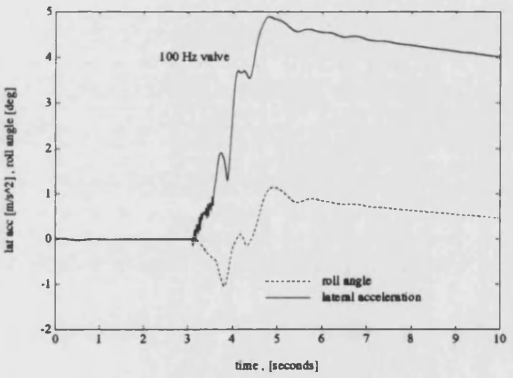


**Fig 6.3** *Roll Response in a Step Steer Test for Active Roll Controlled Vehicle Using 100 Hz Simple Directional Valve*

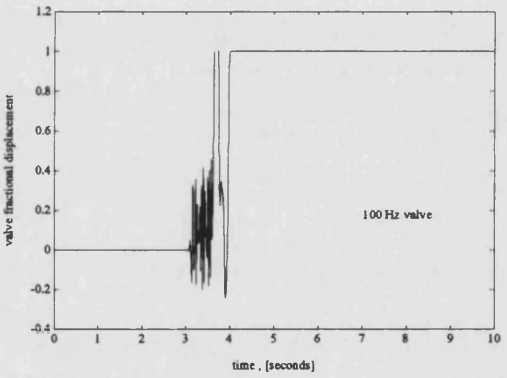


**Fig 6.4** *Valve Spool Fractional Displacement During Step Steer for 100 Hz Simple Directional Valve*

It was concluded that a proportional valve of the type used in the prototype system would be necessary to provide adequate roll reduction without excessive harshness.

### 6.4.2 Proportional Valve Sizing

The mass and cost of the valve used in the prototype vehicle was somewhat prohibitive for use in production. A smaller (and hence cheaper ) valve was required with no degradation in performance

being the major constraint. Since the full flow capacity of the original valve was not utilised, a significant reduction in size was possible.

Figures 6.5, 6.6 show the effect of reducing the valve size on shuttle response. The car body suspension roll angle response deteriorates with reduction in valve size at both speeds. However an increase in valve size is not matched by a proportionate reduction in transient roll. A valve having a nominal flow of 7 L/min appears to be sufficient for this application.

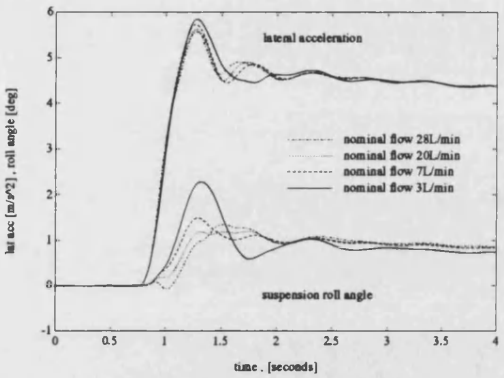


**Fig 6.5** *Effect of Valve Nominal Flow Size on Roll Angle Response in 8 m/s Step Steer Manoeuvre*

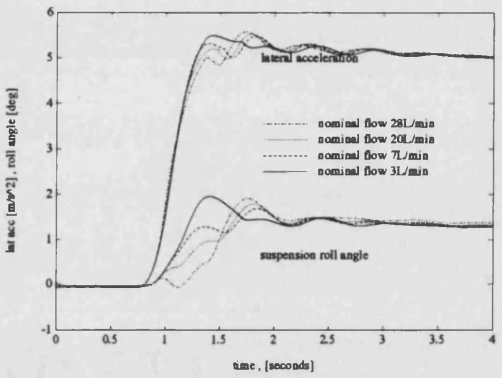


**Fig 6.6** *Effect of Valve Nominal Flow Size on Roll Angle Response in 20 m/s Step Steer Manoeuvre*

### 6.4.3 Proportional Valve Frequency Response

The bandwidth of the valve used in the prototype system was 31 Hz ( information supplied by Vickers Systems Limited ). It is possible that a valve of lower bandwidth ( i.e. slower response ) could be used with little reduction in overall system response. Figures 6.7 - 6.10 show the simulated effect of valve bandwidth on system performance at two different speeds.

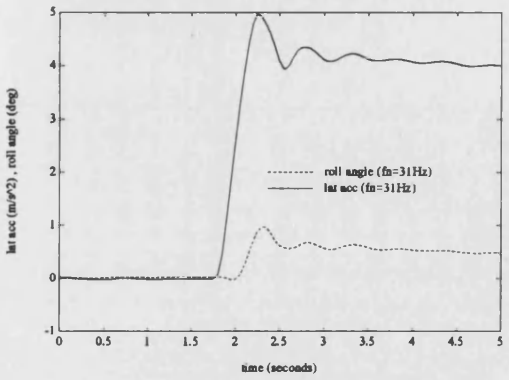


**Fig 6.7** *Lateral Acceleration and Suspension Roll angle in 8.33 m/s Step Steer Test Using 31 Hz Bandwidth Valve*

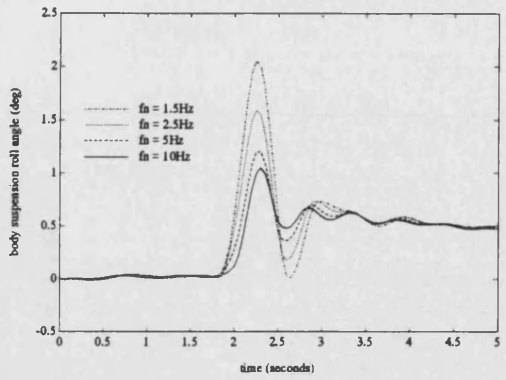


**Fig 6.8** *Effect of Proportional Valve Bandwidth on Roll Angle Response in 8.33 m/s Step Steer Test*

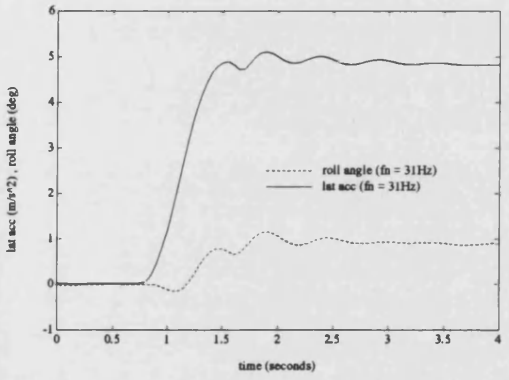


**Fig 6.9** *Lateral Acceleration and Suspension Roll angle in 20 m/s Step Steer Test Using 31 Hz Bandwidth Valve*

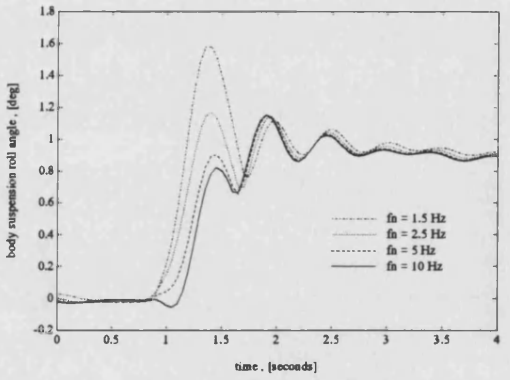


**Fig 6.10** *Effect of Proportional Valve Bandwidth on Roll Angle Response in 20 m/s Step Steer Test*

It is apparent from these results that there is little gain in performance to be achieved from using a proportional valve of greater than 10 Hz bandwidth. Such a valve should be cheaper than the high performance valve used on the prototype vehicle.

## 6.5 Optimisation of the System Loop Gain

In order to test the prototype vehicle, the loop gain was set at a low level in order to ensure stability at low speed. The selection of this gain was therefore rather subjective and almost certainly not optimal. BATH*fp* was therefore used to investigate the effect of the control system loop gain on

stability. An impulse lateral force of 1 kN for 0.2 seconds was applied to the vehicle body at the c.g. position and the resulting body suspension roll response was analysed for a range of loop gain settings at different speeds. The results of this investigation are shown in figures 6.11 - 6.14.

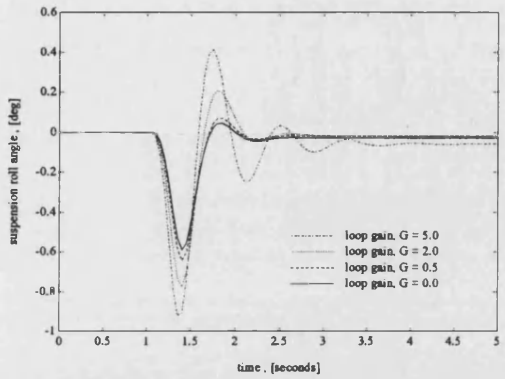


**Fig 6.11** *Effect of Control System Loop Gain on Roll Response to an Applied Lateral Force at 20 m/s*

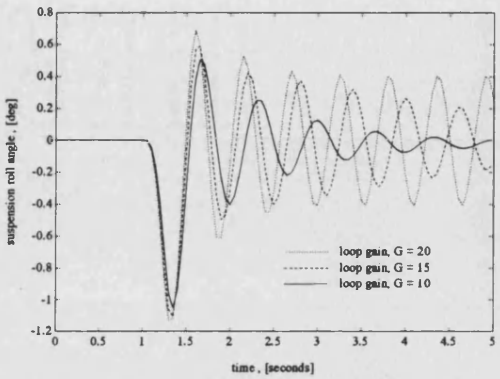


**Fig 6.12** *Effect of Control System Loop Gain on Roll Response to an Applied Lateral Force at 20 m/s*

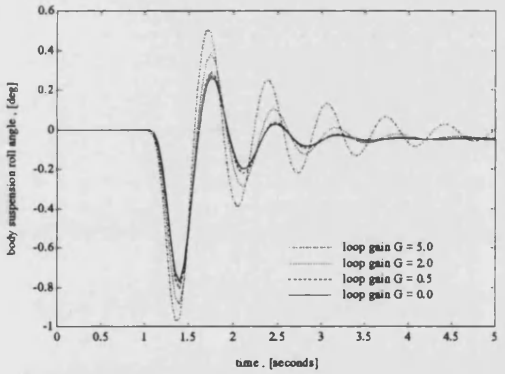


**Fig 6.13** *Effect of Control System Loop Gain on Roll Response to an Applied Lateral Force at 8 m/s*

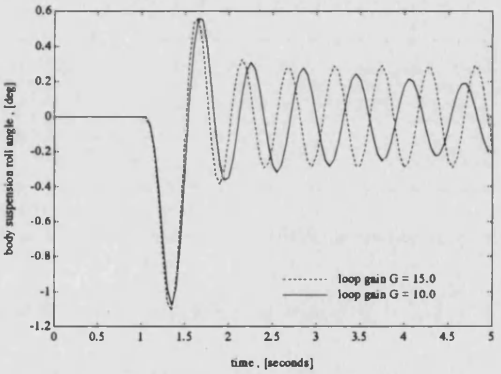


**Fig 6.14** *Effect of Control System Loop Gain on Roll Response to an Applied Lateral Force at 8 m/s*

It is clear from the above figures that the active vehicle roll stability increases with forward speed and therefore the selection of an appropriate loop gain at low speed is important to ensure active system stability. It is also clear that the system becomes unstable as the loop gain is increased. Considering that friction in the real system is considerable, a loop gain of 5, as used in the prototype system, appears to be adequate to maintain stability and provide reasonable shuttle response times.

## 6.6 Performance of the modified system

A circuit diagram of the modified hydraulic actuation system is shown in figure 6.15. The modifications described in this chapter were introduced with the intention of reducing system cost and

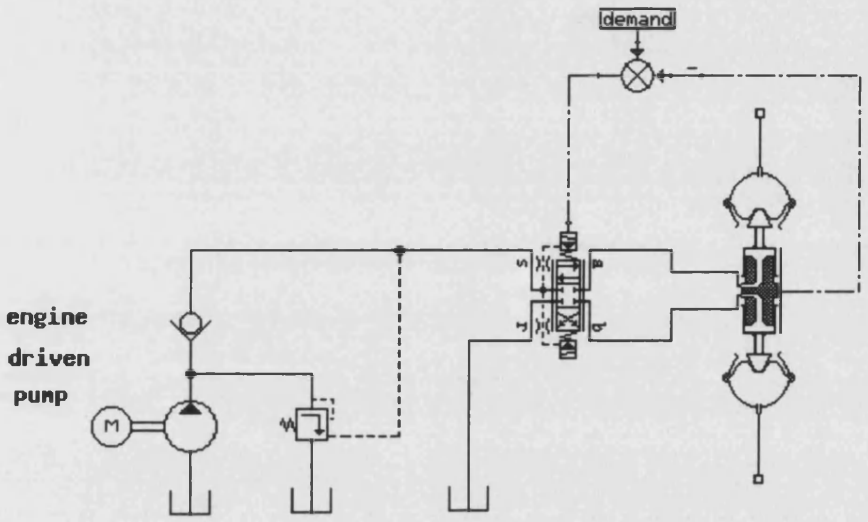


**Fig 6.15** *Modified Hydraulic Circuit for Active Roll Control System*

weight without adversely effecting system performance. The simulated performance of the modified system relative to the prototype set-up used in the experimental vehicle is demonstrated in figures 6.16 - 6.19. The slalom test manoeuvre used in the simulation was a 0.3 Hz sinusoidal steering wheel displacement of magnitude 30°. The vehicle forward speed was 20 m/s. The simulated step steer manoeuvre involved a 40° turn of the steering wheel at 2 Hz, again at 20 m/s.

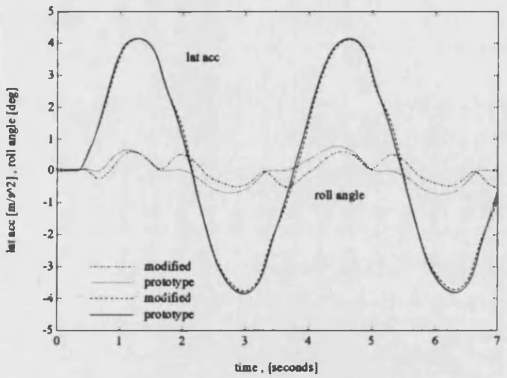


**Fig 6.16** *Lateral Acceleration and Roll Angle for Existing Prototype and Modified Roll Controlled Vehicles in Slalom Manoeuvre*

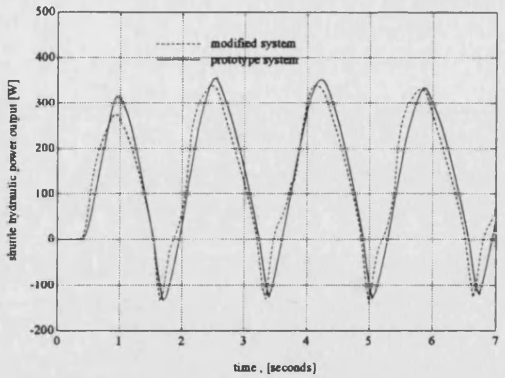


**Fig 6.17** *Shuttle Hydraulic Power Output for Existing Prototype and Modified Roll Controlled Vehicles in Slalom Manoeuvre*

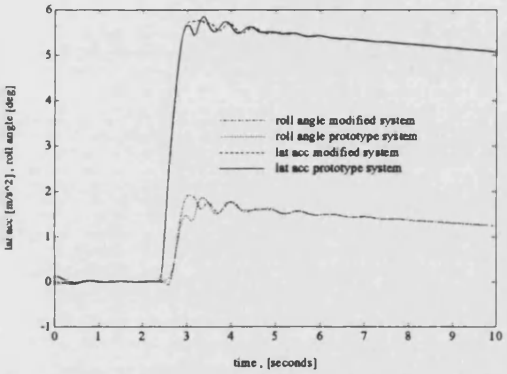


**Fig 6.18** *Lateral Acceleration and Roll Angle for Existing Prototype and Modified Roll Controlled Vehicles in Step Steer*

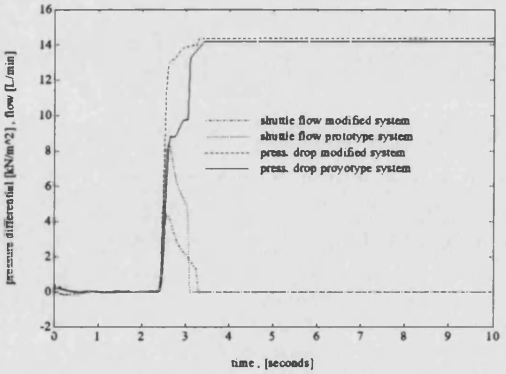


**Fig 6.19** *Shuttle Differential Pressure and Flow for Existing Prototype and Modified Roll Controlled Vehicles in Step Steer*

It is clear from the above figures that the performance of the modified roll control system is not greatly reduced when compared to the over-engineered prototype system. The power outputs of the prototype and modified systems are nearly identical. Since the modified shuttle oil piston bore is smaller than that of the prototype, the flow into the modified shuttle is reduced while the pressure difference across it is increased. As well as the material gains in cost and complexity, the modified system also has the advantage that it can continue to operate under heavy demand since there is no accumulator to become discharged.

## 6.7 Fail-safe Operation

### 6.7.1 Modes of Failure

In the event of a system failure, the vehicle handling performance should not become significantly worse than that of an equivalent passive vehicle. Failures may occur in a number of ways and provision should be made for the active roll control system to fail safely on the occurrence of such a failure. Loss of hydraulic system pressure will lead to a tendency of the shuttle to free-wheel, drastically reducing the vehicle roll rate and resulting in dangerously large roll angles during manoeuvres.

A typical approach to ensure reasonably safe vehicle behaviour in the event of a failure is to install fail-safe pilot operated check valves into one or both of the hydraulic lines supplying the shuttle. These would monitor system pressure and, if a failure occurred, would lock the shuttle in its current position. The main disadvantage of this approach is that when failure occurs the shuttle may be away from its centre position. A resultant roll angle would then be adopted during straight ahead driving, leading to dangerously asymmetrical handling characteristics.

A compromise solution to this problem has been suggested and is outlined below.

### 6.7.2 Proposal for a Hydragas Roll Control Fail-safe Mechanism

It has been suggested that by allowing small bleed holes in the fail-safe valves used to hold the shuttle, the shuttle may be allowed to return slowly to its centre position during straight ahead driving by virtue of the inherent roll taper rate in the Hydragas suspension system. These bleed holes would reduce transient roll during subsequent manoeuvres by heavily damping the roll mode. Steady state roll behaviour will still be poor but it is assumed that the size of these bleed holes will be such that the driver will be able to compensate for the loss of roll control during slower manoeuvres by reducing the vehicle speed. Obviously, any failure of the roll control system should operate a warning light to alert the driver.

### 6.7.3 Performance of the Roll Control System in Failure Mode

Figure 6.20 shows how the unmodified roll controlled vehicle responds following a loss of hydraulic pressure ( for example due to the failure of the pump or a hydraulic hose ). The simulation used a forward speed of 10 m/s and an initial steering wheel angle of 60°. Following the loss of hydraulic system pressure, the steering wheel angle was returned to zero after 5 seconds. Pressure loss occurred after 1 second.

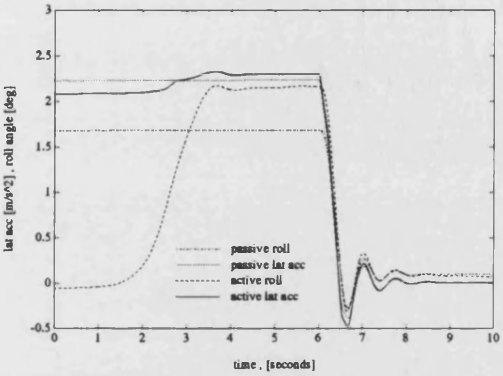


**Fig 6.20** *Roll Response of Standard Active And Passive Vehicles Following Loss of Active System Pressure*

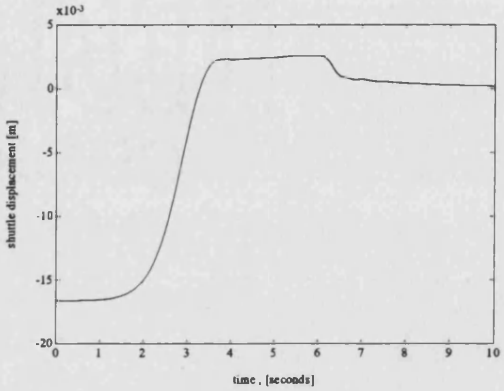


**Fig 6.21** *Shuttle Displacement of Standard Active Roll Controlled Vehicle Following Loss of Active System Pressure*

The failed active system is compared with the equivalent passive system. It is apparent that following the active system failure, the roll angle of the active car becomes worse than that of the passive car. The Hydragas system suspension unit taper rate prevents the shuttle from moving directly to its end stop, as shown in figure 6.21, but the situation is not acceptable. The shuttle returns to the centre-stroke position upon the steering wheel angle returning to zero and body roll also drops to an insignificant value following some oscillation.

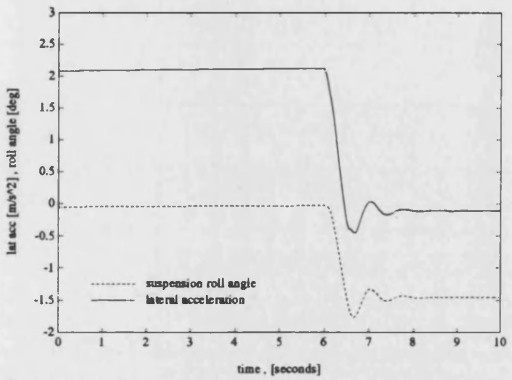


**Fig 6.22** *Roll Response of Active Vehicle With 'Fail-safe' Valves Following Loss of Active System Pressure*

Figure 6.22 shows the effect on body roll of introducing 'fail-safe' valves into the hydraulic lines feeding the shuttle. These close upon the loss of system pressure, locking the shuttle in place. Following system failure, zero suspension roll is maintained by the active vehicle. However when the steering wheel angle is returned to zero, there is a residue roll angle which would be not only uncomfortable for the occupants but also dangerous if a turn in the opposite direction were negotiated.

The performance of the active roll control vehicle utilising the fail-safe method proposed earlier is shown in figures 6.23, 6.24. The roll response of the vehicle is shown for systems allowing varying amounts of bleed flow through the fail-safe valves upon the loss of hydraulic pressure. It appears that allowing some flow across the shuttle following a system failure offers significant benefits in safety. The actual amount of bleed flow allowed should be based on the desired vehicle roll response in terms both of transient roll limitation and the time taken for the system to return to zero roll during straight ahead driving.

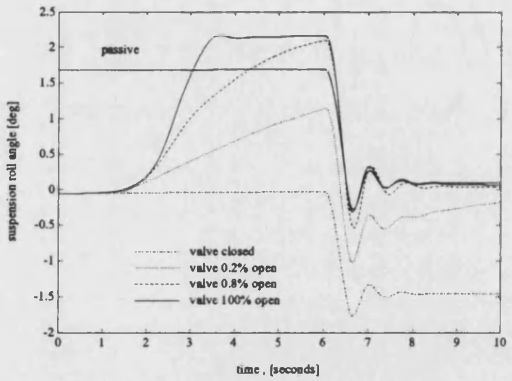


**Fig 6.23** *Effect on Roll Response of Bleed Flow Through 'Fail-safe' Valves Following Loss of Active System Pressure*

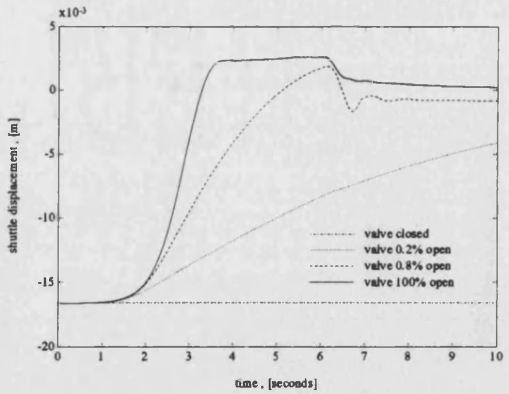


**Fig 6.24** *Effect on Shuttle Displacement of Bleed Flow Through 'Fail-safe' Valves Following System Failure*

## 6.8 Production Considerations

A number of further points need to be considered before a commercially viable system could be developed. These relate to

- Location of the hydraulic roll control system
- Size of the shuttle actuation device
- Integration with other systems

The mounting position of the Hydragas roll control system on the car is not of vital significance as flexible hoses may be used to connect the system to it's fluid supply. However, it would be preferable to mount the shuttle and valve as near to the front of the car as possible in order to minimise pipe pressure losses since the hydraulic power is likely to come from an engine driven pump. It is likely that a system such as this would be available as an optional extra and would not therefore be fitted to all cars of a particular model. Careful Consideration should therefore be given with regards to installing the system around the existing passive suspension and to the coupling between passive and active systems.

The large size of the prototype roll control shuttle was regarded as a considerable problem. It was thought that a number of modifications would need to be made to the shuttle in order to make it

commercially viable, including a reduction in size. A unit of size equivalent to an exhaust pipe silencer would be satisfactory.

The benefits of roll control systems such as that investigated have been shown to be significant. These benefits may be increased further by using the roll control system in conjunction with other ride and handling enhancements. The use of active suspensions in integrated systems including traction control and four wheel steering has already been discussed (chap 1). It has also been proposed [30] that roll control systems may also be used in conjunction with semi active dampers. Since both systems can operate independently; roll control effects attitude during manoeuvres whilst semi active damping controls body motion with respect to road induced disturbances, they may be used together, giving the advantages of both systems.

Other adaptations to the Hydragas suspension system may also be considered, such as lateral interconnection during straight ahead driving and switching of the pitch damper orifices between soft and hard settings.

## 6.9 Costs and Benefits

The primary benefit of active roll control suspensions is the reduction of body roll during cornering manoeuvres which in itself is known to be subjectively appreciated by drivers. There are also a number of secondary benefits associated with the reduction of roll. Firstly the reduction of wheel to road camber is advantageous since it raises the maximum cornering force available from the tyres and negates the need for suspension compliance effects to be built into the suspension system kinematics, allowing simpler linkage geometries. The simplification of suspension linkages could be expected to reduce the cost of manufacture.

The reduction of body roll may also reduce the action of roll steer effects. This may be a disadvantage since a certain degree of roll understeer is built into the existing Metro as a safety feature, giving a less responsive feel. Subjective opinion of the Hydragas® roll controlled car was that it was slightly too responsive.

Testing of the active car showed that the limit handling performance was improved since the suspension deflections were constrained so that the bump or rebound stops were not met. The test driver was able to perform an extreme lane change manoeuvre considerably faster in the active car than the passive car.

It is possible that the active roll control system, responding to a lateral acceleration demand, may have some beneficial effect on vehicle ride quality at low frequency. This is not discussed here; however it is certain that any action of the active system in controlling ride motions would result in a considerable increase in power consumption.

It has been shown that only a modest control system bandwidth is required for effective roll control during fast transient manoeuvres. The cost of the actuation system is therefore likely to be considerably lower than for a single corner of a fully active system. In addition, because of the fluid interconnection between the front and rear suspension units of the Hydragas car, only one actuator (or shuttle) is required to control body roll motion. This compares favourably with the four actuators necessary for a fully active system. It also compares favourably with other roll control systems. Since the active roll moment must be distributed between both axles for reasonable handling behaviour, systems using active roll bars normally use at least two actuators.

The control electronics for the active roll control system are reasonably simple since there is only one controlled variable (suspension linkage roll moment). This compares well with fully active systems, in which there are at least four controlled variables. The transducer costs should also be considerably less than those of even the simplest fully active system.

# 7. Further Simulation Studies and Roll Control Strategies

## 7.1 Introduction

### 7.1.1 Closed and Open Loop Systems

The validated computer model of the Hydragas roll control system gives a sound platform for investigating alternative control methods and strategies. This chapter describes research undertaken into these strategies.

Although the actuation control system used for the prototype vehicle included a feedback term of shuttle position, the roll control system was open loop. In effect, the roll control system estimated the linkage roll moment from a measured variable, the lateral acceleration. The performance of the system was therefore dependent on the size of the external disturbances and on how accurately the measured variables related to the actual linkage roll moment.

Closed loop systems using state information (deriving the roll angle from suspension deflections) have been developed and are outlined in section 2.1.4. For total roll cancellation, the feedback signal should be the absolute body roll angle. In practice however, it is more reasonable to measure only the secondary suspension deflections and hence body suspension roll angle. The error inherent in this approximation is dependent on the tyre stiffness and on operating conditions, however it is likely to be only a small percentage of the overall roll and hence acceptable.

The major difference between open and closed loop systems is that the former respond only to those variables that are directly measured, whereas the latter will respond to any disturbances effecting the controlled variable. The implication is that open loop systems may be designed to be sensitive only to particular disturbances such as cornering induced roll moments associated with lateral acceleration. Closed loop systems on the other hand will attempt to track other disturbance inputs such as road fluctuations, potentially causing a harsh ride. For this reason, a closed loop control system was not investigated here.

In this study, improvements to the open loop roll control system were investigated and, due to instrumentation cost implications, closed loop systems were neglected.

### 7.1.2 Inputs to and Effects of the Control System

Figure 7.1 shows the major influences on the control system and how these effect vehicle behaviour. Bold lines represent the primary function of the system, i.e. the closed loop control of the shuttle position in response to a manoeuvre induced lateral acceleration for the purpose of eliminating or reducing body roll. Feint lines indicate secondary effects on the control system performance, largely due to the large amount of cross-coupling present in the vehicle. Positive and negative signs indicate only relative relationships and should not be taken as absolute values. Therefore, the actual direction of travel is unimportant, a positive demand signal taken to be one which causes the shuttle to move to oppose passive roll.

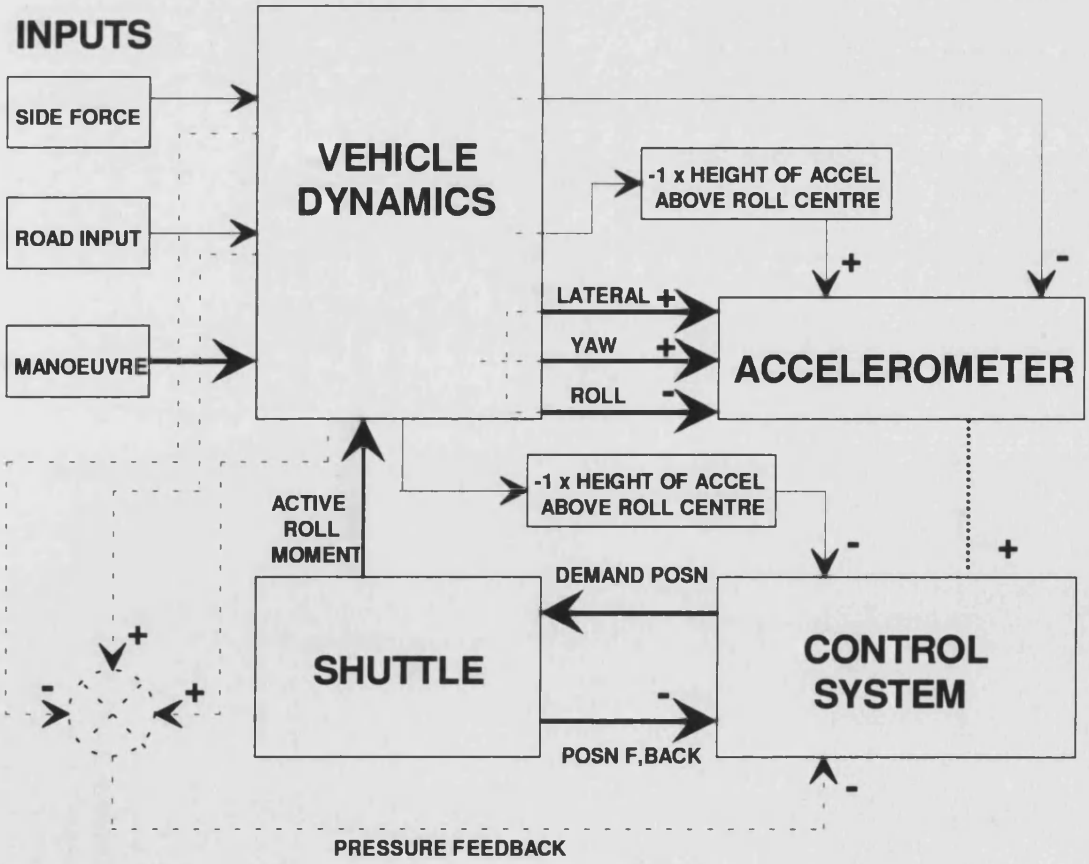


**Fig 7.1** *Inputs to and Effects of Hydragas Active Roll Control System*

The dotted lines in the above figure are included to describe the effects of side-to-side pressure difference feedback. For this case, the position feedback term in the figure should be neglected.

## 7.2 Effect of Pitch Damper Orifice Position on Roll Control

### 7.2.1 Current System

The purpose of the pitch dampers in the interconnection lines of Hydragas equipped cars is to prevent excess body motion following pitch disturbance inputs. They are a necessary compromise to the reduced pitch stiffness and damping associated with fluid interconnection. In the vehicle tested, the pitch dampers were positioned in each interconnection pipe towards the front of the vehicle. It was natural therefore to introduce the fluid lines from the active roll control shuttle behind these dampers. It may be the case that vehicle transient behaviour in cornering could be altered by changing the position of the pitch dampers relative to the active fluid lines. This would have an effect on the transient lateral load transfer distribution of the car.

The subjective opinion of the prototype roll controlled vehicle was that it was somewhat over-responsive, turning sharply into corners. This was because the normal roll understeer associated with suspension deflection was not present.

A contributory factor may be the rearward lateral load transfer bias caused by pumping the Hydragas fluid to and from the interconnection lines rearwards of the pitch dampers. In transient manoeuvres, fluid will pass to and from the rear suspension units marginally before the front units. This has the effect of biasing the lateral load transfer distribution towards the rear. The cornering stiffness at the rear wheels is therefore reduced resulting in a greater slip angle at the rear than would normally be the case.

By switching the fluid supply lines to a position ahead of the pitch dampers, the opposite effect could be achieved. The transient understeer thus achieved would go some way to alleviating the reduced understeer due to suspension geometry effects.

Due to fluid interconnection, the positioning of the active fluid supply lines would have no effect on the steady state lateral load transfer distribution. In order to determine the significance of the pitch damper position during a transient lateral manoeuvre ( step steer ) the computer simulation model was used.

### 7.2.2 Simulation Results

Computer simulations were carried out at a number of different forward speeds for the active system in which fluid was fed into the conventional interconnection lines both in front of and behind the pitch damper orifices. Results are presented for speeds of 8.33 m/s and 20 m/s. Figures 7.2, 7.3 show the effect of the orifice position on lateral load transfer distribution and slip angles for the vehicle travelling at 8.33 m/s. The orifice diameter was 3.3 mm.

With the active system feeding in behind the damper orifice, as in the experimental prototype vehicle, lateral load transfer is biased towards the rear of the car. This is exaggerated in the transient phase because the pitch dampers delay the build-up of pressure in the front suspension units. With the active system connected in front of the damper, the steady state load transfer distribution is also biased towards the rear but the transient load transfer is distributed almost equally between front and rear.

The orifice position has little effect on either the transient or the steady state slip angles, despite the difference in lateral load transfer distribution. Similarly, there is little effect on the lateral and yaw acceleration response of the vehicle. This is probably because the load transfers are insufficient to cause the tyres to operate in the saturation region of their operating curves.

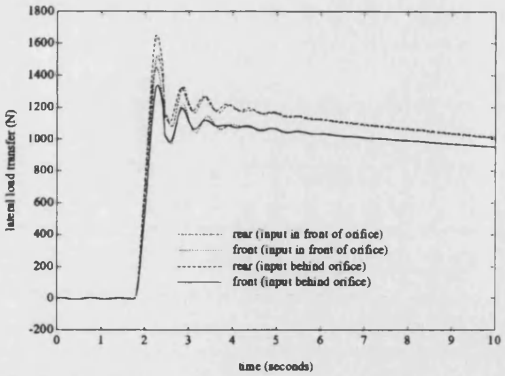


**Fig 7.2** *Effect of Pitch Damper Orifice Position on Lateral Load Transfer Distribution in 8.33 m/s Step Steer*

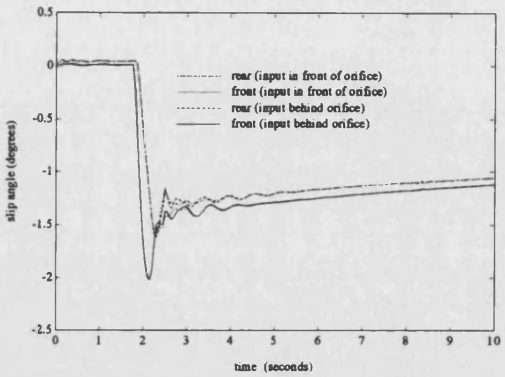


**Fig 7.3** *Effect of Pitch Damper Orifice Position on Front and Rear Axle Slip Angles in 8.33 m/s Step Steer Test*

### 7.2.3 The Effect of Reducing Pitch Orifice Diameters

A hypothetical case was investigated in which the pitch damper orifice diameter was reduced. While this would not be practical due to the resultant change in passive pitch damping, a similar result could be achieved by feeding the supply from the active system directly into the suspension units and placing a suitably sized restriction in the flow path to either the front or rear units.

Results are presented for a pitch damper orifice diameter of 1 mm. Again, the simulation was performed for two forward speeds. Figures 7.3 and 7.4 show the front and rear lateral load transfer and the front and rear slip angles at a vehicle forward speed of 8.33 m/s. Again the orifice position had a significant effect on the transient lateral load transfer distribution but little effect on the difference between slip angles at the front and rear.

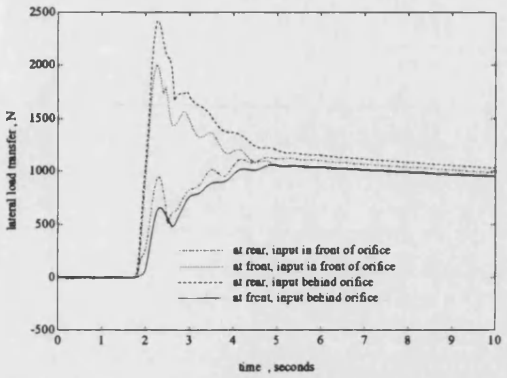


**Fig 7.3** *Effect of 1 mm Pitch Damper Orifice Position on Lateral Load Transfer Distribution in 8.33 m/s Step Steer*

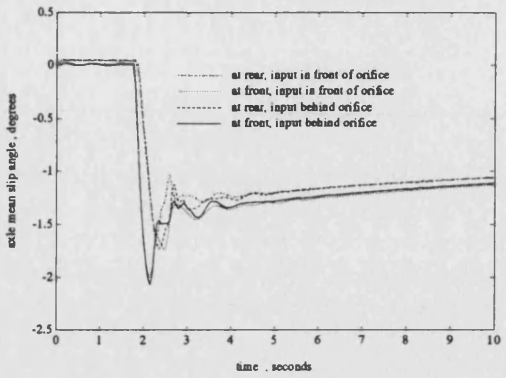


**Fig 7.4** *Effect of 1 mm Pitch Damper Orifice Position on Front and Rear Axle Slip Angles in 8.33 m/s Step Steer Test*

The effects were more noticeable at a forward speed of 20 m/s, as shown in figures 7.5 and 7.6. The lateral load transfer distribution showed a similar trend to those described previously but the effect on front and rear slip angles was considerably greater, probably because the tyres were operating under high load conditions. With the active system feeding into the interconnection pipe behind the pitch damper orifice, as in the prototype vehicle, the transient slip angles at front and rear were approximately equal. However, with the active system feeding into the interconnection pipe in front of the pitch damper, the transient slip angle was greater at the front axle than the rear, suggesting a transient understeer characteristic more closely approximating the understeer built in to the passive car ( figure 7.7 ).

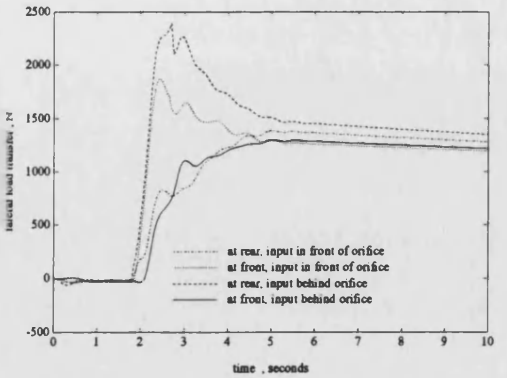


**Fig 7.5** *Effect of 1 mm Pitch Damper Orifice Position on Lateral Load Transfer Distribution in 20 m/s Step Steer*

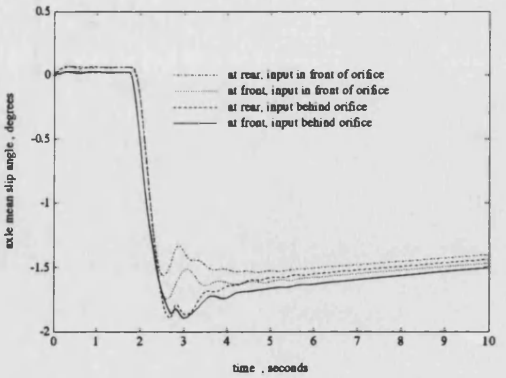


**Fig 7.6** *Effect of 1 mm Pitch Damper Orifice Position on Front and Rear Wheel Mean Slip Angles in 20 m/s Step Steer*

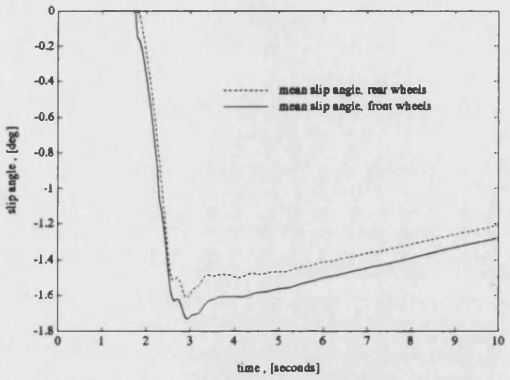


**Fig 7.7** *Passive Vehicle Front and Rear Wheel Mean Slip Angles in 20 m/s Step Steer*

The results of this study indicate that the position at which the active roll control system is joined to the passive interconnected Hydragas system is unlikely to effect transient handling of the vehicle. However lateral load transfer and tyre effects may change the transient handling characteristics at high speed. The current arrangement (active and passive systems joined behind the pitch orifices ) is therefore advised for reasons of simplicity since on the standard vehicle, the orifices are located close to the front suspension units.

There are possible handling benefits to be gained by restricting active fluid flow to the front units still further but it seems unlikely that these will be significant enough to warrant the additional cost and hardware requirements associated with such a system.

## 7.3 Demand Accelerometer Position

### 7.3.1 Vertical position

Control of the Hydragas system has previously been described as 'open loop'. However the effects of coupling between the body yaw, roll and lateral motions may result in the control system input signal being effected by the system output, thus providing a feedback path from output to input. This was demonstrated in figure 4.14 in which the output from the roll control system ( i.e. active roll

moment ) can be seen to have an effect on the input (measured lateral acceleration ). Because of this feedback path, the question of system stability is raised.

The measured acceleration signal, used to drive the control system comprised four elements, their relative magnitudes dependant on accelerometer position:

$$a_{measured} = a_y + x_a a_\varphi - z_a a_\phi + U\dot{\beta} \qquad (7.1)$$

The term due to vehicle forward speed and rate of change of body slip angle will generally be small unless the car is spinning.

Work by Ross-Martin [ 72 ] has shown two important features in acceleration controlled system stability:

(i), the yaw acceleration response to active roll moment input is considerably lower than the roll and the lateral acceleration response.

(ii), such a system is likely to be more unstable at low speeds.

It was also proposed that accelerometer vertical position could have a marked effect on stability by introducing a component of roll acceleration into the demand signal.

The active vehicle body roll response to a step steer input is shown in figures 7.8 and 7.9 for two different speeds at a number of different accelerometer vertical positions. Note that displacements are measured vertically *below* the centre of gravity in accordance with SAE convention.

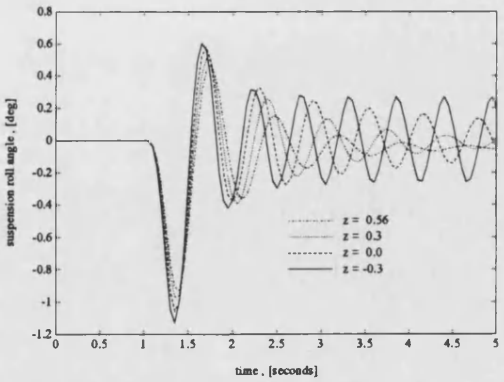


**Fig 7.8** *Influence of Accelerometer Vertical Position ( z ) on Roll Response to a Step Steer Input at 8 m/s*

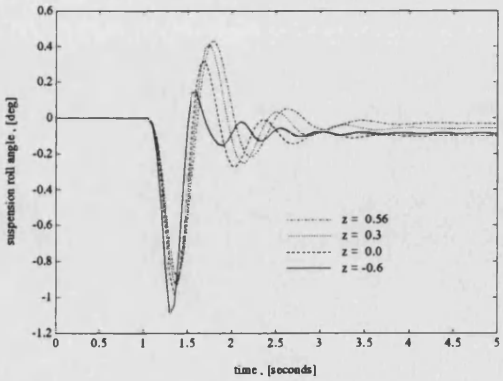


**Fig 7.9** *Influence of Accelerometer Vertical Position ( z ) on Roll Response to a Step Steer Input at 20 m/s*

It is clear that for system stability at low speed the demand accelerometer should be placed as low to the ground as possible. The figures also show that the system is far more likely to be unstable at low speed. At high speed it is evident that a low accelerometer position effectively reduces roll damping and results in undesirable body motion following a lateral disturbance. The value of 0.56m below the vehicle c.g. represents an accelerometer position on the road and is therefore impractical. The value of 0.3m below the c.g. represents the accelerometer position used in the testing of the prototype vehicle and seems to be an appropriate position for further systems.

The reason for this instability with high accelerometer positions can be seen by studying figure 7.1. With the accelerometer positioned above the vehicle roll centre, there is a positive feedback path between the body and the controller. Roll accelerations induced by the active roll control shuttle tend to cause the shuttle to move further in the same direction. The opposite is true when the accelerometer is placed below the roll centre.

### 7.3.2 Longitudinal Position

The aim of the roll control active suspension system is to maintain zero roll attitude by exactly opposing roll moments applied externally to the vehicle due to manoeuvres. However, in the prototype system, linkage roll moment was not available as a measured value and was approximated using a measured acceleration signal. During steady state cornering, linkage roll moment is approximately proportional to lateral acceleration as shown previously (chapter 5), i.e.

$$M_L = K_1 a_y \tag{7.2}$$

Under transient conditions however, the relationship is more complex. A reasonable approximation is given by combining lateral and yaw acceleration terms:

$$M_L = K_1 a_y + K_2 a_\varphi \tag{7.3}$$

The constants $K_1$ and $K_2$ are dependant on front and rear roll centre heights and mass distribution. They may be derived as follows:

The total suspension linkage roll moment may be considered as the sum of the individual front and rear roll moments:

$$M_L = M_{La} + M_{Lb} \tag{7.4}$$

These roll moments may be assumed to be functions of the lateral components of the linkage forces and the roll centre heights only, a reasonable assumption since suspension linkage angles and associated linkage forces are generally small. The total suspension linkage roll moment may be re-written:

$$M_L = F_{Lya} z_{rca} + F_{Lyb} z_{rcb} \tag{7.5}$$

which may be expanded thus:

$$M_L = \frac{\left(F_{Lya} + F_{Lyb}\right)\left(z_{rca} + z_{rcb}\right) + \left(F_{Lya} - F_{Lyb}\right)\left(z_{rca} - z_{rcb}\right)}{2} \tag{7.6}$$

Now, neglecting tyre aligning forces, longitudinal, gyroscopic and aerodynamic forces, the body lateral and yaw accelerations may also be written in terms of the lateral components of the linkage forces.

$$a_y = \frac{F_{Lya} + F_{Lyb}}{m_s} \tag{7.7}$$

$$a_\varphi = \frac{F_{Lya} a - F_{Lyb} b}{I_\Psi} \tag{7.8}$$

which may be rearranged to give

$$F_{Lya} + F_{Lyb} = m_s a_y \tag{7.9}$$

and

$$F_{Lya} - F_{Lyb} = \frac{2I_{\Psi}a_{\varphi} - \left(F_{Lya} + F_{Lyb}\right)(a-b)}{a+b} \tag{7.10}$$

These may be substituted into equation 7.6 to give

$$M_L = K_1 a_y + K_2 a_{\varphi} \tag{7.11}$$

where

$$K_1 = \frac{m_s\left(az_{rcb} + bz_{rca}\right)}{a+b} \tag{7.12}$$

$$K_2 = \frac{I_{\Psi}\left(z_{rca} - z_{rcb}\right)}{a+b} \tag{7.13}$$

The values of $K_1$ and $K_2$ can be easily found for a specific vehicle at a given operating condition. In the BATH*fp* vehicle model, all the necessary components are available as parameters or variables (in the case of the moving roll centre). Therefore it is a simple matter to test the above statements by comparing the predicted linkage roll moment with that estimated using equation 7.11.

Figures 7.10 and 7.11 show the results of such a comparison for a step steer manoeuvre performed at two different speeds. In order to make the comparison, a vehicle model incorporating ideal active roll control was used. An active roll moment equal and opposite to that derived from inertial forces was applied to the vehicle body such that it did not roll. The roll centre heights therefore remained constant throughout the test and the calculation of constants $K_1$ and $K_2$ was simple. The values of the parameters used to calculate $K_1$ and $K_2$ are presented in table 7.1.

| | |
|---|---|
| Sprung Mass, $M_s$ | 780 kg |
| Vehicle Yaw Moment of Inertia, $I_\psi$ | 787 kgm$^2$ |
| Front Axle / c.g. Distance, a | 1.1 m |
| Rear Axle / c.g. Distance, b | 1.163 m |
| Front Roll Centre Height Below c.g, $z_{rca}$ | 0.4063 m |
| Rear Roll Centre Height Below c.g, $z_{rcb}$ | 0.56 m |
| Constant, $K_1$ | 375.0 kgm |
| Constant, $K_2$ | 53.5 kgm$^2$ |

**Table 7.1.** *Parameters Used to Estimate Suspension Linkage Roll Moment*

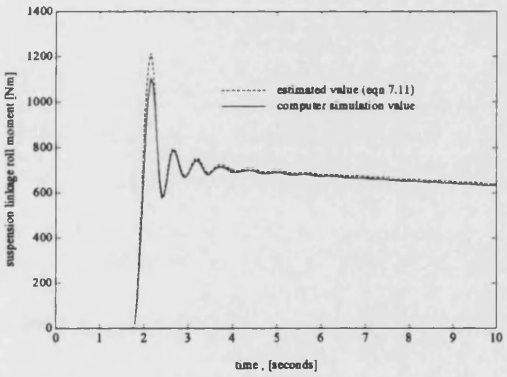


**Fig 7.10** *Estimation of Suspension Linkage Roll Moment in 5m/s Step Steer Using Constants $K_1$ and $K_2$*

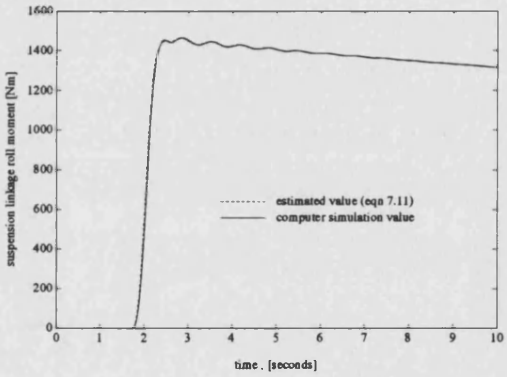


**Fig 7.11** *Estimation of Suspension Linkage Roll Moment in 15m/s Step Steer Using Constants $K_1$ and $K_2$*

A component of yaw acceleration can be introduced into the measured demand signal by positioning the accelerometer forward of the c.g. This also provides an amount of phase lead to the system which can be used to compensate for dynamic lag in the active hydraulic system. The effect of this control system lead varies with forward speed. The positioning of the accelerometer is therefore a matter of some deliberation.

The influence of accelerometer longitudinal position on system response is demonstrated for two different speeds in figures 7.12 - 7.15.

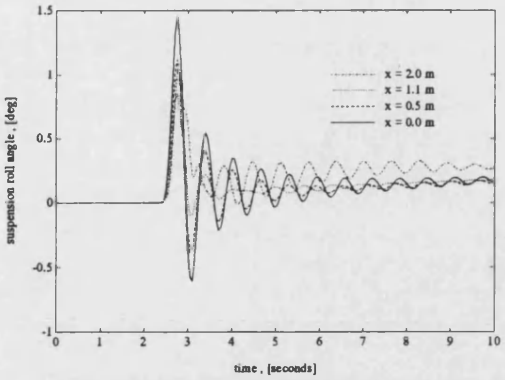


**Fig 7.12** *Effect of Accelerometer Longitudinal Position ( x ) on Roll Angle Response in a 5 m/s Step Steer Test*

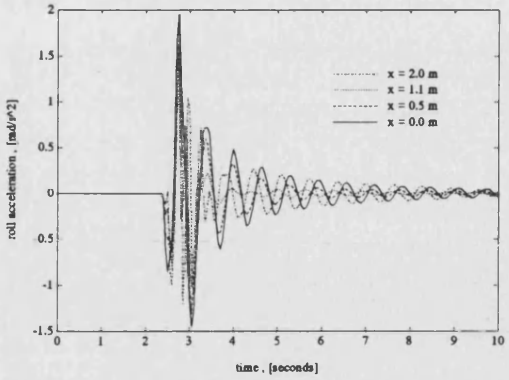


**Fig 7.13** *Effect of Accelerometer Longitudinal Position ( x ) on Roll Acceleration Response in a 5 m/s Step Steer Test*

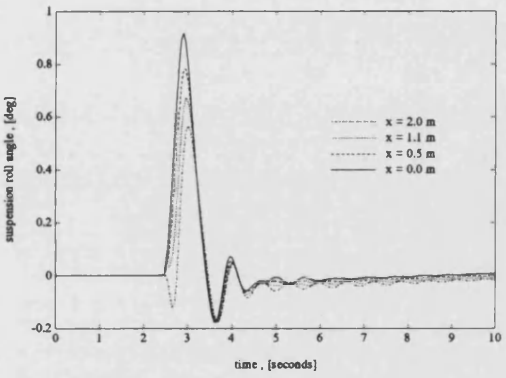


**Fig 7.14** *Effect of Accelerometer Longitudinal Position ( x ) on Roll Angle Response in a 20 m/s Step Steer Test*

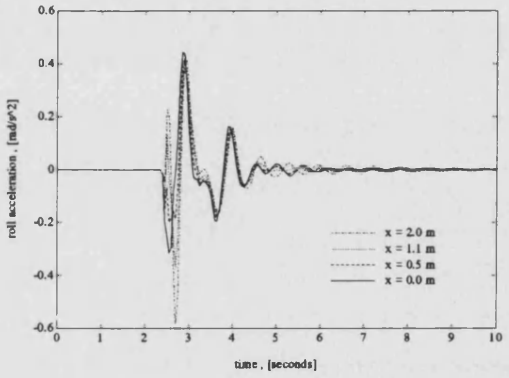


**Fig 7.15** *Effect of Accelerometer Longitudinal Position ( x ) on Roll Acceleration Response in a 20 m/s Step Steer Test*

It is clear that the yaw acceleration component of the measured signal has a greater influence at low speed. It appears that there is a benefit in terms of roll attitude control to be gained from mounting the accelerometer ahead of the c.g. However, a position too far ahead of the c.g. leads to high roll acceleration and instability at low speed. The position on the front bumper, 1.1m ahead of the c.g. appears to offer the best compromise between transient roll control, roll acceleration and stability over the range of vehicle speeds.

## 7.4 Differential Pressure Feedback

### 7.4.1 Introduction

The controlled variable for the prototype active roll control system is suspension roll moment. The forward path term is an estimate of the linkage roll moment, in this case a measured lateral acceleration. The feedback term, also an approximation, is the active shuttle position measured by an LVDT displacement transducer. An alternative to this arrangement is to use shuttle differential pressure.

Such a system would be beneficial from the viewpoint of reduced transducer costs and simpler, sealed shuttle design. For a Hydragas vehicle exhibiting zero roll, the body roll moment in reaction to the applied forces is proportional to the Hydragas unit pressure difference across the car. The most obvious difference between displacement and pressure feedback systems is that the former estimates the active roll moment alone whereas the latter is an estimate of the total roll moment. A consequence of this is that the pressure controlled system will respond to ride disturbances caused by road inputs. The system feedback will seek to move the vehicle body in opposition to the road disturbance, thereby improving ride comfort.

There are two realistic possibilities for the measurement of differential pressure, these being the differential oil pressure across the hydraulic shuttle measured at the valve or the differential water pressure measured between the Hydragas end effectors of the shuttle as measured for the experimental vehicle tests. Pressure measurement at the valve has the disadvantage that it includes any terms associated with losses in the hydraulic system such as pipe pressure drops and actuator friction losses. This study therefore examines the possibility of using differential Hydragas fluid pressure as the control system feedback term.

### 7.4.2 Simulation Results

Figure 7.16 shows the simulated values of shuttle position and pressure feedback for an increasing speed active vehicle steerpad manoeuvre. There is a high level of similarity between the two, the

pressure signal being greater than the position signal at low lateral acceleration and vice versa at high lateral acceleration levels. The gain for the pressure feedback signal is 0.43 V/bar compared with a position feedback gain of 250 V/m. The non-linear effect of the taper rates in both the active displacers and the suspension units is thought to account for the difference between the position and pressure feedback term.

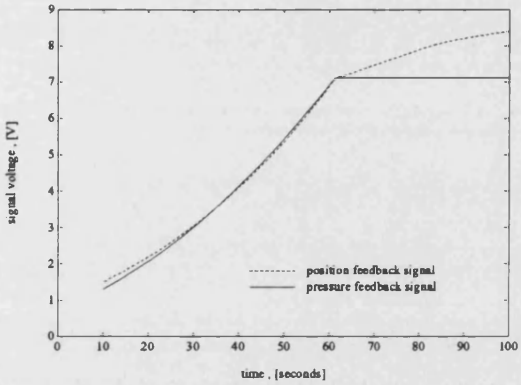


**Fig 7.16** *Simulated Pressure and Position Feedback Signals in Steerpad Manoeuvre*

The effect of using either position or pressure feedback on steady state roll control is shown in figure 7.17. Both systems are capable of maintaining a small suspension roll angle at lateral acceleration levels for which the shuttle is within it's stroke. The system using differential pressure feedback maintains better control of roll attitude over this range of lateral acceleration. This is because the pressure feedback signal at low lateral accelerations is greater than the equivalent position feedback signal, thereby producing less displacement of the shuttle. At lateral acceleration levels above those causing the shuttle to reach it's end stops, the further roll of the vehicle body is independent of the type of feedback used since the roll angle in this region is dependant only on the passive suspension characteristics.

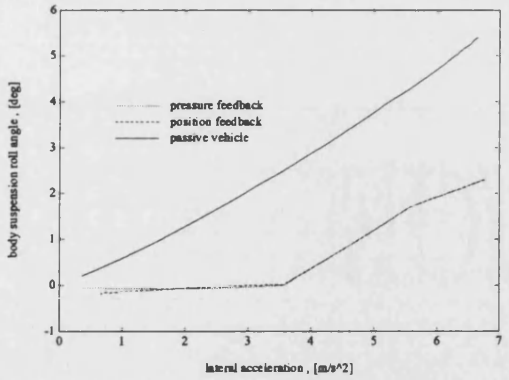


**Fig 7.17** *Suspension Roll Angle for Pressure and Position Feedback Systems and Passive System in Steerpad Manoeuvre*

In a step steer manoeuvre, the pressure feedback system is less able to control the body's transient suspension roll angle, as shown in figure 7.18. This may be explained by examining the feedback signals during the manoeuvre ( figure 7.19 ). It has already been demonstrated (chapter 5) that rapid manoeuvres produce a transient peak in side-to-side differential pressure. The pressure feedback signal during such manoeuvres may therefore be expected to be larger than the equivalent position feedback signal. Therefore the resulting valve control signal is lower during the transient period and the shuttle responds less quickly.

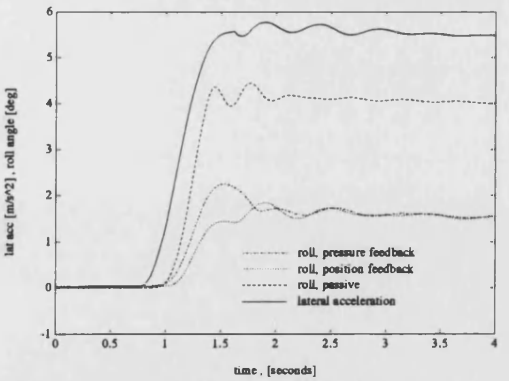


**Fig 7.18** *Suspension Roll Angle Response in Step Steer Using Pressure and Position Feedback Control*

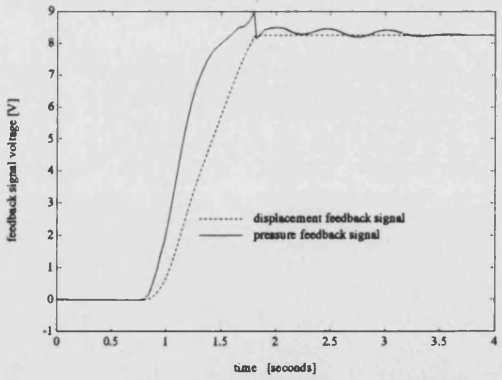


**Fig 7.19** *Differential Pressure and Shuttle Position Feedback Signals During Step Steer Manoeuvre*

### 7.4.3 Lateral Force Disturbance

Figures 7.20 and 7.21 show the effect of an extreme step change lateral force disturbance ( for example a side gust of wind ) on the roll control systems using pressure and displacement feedback. In both systems there is an initial roll motion in the opposite direction to that induced by cornering manoeuvres. This is because in a cornering manoeuvre, the side forces are developed at the tyre contact patches, whereas externally applied forces are assumed to act at the vehicle body centre of gravity. The action of the active roll control system has a detrimental effect on the situation.

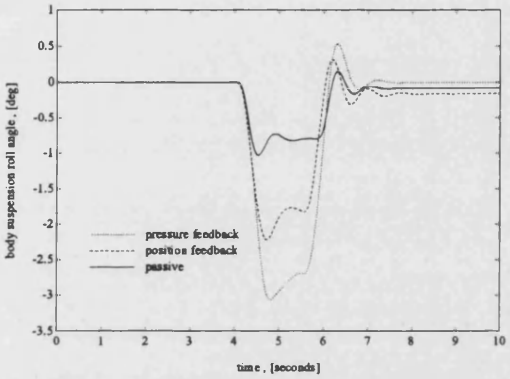


**Fig 7.20** *Lateral Acceleration Response to Lateral Disturbance Force for Both Pressure and Position Feedback Active Systems and Passive System*

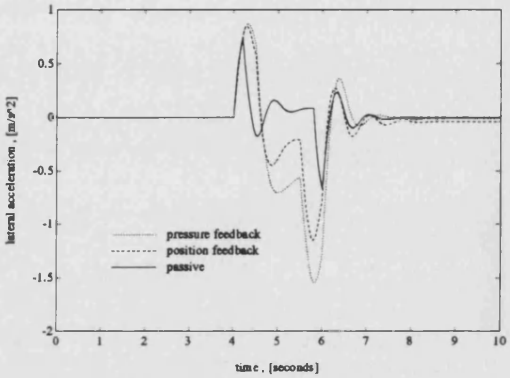


**Fig 7.21** *Roll Angle Response to Lateral Disturbance Force for Both Pressure and Position Feedback Active Systems and Passive System*

The side force induced lateral acceleration results in a shuttle position which is intended to cancel out roll associated with lateral acceleration forces. In this case it is in the opposite direction to that induced by the disturbance force hence it adds to the roll angle of the passive car. The pressure feedback has a further detrimental effect. The Hydragas fluid differential pressure is directly effected by the input disturbance force, such that it reduces the magnitude of the feedback signal, as shown in figure 7.1, causing the shuttle to move to a more extended position than for the position feedback case. The control system demand and feedback signals for both pressure and position feedback control are shown in figures 7.22 and 7.23.

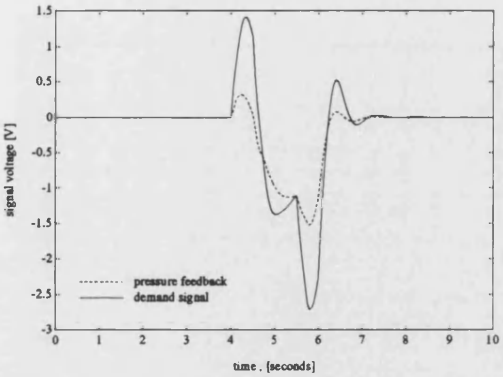


**Fig 7.22** *Control System Demand and Pressure Feedback Signals in Response to a Lateral Disturbance Force*

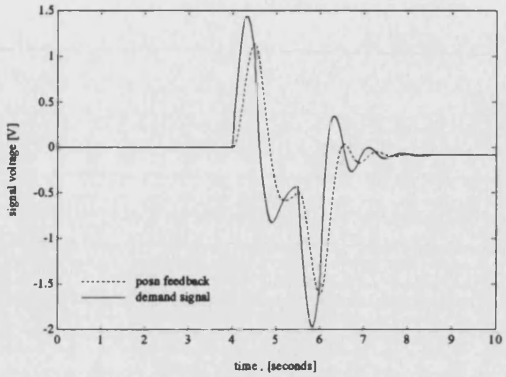


**Fig 7.23** *Control System Demand and Position Feedback Signals in Response to a Lateral Disturbance Force*

### 7.4.4 Road Roll Disturbance

The effect of a road disturbance on both the pressure and position feedback control systems is examined in figures 7.24 - 7.27. A 0.04m impulse input in road vertical displacement was applied to both wheels of one side of the vehicle model, with a suitabie delay for the rear wheel. This simulated the wheels on one side passing over a large stone or a pothole. In both cases a significant roll angle was developed without the high lateral acceleration associated with cornering induced roll. For the pressure feedback system, the roll angle developed is slightly less than for the position feedback system, both having roll angles slightly greater than the passive vehicle.

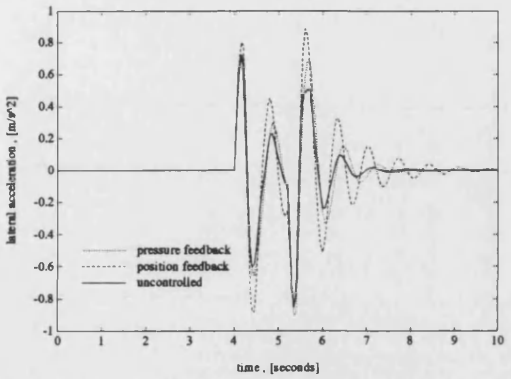


**Fig 7.24** *Lateral Acceleration for Pressure and Position Feedback Systems and Passive System in Response to Road Vertical Input*

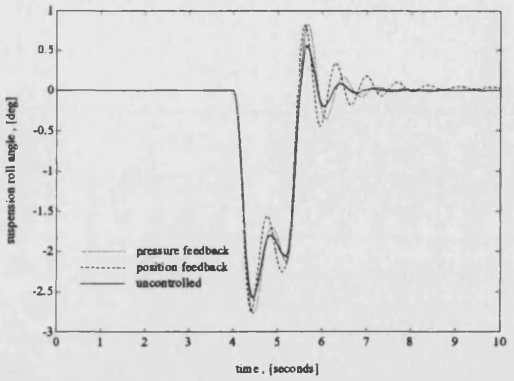


**Fig 7.25** *Roll Angle for Pressure and Position Feedback Systems and Passive System in Response to Road Vertical Input*

This may be explained by examining figure 7.1. The pressure feedback signal response is greater than the shuttle position feedback signal since the pressure differential is affected directly by the disturbance input. A feedback signal greater than the lateral acceleration demand causes the shuttle to move to raise the wheel going over the bump and lower the other wheel, resulting in reduced body roll compared to the position feedback system. The low bandwidth of the roll control system prevents it from having a large effect on roll angles associated with road disturbances

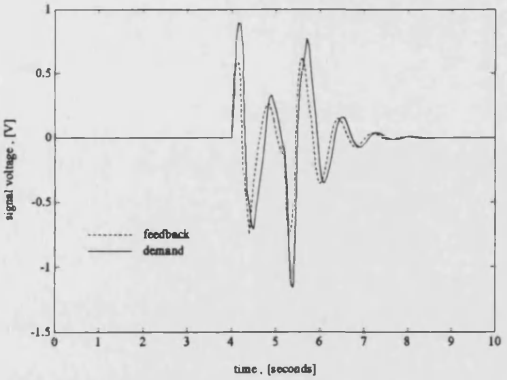


**Fig 7.26** *Control System Demand and Pressure Feedback Signals in Response to a Road Vertical Displacement Input*

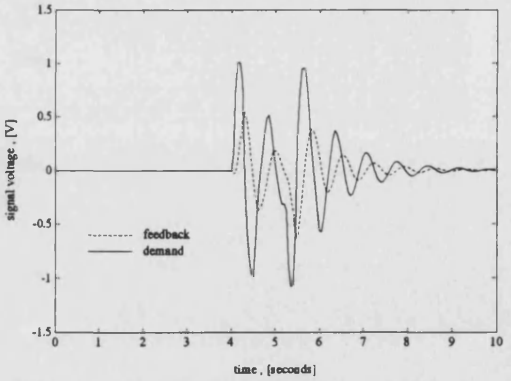


**Fig 7.27** *Control System Demand and Position Feedback Signals in Response to a Road Vertical Displacement Input*

The desirability of reduced body roll caused by road disturbance inputs is subject to question. While a reduction in roll acceleration and displacement is beneficial from a ride perspective it places significant demands on the hydraulic actuation system. Power consumption is therefore greatly increased. Since the control system bandwidth was deliberately selected to be low, it is unlikely that the active system would be able to adequately control road induced motions. It is therefore suggested that steps should be taken to avoid the action of the roll control system in response to road inputs, such as a low pass filter to attenuate high frequency components of the measured signals.

### 7.4.5 The Effect of Varying Payload

The vehicle simulation model was further used to determine the effect of additional loading (increased body mass). Figure 7.28 shows the steady state roll control performance of both systems with the sprung mass increased by 250 kg from the standard ( 2up + 50kg ) conditions. It appears that the performance of the pressure feedback controlled system is worsened by the addition of extra mass to a greater extent than the position controlled system.

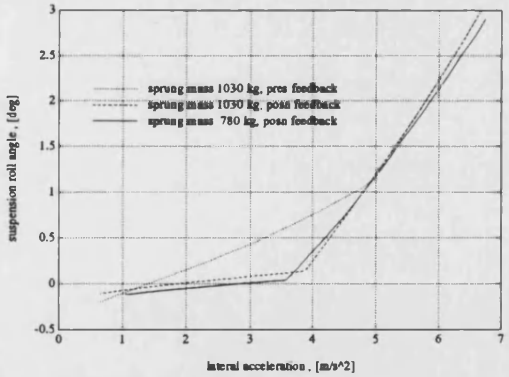


**Fig 7.28** *Effect of Sprung Mass on Steady State Roll Control Performance of Position and Pressure Feedback Systems*

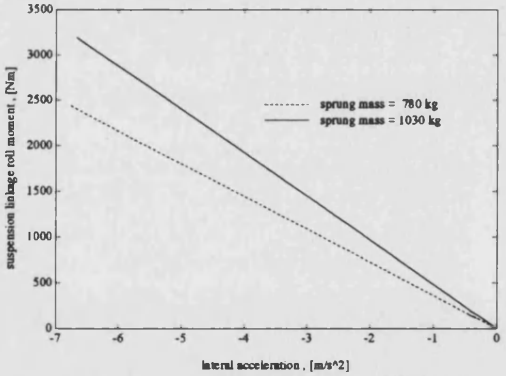


**Fig 7.29** *Relationship Between Lateral Acceleration and Suspension Linkage Roll Moment at Two Sprung Masses*

Both systems control body roll less well upon the addition of extra body mass. This is because the control system gains are established for a particular loading condition. By the addition of extra sprung

mass, the relationship between lateral acceleration and suspension linkage roll moment is changed. Measured lateral acceleration for a particular manoeuvre is not directly effected by the sprung mass, however the suspension linkage roll moment is significantly affected. The relationship between lateral acceleration and suspension linkage roll moment for the two loading cases is shown in figure 7.29.

Since the acceleration measurement in the active system represents an approximation to the suspension linkage roll moment, an error in this approximation due to the addition of extra mass will result in an under-estimation of the demand necessary for roll cancellation. This is shown in figure 7.30, where the shuttle position is shown against lateral acceleration for position feedback controlled systems at both the nominal sprung mass and with an additional 250 kg. The displacement of the shuttle is unaffected by sprung mass, which, in the case of the overloaded vehicle, is insufficient to entirely cancel roll. In the case of a lower sprung mass (than the design value), overcompensation of body roll would occur.

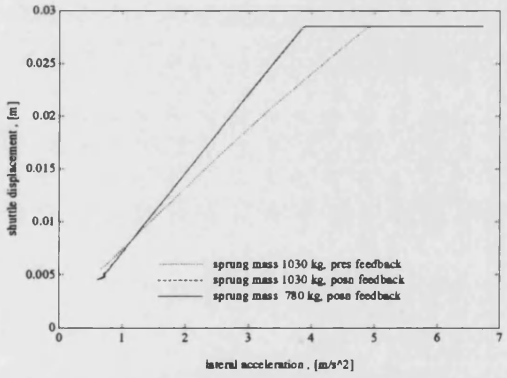


**Fig 7.30** *Shuttle Displacement in Position and Pressure Feedback Roll Control Systems*

The situation is further worsened in the case of the pressure feedback system. The side-to-side pressure differential is directly effected by the sprung mass magnitude. Increasing the sprung mass will increase the lateral load transfer and hence the differential pressure for a given lateral acceleration. The control system feedback signal is therefore dependent on sprung mass and, in the

case of increased body mass, will provide an artificially high signal, resulting in a further under-estimation of required shuttle position. This is shown in figure 7.30.

The transient performance of the position and pressure feedback controlled systems is shown in figure 7.31. Again, the performance of the pressure feedback system is worse than that of the position feedback system. The pressure feedback system is further compromised during transient manoeuvres as shown in figure 7.32. It has been shown previously that flow restrictions in the pipes connecting to the suspension system give rise to sharp transient pressure peaks. These raise the feedback signal to an artificially high level so that the shuttle position demanded is still further an underestimate of that required to eliminate roll.

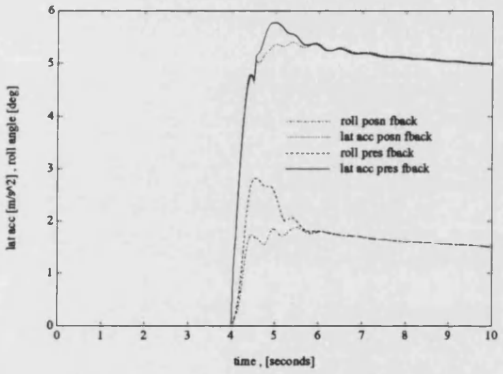


**Fig 7.31** *Performance of Active Roll Control System with Additional Sprung Mass of 250 kg During Step Steer*

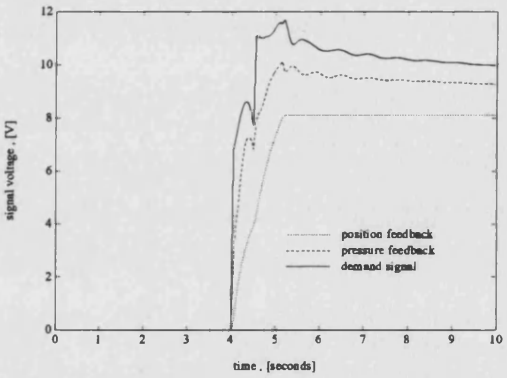


**Fig 7.32** *Demand and Feedback Signals During Step Steer Manoeuvre With Additional Sprung Mass of 250 kg*

## 7.5 Lateral Interconnection

### 7.5.1 Introduction

The concept of longitudinal interconnection is well established and has been proven to offer improved ride performance. It is suggested therefore that there may be a similar benefit to be gained from lateral interconnection. In the case of the Hydragas® system, this would be embodied in a

Hydragas fluid connection between the interconnection lines on each side of the car. Lateral fluid interconnection has been studied by Rakheja et. al. [ 73 ] who suggested that there are ride benefits to be gained by linking the hydro-pneumatic suspension units of each side of the vehicle. They compared an interconnected vehicle supported on a beam axle with a vehicle having non-interconnected independent suspension of a similar static vertical stiffness, and hence their results are not of direct significance here.

The reduction of roll rate may beneficial from a ride perspective but may also result in excessive roll angles during manoeuvres. With the two sides of the car hydraulically connected, the active roll control would have no steady state effect. If lateral interconnection is to be adopted therefore, it is advisable to introduce a solenoid valve into the interconnection line, controlled by the same signals as the active roll control system such that the two sides of the car could be isolated during manoeuvres.

### 7.5.2 The Effect of Lateral Interconnection on Vehicle Ride

The Moulenweg sampled test track ( data supplied by Ford ) was used in a computer simulation using the BATH*fp* non-linear vehicle model to compare the ride performance of a vehicle incorporating lateral interconnection with that of a standard vehicle. Simulated tests were carried out at 10 and 20 m/s. The results of these tests are shown in figures 7.33 and 7.34.

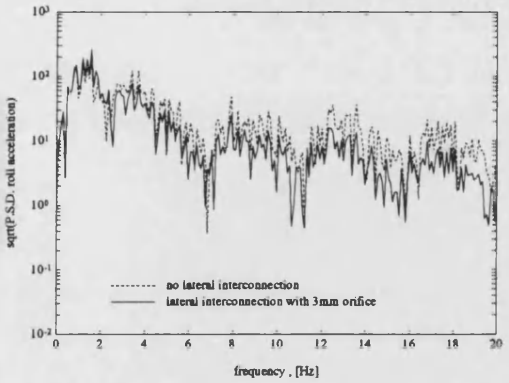


**Fig 7.33** *Effect of Lateral Fluid Interconnection on Ride in the Roll Mode at 10 m/s*

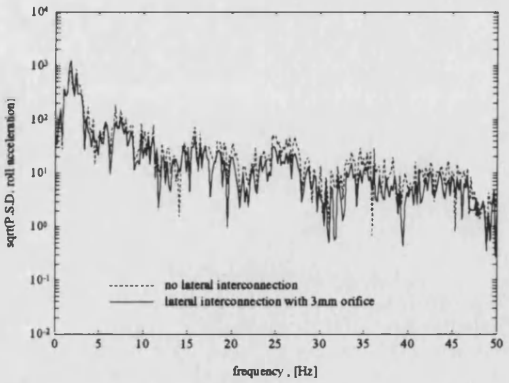


**Fig 7.34** *Effect of Lateral Fluid Interconnection on Ride in the Roll Mode at 20 m/s*

Bounce and pitch ride modes were not effected by the lateral interconnection and are therefore not shown here. A roll damping orifice was introduced into the lateral interconnection line to prevent excessive motion at low frequency. Despite this, the body accelerations at low frequency were higher for the interconnected case. At higher frequency, body accelerations were lower with the interconnection. This suggests that lateral interconnection may reduce ride harshness and noise at high frequency at the expense of reduced control of low frequency roll.

## 7.6 Steering Wheel Measurement Based Roll Control

### 7.6.1 Introduction

The demand signal for the prototype active roll control system studied in this work has previously come from an accelerometer mounted laterally on the vehicle body. This provides an estimation of the suspension linkage roll moment against which the active system reacts. As an alternative to this arrangement, roll moment estimation may be based on the measurement of steering wheel angle input and vehicle forward speed. This has a number of possible advantages:

1. Reduction in transducer costs since steering wheel angle/velocity transducers are widely available and much lower in price than accelerometers. Vehicle speed information is easy and cheap to obtain.
2. Reduction in hydraulic system dynamic requirements since movement of the steering wheel will precede any forces generated at the tyres and any subsequent lateral acceleration.
3. Reduced 'sensitivity' to changes in loading. Lateral acceleration provides an accurate estimation of suspension linkage roll moment for a particular set of loading conditions. If these conditions change however, the approximation becomes less accurate. However, in the case of an understeering vehicle such as the Metro used in this study, steering wheel angle for a particular manoeuvre will

tend to increase with payload, making the relationship less sensitive to load changes.

4. Insensitivity to road input ride disturbances, except those transmitted through the steering linkages to the rack. This will decrease power consumption during straight ahead driving.

Steering wheel angle and forward speed may be mapped to lateral acceleration under a particular set of operating conditions in order to provide an estimate of suspension linkage roll moment. This may be achieved in a number of ways. A typical approach would be to define points which describe the relationship between steering wheel angle, speed and lateral acceleration and interpolate between these. This method requires a substantial data set which would be called every time the controller functions, resulting in a slow response.

Recent years have seen the emergence of the neural network which significantly reduces the computing effort needed to define relationships between any number of dependant variables. In this study, the neural network was investigated as a method of relating speed and steering wheel angle to lateral acceleration.

### 7.6.2 The Neural Network

Neural networks have been used for a variety of applications within the automotive industry. Typical applications include the control of engine management systems and continuously variable transmissions [ 74 ]. Their use has also been investigated with reference to active suspensions [ 75, 76].

A neural network is a structure consisting of a number of simple components which combine to provide a relationship between input and output data. The complexity of the structure depends on the complexity of the relationship and the number of inputs and outputs. The name refers to the biological

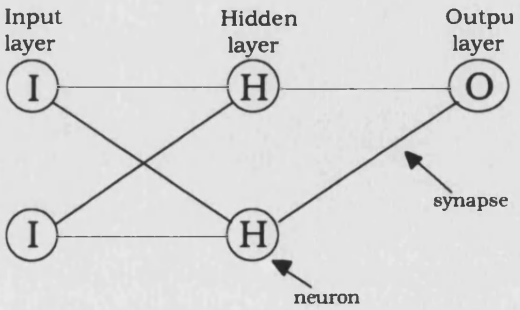


**Fig 7.35** *The structure of a simple neural network*

structures which inspired them. Rather than relying on interpolation between known data points, these networks seek to provide an algebraic relationship between any number of inputs and their corresponding outputs.

The structure of a simple neural network is shown in figure 7.35. Any number of inputs and outputs are possible. This net has two inputs and one output, which is the requirement for mapping speed and steering wheel angle to lateral acceleration. A network such as this is known as a multi-layer perceptron and is commonly used for representing non-linear continuous functions. It consists of three banks of nodes or neurons, the input layer, one or more hidden layers and an output layer. The neurons of each layer are fully connected to each of the neurons of the adjacent layers by a series of links known as synapses. The hidden layer (s) can have any number of neurons.

The size of a network must be optimised for the particular problem. Generally, increasing the number of neurons will increase the accuracy of the network up to a point where accuracy will fall again, but will also reduce the speed of operation [ 74 ]. For this study, the best arrangement was found to have two hidden layers, each with four neurons. The means for selecting this arrangement was somewhat arbitrary, however less complex structures gave inferior predictions whereas networks of an greater complexity offered little increase in accuracy.

$$a_j = \frac{1}{1 + e^{-\left(\sum a_{ij} w_{ij} + \varphi_j\right)}}$$

**Fig 7.36** *Equation at each hidden layer neuron*

Each neuron of the input layer corresponds to an input parameter, which is presented as a floating point number scaled between 0 and 1. Generally the presented data will be scaled to within 10% of the upper and lower limits, so that points outside the measured data envelope can be accommodated. These scaled values pass via the synapses to the first hidden layer, where the data is processed.

Each of the synapses is assigned a weight and each neuron is assigned a bias, with the exception of the input layer, the neurons of which merely pass on the input data unchanged. The neurons of the first hidden layer each receive signals from the input layer via the first bank of synapses. These signals are multiplied by their weighting factor ($w$) and summed. The sum of these weighted signals is added to the bias ($\varphi$) of that neuron. This has the effect of increasing or decreasing the importance of that neuron to the network. The resultant sum is used in a non-linear activation function ( in this

case a sigmoidal curve ). The outputs of each neuron are then passed on to the next layer via the next bank of synapses. A single hidden layer neuron is represented by the equation shown in figure 7.36. '$a$' represents the output from a neuron while '$i$' and '$j$' refer to the previous and current layer respectively. The above process is repeated by the neurons of each hidden layer. The output neurons collect signals from the last hidden layer and present a value between 0 and 1.

In order to make the network represent a real system, the weights and biases must be optimised by an iterative training process. The network is trained by presenting it with measured input and output data. The training data is presented many times, each time known as an epoch. The network parameters are incremented every epoch until the output values match the desired outputs to a specified degree of accuracy. There are a number of algorithms available to do this. The technique used here is known as Stochastic Back Propagation [ 77 ]. This is commonly used in modelling applications. The network effectively learns the relationship between the presented input and output data. It can then predict outputs for input points it has not previously encountered as long as extrapolation is not required.

Several factors will effect the accuracy of the network. Increasing the volume of data presented will generally have a beneficial effect but care must be taken to avoid conflicting data, for example identical inputs with different outputs. There should be enough data to define any non linear behaviour adequately. Data should, where possible, account for any possible range of inputs and outputs as, with any interpolation method, extrapolation is less accurate than interpolation. Input data was therefore supplied over the full range of vehicle speeds and steering wheel angles.

Once trained, the network is treated as a black box. Input values are presented and output values collected. A network can represent a huge volume of data by simple algebraic relationships. Once trained, the values of weights and biases need not be altered and few lines of code are needed to describe the network. It can therefore run very quickly.

### 7.6.3 Training of the Neural Network

Several attempts were made before a suitable network was found to describe the steady state relationship between vehicle speed, steering wheel angle and lateral acceleration. The layout found to

give the best results in the shortest time contained two hidden layers, each with four neurons. The data used to train the network was acquired from quasi-steady state BATH*fp* simulations. Initial data sets consisted of seven runs at constant speed, gradually increasing the steering wheel angle until a maximum lateral acceleration ( about 7.3 $m/s^2$ ) was achieved. This was found to give insufficient definition in the speed axis. A new data set was acquired consisting of seven runs at constant speed (including zero) and six runs at constant steering wheel angle (again including zero). The surface representing the training data is shown in figure 7.37. The stochastic back propagation method presented the training data in random order. This was useful in preventing the network from becoming confused by the periodic nature of the data.

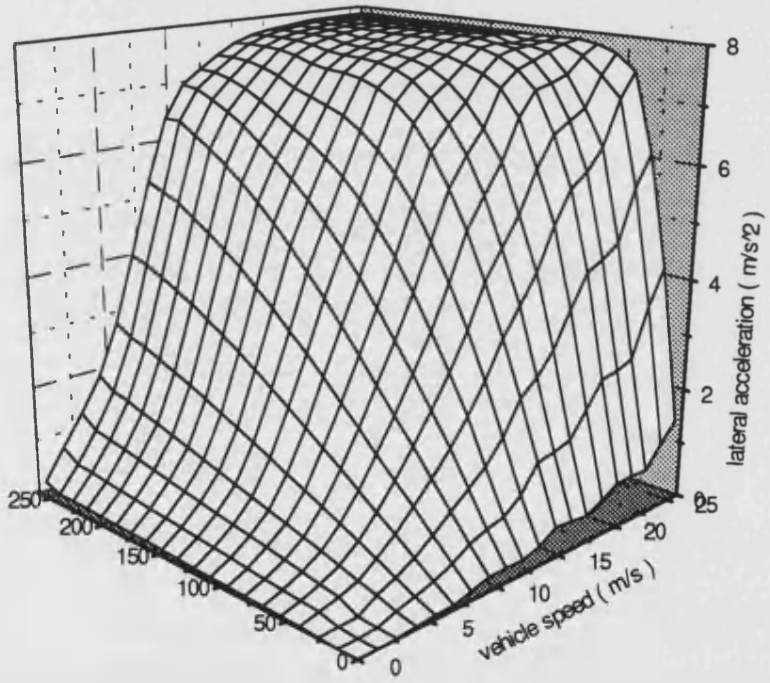


**Fig 7.37** *Surface Plot Representing Data Used to Train the Neural Network*

The vehicle speed data ranged from 0 to 30 m/s (about 70 mph.). In order to aid the network training process, the minimum and maximum scaled values were chosen to be 10 % outside these values. Therefore speed data was scaled between -5 and 35m/s. Negative (reverse) speeds were dealt with by taking the absolute value of speed and multiplying by the sign after the neural network. The

steering wheel was dealt with similarly, steering wheel data being scaled between -50° and 350°. The

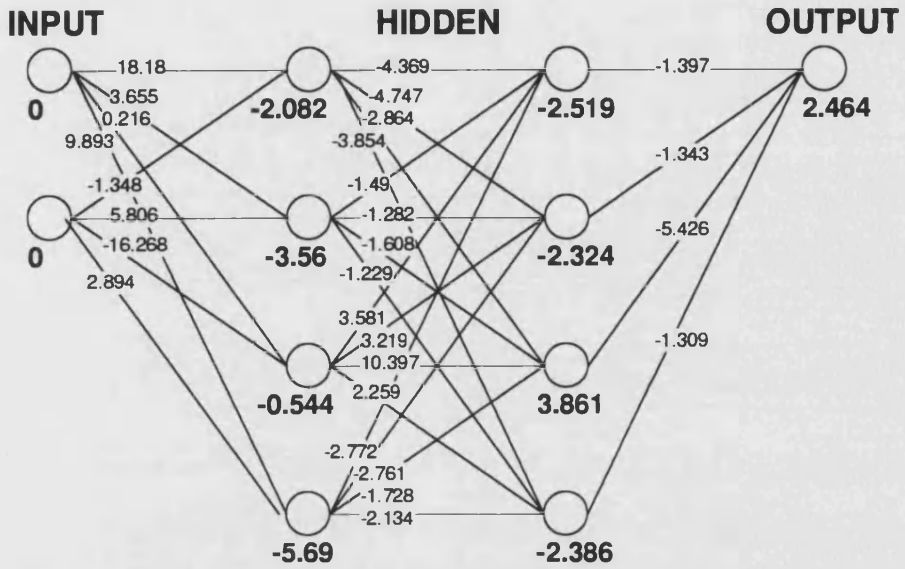


**Fig 7.38** *Trained Neural Network Showing Biases and Weights of Neurons and Synapses*

trained network is shown in figure 7.38.

Overall, just under 200 data points were used. These were sufficient to train the network to within 2.5

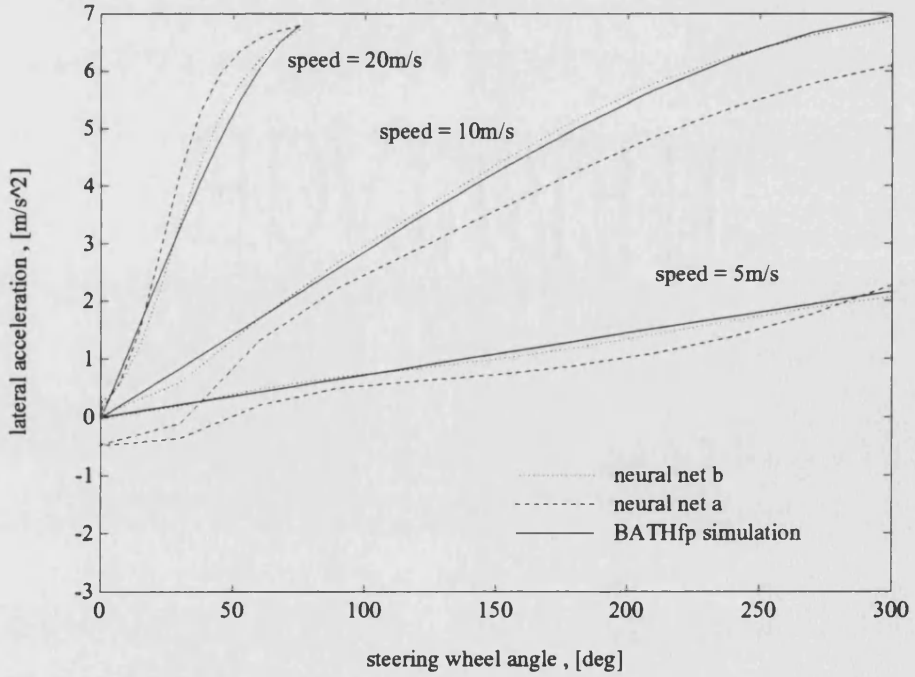


**Fig 7.39** *Performance of Two Neural Networks ( a Simple Network with One Hidden Layer, 'a' and a More Complex Arrangement, 'b') in Estimating Lateral Acceleration*

% average error. The accuracy of the neural net predictions of lateral acceleration for the training data is demonstrated in figure 7.39. The training data for three of the constant speed runs is plotted together with the predicted values for two different neural network structures. The first was a simple network with one hidden layer containing two neurons. The second was the more complex arrangement with two hidden layers, each containing four neurons. It is clear that the more complex arrangement provides a far better approximation of lateral acceleration than the simple network. The comparisons presented here are slightly misleading in that the data used to train the network was

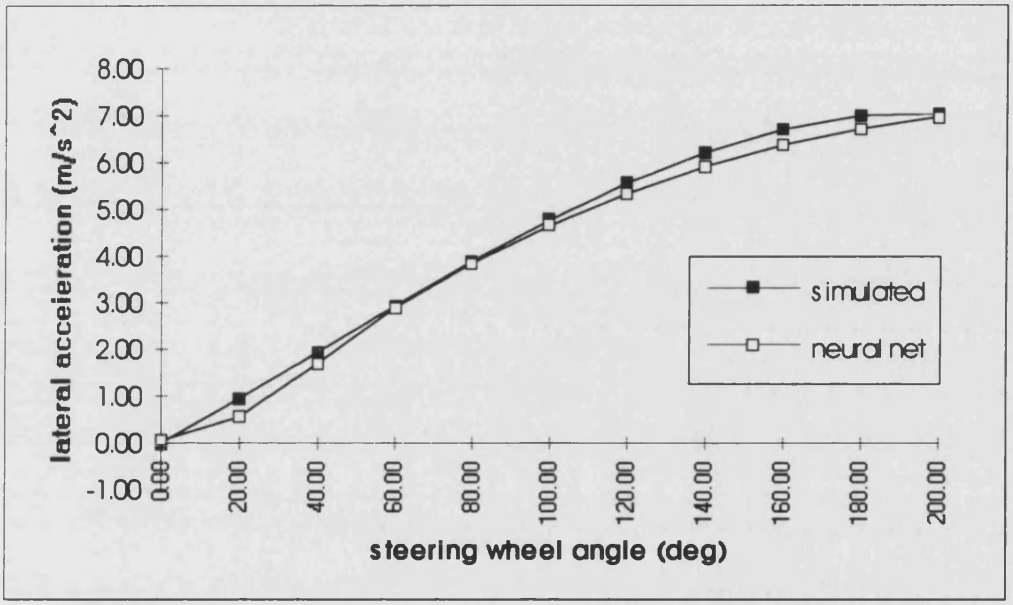


**Fig 7.40** *Neural Network Approximation to Lateral Acceleration for Previously Unencountered Data*

obtained from the computer simulation and therefore free from noise. This was necessary since suitable road data was not available.

The real test of the performance of a neural network is to present it with input data it has not previously encountered. An example of this is given in figure 7.40, for which an additional simulation run was performed at a constant speed of 12 m/s. The neural network was presented with the speed and steering wheel data for which it produced estimated lateral accelerations. These are compared with the values taken directly from the simulation. The neural network provides a reasonable approximation.

### 7.6.4 Implementation of Neural Network into BATH*fp*

The code used to describe a neural network was very simple, consisting of only one main equation ( shown in figure 7.36 ) which was used repeatedly. To produce a satisfactory model for use with the BATH*fp* simulation package, the neural network model had to be self-contained. It was necessary to allow appropriate inputs to be supplied and to supply an output at suitable ports. The scaling of input and output data was performed within the model to ensure simplicity and avoid confusion.

A BATH*fp* model must be linked to an associated graphical *icon*. This allows the model to be inserted in the graphics interface. Port types and positions are specified within the icon. Problems could occur as different icons would be needed for networks containing different numbers of inputs and outputs. The problem could be overcome by streaming all the inputs and outputs through the same ports, although this may in turn require further models to collect together the inputs and separate the outputs. The icons used for the neural network model used here represented any network having 2 inputs and 1 output.

The number of inputs, outputs and internal variables must also be specified for a given model. Therefore, different models would be required for different network layouts. The task of defining a new neural network model has been made easier using a template model written in C. This was originally used for the simulation of an engine management controller [ 78 ]. This reads in the structure of the network and the values of all weights and biases from a data file during the initialisation stage of the simulation. Only minor changes to the model code and to the model definition in BATHmat ( Bath model adding tool ) were then needed to produce a new network model.

The neural network controller model was in fact embodied in a number of adjacent icons describing a pre-processor, the input layer, the hidden and output layers and a post processor. Used in conjunction, these models represented a black box controller which was easily incorporated into the BATH*fp* vehicle model. The neural network model described the two- hidden layer arrangement detailed earlier.

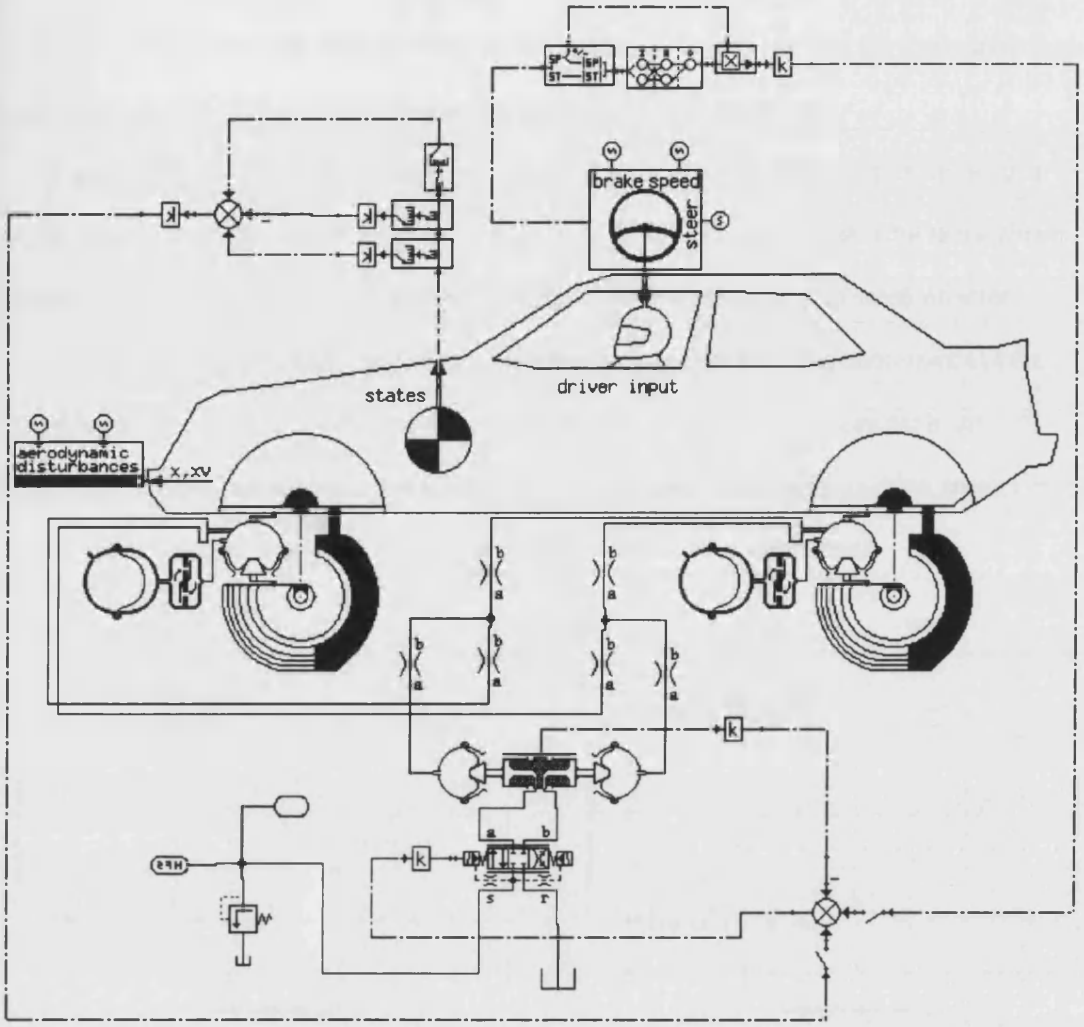


**Fig 7.41** *BATHfp Circuit for Neural Network Controller Testing*

A BATH*fp* vehicle model incorporating both conventional lateral acceleration and neural network controllers is shown in figure 7.41. The acceleration based controller was introduced in parallel with the neural network controller to facilitate performance comparisons. Switch models were used to select uncontrolled, acceleration controlled or steering / speed controlled vehicle modes (and potentially composite control including both acceleration and speed / steer signals). Both speed and steer signals were passed down the line between the vehicle controller and the neural network models.

### 7.6.5 Steady-State Performance of the Neural Network Controller

Having established the accuracy of the neural network in estimating lateral acceleration and having written models to describe the trained network for use in BATH*fp*, the network was used as a

controller for the active roll control circuit. In this capacity, it directly replaced the acceleration signal previously used to provide a demand signal for the active roll control shuttle.

Figures 7.42 and 7.43 show the roll control performance of the neural network controller in a quasi-steady state manoeuvre in comparison with the acceleration based controller for two different speeds. The performance of the acceleration based controller is independent of speed since the suspension linkage roll moment is a function of lateral acceleration only. The performance of the neural network controller is subject to some variations with speed due to inaccuracies in the estimation of lateral acceleration. The neural network controlled system allows a small amount of roll at low lateral accelerations, again due to inaccuracies in acceleration estimation.

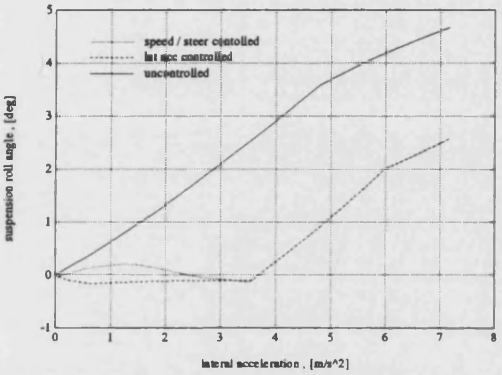


**Fig 7.42** *Performance of Active Systems Using Lateral Acceleration and Speed / Steer Controllers at 12 m/s*

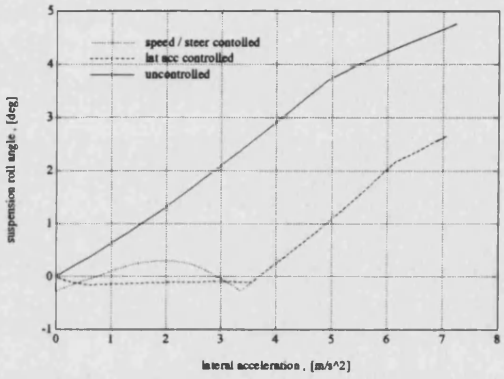


**Fig 7.43** *Performance of Active Systems Using Lateral Acceleration and Speed / Steer Controllers at 20 m/s*

The accuracy of the speed / steer controller in approximating lateral acceleration is dependant on the vehicle operating conditions. Figures 7.44 and 7.45 show the effect of halving the road friction coefficient on roll control for both systems. As expected, the lateral acceleration controlled system is unaffected by the change in friction. The speed / steer controlled system however, tends towards a slight roll-in with the reduced friction. This is because the lateral acceleration predicted by the neural network exceeds that achieved on the slippery surface. The neural network is given no indication of the change in conditions and can not therefore compensate for the change in the relationship between speed, steering wheel angle and lateral acceleration.

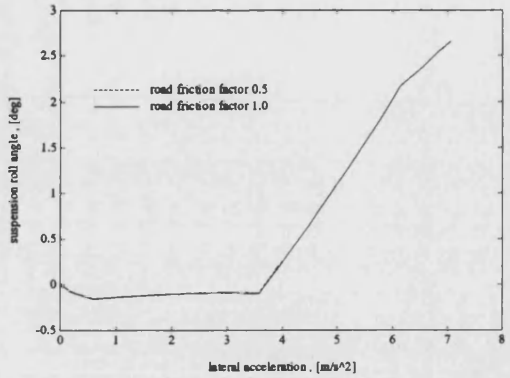


**Fig 7.44** *Performance of Lateral Acceleration Controlled Active System With Reduced Road Friction Coefficient*

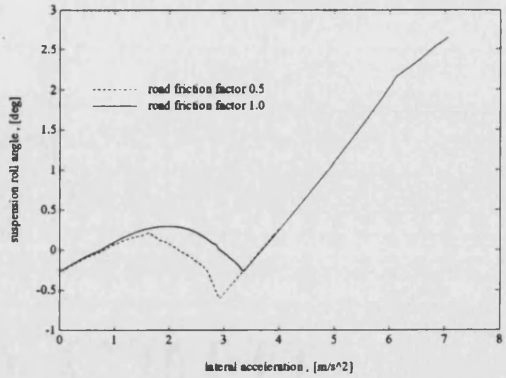


**Fig 7.45** *Performance of Speed / Steer Controlled Active System With Reduced Road Friction Coefficient*

A further test of the neural network controller was provided by increasing the value of the sprung mass in the computer simulation. An additional 250 kg was added at the body c.g. The results of this test are shown in figures 7.46 and 7.47. It is clear that the performance of both controlled systems is worsened by the addition of extra mass. It appears that the performance of the speed / steer controlled system is effected to a greater extent than the acceleration controlled system. This suggests that the neural network under-predicts the lateral acceleration which in turn indicates that the addition of extra load decreases the car's understeer coefficient over the working lateral acceleration range of the shuttle.

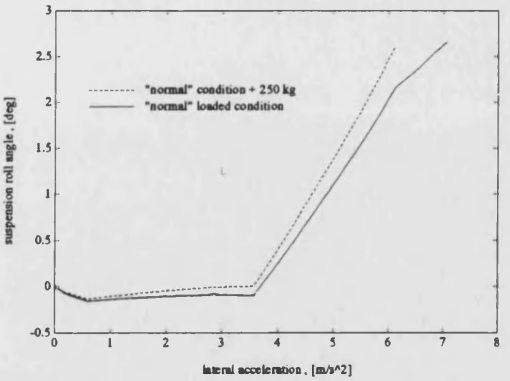


**Fig 7.46** *Performance of Lateral Acceleration Controlled Active System With Increased Sprung Mass*

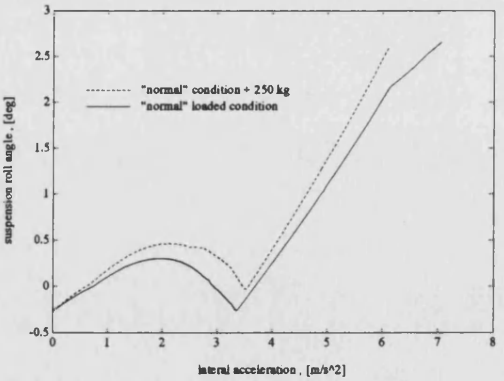


**Fig 7.47** *Performance of Speed / Steer Controlled Active System With Increased Sprung Mass*

### 7.6.6 Transient Performance of the Neural Network Controller

During steady state manoeuvres, the relationship between vehicle speed, steering wheel angle and lateral acceleration is a relatively simple one and is independent of time. For transient manoeuvres however, this simple relationship does not hold as vehicle dynamics play an increasingly important roll. The lateral acceleration response to a steering input is very much time dependant. Supplied with only two input variables, the neural network controller cannot hope to accurately predict transient relationships. Figure 7.48 shows the roll response of a vehicle in a step steer manoeuvre while figure 7.49 shows the actual and predicted lateral acceleration levels during the manoeuvre.

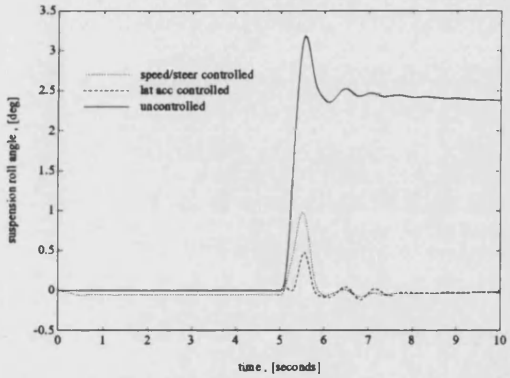


**Fig 7.50** *Roll Response of Passive, Acceleration Controlled and Speed/Steer Controlled Vehicles in Step Steer Manoeuvre*

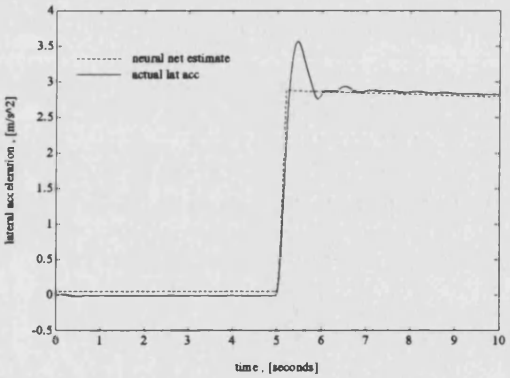


**Fig 7.51** *Actual and Estimated Lateral Acceleration for Speed/Steer Controlled Vehicle in Step Steer*

The neural network did not accurately predict the lateral acceleration response immediately following the steer input, underestimating the overshoot. However this was offset to some degree by the phase lead offered by the steer signal. Therefore the performance of the neural network controller was worse than that of the acceleration controller but not by a significant margin, the difference in transient roll angle between the two controlled systems being approximately 0.25°.

In order to predict transient lateral behaviour more accurately, the neural network must be supplied with more input variables. Steering wheel velocity has often been used as an additional control signal and can be obtained relatively easily using the same sensor as for the steering wheel

angle. This still has limitations though, as lateral acceleration overshoot may continue after the steering wheel is brought to a stationary position.

A possible solution would be to employ steering wheel signals sampled at discrete time intervals before the current time, using these extra signals to train the neural network. This method is known as recursive control and requires a system significantly more complex than that used in the work presented here.

In summary, the neural network controller outlined here offers some advantages over lateral acceleration based systems in terms of hardware requirements and control system costs. The work is not intended to be a thorough investigation of the speed / steer control of active roll control suspensions but an introduction to the possibility of using neural networks. As such it has shown that the approach is feasible.

It is suggested that a more complex neural network structure may predict lateral acceleration more accurately, particularly at low lateral acceleration levels where roll control is poor. It may be advisable to train the neural network only on data which is within the performance limitations of the active shuttle. At lateral accelerations above $4m/s^2$ the shuttle is at one of its end stops and cannot therefore move any further. Accurately predicting lateral acceleration in this region is therefore largely unnecessary. In the operating region below $4m/s^2$ accuracy is crucial and the neural network could be trained on just this data. If this approach were used, checks should be made that approximations to acceleration levels outside this range are sensible.

# 8. Conclusions

This chapter summarises the conclusions drawn from the research work described in this thesis and makes recommendations for further work.

## 8.1 Development of a novel Active Roll Control System

### 8.1.1 Practical Implementation

A novel active roll control system, based on the interconnected Hydragas® suspension system, has been developed. This took the form of a controlled 'shuttle' which displaced Hydragas fluid from the suspension units on one side of the car and to the suspension units on the other according to control signals from transducers mounted on the car. The prototype system was designed using computer simulation and subsequently mounted in the boot of an interconnected Hydragas Austin Metro. The primary aim of the system was to eliminate or reduce body suspension roll during cornering manoeuvres.

The roll control system was initially controlled manually to allow commissioning and static testing of the vehicle. The control system demand signal subsequently came from an accelerometer mounted laterally on the car body with displacement feedback being provided by an LVDT mounted on the shuttle. This lateral acceleration signal provided an estimate of the suspension linkage roll moment, giving 'open loop' control over body roll angle. Roll angle measurement was avoided since the control system could not distinguish between demand signals caused by inertial forces and those caused by road disturbances.

### 8.1.2 Vehicle Testing

Dynamic testing of the active vehicle was carried out at the University of Bath and at the Rover test track at Gayden. Ride testing was also performed using the University four poster road simulator. Measurements were made of front suspension deflections, lateral, yaw and roll accelerations, side-to-side Hydragas fluid differential pressure, steering wheel angle and control system demand and feedback signals.

Ride testing of the vehicle identified the main body natural frequencies and indicated the coupling between roll and bounce modes. Handling tests showed the active roll control system to be effective in eliminating suspension roll up to a lateral acceleration level of $3.5m/s^2$, and substantially reducing it above this value. The system performed well in both steady state and transient manoeuvres but its performance degraded once the hydraulic accumulator became discharged. It was found that the transient performance of the roll control system could be improved by mounting the lateral accelerometer ahead of the vehicle c.g. Active roll control was found to significantly improve vehicle handling during extreme manoeuvres by preventing the suspension from reaching its bump and rebound stops.

The mean power consumption of the active roll control system was below 1.2 kW, even during continuous operation ( slalom manoeuvres ). It was thought that in normal use, power consumption would be even lower.

## 8.2 Vehicle Modelling

### 8.2.1 Modelling of the Passive Interconnected Hydragas Suspension

The Hyrdagas fluid based suspension system has been modelled using semi-empirical models to represent the component parts of the system. These models have been validated under steady state and

dynamic conditions by comparison with experimental data and were found to be accurate. The Hydragas suspension models were then combined with a 10 degree of freedom vehicle ride and handling simulation computer model which had been validated as part of an earlier project.

The computer model was implemented within the BATH*fp* fluid power simulation environment. This made the description of the fluid based suspension a relatively simple matter and standard models were available to simulate the fluid interconnection pipe.

### 8.2.2 Modelling of the Active Roll Control System

The hydraulic active roll control system was modelled using a number of standard hydraulic models available within the BATH*fp* package together with other models written specifically for the active Hydragas system. The control system comprises a similar combination of standard and specifically written models. System parameters were set such that the performance of the simulated system approximated closely that of the physical prototype.

### 8.2.3 Validation of the Complete Vehicle Model

The simulation model's ride behaviour was compared with that measured on the experimental prototype vehicle. The computer model was shown to be qualitatively accurate and successful in identifying the body main natural frequencies. It did not account for ride modes associated with oscillation of the engine on its mounts.

Simulation of the passive vehicle in handling manoeuvres showed good agreement with experimental results although accuracy decreased at high lateral acceleration levels. The variation of steering wheel angle, body suspension roll angle and side-to-side pressure difference with lateral acceleration was comparable with experimental values for a steerpad test. Likewise, the transient performance of the vehicle was modelled accurately by the computer simulation.

The computer simulation of the active roll controlled vehicle was also compared with experimental results. The agreement between the two is good and several key features of the active roll control system were identified, in particular the increased side-to-side pressure difference due to the absence of suspension roll and the jacking effect of the shuttle.

## 8.3 Improvements to the Active Roll Control System

A number of improvements to the prototype roll control system have been suggested, based on improved cost, weight and function and supported by computer simulation. It has been recommended that an engine driven pump be used to power the hydraulic system rather than the existing electric unit. It has also been proposed that a smaller bore shuttle be used to eliminate the need for an accumulator. Computer simulation was used to optimise the size and bandwidth of the control valve. The possibility of using a simple directional valve was also investigated but has been shown to result in excessive valve flutter and ride harshness.

The performance of the vehicle in the event of an active system failure was investigated and a fail-safe system proposed. This system limits transient roll by isolating the shuttle ports and introducing a small cross port bleed path. This was introduced in order to allow the shuttle to return to its central position during straight ahead driving.

The effect of changing the position at which the active fluid flow enters the suspension interconnection lines has been determined. It has been shown that this position has no effect on steady state behaviour and little effect on transient handling properties. Physical constraints on the Hydragas system led to the conclusion that the coupling between active and passive systems should be behind the pitch damper orifice.

## 8.4 Investigation of Alternative Control Strategies

Several alternative control system designs were investigated and their performances compared with that of the existing system.

The position of the control system demand accelerometer was analysed. The vertical and horizontal position of the accelerometer had the effect of introducing elements of roll and yaw acceleration into the control system demand. It has been shown that a degree of roll acceleration, obtainable by mounting the accelerometer below the vehicle c.g. can increase system stability, particularly at low speed when roll damping is minimal.

It has been shown through simulation that the relationship between lateral acceleration and suspension linkage roll moment is approximately linear for steady state manoeuvres. For transient manoeuvres it has been demonstrated that there is a further dependency on yaw acceleration. This may be introduced into the control system by positioning the demand accelerometer ahead of the vehicle c.g. Simulation studies have shown that there is an optimal longitudinal position for the accelerometer at which transient roll is reduced to the greatest degree.

The use of Hydragas fluid side-to-side differential pressure feedback was investigated as an alternative to shuttle position feedback. The steady state performance of such a system was shown to be marginally better than its position controlled counterpart, compensating to a greater degree for the considerable non-linearities in the Hydragas system. The transient performance of the pressure feedback system was found to be somewhat worse than that using position feedback. In addition, the pressure feedback signal was more sensitive to externally applied forces arising from aerodynamic and road disturbances and therefore detrimental to system power consumption.

A simple neural network based speed / steering wheel angle controller has been developed and implemented within the BATH*fp* vehicle model. The performance of this controller was inferior to that of the acceleration based controller, particularly in the case of changing road surface friction. It

has been shown that there are potential benefits during transient manoeuvres arising from the control signal phase lead offered by steering wheel angle measurement but that the current neural network model is incapable of predicting lateral acceleration overshoot.

## 8.5 Recommendations for Further Work

### 8.5.1 Improvements to the Simulation Model

The accuracy of vehicle ride studies may be improved by representing the engine as a separate mass isolated from the main sprung mass by engine mounts. There may also be a case for including fluid inertia effects in the suspension interconnection pipes. This may have a significant effect at high frequency. Vehicle handling studies may be improved by including steering system dynamics and using a more accurate tyre model. It may also be advisable to include temperature effects in the modelling of the Hydragas® suspension units

### 8.5.2 Control System Studies

Further work should be carried out using the computer simulation model to determine the effects of the active roll control system on vehicle ride. The possible advantages and disadvantages arising from any attempt to control vehicle motion to due road undulation inputs should be quantified.

The work presented in this thesis on a neural network controller is intended as a feasibility study only. There remains large scope for improvement to this controller. A more complex network may be necessary to accurately predict low lateral acceleration levels. In addition, further input variables are required to fully describe the relationship between vehicle speed, steering wheel angle and lateral acceleration during transient manoeuvres. A more representative comparison between acceleration and steering controlled systems may then be made. A further possibility is a compound controller, using both lateral acceleration and speed and steering measurement.

### 8.5.3 Production of the Roll Control System

Recommendations are made within this thesis concerning improvements to the prototype roll control system. However there remains a good deal of work to be carried out. The hydraulic shuttle, in its present form, is unsuitable for a production vehicle. The design and long term reliability of the shuttle must be improved, possibly by incorporating a commercially available actuator. A more suitable control valve must also be selected. The electronics used to control the prototype system were bulky and based on analogue circuitry. It is likely that a microprocessor based controller would be developed for a production vehicle. The transducers should also be reduced in cost and selected for durability in a harsh working environment

# Appendix 1 Failure of the Shuttle End Caps

Under continuous testing at the Rover Gayden test track, the original prototype shuttle failed. Inspection showed the fault to be deformation and shear failure of the piston end caps, flush with the inside surface of the oil pistons. The failure is shown in figure A1.1. Analysis showed the end caps to be too thin and the replacement oil pistons were machined from solid with improved thickness of the end sections. The tapered water pistons were also re-designed to accommodate the new oil pistons.

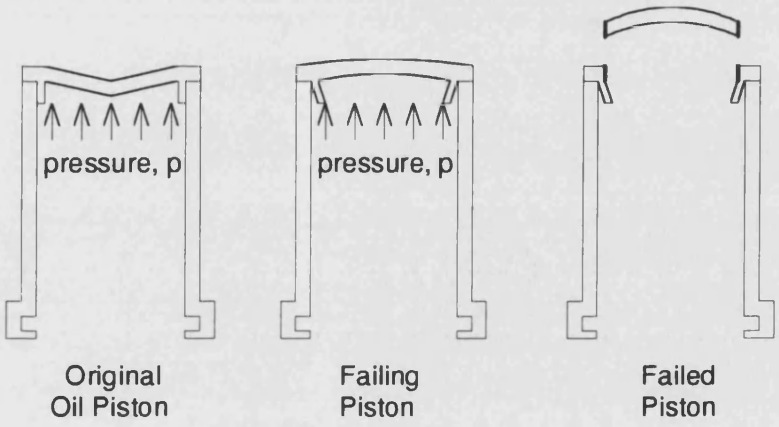


**Fig A1.1.** *Failure of the Original Prototype Oil Piston*

The piston end caps may be analysed by using the theory of plates and shells [ 79 ] assuming a circular plate with clamped edges. This theory gives us the deflection of the plate at any radius, r under a shear load, Q:

$$\frac{d}{dr}\left(\frac{1}{r}\frac{d}{dr}\left(r\frac{dw}{dr}\right)\right)=\frac{Q}{D} \qquad \textbf{(a1.1)}$$

where:

$w$ = plate deflection

$D$ = flexural rigidity

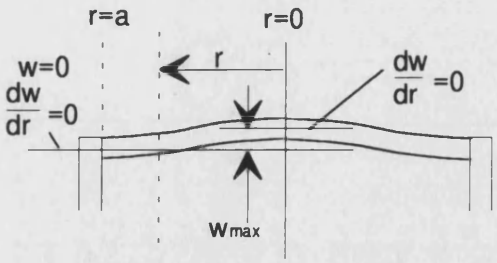


**Fig A1.2** *Relevant Dimensions*

The flexural rigidity, D, is defined thus :

$$D = \frac{Eh^3}{12\left(1-\nu^2\right)} \qquad \textbf{(a1.2)}$$

where

| | | |
|---|---|---|
| $E$ | = | modulus of elasticity |
| $h$ | = | plate thickness |
| $\nu$ | = | Poisson's ratio |

Assuming that the plate is loaded uniformly with pressure, q, the shear load may be expressed in terms of the piston hydraulic pressure

$$2\pi rQ = \pi r^2 q$$
$$Q = {}^{qr}/_{2} \qquad \textbf{(a1.3)}$$

hence :

$$\frac{d}{dr}\left(\frac{1}{r}\frac{d}{dr}\left(r\frac{dw}{dr}\right)\right) = \frac{qr}{2D} \qquad \textbf{(a1.4)}$$

Integrating gives:

$$w = \frac{qr^4}{64D} + \frac{C_1 r^2}{4} + C_2 \log\left({}^{r}/_{a}\right) + C_3 \qquad \textbf{(a1.5)}$$

where:

| | | |
|---|---|---|
| $a$ | = | radius at clamped edge |

and slope:

$$\frac{dw}{dr} = \frac{qr^3}{16D} + \frac{C_1 r}{2} + \frac{C_2}{r} \qquad \textbf{(a1.6)}$$

If the edges of the plate are assumed clamped, the deflection of the plate at $r = a$, i.e. at the edge, will be zero. The slope of the defection will also be zero at $r = a$ and at $r = 0$. Therefore:

$$\left(\frac{qr^3}{16D}+\frac{C_1 r}{2}+\frac{C_2}{r}\right)_{r=0,a}=0 \qquad \textbf{(a1.7)}$$

so

$$C_2 = 0$$

$$C_1 = -\frac{qa^2}{8D} \qquad \textbf{(a1.8)}$$

giving :

$$-\frac{dw}{dr}=\frac{qr}{16D}\left(a^2-r^2\right) \qquad \textbf{(a1.9)}$$

and

$$w=\frac{qr^4}{64D}-\frac{qa^2r^2}{32D}+C_3 \qquad \textbf{(a1.10)}$$

knowing the deflection is zero at $r = a$,

$$C_3=\frac{qa^4}{64D} \qquad \textbf{(a1.11)}$$

so that

$$w=\frac{q}{64D}\left(a^2-r^2\right)^2 \qquad \textbf{(a1.12)}$$

The material used for the original prototype was 0.6% carbon hot rolled steel having a modulus of elasticity, E, of 200 GPa and Poisson's ratio, ν, of 0.25. The thickness of the plate was 3 mm. These values give a flexural rigidity of 480. Based on a maximum pressure in the piston of 140 bar, this gives a deflection at the centre of the end caps of 0.22 mm.

The radial and tangential bending moments on the plate are given by the following two equations:

$$M_r=\frac{q}{16}\left[a^2(1+\nu)-r^2(3+\nu)\right] \qquad \textbf{(a1.13)}$$

$$M_t=\frac{q}{16}\left[a^2(1+\nu)-r^2(1+3\nu)\right] \qquad \textbf{(a1.14)}$$

At the boundary, $r = a$,

$$M_r = -\frac{qa^2}{8} \qquad \textbf{(a1.15)}$$

The maximum stress in the plate is given by

$$\hat{\sigma}_r = -\frac{6M_r}{h^2} = \frac{3}{4}\frac{qa^2}{h^2} \qquad \textbf{(a1.16)}$$

so the minimum plate thickness should be

$$h_{\min} = \sqrt{\frac{3}{4}\frac{qa^2K}{\sigma_{yield}}} \qquad \textbf{(a1.17)}$$

where:

| | |
|---|---|
| $K$ | is the pressure safety factor |
| $\sigma_{yield}$ | is the material's yield stress |

Using 0.6% carbon hot rolled steel having a yield stress of 420 Mpa and adopting a safety factor of 2, the designed maximum system pressure of 140 bar requires a piston end thickness of 6.0 mm. This thickness was used in the second prototype shuttle and the end caps did not fail. The thickness used for the original prototype was 3.0 mm. This was insufficient to deal with the maximum design pressure in the shuttle ( 4.2 mm was required with no safety factor ) and it is clear that pressure peaks due to road disturbances caused the shuttle to fail in the manner outlined.

The maximum deflection of the new end caps may now be calculated. The flexural rigidity, based on a modulus of elasticity of 200 GPa and a Poisson's ratio of 0.25 is 3840. This gives a maximum deflection of 0.03 mm, compared with the value for the original prototype of 0.2 mm.

Stresses in the cylinder wall of the oil pistons were insignificant in comparison with those in the end caps.

# Appendix 2. Theoretical Determination of Hydragas® Piston Taper Rate

Computer models of the Hydragas suspension units and active roll control shuttle were based on experimentally measured data giving the change of diaphragm effective area with piston displacement, i.e. the piston taper rate. It was proposed that the computational efficiency of these models could be improved by employing an analytical method to determine the diaphragm effective area and taper rate based on knowledge of the unit geometry.

This approach could also be of benefit in the design of new geometries for similar suspension elements. In this way, the geometry of a suspension unit could be designed to meet specified criteria without the trial and error of producing and testing numerous prototypes. To this end, a simple computer program was written to provide the effective diaphragm areas and taper rates of a unit with certain user supplied parameters defining the geometry of the unit.

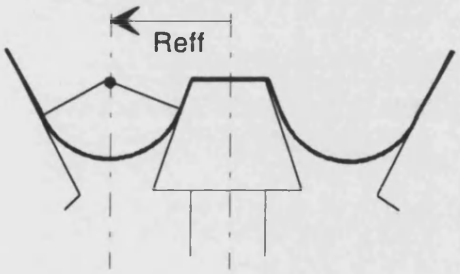


**Fig A2.1.** *Effective Radius of a Rolling Diaphragm Displacer*

The effective radius of a rolling diaphragm fluid displacer has been found to lie at the centre of the curved portion of the diaphragm, as demonstrated in figure A2.1.

Therefore, the determination of this point is central to the theoretical analysis presented here. The following constraints must be assumed for the analysis to continue :

- The length of a radial element of the diaphragm remains constant
- The piston moves only vertically with respect to the unit casing (skirt)
- Any radial section through the curved part of the diaphragm is a perfect circular arc
- The straight sections of the diaphragm remain in contact with the piston or skirt along their entire length

The piston effective area is given by:

$$A_{eff} = \pi R_{eff}^{\ 2} \tag{a2.1}$$

and the taper rate by:

$$\frac{dA_{eff}}{dX} = \pi \frac{dR_{eff}^{\ 2}}{dX} \tag{a2.2}$$

Figure A2.2 shows the basic diagram used in the analysis and defines several of the quantities

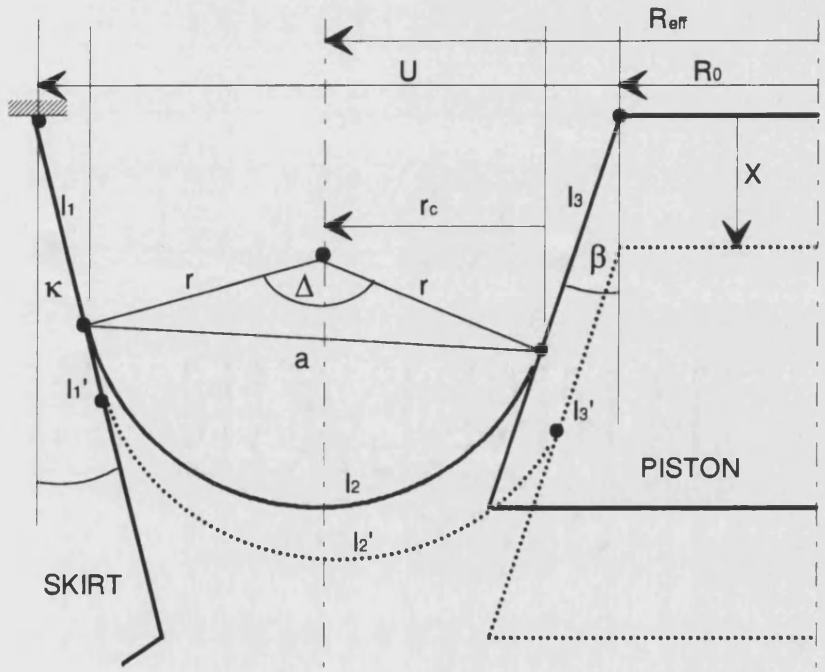


**Fig A2.2.** *Construction for Finding Diaphragm Effective Radius*

used. The diaphragm element is split into three separate lengths, $l_1$ in contact with the unit skirt, $l_2$ being the curved section and $l_3$ in contact with the piston. On a displacement of the piston relative to the skirt, X, the three lengths become $l_1$', $l_2$' and $l_3$'. The overall length of the element, L however remains the same.

The radius of the curved portion is denoted r and it's included angle is Δ. A straight line drawn between the two ends of the curved section has length a. The angles from the vertical of the unit piston and skirt are β and κ respectively. U denotes the horizontal distance between the top corner of the piston and the outermost point on the inside of the skirt. For reference purposes X is defined to be zero when the top of the piston is level with this outermost point on the skirt.

Figure A2.2 gives us :

$$R_{eff} = R_0 + l_3 \sin\beta + r_c$$
$$= R_0 + l_3 \sin\beta + r\cos\beta \qquad \textbf{(a2.3)}$$

and

$$r = l_2 / \Delta \qquad \textbf{(a2.4)}$$

so

$$R_{eff} = R_0 + l_3 \sin\beta + \frac{l_2}{\Delta}\cos\beta \qquad \textbf{(a2.5)}$$

Using the cosine rule, we have

$$a^2 = 2r^2(1-\cos\Delta) \qquad \textbf{(a2.6)}$$

Combining a2.4 and a2.6 :

$$l_2 = \Delta a\sqrt{\frac{1}{2(1-\cos\Delta)}} \qquad \textbf{(a2.7)}$$

since we know

$$l_1 + l_2 + l_3 = L \qquad \textbf{(a2.8)}$$

$$l_1 + \Delta a\sqrt{\frac{1}{2(1-\cos\Delta)}} + l_3 = L \qquad \textbf{(a2.9)}$$

Figure A2.3 shows the construction used to solve $l_1$, $l_2$ and $l_3$ while figure A2.4 shows the derivation of the angle $\phi$.

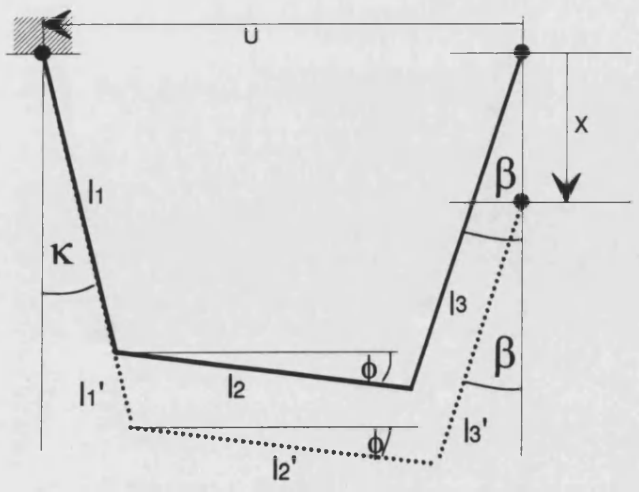


**Fig A2.3.** *Construction to Find Element Lengths*

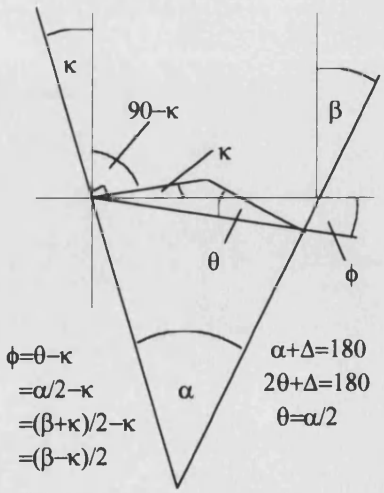


**Fig A2.4.** *Derivation of angle* $\phi$

Resolving in two directions:

$$l_1 \cos\kappa + a\sin\phi - l_3 \cos\beta = X \qquad \textbf{(a2.10)}$$

$$l_1 \sin\kappa + a\cos\phi + l_3 \sin\beta = U \qquad \textbf{(a2.11)}$$

where

$$\phi = \frac{\beta - \kappa}{2} \qquad \textbf{(a2.12)}$$

Equations a2.9, a2.10 and a2.11 may now be solved for $l_1$, a and $l_3$. $l_2$ may easily be found by substituting into equation a2.8. The expressions for $l_2$ and $l_3$ are as follows:

$$l_2 = C\left[\frac{(\sin\kappa - \sin\beta)(L\cos\kappa - X) - (\cos\kappa + \cos\beta)(L\sin\kappa - U)}{(\sin\kappa - \sin\beta)(C\cos\kappa - \sin\phi) - (\cos\kappa + \cos\beta)(C\sin\kappa - \cos\phi)}\right] \qquad \textbf{(a2.13)}$$

$$l_3 = \frac{(L\cos\kappa - X) - (C\cos\kappa - \sin\phi)[l_2 / C]}{(\cos\kappa + \cos\beta)} \qquad \textbf{(a2.14)}$$

where

$$C = \Delta\sqrt{\frac{1}{2(1-\cos\Delta)}} \qquad \textbf{(a2.15)}$$

These terms may then be substituted into equation a2.5 to give an expression for the diaphragm effective radius as a function of piston displacement. The diaphragm effective area can then be calculated for any piston position. The piston taper rate is simply the derivative of the expression for diaphragm area. The above analysis provides a quadratic expression for diaphragm area and a linear expression for taper rate with vertical piston displacement.

The parameters needed to define the geometry of a unit, from which all other constants may be calculated are as follows:

- maximum radius of displacer section, U
- piston taper angle, β
- skirt taper angle, κ

- minimum radius of piston, $R_0$
- overall length of a radial section of diaphragm between the inner and outer bead rings, L
- displacement of the top of the piston relative to the datum position, X

The computer program, based on the analysis set out above, gave a good representation of some of the early incarnations of the Hydragas concept, such as the Telegas unit which had almost linear piston and skirt profiles. For units such as that used on the Hydragas Metro however, the accuracy of the computer program was less good. This was due to the curved profiles of modern Hydragas suspension units. Estimations may be made of the effective diaphragm area at a particular point but not over the range of movement of the shuttle.

For this reason, the analytical approach to determining the piston taper rate was not adopted in the BATH*fp* computer model. There does remain the possibility of extending this theory to cover curved piston and taper profiles. Such a method would be valuable as a design tool for developing new Hydragas units.

# Appendix 3 Vehicle Parametric Data

This appendix gives the values of the vehicle parameters used in the computer simulation of the active roll control Hydragas Metro. These include those describing the vehicle itself, the hydraulic actuation system, the active control system and the controllers used to regulate vehicle speed and course during manoeuvres. The units presented here are as entered in the computer models.

## A3.1 VEHICLE MODEL DATA

### A3.1.1 Tyres

| | |
|---|---|
| linear vertical spring rate | 1.840D+05 N/m |
| vertical damping coefficient | 5.000D+03 N/m/s |
| free radius | 2.660D-01 m |
| relaxation length | 7.000D-01 m |
| longitudinal force relaxation length | 1.000D-02 m |
| longitudinal stiffness factor | 2.000D-02 N |
| tyre / road static friction factor | 1.000D+00 |

### A3.1.2 Unsprung Masses

| | |
|---|---|
| front initial wheel centre vertical displacement | -2.518D-01 m |
| front mass | 3.000D+01 kg |
| front spin inertia about axle axis | 1.000D-01 $kgm^2$ |
| rear initial wheel centre vertical displacement | -2.566D-01 m |
| rear mass | 2.100D+01 kg |
| rear spin inertia about axle axis | 1.000D-01 $kgm^2$ |

### A3.1.3 Sprung Mass

initial conditions:

| | |
|---|---|
| initial front body eyebrow height | -5.600D-01 m |
| initial rear body eyebrow height | -5.600D-01 m |

basic dimensions:

| | |
|---|---|
| nominal track width | 1.332D+00 m |
| nominal wheel base | 2.269D+00 m |
| front eyebrow height above rear at zero pitch | 0.000D+00 m |
| horizontal distance from front axle to body c.g. | 1.100D+00 m |

| | |
|---|---|
| sprung mass | 7.800D+02 kg |
| vehicle yaw moment of inertia (about c.g.) | 7.870D+02 $kgm^2$ |
| sprung mass roll moment of inertia (about c.g.) | 1.520D+02 $kgm^2$ |
| sprung mass pitch moment of inertia (about c.g.) | 7.130D+02 $kgm^2$ |
| sprung mass c.g. height above eyebrow plane | 0.000D+00 m |
| performance parameters | |
| nominal steering ratio | 22:1 |
| front/rear brake torque split | 3:1 |
| vehicle frontal area | 1.820D+00 $m^2$ |
| coefficient of aerodynamic drag | 4.000D-01 |
| suspension kinematic properties: | |
| front ride height at reference condition | 3.082D-01 m |
| rear ride height at reference condition | 3.034D-01 m |
| 1) Wheel Centre Lateral Displacement Polyn. (with ride height) | |
| front constant | 2.990D-01 m |
| front 1st coefficient | 1.546D+00 |
| front 2nd coefficient | -1.586D+00 $m^{-1}$ |
| rear constant | 0.000D+00 m |
| rear 1st coefficient | 0.000D+00 |
| rear 2nd coefficient | 0.000D+00 $m^{-1}$ |
| 2) Wheel Camber Polynomial (with ride height) | |
| front constant | -2.431D+01 deg |
| front 1st coefficient | 1.410D+02 deg/m |
| front 2nd coefficient | -1.978D+02 $deg/m^2$ |
| rear constant | 0.000D+00 deg |
| rear 1st coefficient | 0.000D+00 deg/m |
| rear 2nd coefficient | 0.000D+00 $deg/m^2$ |
| 3) Toe Polynomial (with ride height) | |
| front constant | 3.200D+00 deg |
| front 1st coefficient | -2.560D+01 deg/m |
| front 2nd coefficient | 4.940D+01 $deg/m^2$ |
| rear constant | 1.230D+00 deg |
| rear 1st coefficient | -3.670D+00 deg/m |
| rear 2nd coefficient | 0.000D+00 $deg/m^2$ |

### A3.1.4 Suspension Parameters

| | |
|---|---|
| initial fluid pressure | 2.900D+01 bar |
| initial fluid volume in displacer unit | 2.500D-01 L |

| | |
|---|---|
| fluid bulk modulus | 2.300D+09 $N/m^2$ |
| gas spring total volume | 5.000D-01 L |
| gas spring charge pressure | 2.100D+01 bar |
| gas spring polytropic index | 1.400D+00 |
| front ride height for datum displacer position | 2.960D-01 m |
| front lever ratio | 4.3:1 |
| front parasitic rate | 3.000D+00 kN/m |
| front drop angle rate | -1.050D+00 kN/m |
| front diaphragm effective area polynomial constant | 3.156D+03 $mm^2$ |
| front diaphragm effective area polynomial 1st coefficient | 7.010D+01 mm |
| front diaphragm effective area polynomial 2nd coefficient | 5.072D-01 |
| front diaphragm effective area polynomial 3rd coefficient | 0.000D+00 $mm^{-1}$ |
| front bump /rebound stop position | ± 6.000D+01 mm |
| front bump /rebound stop rate 1st coefficient | 9.369D+01 N/mm |
| front bump /rebound stop rate 2nd coefficient | -8.330D+00 $N/mm^2$ |
| front bump /rebound stop rate 3rd coefficient | 4.960D-01 $N/mm^3$ |
| rear ride height for datum displacer position | 2.990D-01 m |
| rear lever ratio | 5.2:1 |
| rear parasitic rate | 5.000D+00 kN/m |
| rear drop angle rate | 3.500D+00 kN/m |
| rear diaphragm effective area polynomial constant | 3.567D+03 $mm^2$ |
| rear diaphragm effective area polynomial 1st coefficient | 8.230D+01 mm |
| rear diaphragm effective area polynomial 2nd coefficient | 4.900D-01 |
| rear diaphragm effective area polynomial 3rd coefficient | 0.000D+00 $mm^{-1}$ |
| rear bump /rebound stop position | ± 6.000D+01 mm |
| rear bump /rebound stop rate 1st coefficient | 1.350D+01 N/mm |
| rear bump /rebound stop rate 2nd coefficient | 1.496D+00 $N/mm^2$ |
| front damper valve pressure /flow polynomial constant | 0.000D+00 L/min |
| front damper valve pressure /flow polynomial 1st coefficient | 7.437D+00 L/min/bar |
| front damper valve pressure /flow polynomial 2nd coefficient | 9.312D-01 $L/min/bar^2$ |
| front damper valve pressure /flow polynomial 3rd coefficient | 4.890D-02 $L/min/bar^3$ |
| rear damper valve bump region pressure | 4.500D-01 bar |
| rear damper valve bump pressure /flow polynomial constant | -1.021D+01 L/min |
| rear damper valve bump pressure /flow poly. 1st coefficient | 3.664D+00 L/min/bar |
| rear damper valve bump pressure /flow poly. 2nd coefficient | 3.315D+00 $L/min/bar^2$ |
| rear damper valve bump pressure /flow poly. 3rd coefficient | -2.440D-01 $L/min/bar^3$ |
| rear damper valve rebound region pressure | 2.000D+00 bar |
| rear damper valve rebound pressure /flow polynomial constant | 4.190D+00 L/min |

| | |
|---|---|
| rear damper valve rebound pressure /flow poly. 1st coefficient | 1.205D+00 L/min/bar |
| rear damper valve rebound pressure /flow poly. 2nd coefficient | -1.720D-01 L/min/bar$^2$ |
| rear damper valve rebound pressure /flow poly. 3rd coefficient | -2.600D-03 L/min/bar$^3$ |

### A3.1.5 Interconnection Pipe Parameters

| | |
|---|---|
| initial fluid pressure | 2.900D+01 bar |
| overall pipe length | 3.000D+00 m |
| pipe internal diameter | 1.100D+01 mm |
| fluid bulk modulus | 2.300D+09 N/m$^2$ |
| pitch damper orifice diameter | 3.300D+00 mm |
| orifice flow coefficient | 7.000D-01 |

## A3.2 ACTIVE ROLL CONTROL SYSTEM PARAMETERS

### A3.2.1 Active Shuttle Parameters

| | |
|---|---|
| displacer initial displacer fluid pressure | 2.900D+01 bar |
| displacer initial displacer fluid volume | 2.500D-01 L |
| displacer fluid bulk modulus | 2.300D+09 N/m$^2$ |
| shuttle initial displacement | 0.000D+00 m |
| shuttle oil bore | 5.300D+01 mm$^2$ |
| shuttle stroke | 5.700D-02 m |
| shuttle moving mass | 1.000D-01 kg |
| oil bulk modulus | 1.900D+09 N/m$^2$ |

### A3.2.2 Control Valve

| | |
|---|---|
| supply to port A flow rate | 2.800D+01 L/min |
| supply to port A pressure drop | 5.000D+00 bar |
| port B to return flow rate | 2.800D+01 L/min |
| port B to return pressure drop | 5.000D+00 bar |
| supply to port B flow rate | 2.800D+01 L/min |
| supply to port B pressure drop | 5.000D+00 bar |
| port A to return flow rate | 2.800D+01 L/min |
| port A to return pressure drop | 5.000D+00 bar |
| valve natural frequency (-90 degrees phase lag) | 3.100D+01 Hz |
| valve rated current | 2.500D+02 mA |
| % current defining null flow gain | 1.000D+00 |
| flow gain corresponding to null current | 1.000D+00 L/min |
| null internal leakage | 0.000D+00 L/min |
| corresponding null leakage pressure differential | 0.000D+00 bar |

### A3.2.3 Miscellaneous Hydraulic Circuit Parameters

| | |
|---|---|
| pump supply flow | 4.800D+00 L/min |
| pressure relief valve cracking pressure | 1.400D+02 bar |
| accumulator volume | 1.000D+00 L |
| accumulator charge pressure | 6.000D+01 bar |

### A3.2.4 Controller Parameters

| | |
|---|---|
| accelerometer lateral sensitivity | 1.000D+00 |
| accelerometer roll sensitivity | 3.000D-01 |
| accelerometer yaw sensitivity | 1.100D+00 |
| forward path gain | 2.000D+00 |
| shuttle position feedback gain | 2.500D+02 |
| proportional gain | 5.000D+00 |

## A3.3 STEERPAD CONTROLLER PARAMETERS

1) Steering Controller

| | |
|---|---|
| reference point vehicle x-axis displacement | 5.000D+00 m |
| derivative gain | 5.000D-02 s |
| proportional gain | 1.000D+00 |
| integral gain | 3.300D-02 $s^{-1}$ |
| output gain | 5.000D+01 deg/m |

2) Speed Controller

| | |
|---|---|
| proportional gain | 5.000D+02 Ns |
| integral gain | 5.000D+01 N |

# REFERENCES


[ 1 ] S.A.E. J670e, Vehicle Dynamics Terminology, 1978

[ 2 ] Wong J Y, 1993, Theory of Ground Vehicles, 2nd Edition, ISBN 0-471-52496-4

[ 3 ] Higuchi A, Yano T, Hashimoto T, 1992, Trend of Suspensions of Front-Wheel Drive Vehicles, J.S.A.E. Review, Vol. 13, no 2

[ 4 ] Anderson J E, Bane O, Larsson A, 1989, Volvo 760 GLE Multi-Link Rear Axle Suspension, S.A.E. paper 890082

[ 5 ] Randle S J, 1993, Concept and Design of the MacLaren F1 Suspension Systems, Proc. IMechE paper C466 / 007

[ 6 ] Curtis A, 1991, Ride Revolution, Car Design and Technology, June/July Issue

[ 7 ] Bhave S Y, 1992, Effect of Connecting the Front and Rear Air Suspensions of a Vehicle on the Transmissiblity of Road Undulation Inputs, Vehicle System Dynamics, Vol. 21, pp225-245

[ 8 ] Moulton A E, Best A, 1979, Hydragas Suspension, S.A.E. paper 790374

[ 9 ] Oldaker A R, Waide D N, Rover Metro / 100 Series Suspension Engineering, Internal Report

[ 10 ] Olley M, 1934, Independent Wheel Suspension - Its Whys and Wherefores, Society of Automotive Engineers Journal, vol. 34 no. 3, pp73-81

[ 11 ] Dynamic Stability Control D.S.C. - A New B.M.W. Control System to Improve Vehicle Stability and Handling, 1993, Leffler H, Proc. IMechE paper C466 / 028 / 93

[ 12 ] Yokoya Y, Kizu R, Kawaguchi H, Ohashi K, 1990, Integrated Control System Between Active Controlled Suspension and Four Wheel Steering for the 1989 Celica, S.A.E. paper 901748

[ 13 ] Tanaka H, Inoue H, Iwata H, 1992, Development of a Vehicle Integrated Control System, Proc. IMechE paper C389 / 220

[ 14 ] Sharp R S, Crolla D A, 1987, Road Vehicle Suspension System Design, Vehicle System Dynamics Vol. 16

[ 15 ] Sharp R S, Hassan A, 1986, The Relative Performance Capabilities of Passive, Active and Semi-Active Suspension Systems, Proc. IMechE Vol. 200 no d3

[ 16 ] Sharp R S, 1988, Development of Adaptive Suspension, Mechanique et Structure, S.I.A. 88081

[ 17 ] Wright P G, Williams D A, 1989, The Case for an Irreversible Active Suspension System, S.A.E paper 890081

[ 18 ] Hillebrecht P, Konik D, Pfeil D, Wallentowitz H, Zieglmeier F, 1992, The Active Suspension Between Customer Benefit and Technological Competition, IMechE paper C389 / 378

[ 19 ] Aoyama Y, Kawabata K, Hasegawa S, Kobari Y, 1990, Development of the Full Active Suspension by Nissan, S.A.E. paper 901747

[ 20 ] Csere C, 1988, Lotus Active Suspension, Car and Driver , June Issue

[ 21 ] Garret K, 1988, Hydraulically Damped Vehicle Suspension is Automatically Controlled, Engineering Materials and Design, October Issue

[ 22 ] Dryden C, End to Things that go Bump in the Night, Daily Telegraph, 21st September 1988

[ 23 ] Tsutsumi Y, Sato H, Kawaguchi H, Hirose M, 1990, Development of Piezo TEMS ( Toyota Electronic Modulated Suspension ), S.A.E. paper 901745

[ 24 ] Dymock E, Citroen Corners the Market in Suspension, The Sunday Times, 25th September 1994

[ 25 ] Sharp R S, Pilbeam C, 1993, Achievability and Value of Passive Suspension Designs for Minimum Pitch Response, Proc. IMechE C466 / 028 / 93

[ 26 ] Hegel R, 1973, Vehicle Attitude Control Methods, S.A.E. paper 730166

[ 27 ] Alirand M, Lachaize H, Lebrun M, 1993, Study and Analysis of an Active Self-Levelling Suspension, Proc. I.E.E.E. International Conference on Systems, Man and Cybernetics pp222-227

[ 28 ] Sun Y, Parker G A, 1993, A Position Controlled Disc Valve in Vehicle Semi-Active Suspension Systems, Control Engineering Practice, Vol. 1 no 6, pp927-935

[ 29 ] Wu H C, Yan W Z, Mo C, Patten W N, 1993, A Prototype Semi-Active Damper, A.S.M.E. Dynamic Systems and Control Division Advanced Automotive Techniques, Vol. 52, pp51-57

[ 30 ] Williams R A, 1994, Electronically Controlled Automotive Suspensions, Computing and Control Engineering Journal, June Issue, pp143-148

[ 31 ] Pham A T, Ugazio P, 1989, Basic Developments of an Active Air Suspension for Passenger Cars, S.A.E. paper 890095

[ 32 ] Konishi J, Shiraishi Y, Katada K, Ito H, 1989, Development of an Electronically Controlled Air Suspension System, S.A.E. paper 881770

[ 33 ] Sharp R S, Hassan J H, 1988, Performance Predictions for a Pneumatic Active Car Suspension System, Proc. IMechE Vol. 202 no d4

[ 34 ] Goto T, Kizu R, Sato H, Onuma T, Ohno H, 1990, Toyota Active Control Suspension System for the 1989 Celica, ISATA, 14-18th May, Florence, Italy, paper 90007

[ 35 ] Crolla D A, Pitcher R H, Lines J A, 1987, Active Suspension Control for an Off-Road Vehicle, Proc IMechE Vol. 201 no d1

[ 36 ] Milliken W F, 1988, Active Suspension, S.A.E. paper 880799

[ 37 ] Williams D, Active Suspension for Automobiles - a Further Progress Report, Cranfield Flight Systems and Measurement Laboratories Internal Report

[ 38 ] Anon, 1989, Active Suspension: Making it Happen, Automotive Engineer, February Issue

[ 39 ] Cropley S, 1986, Re-inventing the Wheel, Car Magazine, October Issue

[ 40 ] Brunning A D, 1993, Adaptive Damping for Small Cars, Proc. IMechE C466 / 028 / 93

[ 41 ] Sharp R S, Pilbeam C, 1993, On the Preview Control of Limited Bandwidth Vehicle Suspensions, Proc. IMechE Vol. 207, pp185-193

[ 42 ] Crolla D A, Abdel-Hady M B A, 1991, Active Suspension Control; Performance Comparisons Using Control Laws Applied to a Full Vehicle Model, Vehicle System Dynamics 20, pp107-120

[ 43 ] Dixon J C, 1987, Roll-Centre Concept in Vehicle Dynamics, Proc. IMechE Vol. 201 no d1

[ 44 ] Dixon J C, 1988, Linear and Non-linear Steady State Vehicle Handling, Proc. IMechE, vol. 202 no d3

[ 45 ] Ross-Martin T J, Dorey R E, Darling J, 1990, A Low Cost Active Anti-Roll Suspension for Passenger Cars, A.S.M.E. Winter Annual Meeting, Dallas, Texas, November 1990

[ 46 ] Baker A, 1978, Anti-roll Vehicle Suspension with Hydraulically Powered Actuation, Hydraulic and Pneumatic Power, vol. 24 no 281, pp235-238

[ 47 ] Scott D, 1992, Active Roll Reduction, Automotive Engineer, August / September Issue

[ 48 ] Sharp R S, Pan D, 1993, On the Design of an Active Roll Control System for a Luxury Car, Proc. IMechE Vol. 207, pp275-283

[ 49 ] Hickson L R, Darling J, 1994, Hydraulic Systems Modelling Within Automotive Applications, 6th Intl. Congress on Hydraulic Engineering in the Vehicle, Angers, France, May 1994

[ 50 ] Broos P, 1993, Keeping an Even Keel, Delft Outlook, Delft University of Technology Magazine, Netherlands

[ 51 ] Anon, 1994, Active Suspension for Luxury Cars, Professional Engineer, Vol. 7 no 3, p31

[ 52 ] Williams R A, Best A, Crawford I L, 1993, Refined Low Frequency Active Suspension, Proc. IMechE C466 / 028 / 93

[ 53 ] Shuttlewood D W, Crolla D A, Sharp R S, 1992, Theoretical Results of an Electrically Actuated Hydro-Pneumatic Slow-Active Suspension, IFToMM-jc International Symposium on Theory of Machines and Mechanisms

[ 54 ] Sharp R S, Hassan S A, 1987, Performance and Design Considerations for Dissipative Semi-Active Suspension Systems for Automobiles, Proc IMechE Vol. 201 no d2

[ 55 ] Thompson A G, 1971, Design of Active Suspensions, Proc IMechE Vol. 185

[ 56 ] I.S.O. 2631, A Guide for the Evaluation of Human Exposure to Whole Body Vibration

[ 57 ] Best A, 1984, Vehicle Ride - Stages in Comprehension, Physics Technology Vol. 15

[ 58 ] Blundell M V, 1991, Full Vehicle Modelling and Simulation Using the ADAMS Software System, Autotech '91 c427 / 16 / 170

[ 59 ] Orlandea N, Chace M A, 1977, Simulation of a Vehicle Suspension with the ADAMS Computer Program, S.A.E. paper 770053

[ 60 ] Richards C W, 1990, BATH*fp* - A Second Generation Simulation Package for Fluid Power Systems, Proceedings B.H.R.A. 9th International Fluid Power Symposium

[ 61 ] Ross-Martin T J, 1990, The Development of a Computer Model for the Simulation of Passenger Car Ride and Handling Dynamics, Bath University Internal Report no. 1019

[ 62 ] Ross-Martin T J, 1990, Improvements to the BATH*fp* Model for the Simulation of Passenger Car Ride and Handling Dynamics, Bath University Internal Report no. 1020

[ 63 ] Ross-Martin T J, Darling J, Woolgar R, 1992, The Simulation of Vehicle Dynamics Using the Roll Centre Method, F.I.S.I.T.A. Congress London, paper 925048

[ 64 ] Bakker E, Pacejka H B, Lidner L, 1989, A New Tyre Model with an Application in Vehicle Dynamics Studies, S.A.E. paper 890087

[ 65 ] I.S.O. 7401, 1988, Road Vehicles - Lateral Transient Response Methods, British Title : BS AU230, 1989, Lateral Transient Response and Behaviour of Passenger Cars

[ 66 ] I.S.O. 4138, 1982, Road Vehicles - Steady State Test Procedure, British Title : BS AU189, 1983, Steady State Cornering Behaviour for Road Vehicles

[ 67 ] Els P S, Grobbelaar B, Investigation of Time- and Temperature- Dependency of Hydro-Pneumatic Suspension Systems, S.A.E. special paper 952, Vehicle Suspension and Steering Systems pp55-65

[ 68 ] Anon, 1992, MATLAB User's Guide, The Mathworks Inc. Nantick, Mass. 01760, USA

[ 69 ] Lechner D, Perrin C, 1993, The Actual Use of the Dynamic Performance of Vehicles, Proc. IMechE vol. 207

[ 70 ] Bastow D, 1987, Car Suspension and Handling, 2nd Edition, Pentech Press, London, ISBN 0-7273-0316-3

[ 71 ] Handbook of Perception and Human Performance, 1986, Section VII 36-39, vol. II, Cognitive Processes and Performance, John Wiley and Sons, New York

[ 72 ] Ross-Martin T J, 1994, Low Bandwidth Active Roll and Warp Control Suspension, PhD Thesis, University of Bath

[ 73] Rakheja S, Peijun L, Ahmed A K W, Su H, 1993, Analysis of an Interlinked Hydro-pneumatic Suspension, ASME Dynamic Systems and Control Division - Advanced Automotive Techniques, vol. 52 pp279-287

[ 74 ] Brace C J, Deacon M, Vaughan N D, Charlton S J, Burrows C R, 1994, Prediction of Emissions from a Turbocharged Passenger Car Diesel Engine Using a Neural Network, Proc. IMechE, C484 / 046 / 94

[ 75 ] Hampo R, Marko K, 1992, Neural Network Architectures for Active Suspension Control, Proc. I.J.C.N.N. Intl. Joint Conference on Neural Networks, Seattle, pp765-770

[ 76 ] Smith J C, Cheok K C, Huang N, 1992, Optimal Parametric Control of a Semi-Active Suspension System Using Neural Networks, Proc. American Control Conference Vol. 2, pp963-967

[ 77 ] Neural Desk User's Guide, 1992, Neural Computer Sciences

[ 78 ] Deacon M, Brace C J, Guebeli M, Vaughan N D, Burrows C R, Dorey R E, 1994, A Modular Approach to the Computer Simulation of a Passenger Car Powertrain Incorporating a Diesel Engine and Continuously Variable Transmission, I.E.E. Intl. Conference, University of Warwick, 21-24 March

[ 79 ] Timoshenko S P, Woinowsky-Krieger S, 1959, Theory of Plates and Shells, 2nd Edition, McGraw-Hill, London, ISBN 0070858209